



INVESTIGATING TELOMERE LENGTH DYNAMICS IN HUMAN ENDOTHELIAL CELLS

Thesis submitted for the degree of
Doctor of Philosophy
at the University of Leicester

By

Meeta Suresh Patel BSc (Hons), MSc

Department of Cardiovascular Sciences
University of Leicester

2019

Investigating Telomere Length Dynamics in Human Endothelial Cells

Meeta Patel

Abstract

Numerous previous studies have shown an association between shorter TL and CAD. Prospective and family-based studies have suggested that shorter TL precedes disease onset. Recent genetic studies have provided evidence to support causality, however the biological mechanism is not understood. There is evidence that catastrophic telomere loss induces endothelial dysfunction through senescence. Such changes in TL do not reflect the modest changes observed at an inter-individual level. The aim of this study was to develop a model system in which TL could be manipulated to investigate potential mechanisms through which TL modulates disease risk.

The model utilised the addition of a removal *TERT* transgene (encoding the catalytic subunit of telomerase, which is normally repressed in somatic cells) to enable TL lengthening or stabilisation in endothelial cell lines. Removal of *TERT*, through Cre excision at different time points, would allow the generation of subcultures with short and long TL in the absence of potential confounding factors. In total *TERT* was transduced into nine HUVEC lines, four successfully immortalised and showed TL stabilisation. Three lines stabilised with relatively long TL. One of these lines was taken forward to generate long and short TL subcultures which were tested with and without the presence of a pro-inflammatory stimulus, for markers of endothelial dysfunction.

Cells with shorter TL displayed differences in basal expression of the cellular adhesion molecule ICAM-1 at both an mRNA and protein level. Cells with shorter TL were further shown to recruit higher numbers of monocytes using an *in-vitro* cellular adhesion assay. It was further shown that these differences are not the result of inducing senescence in these cells. This data provides preliminary evidence that TL may regulate monocyte adhesion to endothelial cells, contributing to the early stages of atherosclerosis and providing a potential mechanism through which TL contributes to disease risk.

Acknowledgements

I will like to thank and express my appreciation to my PhD supervisors Dr. Veryan Codd and Professor Sir Nilesh Samani. I am also thankful to the Medical Research Council and the NIHR Leicester Cardiovascular Biomedical Research Centre for funding my PhD project. A special thank you to Veryan, for the constant guidance and academic support throughout my PhD. Not only have you have helped me develop as a scientist, but you have been an approachable and caring mentor throughout my time at CVS. A sincere thank you to Sir Professor Nilesh Samani for the opportunity to work in his group; I am grateful to have been able to work with such excellent academics.

I would like to acknowledge many members of the Department of Cardiovascular Sciences who have helped me throughout my PhD, a particular huge thank you to Martha Hardy, Pete Braund, Matthew Denniff, Sarah Andrews, Mike Kaiser, Julie Chamberlain, Frederik Gibson, Sukhvir Rai, Pete Jones and Gavin Morris for their technical help and expertise. Thank you to Richard Mbasu, Abisola Sanusi, Maryam Ghaderi Najafabadi, Shilpi Sheth and Manish Asiani for all the laughs over the years in CVS and beyond.

Thank you Jitesh for your unwavering love and for your kind words of encouragement that kept me going. I would like to acknowledge my wonderful family; particularly my sisters, Fiona and Krishna, brother Hiren, and my dear friend Aneela; thank you for the support and cheering me on from the very start.

And finally, I dedicate this thesis to my incredible humble parents and would like to thank them for their endless love, encouragement, and continuous support they have given me throughout my life; I hope this makes you proud.

Table of Contents

Abstract	i
Acknowledgements	ii
Table of Contents	iii
List of Tables	vi
Table of Figures	vii
Abbreviations	x
CHAPTER 1 INTRODUCTION	1
1.1 The dynamic aspect of telomeres.....	2
1.1.1 Telomere function and maintenance	2
1.1.2 Semiconservative telomeric DNA replication	6
1.1.3 Telomerase and telomere elongation	6
1.2 Telomere length as a marker of biological age.....	8
1.2.1 3' End Replication problem.....	8
1.2.2 The Hayflick Limit- Replicative senescence	8
1.2.3 Telomere length and premature ageing syndromes.....	11
1.2.4 Telomere Length and Age-related Diseases.....	12
1.3 Telomere length and CAD.....	16
1.3.1 Epidemiological studies associating a positive relationship between TL, Ageing and cardiovascular disease	17
1.3.2 Inheritance and Genetics of Telomere Length	19
1.4 How may Telomere Length influence Coronary Artery Disease?.....	22
1.4.1 Coronary Artery Disease.....	22
1.4.2 Endothelial cell homeostasis	23
1.4.3 Stages of atherogenesis.....	26
1.5 The Causality Telomere Hypothesis	35
1.6. <i>In-vitro</i> model systems to generate primary cells lines with different telomere lengths	36
1.6.1 Historical studies to generate lines of different telomere lengths	36
1.6.2 Established models to generate isogenic lines of short and long TL.....	37
1.6.3 Lentiviruses	39
1.6.4 Cre-Lox system.....	43
1.7. Aims of the Project	47

CHAPTER 2 Materials & Methods	50
2.1 Materials	50
2.1.1 Bacterial culture	50
2.1.2 Nucleic acid extraction from human cells	50
2.1.3 PCR and RT-qPCR reagents	50
2.1.4 Gel electrophoresis	51
2.1.5 Plasmid preparation and cloning	51
2.1.6 Cell Culture.....	52
2.1.7 Production of Lentivirus.....	53
2.1.8 Protein detection by flow-cytometry	53
2.1.9 TRAP assay for telomerase activity.....	54
2.2.0 Equipment.....	54
2.2.1 Software.....	54
2.2 Methods.....	55
2.2.1 Cell Culture.....	55
2.2.2 Lentivirus Generation	60
2.2.3 Genomic DNA Extraction	61
2.2.4 Plasmid DNA.....	62
2.2.5 RNA Extraction	69
2.2.6 Polymerase chain reaction.....	71
2.2.7 Cellular Senescence	91
2.2.8 THP-1 monocyte cell adhesion assay.....	92
2.2.9 Cell surface target detection by flow cytometry	92
2.3.0 Statistical analysis	93
 CHAPTER 3	
GENERATION OF LOX-TERT PRIMARY HUMAN ENDOTHELIAL CELL LINES	95
3.1 Introduction.....	95
3.2 Methods	98
3.2.1 Lentivirus Generation	98
3.2.2 Biological Titration of TERT Lentivirus by quantitative PCR	99
3.3 Results.....	104
3.3.1 Telomere shortening in HUVEC under standard culturing conditions	104
3.3.2 Generation of a Lox-TERT line	107
3.3.3 Growth of TERT+ HUVEC under standard culturing conditions.....	107

3.3.4 Under standard culture conditions TERT is protective against stress induced senescence but does not maintain telomere length	111
3.3.5 Establishment of further Lox-TERT cell lines	115
3.3.6 Successful Immortalisation of HUVEC using human TERT	120
3.3.7 Ability to generate isogenic lines of varying telomere lengths from iHUVEC.....	135
3.4 Conclusion	140

CHAPTER 4

CHALLENGING ISOGENIC CELL LINES OF SHORT AND LONG TELOMERE LENGTHS WITH PRO-ATHEROGENIC STRESS TO ASSESS ENDOTHELIAL DYSFUNCTION..... 145

4.1 Introduction.....	145
4.2 Methods	146
4.2.1 Creation of isogenic lines	146
4.2.2 Functional experiments	147
4.3 Results	148
4.3.1 Experimental HUVEC isogenic lines with long and short telomeres	148
4.3.2 Increased <i>ICAM-1</i> and <i>E-SELECTIN</i> gene expression at basal level in the short TL clone.....	153
4.3.3 Increased <i>ICAM-1</i> gene expression in response to TNF- α stimulation	154
4.3.4 Isogenic lines with short telomere length show increased protein expression of ICAM-1 at the cell surface.....	154
4.3.5 HUVEC-monocyte adhesion in the short TL clone is higher at a basal and further increases upon TNF- α stimulation	159
4.3.6 Higher levels of endothelial dysfunction in cells with short TL is not associated with senescence.....	162
4.4 Conclusion	164

CHAPTER 5 DISCUSSION 169

5.1 Summary of key findings.....	169
5.2 Limitations of the <i>in-vitro</i> experimental model system	176
5.3 Future Work.....	180

APPENDIX 187

REFERENCES..... 199

List of Tables

Table 1.1	Cellular effects of normal (atheroprotective) endothelial cell compared to endothelial cell dysfunction (pro-atherogenic)	25
Table 2.1	Plasmid DNA vector name, bacterial growth strain, supplier/source and catalogue number	52
Table 2.2	Information on human primary cell lines and non-primary human cells lines	59
Table 2.3	Plasmid DNA vector	64
Table 2.4	Restriction enzymes and the expected fragment sizes for each of the plasmid vectors	66
Table 2.5	DNA restriction digest reaction set-up	67
Table 2.6	Criteria for optimum forward and reverse primers.....	71
Table 2.7	The components of a standard PCR set up reaction	72
Table 2.8	Standard PCR cycling conditions	72
Table 2.9	Blunt ended digestion of genomic DNA to generate viral integration libraries	73
Table 2.10	Integration Site Analysis primer sequences for the primary and Secondary PCR.....	75
Table 2.11	Forward and reverse primer sequences and cycling conditions.....	79
Table 2.12	Telomere and Single Copy gene (36B4) primer sequences for telomere length PCR.....	82
Table 2.13	Mastermix PCR set up for the TRAP assay.....	87
Table 2.14	PCR cycling conditions for the TRAP assay	88
Table 2.15	Human isotope antibodies and the corresponding human isotope control antibody used for the detection of specific cell surface proteins	93

Table of Figures

Figure 1.1. Telomere Biology.....	4
Figure 1.2 Schematic diagram of the DNA end-replication problem during mitosis in the absence of telomerase and progressive telomere shortening with each round of cell division	9
Figure 1.3 Telomere length variants and risk of CAD	21
Figure 1.4 Structural layers of a normal artery vessel.....	23
Figure 1.5 Stages in atherogenesis	27
Figure 1.6 Schematic overview of a HIV-1 I replication and life cycle	42
Figure 1.7 Schematic diagram of the Lox-TERT lentivirus and the Lox 3'LTR region of the integrated <i>TERT</i> provirus.	45
Figure 2.1 Example of DNA restriction double digest products on a gel	68
Figure 2.2 Melt Curve Analysis of <i>ICAM-1</i> standard curve	78
Figure 2.3 Standard curve for <i>ICAM-1</i> primer set	80
Figure 2.4 Concentration-response of Acycloguanosine on untransduced HUVEC.....	86
Figure 2.5 TRAP assay gel image and densitometry.....	90
Figure 3.1 Schematic experimental design to show the generation of short and long telomeres sublines from an single immortalised TERT+ HUVEC line	97
Figure 3.2 Flow diagram to show the process of lentivirus production, concentration, titration and infection into the host cell.	98
Figure 3.3 Pro-viral copy number, Titre (TU/ml) and MOI for transduced <i>TERT</i> and transduced <i>GFP</i> lines	101
Figure 3.4 HCT116 single cell GFP clone screening and Cre titration using clone 4....	103
Figure 3.5 Growth curve and telomere length of HUVEC single donor cell Line 7 cultured under standard conditions	106
Figure 3.6 Confirmation of <i>TERT</i> pro-viral integration and <i>TERT</i> expression.....	109
Figure 3.7 Line 7 growth curves and cellular senescence levels for parental (un-transduced) and TERT+ cells, grown under standard culturing conditions.....	110
Figure 3.8 Line 7 growth and telomere measurements reveal TERT+ cells fail to immortalise	113
Figure 3.9 Continued growth and TL stabilisation in TERT+ cells grown under 5% oxygen	114

Figure 3.10	Growth curves, <i>TERT</i> pro-viral integration data and <i>TERT</i> expression for the unsuccessful HUVEC lines	117
Figure 3.11	Failure to immortalise HUVEC (loss of <i>TERT</i> expression)	118
Figure 3.12	Failure to immortalise HUVEC (Telomere length shortening in the TERT+ line)	119
Figure 3.13	Successful immortalisation of four HUVEC lines	121
Figure 3.14	Immortalised HUVEC bypass senescence.....	122
Figure 3.15	Telomerase Activity in iHUVEC	124
Figure 3.16	Growth rates and Telomere length measurements for control (uninfected) and iHUVEC TERT	126
Figure 3.17	<i>TERT</i> mRNA expression in Line 1	127
Figure 3.18	Pro-viral <i>TERT</i> Integration site analysis of Line 7, 2 and 10 iHUVEC.	129
Figure 3.19	<i>MOB4</i> gene expression in control (un-transduced) and TERT+ transduced (iHUVEC) cells.....	132
Figure 3.20	iHUVEC phenotypic profiling to normal HUVEC.	134
Figure 3.21	Addition of Cre recombinase by transient transfection does not remove Lox-TERT	136
Figure 3.22	Successful removal of <i>TERT</i> from iHUVEC following the viral Cre test excision	138
Figure 3.23	<i>TERT</i> expression in Line 10 immortalised HUVEC excised with Cre.	139
Figure 4.1	Creation of experimental isogenic lines with short and long telomere lengths	150
Figure 4.2	<i>MOB4</i> gene expression in iHUVEC and short and long TL lines.....	151
Figure 4.3	Phenotypic profiling of isogenic lines to parental HUVEC.....	152
Figure 4.4	Gene expression of endothelial dysfunction markers in untreated and TNF- α stimulated cells	156
Figure 4.5	Upregulation of endothelial dysfunction marker gene expression in response to TNF- α	157
Figure 4.6	ICAM-1 protein expression in the isogenic lines with and without TNF- α stimulation.	158
Figure 4.7	Increased HUVEC-THP-1 monocyte cell adhesion at basal in the shorter TL clone, adhesion is further increased upon TNF- α (10ng/ml) stimulation.....	161
Figure 4.8	Minimal senescence detected in the short and long TL lines at basal and upon TNF- α treatment	163

Figure S1 (1)	Plasmid map pLOX-CW-CRE	187
Figure S1 (2)	Plasmid map pLOX-TERT-iresTK	188
Figure S1 (3)	Plasmid map pLOX-GFP-iresTK	189
Figure S1 (4)	Plasmid map pCMVR8.74	190
Figure S1 (5)	Plasmid map pUMVC	190
Figure S1 (6)	Plasmid map pCMV-VSV-G	191
Figure S1 (7)	Plasmid map pBABE-GW-GFP	191
Figure S1 (8)	Plasmid map pMD2.G	192
Figure S1 (9)	Plasmid map and gel image of restriction digest of pOG231	193
Figure S1 (10)	Plasmid map and gel image of restriction digest for pCre-pac	194
Figure S2	Integration site analysis of pro-viral <i>TERT</i> in Line 7 iHUVeC.....	195
Figure S3	PCR suppression effects during DNA walking (Integration Site Analysis)	196
Figure S4	Flow cytometric detection (Histoplots) of endothelial cell surface markers CD31, CD309 and CD144 (Line 1, 2, 7 and 10 parental HUVEC and iHUVEC).....	197
Figure S5	Flow cytometric detection (Histoplots) of endothelial cell surface markers CD31, CD309 and CD144 (parental HUVEC, iHUVEC, short TL and long TL lines)	198

Abbreviations

* may refer to a gene or the corresponding protein; standard nomenclature is applied within the text (all capitals, italicised = human gene; all capitals, not italicised = human protein, initial capital, remaining lower case, italicised = mouse gene)

36B4*	Ribosomal protein, large, P0
AA	Aplastic anemia
ACG	Acycloguanosine
AD	Alzheimer's disease
ADPase	Adenosine diphosphatase
AGEs	Advanced glycation end-products
Alb	Albumin
Alu	Arthrobacter luteus
APC	Allophycocyanin
APC*	Activated protein C
ATIII*	Antithrombin III
ATM*	Ataxia-telangiectasia mutated
ATR*	Ataxia telangiectasia and Rad3related protein
AUC	Area Under the Curve
Bcl-2*	B-cell lymphoma-2
BLAST	Basic Local Alignment Search Tool
BLAT	BLAST -like alignment tool
BMI	Body Mass Index
bp	Base pairs(s)
BSA	Bovine Serum Albumin
c-IAP-1*	Baculoviral IAP repeat-containing protein 2
c-NHEJ	classical non-homologous end-joining
C8orf33*	chromosome 8 open reading frame 33
CAD	Coronary artery disease
cAMP	Cyclic adenosine monophosphate
CARDIoGRAM	Coronary ARtery DIsease Genome Wide Replication and Meta-analysis
CCL2*	C-C motif chemokine ligand 2
CCR2*	C-C Chemokine receptor type 2
CD309*	cluster of differentiation 309
CDH5*	Cadherin 5
CDK4*	Cyclin dependent kinase 4
cDNA	Complimentary DNA
cGMP	cyclic guanosine monophosphate
CHAPS	3-((3-cholamidopropyl) dimethylammonio)-1-propanesulfonate)
CM	Cardiomyocytes
CMV	Cytomegalovirus

CN	Copy Number
CRP*	C-Reactive Peptide
CTC1*	CST telomere replication complex component 1
CX3CL1*	Fractalkine
CXCL2*	Chemokine (C-X-C motif) ligand 2
CXCL6*	C-X-C Motif Chemokine Ligand 6
DDR	DNA damage response
Dil-Ac-LDL	1,1'-dioctadecyl-3,3',3'-tetramethyl-indocarbocyanine perchlorate acetylated-low density lipoprotein
DKC	Dyskeratosis congenita
DKC1*	Dyskeratosis congenita 1
DL	DNA library
DMEM	Dulbecco's modified Eagle's medium
DMEM/F12	Dulbecco's Modified Eagle Medium: Nutrient Mixture F-12
DMSO	Dimethyl sulfoxide
DNA	Deoxyribonucleic acid
dNTPs	Deoxyribose nucleoside triphosphates
dsDNA	Double stranded deoxyribonucleic acid
EC	Endothelial cells
ECGM	Endothelial cell growth media
ECM	Extracellular matrix
ED	Endothelial dysfunction
EDHF*	Endothelium derived hyperpolarizing factor
EDTA	Ethylenediaminetetraacetic acid
eNOS*	endothelial nitric oxide synthase
ET-1*	Endothelin-1
Ex1	Excision 1
Ex2	Excision 2
FACS	Fluorescence-activated cell sorting
FBS	Fetal Bovine Serum
FGF*	Fibroblast growth factor
FITC	Fluorescein isothiocyanate
gDNA	Genomic Deoxyribonucleic acid
GFP*	Green Fluorescent Protein
H ₂ O ₂	Hydrogen peroxide
HCl	Hydrochloric acid
HCT116	Colon adenocarcinoma cell line
HDR	Homology directed repair
HEK293T	Human Embryonic Kidney 293T
HEPES	4-(2-hydroxyethyl)-1-piperazineethanesulfonic acid
HIV-1	Human immunodeficiency virus 1
HO ⁻	Hydroxyl radical

HS	Hot start
HSPC	Haematopoietic stem and progenitor cells
HSV TK*	Herpes simplex virus type 1 thymidine kinase
HUVEC	Human Umbilical Vein Endothelial cells
IC	Internal Control
ICAM-1*	Intracellular adhesion molecule 1
iDDR	Inhibitor of the DNA damage response pathway
IFN- γ *	Interferon gamma
IFU	infectious pseudoviral particles
IGF-1*	Insulin-like growth factor
iHUVEC	Immortalised Human Umbilical Vein Endothelial cells
IL-1*	Interleukin-1
IPF	Idiopathic pulmonary fibrosis
ITGAV*	Integrin subunit alpha V
ITGB1*	Integrin subunit beta 1
ITGB3*	Integrin subunit beta 3
K562	Lymphoblastoid cell line
KCl	Potassium Chloride
KDR*	kinase insert domain receptor
KH ₂ PO ₄	Monobasic potassium phosphate
LB	Luria Broth
LDL	Low-density lipoprotein
LOX-1*	Lectin-like oxidised low density lipoprotein receptor 1
LTR	Long terminal repeat
LV	Lentiviral
LV- <i>TERT</i>	Lentiviral <i>TERT</i>
MAE	Mean amplification efficiency
MCF-1*	Monocyte chemoattractant protein-1
MFI	Mean Fluorescence Intensity
MI	Myocardial Infarction
miR-128*	Micro Ribonucleic acid-128
MMP*	Matrix metalloproteinase
MMTV	Mouse mammary tumor virus
MOB4*	Family Member 4, Phocein
MOI	Multiplicity of Infection
MR	Mendelian randomization
mRNA	Messenger Ribonucleic acid
MST-1*	sterile 20-like kinase 1
Na ₂ HPO ₄	Disodium hydrogen phosphate
NaCl	Sodium Chloride
NCBI	National Center for Biotechnology Information
NCOA6*	Nuclear receptor coactivator 6
NF- κ B*	Nuclear factor kappa-light-chain-enhancer of activated B cells

NHEJ	Non-homologous end joining
NHP2*	NHP2 ribonucleoprotein
NO	Nitric oxide
NOP10*	NOP10 ribonucleoprotein
NRT	No reverse transcriptase
NTC	No template control
O ₂ ⁻	Superoxide anion
OBFC1*	OB fold-containing protein 1
OR	Odds Ratio
Ox-LDL	Oxidised low density lipoprotein
p16 ^{INK4A} *	Cyclin dependent kinase inhibitor 2A
PAF	Platelet activating factor
PAGE	Polyacrylamide gel electrophoresis
PBS	Phosphate Buffered Saline
PCR	Polymerase chain reaction
PDGF*	Platelet-derived growth factor
PD	Population Doublings
PECAM-1*	Platelet endothelial cell adhesion molecule 1
PEG	Polyethylene glycol
PGI ₂	Prostacyclin
pHUVEC	Parental human umbilical vein endothelial cells
Polα	DNA polymerase-α
POT1*	Protection of telomeres 1
PR	Protease
PSGL-1*	P-Selectin glycoprotein ligand-1
PTEN*	Phosphatase and tensin homolog
RAP1*	Repressor/activator protein 1
Rb	Retinoblastoma
RNA	Ribonucleic acid
RNF168*	Ring Finger Protein 168
ROS	Reactive oxygen species
RPMI	Roswell Park Memorial Institute
RRE	Rev-responsive elements
rRNA	Ribosomal ribonucleic acid
RT	Reverse transcriptase
RT-qPCR	Real-time quantitative polymerase chain reaction
RTA	Relative telomerase activity
RTEL1*	Regulator Of Telomere Elongation Helicase 1
SA β-gal	Senescence associated β-galactosidase
SAPS	Senescence associated secretory phenotype
SD	Standard Deviation
SFM	Serum Free Media

SIN	Self in-activating
SNP	Single Nucleotide Polymorphism
SOC	Super Optimal Broth
SV40	Simian virus 40
T/S	Relative Telomere to Single copy
TAE	Tris-acetate-EDTA
TBE	Tris-borate-EDTA
TEN1*	TEN1 subunit of CST complex
TERC*	Telomerase RNA component
TERT*	Telomerase Reverse Transcriptase
TF*	Tissue factor
TFPI*	Tissue factor pathway inhibitor
TGF- β *	Transforming growth factor
THP-1	Human monocytic leukaemia
TIN2*	Telomeric repeat-binding factor 1-interacting nuclear factor 2
TINF2	TERF1 interacting nuclear factor 2
TL	Telomere length
TNF- α *	Tumour necrosis factor- α
TPE	Telomere Position Effect
TPP1*	Tripeptidyl peptidase
TRAP	Telomeric repeat amplification protocol
TRF1*	Telomeric repeat binding factor 1
TRF2*	Telomeric repeat binding factor 2
TRFH*	Telomeric repeat factors homology
tRNA	Transfer ribonucleic acid
TS	Telomerase substrate
TU	Transducing Units
TXA ₂	Thromboxane
UCSC	The University of California Santa Cruz
UoL	University of Leicester
UTR	Untranslated region
UV	Ultraviolet
VCAM-1*	Vascular cell adhesion molecule 1
VE-Cadherin*	Vascular endothelin cadherin
VEGFR-2*	Vascular endothelial growth factor receptor 2
VLA-4 $\alpha_4\beta_1$ *	Very late antigen-4 $\alpha_4\beta_1$ integrin
VSMC	Vascular smooth muscle cells
VSV-G	Vesicular stomatitis virus
vWF*	von Willebrand Factor
WBC	White blood cell
WRAP53*	WD Repeat Containing Antisense To TP53
X-Gal	X-Galactosidase
β -Gal	β -Galactosidase

CHAPTER 1

Introduction

CHAPTER 1 INTRODUCTION

1.1 The dynamic aspect of telomeres

Derived from the Greek *telos* (end) and *meros* (part), telomeres are non-coding, protein bound structures located at the ends of eukaryotic chromosomes. In humans the telomere sequence consists of tandem repeats of 'TTAGGG' ending with a 3' single guanine strand overhang (Blackburn & Gall 1978; Moyzis *et al.*, 1988; Henderson *et al.*, 1989). In healthy humans, the average length of the telomere ranges from 2kb to 12kb (Henderson & Blackburn 1989; Meyer *et al.*, 2018). The main role of telomeres is in maintaining genomic stability (Podlevsky *et al.*, 2008).

1.1.1 Telomere function and maintenance

At the proximal end of chromosomes, telomeres are isolated from chromatin by a dynamic stretch of conserved DNA sequences. The 3' G-rich overhang strand invades the doubled-stranded DNA region to form a large duplex D-loop T-loop 'cap', which in essence neatly tucks away the ends of telomeres and offers telomere protection (Sfeir *et al.*, 2009) (**Figure 1.1 A**). This complex structure protects the 3' overhang from being incorrectly recognised as a DNA break and thereby preventing inappropriate activation of the DNA damage response pathway. Telomeres also protect against DNA damage repair processes including Non-Homologous End Joining (NHEJ) and Homology Directed Repair (HDR) and subsequent chromosomal fusion and degradation (Yu *et al.*, 1990). The activation of these processes can incorrectly lead to homologous recombination as well as chromosome end-to-end fusions chromosome aberrations; such genomic instability is a hallmark of cancer (De Lange 2005; Wolman *et al.*, 1964; Benn 1976). In preventing chromosomal fusion, telomeres ensure the stable integrity of genetic material and the correct segregation of genetic material into daughter cells during each mitotic cell division (Henderson & Blackburn 1989).

The tight structure and regulation of the telomeric cap structure is dependent on the association and dynamics of specific telomere associated proteins known as the shelterin complex (Ye *et al.*, 2004) (**Figure 1.1 A & B**) and telomerase (**Figure 1.1 B**). The shelterin complex encompasses six core proteins; TRF1, TRF2, POT1, RAP1, TIN2 and TPP1. The telomeric repeat binding factors 1 (TRF1) and 2 (TRF2) directly bind

independently to telomeric double stranded DNA (Broccoli *et al.*, 1997). The protection of telomeres protein 1 (POT1) binds at a high affinity to the single stranded G-rich 3' overhang as well as the displaced G-strand at the D-loop site (Lei *et al.*, 2001) (**Figure 1.1 C**). TIN2 binds to both TRF1 and TRF2 through independent molecular domains and recruits the TIN2- and POT1-organizing protein (TPP1)-POT1 complex to telomeric DNA (**Figure 1.1 C**) (Ye *et al.*, 2004; Chen *et al.*, 2008). Through this interaction, TRF-1 interacting nuclear protein 2 (TIN2) creates a bridge between the different shelterin proteins to structurally maintain the telomere cap. TPP1 possesses a telomerase-interacting domain within its amino terminus (Xin *et al.*, 2007) and recruits an essential telomere binding protein, Telomerase, which has an important role in elongating the invading telomeric strand.

Inhibition of DNA Damage Response and Repair Pathways by Telomere Binding Proteins

Telomere protection is predominantly dependent on the shelterin complex (Griffith *et al.*, 1999; Kim *et al.*, 1999; Abreu *et al.*, 2010; Guo *et al.*, 2007) and is crucial in preventing the activation of the DNA Damage Response and DNA repair pathways. Telomere protection is acquired through the inhibition of conventional DNA damage response (DDR) pathways, the Ataxia telangiectasia mutated (ATM) kinase pathway and the Ataxia telangiectasia and Rad3-related protein (ATR) kinase pathway. The ATM and ATR kinases induce cell cycle arrest through the inhibition of cell cycle checkpoint proteins via independent signalling pathways. Okamoto *et al.*, (2013) found the direct role of TRF2 in the suppression of the ATM pathway via a two-step mechanism. Firstly, the dimerization domain of TRF2, TRFH, is essential to inhibit early ATM activation. Secondly, an iDDR region is present within TRF2 which prevents the recruitment of an E3 ubiquitin ligase, RNF168, thereby suppressing chromosome end to end fusions. TRF2 also plays a role downstream the ATM kinase signalling pathway, in the direct repression of the classic (c-NHEJ) pathway (Karlseder *et al.*, 2004). During c-NHEJ, the Ku70-Ku80 heterodimer is normally recruited and binds to the site of double stranded DNA (dsDNA) breaks (Rai *et al.*, 2010). Prior to DNA replication, TRF2 binds and inhibits the helix 5 (α 5) domain of Ku70, thereby blocking the activation of the c-NHEJ repair pathway and preventing synapsis of chromosome ends (Ribes-Zamora *et al.*, 2013).

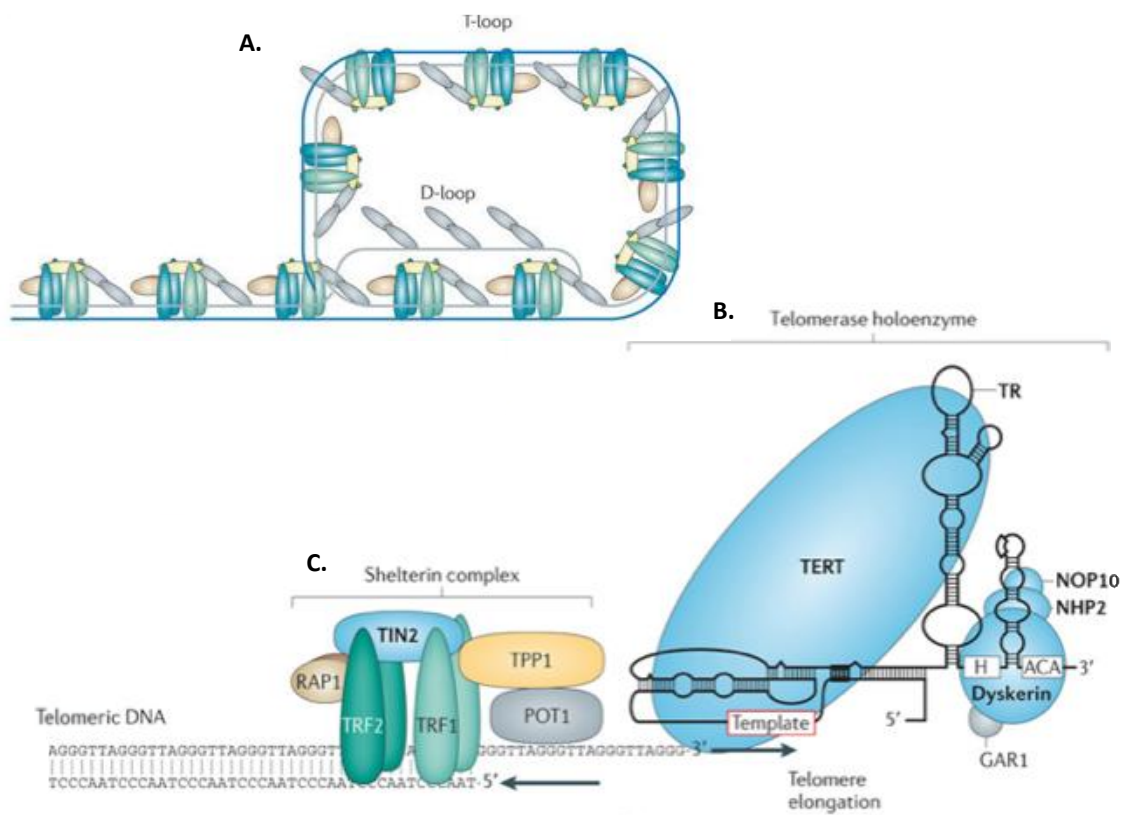


Figure 1.1. Telomere Biology. A. Schematic model of the shelterin complex bound to a telomere in a T-loop configuration adopted by the 3' G-strand overhang. B. The telomerase enzyme is comprised of TERT (the reverse transcriptase) and the RNA template TR (TERC) which recognizes the hydroxyl group (OH) at the 3' end of the G-strand overhang and elongates the telomere. The dyskerin complex is a component of telomerase and consists of NHP2, NOP10 and GAR1 (ribonucleoprotein). C. The shelterin complex is composed of telomeric repeat binding factor 1 (TRF1), TRF2, repressor-activator protein 1 (RAP1), the protection of telomeres protein 1 (POT1), TIN2, and an organizing protein (TPP1) (Ye *et al.*, 2004; Armanios (2009)). Images taken from Martínez & Blasco (2011) and Armanios & Blackburn (2012).

The telomere binding protein, RAP1, alone is unable to bind directly to telomeric DNA and its functional role is reliant on interaction with TRF2. It is known that RAP1 supports TRF2 in inhibiting ATM activation/c-NHEJ pathways, through a direct association with TRF2 at the t-loop formation (Arat *et al.*, 2012). The RAP1–TRF2 complex, compared to TRF2 alone, binds at a higher affinity to the telomeric 3' end. One study confirmed the repression of RAP1 does not alter the heterochromatic structure of telomeres or affect binding of the other shelterin proteins but does cause telomere recombination in the presence of POT1a/b (Sfeir *et al.*, 2010). These findings show in addition to TRF2, RAP1 also blocks HDR but in a TPP1/POT1 dependent manner. At the site of stalled replication forks, TPP1-POT1 is recruited by TRF1-TIN2 to prevent ATR activation (Sfeir *et al.*, 2009). Inhibition is achieved through the exclusion of a replication protein A (RPA) from the G-rich single-stranded overhang at the site of stalled replication forks (Gong & de Lange 2010; Litman *et al.*, 2012). Despite TRF2 and TRF1 belonging in the TRF (DNA topoisomerase I-related function) family of proteins, TRF1 serves a distinct function in telomere regulation. TRF1 suppresses telomere elongation through a negative feedback mechanism that stabilises telomere length (van Steensel & De Lange 1997). As TRF1 does not directly affect the expression of telomerase; the authors speculate this may be through TRF1 repression *in cis* by inhibiting the action of telomerase at the telomeric strands. TRF1 also facilitates the replication of telomeres during S-phase. Loss of TRF1 activates ATR at stalled replication forks during G and S2 phase of the cell cycle, where despite this replication stress, TIN2–TPP1–POT1 bind to TRF2 to suppress the ATR activation (Sfeir *et al.*, 2009).

Long non-coding telomeric repeat-containing RNA, TERRA are transcribed at subtelomeric regions and regulate various aspects of telomere function (Azzalin *et al.*, 2007; Cusanelli *et al.*, 2014; Wang *et al.*, 2015). A recent review by Bettin and colleagues (2019) highlights the proposed function of TERRA in telomere maintenance. TERRA transcripts may facilitate DNA replication at telomeres through the formation of DNA-RNA hybrids (R-loops) which promote homologous recombination and protects replication forks from collapsing and becoming dysfunctional during replication stress (Bettin *et al.*, 2019). TERRA interacts with a histone methyltransferase (Suv39h1), in TRF2-depleted cells, this interaction promotes H3K9me3 accumulation at dysfunctional

telomeres, sustaining the DNA damage response (Porro *et al.*, 2014). Therefore, TERRA sustains the DNA damage response at dysfunctional telomeres.

1.1.2 Semiconservative telomeric DNA replication

During semiconservative telomeric DNA replication, DNA polymerase- α (part of a Pol α –primase (PP) complex) incorporates nucleotides using Watson Crick base pairing extending along the template strand. Telomeric repeats are lengthened on the leading strand via a reverse transcription reaction (**Figure 1.2A**). Due to the unidirectional nature of DNA replication, during replication of the 5′-3′ template strand, a complementary lagging strand is synthesised by Pol α with deoxyribonucleotides by conventional RNA priming (Pellegrini *et al.*, 2012). The RNA primers provides a hydroxyl group to prime DNA synthesis at regular intervals along the strand (**Figure 1.2 A**) (Watson 1972). The RNA primers are subsequently degraded, the gaps are filled by DNA polymerase- δ using Okazaki fragments and ligated by DNA ligase to synthesis the lagging strand (Blasco 2005). During S-phase, at the 5′ end of telomeres, the ‘final’ RNA primer (positioned 70–100 nucleotides) is removed as no 3′ –OH group is available to prime DNA synthesis at the end of the lagging strand (**Figure 1.2 A**) (Chow *et al.*, 2012) leaving a 3′ G-rich overhang strand.

1.1.3 Telomerase and telomere elongation

After the replication of telomeric DNA, the 5′ and 3′ telomere DNA strands (the G and C strands respectively) are sequentially extended by telomerase and the PP complex (Blasco 2005). Telomerase is a ribonucleoprotein polymerase which uses a reverse transcriptase catalytic subunit (TERT) and an integral RNA component with a short template element (TERC) (**Figure 1.1. B**) (Greider & Blackburn 1985) for the de-novo addition of telomere repeat sequences. In humans, the TERC RNA sequence spans 451 nucleotides, within this is a recognition sequence 5′-AAUCCC. The TERC RNA template sequence complementary binds to the subtelomeric 3′ single strand overhang TTAGGG region (of a sequence bearing TTAGGGn) to lengthen the G strand via reverse transcription (Greider & Blackburn 1985). The presence of telomerase is critical for the binding of a CST complex (CTC1-TEN1-OBFC1) to this extended 3′ end (telomerase

dependent) which occurs during S/G2 phase. CST binding suppresses telomerase access, and subsequently the C strand is synthesised by the CST complex, thereby lengthening the C strand (Reveal *et al.*, 1997; Martínez & Blasco 2015; Gu *et al.*, 2012). This process is highly stringent and is reliant on the spatial association of telomerase. The Dyskerin complex of telomerase is composed of proteins GAR, NHP2 and NOP10 (Mitchell *et al.*, 1999; Podlevsky *et al.*, 2012) (**Figure 1.1 B**). TERC contains a 3' H/ACA box motif that binds the dyskerin protein DKC1, this complex plays a key role in TERC stabilization (Counter *et al.*, 1992).

Telomerase expression is high in specific cell types of regenerative tissues, telomerase is particularly active during human embryonic development (Wright 1996), enabling rapid cell division to support growth of the developing embryo. Furthermore, telomerase is expressed in human germ cells and activated lymphocytes and to a lesser extent in adult stem cells (of the gut, skin and blood), all of which have infinite cellular lifespans (Kim *et al.*, 1994; Wright 1996; Broccoli *et al.*, 1995; Tahara *et al.*, 1995).

In humans, both the TERC and dyskerin components of telomerase are ubiquitously expressed in somatic cells (Mitchell *et al.*, 1999; Feng *et al.*, 1995). Human telomerase is primarily regulated through the transcriptional silencing of the *TERT* gene. This is achieved through *TERT* transcriptional repressors and epigenetic modifications (Counter *et al.*, 1998; Won *et al.*, 2002; Cong *et al.*, 2002; Nakayama *et al.*, 1998). TERT is the rate-limiting determinant of enzymatic activity of human telomerase. The ectopic expression of *TERT* in normal human somatic cells has been shown to reconstitute telomerase activity and extend the replicative lifespan of human somatic cells (Bodnar *et al.*, 1997, Bodnar *et al.*, 1998). This evidence is highly suggestive that the repression of TERT accounts for telomerase activity to be switched off in most somatic cells. Reactivation of telomerase in somatic cells is associated with tumorigenesis (Counter *et al.*, 1998). *TERT* overexpression alone has been shown to be insufficient for cell transformation, unless cells lose the function of tumour suppressor genes *p53*, *PTEN*, *RB* (Boehm *et al.*, 2005) or *TERT* is overexpressed in combination with viral oncogenes such as the large T antigen of *SV40* or *E6/E7* genes of human papilloma virus (which exert their inhibitory effects on *p53* and *Rb*, respectively) (Fontijn *et al.*, 1995; Kiyono *et al.*, 1998).

1.2 Telomere length as a marker of biological age

1.2.1 3' End Replication problem

A caveat with the maintenance of telomerase dependent elongation of telomeric DNA discussed previously is telomerase is not expressed in somatic cells. To maintain the telomere length (TL) as associated with cell division throughout life, the presence of telomerase is necessary. The previous section discussed the inability to replicate the 3' ends of linear chromosomes due to conventional DNA replication machinery (**1.1.2 semiconservative telomeric DNA replication**). Therefore, in the absence of telomerase, 3' telomeric sequence of the C strand is lost at each round of DNA replication (Olovnikov 1973; Samani & van der Harst 2008), a process known as the 3' End Replication Problem (**Figure 1.2 A**). Owing in part to the 3' End Replication problem, chromosomes progressively shorten from both ends during each round of DNA replication which contributes to progressive telomere shortening with cellular ageing.

1.2.2 The Hayflick Limit- Replicative senescence

Due to the 3' end replication problem discussed in the previous section, as human somatic cells actively divide, TL progressively shorten, a theory postulated by Olovnikov in 1973. During telomere attrition, once telomeres reach a crucially short TL, known as the 'Hayflick Limit', somatic cells undergo replicative senescence which results in cell cycle growth arrest (Hayflick, Moorhead 1961). As shown in **Figure 1.2 B**, the Hayflick Limit model is proposed to be one of the molecular mechanisms of cellular ageing. Hayflick concluded both adult and fetal cells undergo a finite number of cell divisions before undergoing cell arrest. Hayflick's hypothesis denoted 'the finite lifetime of diploid cell strains in vitro may be an expression of ageing or senescence at the cellular level' (Hayflick 1965). The limited replicative capability of a cell is related to cellular ageing; this finite lifespan of human somatic cells is fundamental. A common denominator of cellular ageing is the accumulation of DNA damage throughout life (Moskalev *et al.*, 2013). This includes exogenous stress such as UV damage as well as endogenous stress including DNA replication errors (such as somatic cell mutations), hydrolytic reactions and reactive oxygen species (ROS). Although there is a complex network of DNA repair mechanisms (Lopez-Otin *et al.*, 2013), the concept of cellular ageing places a limit on how much DNA damage a cell can accumulate prior to the finite lifespan of that cell.

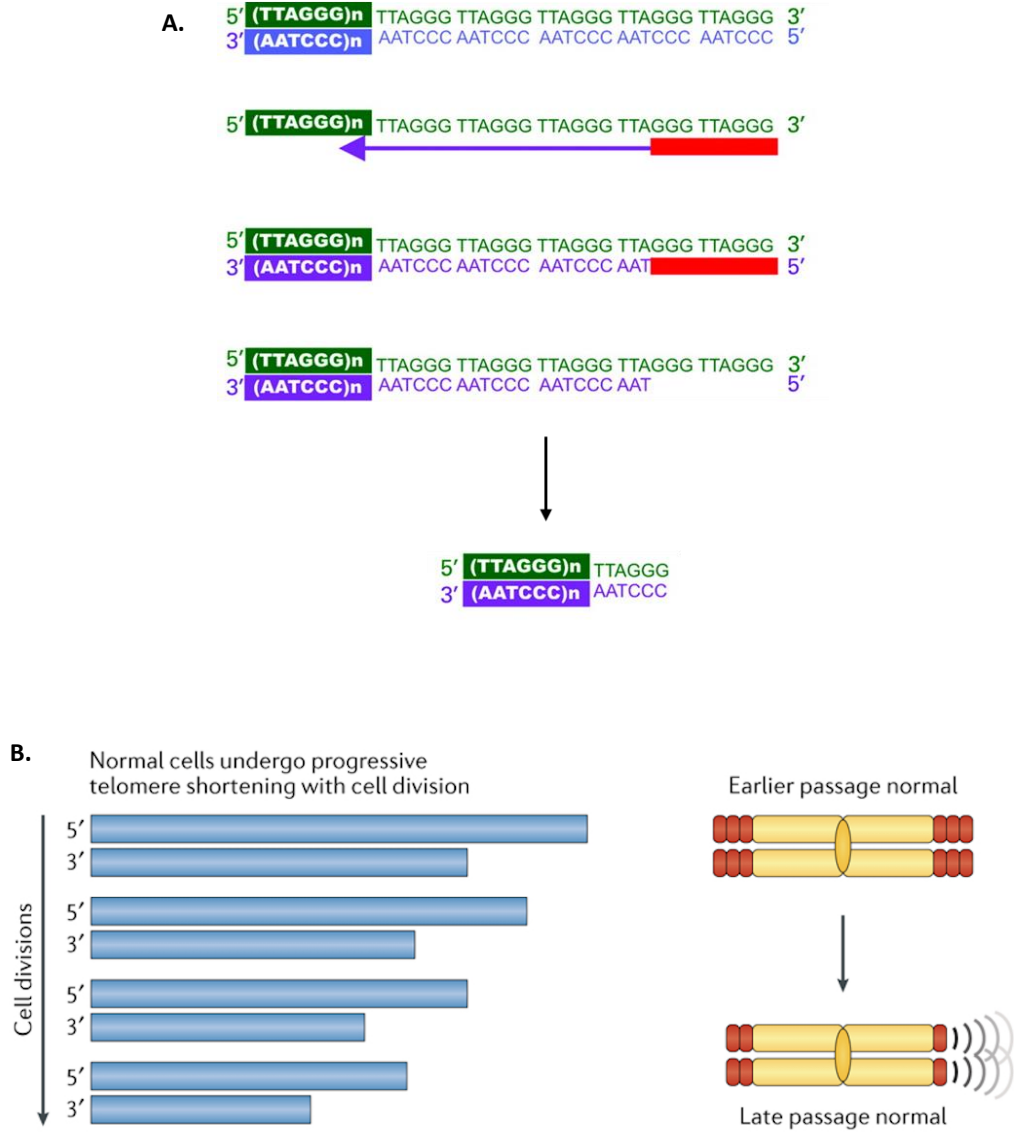


Figure 1.2 A. Schematic diagram of the DNA end-replication problem during mitosis in the absence of telomerase. B. Depiction of progressive telomere shortening with each round of cell division.

During conventional DNA replication, DNA is copied during the S phase of the cell cycle. RNA primers (red block) and DNA polymerase synthesises the lagging strand (3' → 5') by copying the parental strand. As the final RNA primer is removed, there is an inability to replicate the end of chromosomes leaving a 5' terminal gap on bottom strand. Degradation of this 3' single-stranded overhang results in loss of the telomeric sequence. This leads to progressive telomere shortening with increased cell division. B. Due to the 3' end replication problem in normal human somatic cells, telomeres shorten each time the cell divides. Eventually telomeres reach a critical short length, known as the 'Hayflick Limit' at which cells enter replicative senescence (Olovnikov 1973; Watson 1972; Hayflick 1965; Harley 1990, Stewart *et al.*, 2003). A & B. Adapted from Samani & Van der Harst (2008) and Shay & Wright (2019) respectively.

As telomerase activity is silenced in most human adult somatic cells, the Hayflick Limit, is an important determinant of the limited lifespan of these cells. Based on this concept of cellular ageing, TL is proposed as a marker of biological ageing, with shorter mean TL signifying an increased biological age (Watson 1972; Bodnar *et al.*, 1998; Harley & Greider 1990).

Numerous cross-sectional human studies support the cellular ageing hypothesis; a significant inverse relationship is observed between TL and chronological age (Bakaysa *et al.*, 2007; Nordfjall *et al.*, 2009; De Meyer *et al.*, 2008; Aviv *et al.*, 2009; Martin-Ruiz *et al.*, 2005). Mean adult TL attrition rates have been reported of ~30bp/year from cross-sectional studies (Daniali *et al.*, 2013; Slagboom *et al.*, 1994). Genetic heritability is proposed to be the major mechanism that accounts for inter-individual differences in TL between individuals; 78-84% of mean TL is genetically determined in twin and family studies (Slagboom *et al.*, 1994; De Meyer *et al.*, 2007; Jeanclos *et al.*, 2000; Broer *et al.*, 2013). Human studies show wide variability in TL between individuals of the same chronological age and this difference exists at birth (Belsky *et al.*, 2015). This variation reflects inherited and environmental differences between subjects. Lifestyle factors such as smoking, obesity and chronic psychological stress (increased cortisol levels) are also factors implicated in TL shortening through the biological effects of oxidative stress and inflammation (Epel *et al.*, 2006; Bekaert *et al.*, 2007; Valdes *et al.*, 2005).

1.2.3 Telomere length and premature ageing syndromes

Further support for TL as a marker for biological age comes from studies of TL in premature ageing syndromes (Vulliamy *et al.*, 2001; Armanios *et al.*, 2007; Panossian *et al.*, 2003). Such telomeropathies are strongly linked to telomere shortening and telomere dysfunction, through deleterious mutations in *TERT*, *TERC* and components of other telomere binding proteins involved in telomere protection (Du *et al.*, 2009).

An example of a telomeropathy is Dyskeratosis Congenita (DKC), a severe multi-system ageing disorder to which bone marrow disorder develops into mucocutaneous manifestations including oral leukoplakia, abnormal skin pigmentation, and nail dystrophy. X-linked recessive DKC is associated with telomere dysfunction, primarily through mutations in the *DKC1* gene encoding the dyskerin protein of telomerase (Mitchell *et al.*, 1999). Patients with the autosomal dominant form of DKC are haploinsufficient for *TERT* (missense mutation) and *TERC* (several deletions and nucleotide substitutions) and have a shorter TL compared to age matched controls (Armanios *et al.*, 2005; Vulliamy *et al.*, 2001, 2004 & 2005). DKC is a genetically heterogenous disorder, but universally almost all molecular features of this disease are excessively short telomeres. Studies with DKC associated *WRAP53*, *TERT*, *TERC* and *DKC1* mutations have demonstrated decreased telomerase activity levels or loss of telomerase recruitment to telomeres (Nelson & Bertuch 2012). In DKC (autosomal recessive form of the disease), *NOP10* and *NHP2* are associated with decreased *TERC* levels, re-emphasising telomere shortening is through decreased levels of telomerase activity (Walne *et al.*, 2007, Vulliamy *et al.*, 2008). In contrast, the DKC associated genes, TRF1 interacting nuclear factor 2 (*TINF2*) affects TL independent of telomerase. *TINF2* encodes protein TIN2 of the shelterin complex, *TINF2* mutations in children (most frequently present during early childhood) are presented with bone marrow failure prior to the development of the clinical mucocutaneous features of DKC mentioned above (Gramatges & Bertuch 2013). Onset and severity of DKC has been shown to correlate with progressive telomere shortening in later generations (Goldman *et al.*, 2005).

In addition to telomere attrition, López-Otín and colleagues (2013) propose further hallmarks of premature ageing which include genomic instability, epigenetic alterations,

loss of proteostasis, deregulated nutrient sensing, mitochondrial dysfunction, cellular senescence, stem cell exhaustion and altered intercellular communication (López-Otín *et al.*, 2018).

Increased DNA damage accumulation (including genomic nuclear DNA and mitochondrial DNA) contributes to premature ageing diseases such as Werner syndrome and Bloom syndrome, however genetic instability as previously mentioned is in part owed to various exogenous and endogenous threats (Hoeijmakers 2009). Ageing is also accompanied by epigenetic alterations (such as histone modifications, chromatin remodelling, DNA methylation and transcriptional alterations of mRNA) in various progeroid syndromes (Shumaker *et al.*, 2006). The hallmark, loss of proteostasis results in the chronic expression of unfolded, misfolded, or aggregated proteins which contributes to the development of some age-related pathologies, such as Alzheimer's disease, Parkinson's disease, and cataracts (Powers *et al.*, 2009).

Stem cell exhaustion results in a decline in the regenerative potential of tissues, e.g. hematopoiesis declines with age and due to immunosenescence a diminished production of immune cells. Such a phenotype is typical of myeloid malignancies and anemia (López-Otín *et al.*, 2013), which are further discussed in the next section.

1.2.4 Telomere Length and Age-related Diseases

Aplastic Anemia

Aplastic anemia (AA) is a fatal bone marrow heterogenous disorder characterised by peripheral pancytopenia and marrow hypoplasia (Marsh *et al.*, 2009). In AA, there is an inability of immature haematopoietic stem and progenitor cells (HSPCs) in the body to produce sufficient new erythrocytes, leukocytes and platelets (Scopes *et al.*, 1994, Yamaguchi *et al.*, 2003), in an otherwise natural process.

AA can be acquired, caused by T-cell triggered autoimmune processes against the hematopoietic stem cell compartment (Nakao 1997) or inherited caused by mutations

in genes involved in DNA repair, ribosome biogenesis and telomere biology (Dokal & Vulliamy 2010; Fogarty *et al.*, 2003).

Sequencing from AA blood samples revealed telomere dysfunction due to *TERT* haploinsufficiency (Vulliamy *et al.*, 2005; Yamaguchi *et al.*, 2005). Significant TL shortening was observed in patients with AA of varying disease severity and duration (Ball *et al.*, 1998). Telomerase activity in HSPCs is insufficient to maintain telomeres with ageing, this prematurely limits the high proliferation potential of the cells. Eventually this leads to a loss in the regenerative potential of these cells and the decreased tissue renewal capacity of the hematopoietic system (Vulliamy *et al.*, 2002). Furthermore, further TL loss may be linked to the increased loss of primitive progenitor cells (e.g. CD34+ cells) associated with AA through apoptosis (Philpott *et al.*, 1995).

In autoimmune-mediated AA, as a compensatory mechanism, HPSCs cells undergo an increased number of cell divisions to achieve the generation of mature progenitor cells in comparison to normal. Using a mouse model, it was shown conditional *Trf1* deletion causes acute telomere uncapping and activation of a DNA damage response at telomeres, leading to fast elimination of HPSC (Beier *et al.*, 2012). This study recapitulates the high turnover and hyper-proliferation observed in patients with AA of autoimmune origin, as well as demonstrating the presence of catastrophic telomere loss owing to direct mutations in telomere maintenance genes. Furthermore, Bär and colleagues (2016) showed telomerase reactivation using adeno-associated virus (AAV)9-*Tert* gene therapy vector, in 2 independent mouse models of AA due to very short telomeres (*Trf1*- and *Tert*-deficient) rescues AA in HSPC and mouse survival. Improved survival is associated with a significant increase in TL in both peripheral blood and bone marrow cells and improved blood counts (Bär *et al.*, 2016).

Conversely in another subset of AA, Fanconi Anemia, rather than direct mutations in telomere associated genes, telomeres are affected through breaks at telomere sequences, accumulation of breaks due to defective DNA repair mechanisms and impaired response to oxidative stress (Sarkar and Liu 2016)

Idiopathic pulmonary fibrosis

Idiopathic pulmonary fibrosis (IPF) is a progressive, fatal lung disease characterized by lung scarring and abnormal gas exchange. A clinical study shows both familial IPF (heterozygous mutations in *TERT*) and sporadic IPF (mutation in *TERC*) patients had shorter leukocyte TL compared to age matched controls. Asymptomatic subjects with mutant telomerase also had short telomeres, suggesting that they may be at risk for the disease (Armanios *et al.*, 2007). Povedano and colleagues (2015) provided a proof of principle study, of the causal role of DNA damage stemming from either critically short telomeres (telomerase-deficient mice) or severe telomere dysfunction (in mice with *Trf1* deletion in type II alveolar cells) in IPF development (Povedano *et al.*, 2015).

Alzheimer's Disease

Telomere dysfunction is a potential contributor to the pathogenesis of Alzheimer's disease (AD), an ageing-associated progressive neurodegenerative disorder. Different brain cell types are shown to exhibit diverse telomere dynamics. Neurons are terminally-differentiated post-mitotic brain cells while microglia exhibit significant mitotic potential and are therefore susceptible to telomere shortening. Microglial cells exhibit significant TL shortening and a reduction in telomerase activity is observed in ageing rats. In humans there is a tendency towards telomere shortening with the presence of dementia Flanary *et al.*, 2007. The authors suggested the increase in amyloid pathology with a higher degree of microglial dystrophy may play a contributing factor in the pathogenesis of AD (Flanary *et al.*, 2007). Patients with AD have significantly shorter telomeres in WBC and buccal cells relative to healthy age matched controls (Panossian *et al.*, 2003; Thomas *et al.*, 2008). These cell types have diverse cellular replicative potentials. TL are particularly shorter in buccal cells compared to WBC in patients with AD; buccal cells have a higher turnover rate of 21 days relative to that of lymphocytes (which is 6months or greater) (Zhang *et al.*, 2003).

Increased TL shortening in T-cells of patients also correlates with the severity of AD (Panossian *et al.*, 2003). Furthermore, in AD patients, increased telomerase activity and decreased proliferation of T-lymphocytes correlates with the severity of dementia (Zhang *et al.*, 2003). AD patients show partial impairment of immune cell (T-cell and B-

cell) function (Martorana *et al.*, 2012). Immune cell populations undergo rapid clonal expansion and are subject to high levels of replicative stress and therefore are particularly susceptible to telomere attrition (Zhang *et al.*, 2003). Whether leukocyte TL is associated with AD is still unclear (Boccardi *et al.*, 2015).

Cancer

One of the many hallmarks of cancer is loss of genomic stability (Hanahan & Weinberg 2000). Associations between TL and numerous human cancers have been identified (Wentzensen *et al.*, 2011; Shay 1997; Blasco 2005). Due to the loss of function of the tumour suppressor proteins RB/P53, cancer cells bypass cell cycle arrest. At the early stages of tumorigenesis, the telomere end protection capping process is disrupted in a small subset of precursor cells (Gilley & Herbert 2005) which may alter telomerase activity, for example mutations in *POT1* of glioma patients (Walsh *et al.*, 2015). The uncapped short telomeres evade being recognised as DNA breaks and this causes high chromosomal instability. End to end telomere fusions lead to breakage fusion bridge cycles and aberrant chromosomes leading to chromosomal translocations, aneuploidy and gene amplifications/deletions (Gilley & Herbert 2005; Artandi *et al.*, 2000; DePinho 2000; Sprung *et al.*, 1999). The late tumour metastasis stage involves a complexity of changes in expression levels of telomere associated proteins. For example, TRF1, TRF2, POT1 and TIN2 are vastly upregulated during the late tumour metastasis stage which induces changes in telomere dynamics thereby promoting late tumorigenesis of human cancers (Oh *et al.*, 2005, Kondo *et al.*, 2004, Hackett & Greider 2002).

A small subset of tumours activate alternative lengthening of telomeres-based mechanisms to cap the chromosome ends (Bryan *et al.*, 1997; Bechter *et al.*, 2004), although telomerase reactivation is observed in up to 90% of all types of malignant tumours (Shay 1997) where short telomeres are rescued and cancer growth is sustained (Kim *et al.*, 1994). However, it has been shown telomerase expression alone is not enough to transform cells; neoplastic transformation of human cells was first achieved by the combination of hTERT, SV40 TAg, and Ras^{G12V} (Hahn *et al.*, 1999). Recent work shows AAV9-mediated *TERT* over expression in the context of an oncogenic *K-RAS*

induced lung cancer mouse model does not accelerate tumorigenesis (Muñoz-Lorente *et al.*, 2018) showing defined genetic elements are required in addition to telomerase.

The tumour promoting effects of telomere dysfunction in humans is complex; different mechanisms module telomere homeostasis and aberrant telomeres (Bernal & Tusell 2018). Unlike other ageing diseases, changes in TL and telomerase activation are observed during tumorigenesis. Short TL is observed in early metastasis whilst longer telomeres are present in telomerase positive cancer cells during late tumour metastasis (Blasco 2005). To further strengthen this point, a genome wide association study shows TERT and TERC alleles associated with both shorter and longer telomeres are associated with increased risk of specific cancers (Codd *et al.*, 2013).

1.3 Telomere length and CAD

Coronary Artery Disease (CAD) is becoming increasingly prevalent in the ageing population. At a population level, environmental, lifestyle and genetic risk factors all play a role in CAD development. However, at an individual level CAD onset varies considerably even for subjects with similar risk factor profiles (Samani & van der Harst 2008). Due to this, human studies were initially performed using TL as a marker of biological age to address this issue of inter-individual variability observed in the susceptibility to, and in age of onset of CAD.

TL and telomere attrition rate have been shown to strongly correlate between different somatic tissues (Daniali *et al.*, 2013), therefore straightforward 'systemic' TL had been measured in leukocytes or mononuclear cells for the following epidemiological studies that will be discussed. Furthermore, different laboratory methods were used to measure leukocyte TL. Traditional methods include telomere restriction fragment analysis which requires enzymatic DNA digestion and subsequent Southern Blot analysis (Harley & Greider 1990) which measures subtelomeric fragments. Recent high-throughput methods include quantitative PCR (telomeric repeat DNA) to measure mean TL (Cawthorn *et al.*, 2003) and fluorescence in situ hybridisation, where it is possible to measure the shortest telomeres in large human sample sets (Canela *et al.*, 2007).

Nonetheless all 3 established methods to measure TL detect at least large differences between individuals.

1.3.1 Epidemiological studies associating a positive relationship between TL, Ageing and cardiovascular disease

A vast number of epidemiological studies have suggested shorter TL is associated with cardiovascular disease therefore centring TL and ageing to CAD risk (De Meyer *et al.*, 2018). One of the initial studies investigating TL and CAD found patients with severe (triple vessel) CAD had a shorter mean TL than age matched individuals with normal coronary angiograms. The mean TL in CAD patients was equivalent to those without CAD who were 8.6years younger (Samani *et al.*, 2001), this first study identified a link between shorter TL and increased risk of CAD. Other studies have shown a consistent difference equivalent to between 6-12 years (with the exception in elderly subjects) (Brouillette *et al.*, 2003; Brouillette *et al.*, 2008; Brouillette *et al.*, 2007; Willeit *et al.*, 2010) suggestive that subjects with CAD are biologically older. Whether this association is ultimately causal or due to reverse causation with the inclusion of confounding factors remained to be elucidated.

The relationship of shorter TL with increased CAD was confirmed and greatly extended on a retrospective study with a larger cohort of subjects at a later stage in the CAD process, with premature Myocardial Infarction (MI) (<50years) (Brouillette *et al.*, 2003). The limitation with cross-section observational studies (Samani *et al.*, 2001; Brouillette *et al.*, 2003) is the possibility that shorter TL may be a consequence of the development of CAD rather than a causative factor.

In a prospective study, leukocyte TL was analysed in statin naïve men aged between 45-65years (with no history of an MI) (Brouillette *et al.*, 2007). Subjects with a shorter baseline TL have an increased risk of developing a future CAD end-point event, compared to those with longer telomeres (Brouillette *et al.*, 2007). In poor socio-economic areas (for example West of Scotland), due to the poor lifestyle and dietary choices, CAD risk factors are more prevalent (Lowe *et al.*, 2000). The association

between shorter TL and increased CAD risk is independent of other established CAD risk factors such as smoking (oxidative stress through the generation of reactive oxygen species), body mass index, dyslipidemia, hypertension, diabetes or markers of systemic inflammation (CRP, WBC, fibrinogen) (Samani *et al.*, 2001; Brouillette *et al.*, 2003; Brouillette *et al.*, 2008; Brouillette *et al.*, 2007; Willeit *et al.*, 2010). These factors are also known to be implicated in telomere shortening (Valdes *et al.*, 2005; Lowe *et al.*, 2000; von Zglinicki 2002; Kurz *et al.*, 2004; Zhao *et al.*, 2013). Such findings support a causal relationship where shorter leukocyte TL increases the likelihood of a future CAD event occurring or CAD progression. Interestingly with shorter baseline TL this increased risk is attenuated in individuals receiving statins (Brouillette *et al.*, 2007), suggesting that patients with shorter telomeres preferentially gain advantage from taking statin treatment.

Within the scope of the prospective population-based Bruneck Study, leukocyte TL were measured in both men and women within a broader age range (45-94yrs). This study analysed the association of TL and atherosclerosis progression and manifestation of the CAD end-points stroke and myocardial infarction (Willeit *et al.*, 2010). As observed with previous epidemiological studies, age adjusted TL was shorter in men than in women and inversely correlated to age (Epel *et al.*, 2008). Participants with cardiovascular disease events during follow-up had significantly shorter TL. Furthermore, baseline shorter TL emerged as a significant and independent risk predictor for MI and stroke during a follow up period of twenty years (Willeit *et al.*, 2010). This observed effect is probable of a more causal (over a reverse causation) effect of shorter TL with CAD risk. The study shows TL is associated with the progression of advanced rather than early atherosclerosis. However, there are some limitations with aspects of this study; despite being a large cohort study (of 800 subjects), the level of significance associating TL to the risk of advanced compared to early atherosclerosis was low due to a wide error in the multivariable odds ratios of advanced atherogenesis between the data sets (Willeit *et al.*, 2010).

Atherosclerosis is a disease process which develops over decades; the time frame of the follow-up in the longitudinal studies discussed (Brouillette *et al.*, 2007; Willeit *et al.*, 2010) was relatively short. Therefore, it is difficult to interpret in such studies whether

the underlying pathophysiology of atherosclerosis, particularly early in the disease process, was already present at the time patients were recruited. In addition, confounding factors for both telomere shortening and CAD risk may still be implicated which means reverse causation cannot be completely ruled out.

To explore the familial risk of CAD in subjects with shorter TL, in a case-control study, TL measured in healthy young offspring with contrasting familial risks of CAD were compared to offspring from families without such a history of CAD (Brouillette *et al.*, 2008). TL of the case offspring was significantly shorter compared to that of the control offspring and the difference in mean TL (adjusted for age, sex, BMI and recruitment phase) between offspring of cases and controls was 472 base pairs. Furthermore, there was a significant positive correlation in mean TL between offspring and their parents. Shorter TL was observed quite early in the adult life of the healthy offspring (29years) with a family history of CAD. Therefore, it is unlikely that the shorter TL in these individuals is a consequence of significant existing but undetected disease. The observation that inherited short telomeres primarily increases familial CAD risk provides support that shorter TL may be causally implicated in the pathogenesis of CAD (Brouillette *et al.*, 2008).

1.3.2 Inheritance and Genetics of Telomere Length

There is some evidence to suggest that exogenous environmental factors such as smoking, obesity and chronic psychological stress affect TL (due to oxidative stress and inflammation) during an individual's life span (Epel *et al.*, 2004; Bekaert *et al.*, 2007; Valdes *et al.*, 2005; von Zglinicki 2002; Kurz *et al.*, 2004). However, the observational studies that have identified the link between shorter TL and increased risk of CAD found the association to be independent of these factors and also established CAD risk factors (smoking, high BMI, hypertension, diabetes, high cholesterol and high C-reactive peptide/fibrinogen/WBC/homocysteine) (Samani *et al.*, 2001; Brouillette *et al.*, 2003; Brouillette *et al.*, 2008; Brouillette, *et al.*, 2007; Willeit *et al.*, 2010). Such factors do not confound or explain the association between shorter telomeres and increased risk of CAD.

Genetic heritability is proposed to be the major mechanism that accounts for inter-individual differences in TL (Andrew *et al.*, 2006). Mendelian randomization (MR) is a broadly applicable methodological approach to assess the relationship between a biomarker and disease (Jansen *et al.*, 2014; Voight *et al.*, 2012). MR is based on the principle that, due to the nature of Mendelian Inheritance, genetic variants are randomly assigned during meiosis and are not affected by lifestyle or environmental factors. Therefore if genetic variants associated with TL associate with risk of CAD one can infer that the relationship is causal and not due to either reverse causation or confounding.

Genome-wide association studies have identified genetic determinants of TL (*TERC* and *OBFC1*) (Codd *et al.*, 2010; Levy *et al.*, 2010). This was expanded in a larger study that identified 7 genetic loci that affect TL (Codd *et al.*, 2013). The reported loci harbour genes are involved in the formation and activity of telomerase (*TERC*, *TERT*, *NAF1*) or telomere binding/replication (*OBFC1* and *RTEL1*). Most interestingly, a combined genetic risk score using all seven lead variants in cases of CAD compared to controls found a significant association between the alleles associated with shorter leucocyte TL with increased risk of CAD (**Figure 1.3**). This was the first study to establish an association between shorter TL and increased risk of CAD. The findings was later confirmed using a larger dataset of the same Coronary ARtery Disease Genome wide Replication and Meta-analysis (CARDIoGRAM) consortium and the Coronary Artery Disease (C4D) Genetics (CARDIoGRAMplusC4D) consortium (Madrid *et al.*, 2016). In addition, the observational and genetic studies, determined 200-bp-shorter TL was associated with a higher risk of ischemic heart disease (OR 1.10) (Madrid *et al.*, 2016).

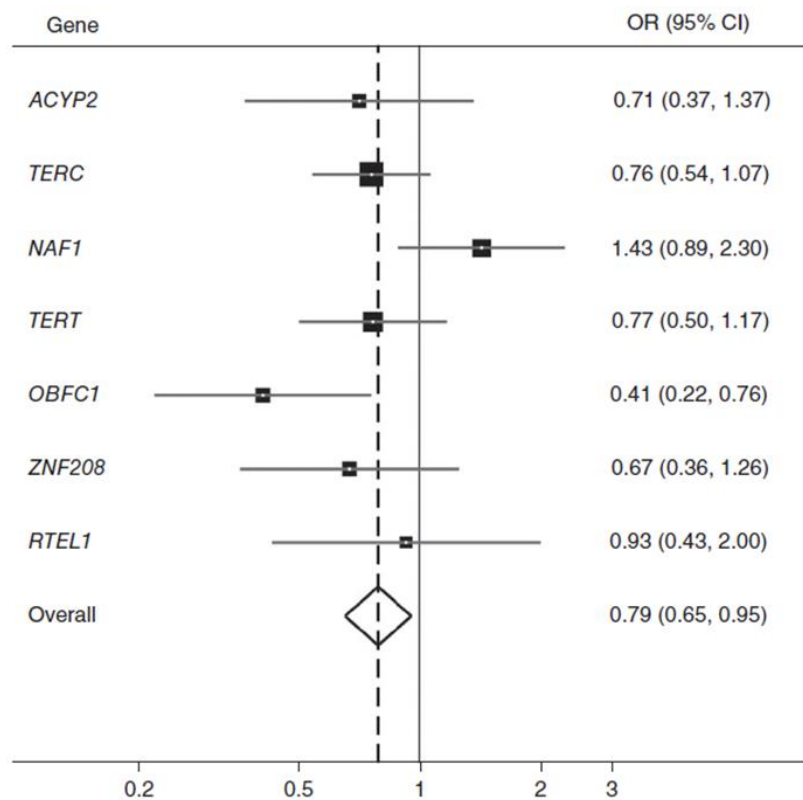


Figure 1.3. Telomere length variants and risk of CAD. Forest plot showing the effect of TL on CAD risk obtained for each SNP using a risk score analysis for each individual SNP. Effect sizes are plotted with 95% confidence intervals. The overall estimate is from a fixed-effects meta-analysis over all combined 7 SNPs, where the odds ratio (OR) relates to the change in CAD risk for a standard deviation change in telomere length. From Codd *et al.*, 2013.

The key findings discussed strengthen the hypothesis that shorter leucocyte TL is causal to CAD (Codd *et al.*, 2013; Madrid *et al.*, 2016; De Meyer *et al.*, 2018; Said *et al.*, 2017), to a level where one can confidentially progress research in this area to investigate the biological mechanisms by which shorter TL leads to increased CAD risk.

1.4 How may Telomere Length influence Coronary Artery Disease?

1.4.1 Coronary Artery Disease

The supply of oxygen to the myocardium is through an independent coronary circulation via the left and right epicardial coronary arteries. CAD is a disease of plaque (atheroma) formation in the coronary arteries; a process known as atherosclerosis. Cardiovascular heart disease is the biggest single cause of death around the world; with CAD the leading cause of death (Benjamin *et al.*, 2019).

Depending on the severity of CAD, atherosclerotic plaques can form in one or more of the following coronary vessels; the left coronary artery, the left anterior descending (LAD) artery, the right coronary artery or the circumflex artery (Roberts 1972). A severe case of CAD is triple-vessel disease. This is defined by the presence of $\geq 50\%$ diameter luminal narrowing at sites in three of the major coronary vessels. At the final stages of the atherosclerosis process, fibrous plaque formation and plaque rupture may lead to blockage of any of the coronary vessels. This causes localised ischaemia of the heart muscle and leads to a MI (Roberts 1972; De Maria *et al.*, 2013).

Structure of the vessel wall

The arterial vessel wall consists of three layers (**Figure 1.4**). The innermost tunica intima is lined with a monolayer of endothelial cells (EC) on the luminal side, and an internal elastic lamina on the peripheral side. The tunica media layer is made up of primarily vascular smooth muscle cells (VSMC) embedded in the extracellular matrix. Tunica adventitia (the outer layer) comprises of fibroblasts, VSMC, mast cells, nerve endings and microvessels (Libby *et al.*, 2011; Lusis 2000).

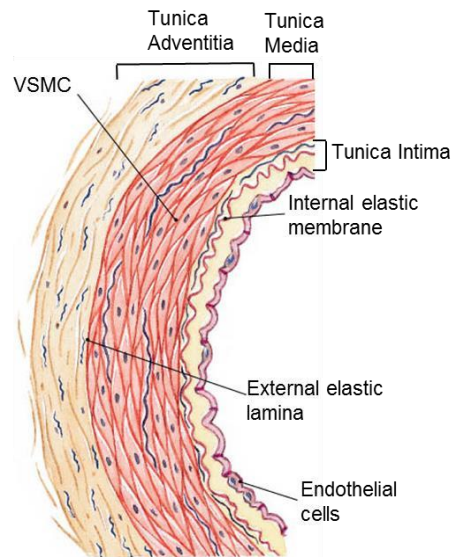


Figure 1.4. Structural layers of a normal artery vessel. The tunica intima (inner most layer) is lined with a monolayer of EC and a subendothelial connective tissue layer, limited by the internal elastic lamina. The tunica media layer is made up of primarily VSMC and ECM components, including elastin, collagen and proteoglycans. The adventitia is the outer layer of the vessel and comprises of fibroblasts, VSMC, mast cells, nerve endings and microvessels. Adapted from Lusis (2000).

1.4.2 Endothelial cell homeostasis

The healthy endothelium is a highly selective permeable barrier between the circulating blood and the vessel wall. EC control vascular function by responding to various chemical substances including vasoactive factors, which affect vasomotion, thrombosis, platelet aggregation and inflammation. As highlighted in **Table 1.1**, the healthy endothelium exerts favourable and atheroprotective effects to carry out its function (Davignon 2004; Sandoo *et al.*, 2010).

Vascular Tone

A healthy endothelium secretes vasoactive factors to tightly control vascular tone. Vasodilatory factors include nitric oxide (NO), prostacyclin (PGI₂) and endothelium derived hyperpolarizing factor (EDHF). The vasoconstrictive factors secreted by the endothelium are thromboxane (TXA₂), endothelin-1 (ET-1) and platelet-activating factor (PAF). The balanced production of these vasoactive factors is atheroprotective, whereas a damaged endothelium causes disrupted production of these factors (Sandoo *et al.*, 2010) (**Table 1.1**).

Endothelial cell barrier

The endothelial lining of the vessel wall forms a tight selective barrier for the transport of molecules between blood and tissues. The monolayer of endothelial cells is formed by cells tightly linked to adjacent cells by adhesive structures or cell to cell junctions (tight junctions, adherens junctions and gap junctions) (Bazzoni & Dejana 2004). Endothelial cell to cell contact is an important phenotype of EC and allows for blood vessels to sprout and lengthen (angiogenesis). Adhesion molecules such as vascular cell adhesion molecule 1 (VCAM-1), intracellular adhesion molecule 1 (ICAM-1), E-SELECTIN and platelet EC adhesion molecule 1 (PECAM-1) expressed on the surface of EC (Cines *et al.*, 1998) (**Table 1.1**) are implicated in this process. The adhesion molecules control the vascular permeability to circulating inflammatory cells (Bazzoni & Dejana 2004). In a healthy resting endothelium expression of these adhesion molecules is low therefore there is little leukocyte and lymphocyte cell recruitment to the intima (Michiels 2003).

Coagulation and Thrombotic properties

EC control the intrinsic coagulation cascade and platelet aggregation to exert anti-coagulant and antithrombotic effects (**Table 1.1**). EC secrete anti-platelet molecules such as NO and PGI₂ which act synergistically to increase cAMP in platelets, thereby preventing platelet aggregation. Furthermore, EC secretes protein thrombomodulin, and heparin like glycosaminoglycans at its cell surface which inhibit thrombin (a critical component of the coagulation cascade). Furthermore, EC release tissue factor pathway inhibitor (TFPI), an anti-coagulation protein, which specifically inhibits the extrinsic pathway of blood coagulation; the tissue factor pathway (Michiels 2003).

Vascular Effect	Atheroprotective Healthy Endothelial cell	Pro-atherogenic Endothelial cell dysfunction
Vascular tone	Pro-Vasodilatory Increased secretion of vasodilators (NO, PGI ₂)	Pro-vasoconstrictive Increased secretion of vasoconstrictors (ET-1, angiotensin II, TXA ₂)
Coagulation & Platelet activity	Anti-coagulant/ anti-thrombotic Inhibits platelet aggregation and adhesion, PGI ₂ , NO and ADPase produced and stored by platelets Glycosaminoglycans/ATIII Thrombomodulin TFPI	Pro-coagulant/ Pro-thrombotic Promotes platelet aggregation and adhesion, vWF, PAF, Fibrinogen, FV and FXI Binding sites for, fibrin, FIX, IXa, X, Xa, FXII, kallikrein, thrombin receptor for protein C/APC TF
Cell recruitment	Low inflammatory cell recruitment VCAM-1 absent, downregulation of ICAM-1 and E-SELECTIN expression, decreased chemokine secretion	High inflammatory cell recruitment Up-regulation of VCAM-1, ICAM-1 and E-SELECTIN expression, increased chemokine secretion, monocyte & T-cell recruitment
EC permeability	Decreased cell permeability to blood molecules	Increased cell permeability to LDL

Table 1.1. Cellular effects of normal (atheroprotective) endothelial cell compared to endothelial cell dysfunction (pro-atherogenic). A healthy endothelium exerts favourable and atheroprotective effects to carry out its function and in response to pro-atherogenic stimuli undergoes endothelial cell dysfunction. During this process the following changes in vascular tone (pro-vasoconstrictive), coagulation & platelet activity (pro-coagulant and pro-thrombotic), high inflammatory cell recruitment, and increased EC permeability occurs. Endothelial cells (EC), Nitric oxide (NO), prostacyclin (PGI₂), endothelin-1 (ET-1), Thromboxane TXA₂, Von-Willibrand factor (vWF), Antithrombin III (ATIII), tissue factor pathway inhibitor (TFPI), activated protein C (APC), platelet activating factor (PAF), Coagulation factor V (FV), factor XI (FXI), Tissue Factor (TF), vascular cell adhesion molecule 1 (VCAM-1), intracellular adhesion molecule 1 (ICAM-1) and E-SELECTIN. (Michiels 2003; Mudau & Mashudu 2012; Cines *et al.*, 1998; Schachinger *et al.*, 2000; Gimbrone & García-Cardeña 2016).

1.4.3 Stages of atherogenesis

The earliest change in the vessel wall that precedes atherogenesis is endothelial dysfunction (ED) (**Figure 1.5 A**). This triggers a plethora of cellular and molecular changes at the vessel wall which drives atherogenesis (Lusis 2000; Pober & Sessa 2007).

Upon the activation of endothelial cells, blood monocytes migrate into the intima where they mature into macrophages (**Figure 1.5 B**). The intracellular accumulation of oxidised LDL within macrophages, forms a 'foam cell'. The accumulation of lipid-laden foam cells together with T-lymphocytes and VSMC forms a 'fatty streak' (Pober & Sessa 2007, Rudijanto 2007) (**Figure 1.5 B**).

During the late stages of atherogenesis increased migration and proliferation of VSMC contributes to the formation of a fibrous plaque. The increased synthesis and secretion of mainly collagen by VSMC forms the protective fibrous cap (Rudijanto 2007). Monocytes, macrophages and VSMC within the atheroma die to produce a lipid-rich necrotic core consisting of oxidized lipoproteins, cholesterol crystals and cellular debris which is accompanied by varying degrees of matrix remodelling and calcification (**Figure 1.5 C**) (Hansson 2005).

The last stage of atherosclerosis involves plaque rupture and thrombosis (**Figure 1.5 D**). Thinning of the fibrous cap and plaque instability is due to the action of proteolytic enzymes which are released by VSMC in response to cell contact by activated T-lymphocytes (Schonbeck *et al.*, 1997). Upon plaque rupture, thrombogenic plaque material enters the blood, thrombosis occurs where the thrombus (platelets and fibrin crosslinks) extends into the lumen of the vessel impeding blood flow to the heart causing tissue ischaemia (Wang & Bennett 2012). Each of these stages of atherosclerosis are discussed in detail in the next section.

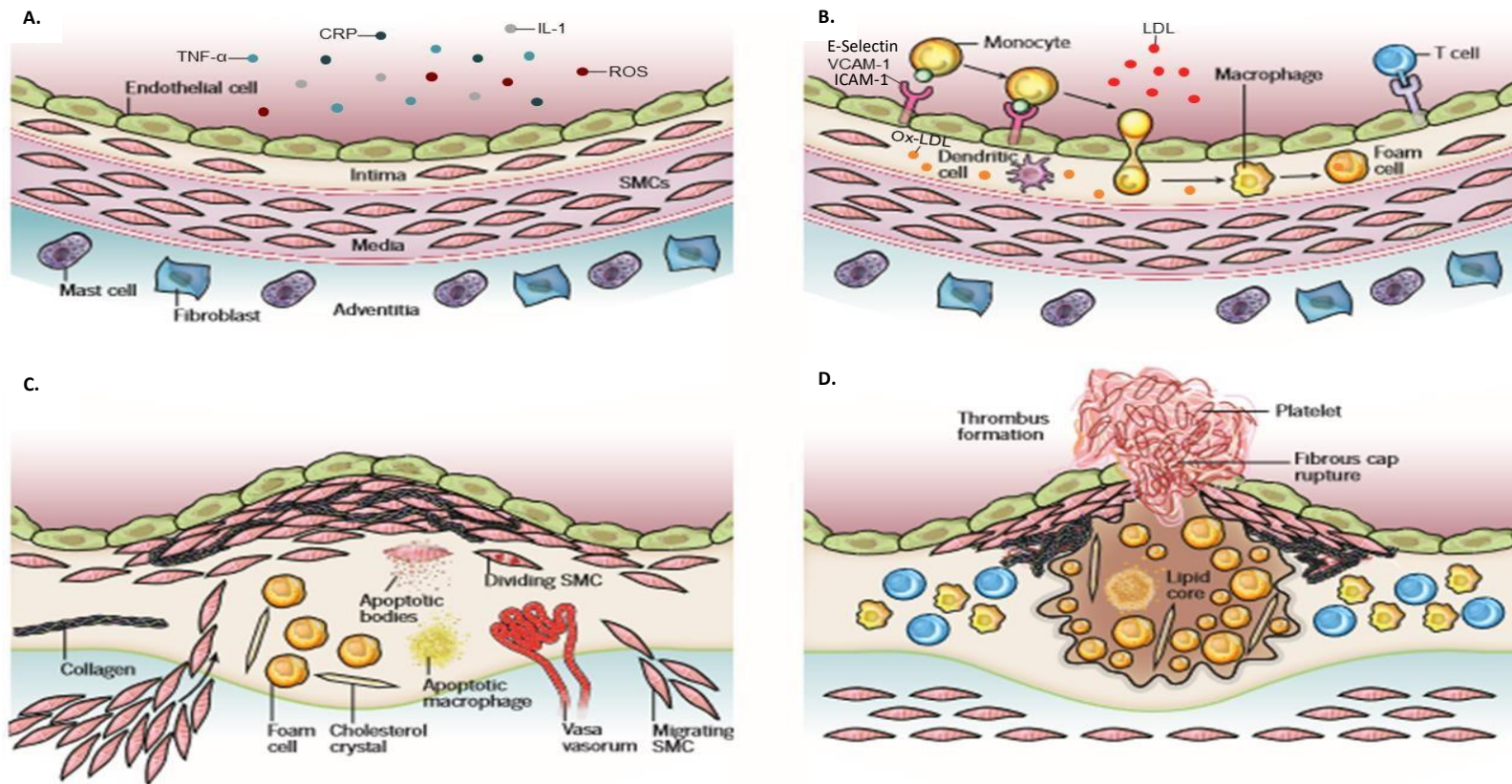


Figure 1.5. Stages in atherogenesis. A. Endothelial dysfunction is the earliest stage of atherogenesis, EC are activated by inflammatory mediators TNF- α , IL-1 β , CRP and ROS. B. The upregulation of adhesion molecules VCAM-1/ICAM-1/E-SELECTIN permits monocytes to adhere and migrate into the intima where they differentiate into macrophages. These macrophages take up oxidised LDL, resulting in foam cell formation. C. Accumulation of foam cells and cytokine-induced VSMC migration/proliferation leads to a fibrous plaque formation. Apoptotic bodies/macrophages release lipid and cholesterol crystals into the plaque to form a hard necrotic core. D. Upon plaque rupture and thrombosis the fibrous cap releases the contents of the necrotic core into the lumen, inducing thrombosis formation that may lead to a myocardial infarction. Adapted from Libby *et al.*, (2011). VCAM-1 (vascular cell adhesion molecule-1), LDL (low density lipoprotein), Ox-LDL (oxidised low density lipoprotein), TNF- α (Tumour necrosis factor- α), CRP (C-reactive peptide), IL-1 (Interleukin-1), ROS (Reactive oxygen species).

Endothelial cell activation and dysfunction

Healthy EC are activated according to the needs of the microenvironment of the cells e.g. for repair processes upon injury. ED is the initial stage of atherogenesis (**Figure 1.5 a**) (Liao *et al.*, 2013). As proposed by Ross and Glomset (1976), the 'response-to-injury' hypothesis is the initial step in atherogenesis and involves endothelial denudation in response to noxious substances (oxidised cholesterol, cigarette smoke, hyperhomocystemia, hyperglycemia) or altered hemodynamic forces (shear stress) (Gimbrone & García-Cardena 2016). To understand how this process is initiated, it is important to first discuss inducers of ED in the context of how ED drives a pro-atherogenic environment.

Shear stress

NO plays a pivotal role in the regulation of endothelial function. NO is synthesised in healthy endothelial cells and is a potent vasodilator. In NO synthesis, L-citrulline is formed from L-arginine. This oxidative reaction is catalysed by endothelial NO synthase (eNOS) in the presence of cofactors (Davignon 2004). In response to shear stress, NO diffuses into VSMC where it activates soluble guanylate cyclase. As a consequence, the substantial increase in the secondary messenger cGMP activates cGMP-dependent kinase causing a decrease in Ca^{2+} and vasorelaxation (Münzel *et al.*, 2008). Non-laminar blood flow induces shear stress and disrupts the balance in vascular tone. Impaired endothelium dependent vasorelaxation is caused by the loss of bioavailability of NO and is a critical hallmark of endothelial cell dysfunction (Ludmer *et al.*, 1986) (**Table 1.1**).

Oxidative stress

ED is primarily due to the increased production of reactive oxygen species (ROS) which affects the bioavailability of NO (Cai & Harrison 2000). ROS include the free radicals, superoxide anion ($O_2^{\bullet-}$) and the hydroxyl radical (HO^{\bullet}). Hydrogen peroxide (H_2O_2) is also a ROS that contributes to oxidative stress. Decreased bioavailability of NO may be due to changes in the activity/and or decreased expression of eNOS or due to increased formation of $O_2^{\bullet-}$ (due to uncoupled eNOS) (Wilcox *et al.*, 1997; Mudau *et al.*, 2012). The subsequent imbalance in NO and $O_2^{\bullet-}$ leads to accelerated degradation of NO (Harrison

1997). Increased $O_2^{\bullet -}$ is released from endothelial cells and macrophages which along with other ROS contribute to the oxidation of LDL. Ox-LDL are scavenged by macrophages and once internalised undergoes modification to form foam cells (**Figure 1.5 B**). Lipid laden macrophages primarily serve as the hallmark of the fatty streak (**Figure 1.5 B**). During atherogenesis, mediators of inflammation TNF- α , IL-1 and MCP-1 increase transcription of the LDL-receptor gene and also subsequent LDL binding to EC and VSMC (Ross 1999; Steinberg 2009).

Inflammation

In ED, oxidative stress is an important promotor of inflammation. All stages of atherosclerosis from initiation to the advanced plaque formation and thrombosis are considered a chronic inflammatory response (Libby *et al.*, 2002). At sites of inflammation during atherogenesis, inflammatory leukocytes are recruited (T cells, neutrophils, monocytes, and mast cells (**Figure 1.5 A and B**) (Weber & Noels 2011; Libby *et al.*, 2002). C-reactive peptide (CRP) is an inflammatory marker present within atherosclerotic lesions (Torzewski *et al.*, 1998). CRP is found in the vascular intima, where it co-localizes with monocytes, monocyte-derived macrophages and lipoproteins (Torzewski *et al.*, 1998). CRP is an activator of EC and is known to play a role during the inflammatory stages of stages of atherosclerosis (Bazzoni & Dejana 2004) through decreasing the secretion of both NO and PGI_2 (Paffen & DeMaat 2006). EC undergo type II activation in response to inflammatory cytokines TNF- α , IL-1 and IFN- γ and results in the activation of the pleiotropic nuclear factor- κ B which leads to the upregulation of pro-inflammatory effector proteins as further discussed in the next section.

Adhesion Molecules

Accumulated oxidised-LDL and markers of inflammation (CRP, IL-1, TNF- α) stimulate overlying EC to express the adhesion proteins vascular cell adhesion molecule 1 (VCAM-1) intracellular adhesion molecule 1 (ICAM-1), E-SELECTIN and P-SELECTIN (**Figure 1.5 A & B**) (Pober & Sessa 2007; Paffen & DeMaat 2006; Albrecht *et al.*, 2004). Such proteins are expressed on the surface of activated EC and have been observed in EC of atherosclerotic vessels (Lusis 2000, Pober & Sessa 2007; Davies *et al.*, 1993). These pro-inflammatory mediators are important in monocyte and T-lymphocyte cell recruitment

to the endothelium during the initial stages of atherogenesis (Lusis 2000; Chi 2007) **Figure 1.5 B).**

Chemokines/cytokines

Activated EC locally secrete the inflammatory mediators, TNF- α and chemokines monocyte chemoattractant protein-1 (MCP-1), IL-8 and fractalkine (CX3CL1), to stimulate the adhesion of different monocytic subsets to the intima (Čeiková *et al.*, 2016). Proinflammatory monocytes, identified by the high expression of a cell surface marker Ly6C, express a CCR2 receptor at its cell surface (Gordon & Taylor 2005). MCP-1 is a critical cytokine responsible for the recruitment and trafficking of classical and intermediate subsets of Ly6C^{high} CCR2⁺ monocytes, via the β 2-integrin adhesion signalling pathway (binding to ICAM-1) (Maus *et al.*, 2002). CX3CL1 mediates the transendothelial migration of non-classical CD16⁺ monocyte subset (Ancuta *et al.*, 2003).

The adhesion cascade

It has been discussed how endothelial dysfunction drives the earliest stage of atherogenesis. The pro-inflammatory microenvironment of the endothelium is favourable for monocyte recruitment which ultimately leads to formation of the atherosclerotic plaque via a multistep regulated process known as the 'adhesion cascade' (Čeiková *et al.*, 2016). An and colleagues (2008) found P-SELECTIN glycoprotein ligand-1 (PSGL-1) is expressed at a much higher level by Ly6C^{high} monocytes compared to resident Ly6C^{low} monocytes which facilitates the adhesion cascade in mice atherosclerotic lesions. During monocyte capture, P-selectin binds to its PSGL-1 this association is however weak. Firm adhesion of pro-inflammatory monocytes and subsequent 'rolling' requires the binding of Very Late Antigen-4 $\alpha_4\beta_1$ (VLA-4 $\alpha_4\beta_1$) integrin, VCAM-1 and ICAM-1 (Tan *et al.*, 2000; Gerhardt & Ley 2015). Recent attention has focused on specific carbohydrate antigens (glycosaminoglycans) present on the surface of EC called glycocalyx (Kolářová *et al.*, 2014; Chacko *et al.*, 2011). TNF- α is known to induce the shredding of glycosaminoglycans (Henry & Duling 2000) thereby decreasing the glycocalyx size at the endothelium. This allows circulating adhesion molecules to undergo N-glycosylation at sites of endothelial junctions (Scott & Patel

2013) which attracts circulating monocytes to recruit and roll (Chacko *et al.*, 2011). Such a cascade at the endothelium develops to the formation of the atherosclerotic plaque.

Endothelial cell senescence

The concept of cellular senescence has previously been discussed (**section 1.2.2**). Using β -Galactosidase as a marker of cellular senescence, senescent EC are detected within human atherosclerotic plaques obtained from the carotid arteries of patients with CAD (Minamino *et al.*, 2002). Numerous In-vitro studies have shown senescent EC are dysfunctional and pro-inflammatory. Endothelial vasodilation is impaired in aged EC and the production of TXA₂, ET-1 and PGI₂ is markedly augmented (Sako *et al.*, 1993), contributing to atherogenesis. Senescent EC also show decreased expression of eNOS and NO production (Sato *et al.*, 1993, Matsushita *et al.*, 2001). Furthermore, there is an upregulation of ICAM-1, VCAM-1 and the pro-inflammatory cytokine (IL-15) (Minamino *et al.*, 2002, Matsushita *et al.*, 2001; Shelton *et al.*, 1999). As discussed previously, this contributes to the adhesion cascade; interactions between monocytes EC are enhanced in senescent EC (Maier *et al.*, 1993).

Plaque Formation

After intimal injury, cell types including EC, platelets and various inflammatory cells release growth factors (platelet-derived growth factor (PDGF) and fibroblast growth factor (FGF) and inflammatory cytokines (IL-1, IL-4, TNF- α) (Willis *et al.*, 2004). These growth factors and inflammatory cytokines act synergistically to induce the migratory and proliferative activities of VSMC. These mediators also induce matrix metalloproteinase (MMPs). MMPs remodel the basement membrane around VSMC to enable their migration (Newby 2005). The concurrent migration and proliferative properties of VSMC are regulated by additional growth promoters (ET-1, thrombin, FGF, interferon gamma (IFN- γ) and inhibitors (heparin sulfates, NO, and transforming growth factor (TGF)- β)) (Rudijanto 2007). Under physiological conditions, VSMCs within the medial layer of the vessel wall are of a 'synthetic' phenotype, where the secretion of extracellular matrix (ECM) proteins is reduced. VSMC then transits into a normal 'contractile' state where in physiological conditions they function to regulate blood pressure and flow (by contraction and dilation of the blood vessel wall). During early

atherogenesis, VSMC undergo a phenotypic shift from the normal contractile state to synthetic, consequently VSMC can migrate from the media into the intima and proliferate following injury (**Figure 1.5 C**). VSMC in a synthetic state contribute to the accumulation of fibrous tissue in advanced lesions. VSMC achieve this through the increased synthesis of collagen, elastin, proteoglycans, and elaborate growth factors and cytokines. This fibrous tissue makes up fibrous cap (**Figure 1.5 C**). The fibrous cap overlies a lipid core and necrotic tissue; this is made up of accumulated foam cells and collagen and other extracellular matrix molecules (secreted by VSMCs) (**Figure 1.5 C**). This forms a more advanced atherosclerotic plaque, which stabilises the plaque (Rudijanto 2007).

Plaque Rupture

VSMC within the vessel wall are capable of both dividing and undergoing apoptosis during their cellular lifespan. VSMC of atherosclerotic plaques show reduced proliferation, early senescence, and increased susceptibility to apoptosis (Geng & Libby 1995). In atherosclerosis, the presence of inflammatory cells, cytokines, modified cholesterol, and systemic factors such as hyperglycaemia, blood pressure and flow are all involved in regulating apoptosis (Bennett 2002). These factors substantially alter the normal balance of VSMC proliferation and apoptosis; where apoptosis predominates (Bennett *et al.*, 1995).

Survival growth factors such as PDGF and insulin-like growth factors (IGF-1) are also increased in atherosclerotic plaques (Poston *et al.*, 1996). Such mitogenic signals are normally protective against apoptosis and promote cell proliferation but are evaded in atherogenic VSMC. VSMC in advanced atherosclerotic plaques possess a senescence associated apoptotic phenotype, where even in the presence of mitogenic signal, they are unable to proliferate, show increased markers of cellular senescence, and upon re-entering the cell cycle are forced to undergo apoptosis (Bennett *et al.*, 1998; Minamino *et al.*, 2003). The apoptosis pathway in VSMC is induced primarily through interplay between the different atherogenic cell types. Human VSMC express a death receptor known as the Fas receptor whilst inflammatory cells (EC, macrophages and T-lymphocytes) secrete the Fas ligand. Fas-mediated apoptosis in VSMC has been

observed in plaque VSMC *in vitro* (Boyle *et al.*, 2001). Atherogenic factors which drive this process include ox-LDL, CRP, cytokines IL-1 β , interferon (IFN)- γ , and TNF- α (Bazzoni & Dejana 2004; Chau 2001). During the process of plaque rupture, infiltration of inflammatory cells in the fibrous cap, results in the loss of plaque stability (**Figure 1.5 D**). Loss of plaque stability and thinning of the fibrous cap is achieved through VSMC apoptosis. Apoptotic VSMC are observed in advanced atherosclerotic plaques which suggests VSMC apoptosis promotes plaque rupture leading to thrombosis (Newby *et al.*, 1999).

Senescence of VSMC within the fibrous cap may also contribute significantly to inefficient plaque repair and loss of plaque stability. Furthermore, senescence cells upregulate genes (adhesion molecules (*ICAM-1*), a regulator of homeostasis (*plasminogen activator inhibitor 1*) and MMPs (collagenases) which all directly induce plaque instability (Gorenne *et al.*, 2006). The lateral edges of the fibrous plaque (where underlying VSMC are present) also contain inflammatory cells (activated macrophages and T cells, natural killer T cells and dendritic cells) which further modulates the EC proinflammatory phenotype (Hansson 2005). Proteolytic modifications of the extracellular matrix, contributes to plaque instability which is prone to rupture (**Figure 1.5 D**) (Hansson & Libby 2006; Gimbrone & García-Cardeña 2016). During plaque rupture highly thrombogenic contents are released from the necrotic core triggering an atherothrombotic occlusion (Fuster *et al.*, 2005; Libby 2013).

Endothelial cell apoptosis

EC apoptosis occurs in lesion prone regions and accounts for the EC turnover suggesting a mechanistic link between the atherosclerotic plaque development and rupture (**Figure 1.5 D**). EC apoptosis has been shown to be directly involved in the formation of coronary thrombotic atherosclerotic plaques (Xu *et al.*, 2009). EC apoptosis may be due to the infiltration of inflammatory cells (T cells, mast cells and some B cells) and the subsequent secretion of pro-apoptotic cytokines from these cells (Chi & Melendez 2007). Additional pro-apoptotic mediators also include glucose, angiotensin II, liposaccharide and ROS (Dimmeler *et al.*, 1998). One mechanistic study showed the binding of oxLDL to the LOX-1 receptor, caused EC apoptosis via the suppression of anti-apoptotic proteins, Bcl-2 (B-

cell lymphoma-2) and c-IAP-1 (Baculoviral IAP repeat-containing protein 2) (Chen *et al.*, 2004). The fibrous cap is covered by a monolayer of EC, which sequesters peripheral blood from the sub-endothelial lesion prior to plaque rupture (**Figure 1.5 D**) (Chi 2007). Clinically, superficial intimal erosions are present without evidence of plaque rupture and is a due to EC apoptosis coupled with endothelial denudation and triggering of thrombus formation (Quillard *et al.*, 2016, Gimbrone & García-Cardeña 2016).

CAD Risk Factors

Risk factors of CAD such as hyperlipidaemia, hypertension, diabetes, and smoking promotes atherogenesis (particularly ED) by primarily causing oxidative stress and inflammation (Soldatos *et al.*, 2005; Böger *et al.*, 2003; Burke & FitzGerald 2003). In hypercholesterolemia, elevated concentrations of total and LDL cholesterol are associated with ED, driven by oxidative stress. Cigarette smoking profoundly impairs endothelial function; high levels of free radicals are present in cigarette smoke which facilitates the release of ROS in activated inflammatory cells (Burke & FitzGerald 2003). Whereas, smoking cessation was found to reverse the impairment of endothelium-dependent dilation (Celermajer *et al.*, 1993). ED is prominent in hypertension due to the vasoconstrictive change in the vascular tone. Patients with hypertension show decreased NO bioavailability and increased synthesis of ROS and potent vasoconstrictors (Burke & FitzGerald 2003).

Diabetes is CAD risk factor clinically associated with impaired endothelial function and contributes to the atherogenic process. In diabetes mellitus, hyperglycaemia leads to the increased formation of advanced glycation end-products (AGEs). AGEs accumulates in the vessel wall and quench NO, causing NO inactivation (Soldatos *et al.*, 2005). Furthermore, AGEs have been shown to enhance *VCAM-1* and *ICAM-1* gene expression and induce macrophage infiltration, in an *in-vivo* rabbit model (Vlassara *et al.*, 1995). In hyperglycaemia, glycated proteins and growth factors have also been shown stimulate the proliferation of smooth muscle cells. Diabetes is also associated with elevations in LDL cholesterol and reductions in HDL cholesterol (Johnstone *et al.*, 1993). This evidence is highly suggestive that diabetes contributes to atherogenic process through independent several mechanisms.

1.5 The Causality Telomere Hypothesis

The Telomere Hypothesis has been suggested by Samani & Van der Harst (2008) which links how shorter telomere length may be causally implicated to CAD. The Hayflick Limit states, once telomeres reach a critically short length cells undergo replicative senescence. Therefore, cells with shorter TL may become senescent faster.

The effects of atherosclerosis are superimposed on normal vascular ageing of both endothelial cells and smooth muscle cells; where cellular senescence is an important and early feature of the atherosclerotic plaques (Minamino *et al.*, 2002, Matthews *et al.*, 2006). Senescence associated β -galactosidase (SA β -gal) activity correlates with cellular ageing and is a biomarker for cellular senescence (Dimri *et al.*, 1995). SA β -gal-positive VSMCs are detected in the intima of advanced atherosclerotic lesions (Minamino *et al.*, 2003). Another study showed in addition to SA β -Gal, cyclin-dependent kinase inhibitors p16 and p21 (additional markers of senescence) are detected in VSMC of the fibrous plaque (at a later stage of the atherosclerotic process) (**Figure 1.5 C**) (Matthews *et al.*, 2006). In VSMC, telomere shortening is closely associated with increasing severity of atherosclerosis. *In-vitro* plaque VSMC exhibited markedly shorter telomeres compared with normal medial VSMC, where telomerase expression alone rescued plaque VSMC senescence and normalised p16/p21 levels (Matthews *et al.*, 2006).

Shorter TL measured in leucocytes derived from both circulating blood and within the vascular wall is associated with increased atherosclerosis (Brouillette *et al.*, 2003; Brouillette *et al.*, 2008; Brouillette *et al.*, 2007; Willeit *et al.*, 2010). Furthermore, telomeres of EC from the coronary vessel are shorter in patients with atherosclerosis compared with healthy age-matched controls; suggesting telomere shortening of EC may play a role in atherogenesis (Ogami *et al.*, 2004). SA β -gal-positive EC are observed on the luminal surface of atheromas in coronary arteries from patients with ischaemic heart disease (Minamino *et al.*, 2002). Studies show that normal aged EC are dysfunctional and pro-inflammatory; senescent EC show reduced *NO*, increased *ET-1*, increased activation of *NF- κ B* and predisposition to apoptosis (Khaidakov *et al.*, 2011,

Sato *et al.*, 1993; Donato *et al.*, 2009). Furthermore, there is an enhanced uptake of acetylated LDL in normal aged EC (Hashimoto *et al.*, 1991).

It is currently unclear as to how shorter telomeres may contribute to the atherosclerotic process. In one study, a dominant negative TRF2 (lacking the TRF2 binding domain) was introduced in EC to induce telomere dysfunction (Minamino *et al.*, 2002). Catastrophic telomere loss increased the number of SA β -gal-positive EC and altered levels of endothelial dysfunction markers (increased *ICAM-1* expression, decreased *eNOS* activity). Conversely, introducing *TERT* significantly extended the lifespan of the cells, reversed the changes in *ICAM-1* and *eNOS* and inhibited the functional alterations associated with senescence (Minamino *et al.*, 2002). This is a key finding and is the first line of evidence for the direct link between telomere shortening and ED, where the changes in expression levels of *ICAM-1* and *eNOS* are implicated in atherogenesis (Lusis 2000, Pober & Sessa 2007; Davignon 2004). Therefore, one hypothesis is that shorter TL may induce ED and inflammation to drive early atherogenesis. As severe dysfunction, via removal of TRF2 function (Minamino *et al.*, 2002) will not reflect the subtle changes in telomere length associated with CAD risk it is necessary in the current context to establish a model system in which one could manipulate telomere length to examine the ED effects of more subtle changes in telomere length.

1.6. *In-vitro* model systems to generate primary cells lines with different telomere lengths

1.6.1 Historical studies to generate lines of different telomere lengths

Historically, to generate cell lines with different telomere lengths, cells would be grown over time in culture and experiments performed on sub-cultures at different time points (Harley & Greider 1990; Chang *et al.*, 1995). Cells from an early time point in culture would have longer telomeres than those at later time points due to the natural decline in telomere length. However, with this approach culturing of the cells for different lengths of time induces potential stress conditions to different sub cultures therefore it would not be possible to distinguish whether any difference in cellular behaviour is due

to the different telomere length or whether it simply reflects different culture conditions. Another method would be to test human primary cells from donors with short telomeres versus cells from donors with long telomeres (Allsopp *et al.*, 1992). A limitation with this approach is the diverse genetic backgrounds between donors, therefore it is difficult to distinguish whether any effects are due to telomere length differences or differences in donors, particularly with small sample sizes.

The telomere lengths between different chromosome ends within an individual cell *per se* are highly variable (Barbieri *et al.*, 2009). This is problematic when working with primary human cells *in-vitro* due to the diverse proliferative lifespan of these cells. Another implication is clonal succession, which occurs in human primary cell cultures (Martin *et al.*, 1974). In clonal succession, an individual clone dominates the cell population but is then attenuated and replaced in turn by a different clone as the cells are passaged. Clonal succession would be a problem specifically with regards to telomere length, during passaging of the cells, one clone may have a different TL to another that replaces it. This is an issue for the older models where cells were grown in culture for different lengths of time (Harley & Greider 1990; Chang *et al.*, 1995).

1.6.2 Established models to generate isogenic lines of short and long TL

The aim of this project is to utilise a more elegant approach to eradicate the confounding factors that have been discussed. Isogenic (from the same genotype) endothelial cell lines of varying TL will be generated and cells will be subjected to the same length of time in culture. This established model has been applied in a number of studies to immortalise myoblast clonal cell lines isolated from patients with Facioscapulohumeral muscular dystrophy with the aim to investigate an occurrence known as Telomere Position Effect (Stadler *et al.*, 2011; 2013; Robin *et al.*, 2014). Using this strategy, the telomere lengths in clonal cell lines can be controlled. It is necessary to first immortalise the cells using a removable TERT cDNA flanked by LoxP sites (Stadler *et al.*, 2011; 2013). Telomerase is recruited to the shortest telomeres, consequently short TL are preferentially elongated over longer TL which ensures a uniform TL distribution within the cell (Fakhoury *et al.*, 2010). To address the issue of clonal succession within the resulting mixed TERT+ population, this model is particularly advantageous as it is thought to homogenise the TL between different chromosome ends (Londono-Vallejo

et al., 2001; Arnoult *et al.*, 2010), therefore minimising the effects of TL variation on different chromosomes (Bodnar *et al.*, 1998). *TERT* can then be excised at an earlier and later time points using Cre Recombinase. Isogenic lines are then grown for the same length of time in culture. Telomere length shortening occurs, due to the natural decline in TL during each cell division and isogenic lines with short and long TL are generated (Robin *et al.*, 2014).

Bypass of Stress induced senescence (Telomere length Independent) during immortalisation

Using a prototypic approach it is feasible for primary cells isolated *in-vivo* to grow indefinitely *in-vitro*, a process known as immortalisation. Previous efforts to immortalise Human Umbilical Vein Endothelial cells (HUVEC) endothelial cells include the expression of viral oncogenes such as the large T antigen of SV40 (Ades *et al.*, 1992; Candel *et al.*, 1996) and E6/E7 genes of human papilloma virus (Fontijn *et al.*, 1995) which exert their inhibitory effects on p53 and Rb, respectively (Shay *et al.*, 1991; Kiyono *et al.*, 1998; Coppe *et al.*, 2008).

An important aspect to the model system to consider is, in addition to telomere dependent replicative stress, cells may also undergo cell cycle arrest via alternative (non-telomere length) pathways, such as stress induced senescence. Stress induced cellular senescence can particularly occur when primary cells are cultured for extended periods of time (Toussaint *et al.*, 2002) for example during the immortalisation process. Overexpression of the cell cycle regulator cyclin dependent kinase 4 (CDK4) will bypass the premature growth phase arrest, without affecting normal cell-cycle kinetics or the ability of cells to differentiate normally (Ramirez *et al.*, 2003; Stadler *et al.*, 2011). The tumour suppressor protein, p16^{INK4a} is a major negative regulator of CDK4 and drives premature growth arrest via the p16^{INK4a}/retinoblastoma protein (p16/Rb) pathway (Dickson *et al.*, 2000; Kiyano *et al.*, 1998). Therefore, previous studies have achieved the immortalisation of primary cells by over-expressing CDK4 in addition to telomerase (Stadler *et al.*, 2011; Zhu *et al.*, 2007). Alternatively, a CDK4 (R24C) mutant can be introduced, which is insensitive to inhibition by p16^{INK4a} (Hahn *et al.*, 2002). However, studies have shown that it is possible to successfully immortalise EC using *TERT* alone

(Yang *et al.*, 1999; Wen *et al.*, 2006; Kan *et al.*, 2012). In certain primary cell lines, p16^{INK4a} is directly repressed upon immortalisation, through CpG island methylation (Wen *et al.*, 2006; Kan *et al.*, 2012; Dickson *et al.*, 2000; Graham *et al.*, 2017), thereby permitting immortalised cells to bypass premature growth arrest. Normal EC express low levels of p16^{INK4a} (Kan *et al.*, 2012), therefore in this cell type levels of endogenous CDK4 may exceed that of p16^{INK4a} to enable cell cycle progression. Previous studies that have immortalised EC have not over-expressed CDK4, this model also did not utilise this approach, in part to avoid use of a viral CDK4 which would introduce further viral integration events in the host genome which may be more deleterious to the cell.

1.6.3 Lentiviruses

Replication life cycle of HIV-1

It is possible to achieve the immortalisation of primary cells lines by expressing human TERT using a lentiviral transfer technique; a method developed by the Trono Lab (Salmon *et al.*, 2000). Lentiviruses are capable of governing the efficient delivery, integration and long term expression of transgenes into both proliferating and non-dividing cells (Zufferey *et al.*, 1997). Lentivectors are based on the human immunodeficiency virus type 1 (HIV-1) virus and therefore consists of HIV-1 core viral proteins and viral genome (Salmon & Trono 2007).

To understand lentiviral technology, it is useful to first discuss the replication life cycle of a HIV-1 virus, as shown in **Figure 1.6**. Glycoproteins present on the viral envelope accounts for viral tropism during attachment and subsequent entry into the host cell (via membrane fusion), the matrix and capsid proteins are then disassembled releasing integrase and reverse transcriptase (RT) (Harrison 2005; Salmon & Trono 2007) (**Figure 1.6 (1, 2 & 3)**). Using viral RNA as a template, RT synthesises pro-viral DNA (Naldini *et al.*, 2016) (**Figure 1.6 (4)**); the virus takes advantage of the host genome in order to replicate and have the capacity to store their genome as RNA within the host cell. Pro-viral DNA is imported into the nucleus and integrated into the host genome with the aid of the viral integrase (Fanales-Belasio *et al.*, 2010) (**Figure 1.6 (5 & 6)**). Following pro-

viral integration, the 5' end of the viral genome is an enhancer and promoter, which allows RNA polymerase II to begin the transcription process and express a full length copy of the transgene (**Figure 1.6. (7)**) (Sakuma *et al.*, 2012).

Synthesised viral transcripts are multiply spliced into short transcripts encoding the non-structural proteins Tat, Rev and Nef, which progress through to the viral protein synthesis and assembly (Wei *et al.*, 1998) (**Figure 1.6 (8)**). mRNA transcripts synthesised include multiple spliced (encoding accessory factors Tat, Rev and Nef), singly spliced (env, Vif, Vpu and Vpr) and un-spliced transcripts (Gag, Pol and the viral genome) (Baeyens *et al.*, 2016). The nuclear export of both singly spliced and un-spliced viral mRNA transcripts is reliant on a protein Rev binding to the Rev-responsive elements (RRE) within the viral transcripts (Malim *et al.*, 1989; Fischer *et al.*, 1995). The exported viral proteins and viral genome are then assembled to generate a viral particle which is released from the host cell via budding. The Gag and Gag-Pol viral components dimerize to activate a viral protease (PR), cleavage of this PR leads to the maturation of an infectious particle (Sundquist *et al.*, 2012; Shehu-Xhilaga *et al.*, 2001) (**Figure 1.6. (9 & 10)**).

Proviral Integration

Lentiviruses have a particular selection criteria for integration; they have a unique ability to translocate across the nuclear pore where they access chromosomes by active transport (Yamashita *et al.*, 2004). This permits lentiviral integration into non-dividing cells. The long terminal repeat (LTR) sequence within the transgene lentivector is a non-coding region and facilitates the reverse transcription process (**Figure 1.7 A**). Such a feature allows for the full control of transgene expression to the exogenous promoter inserted in the lentivector (Miyoshi *et al.*, 1998). The LTR is recognised by integrase, which helps mediate integration of the virus genome into the host chromosome (Zufferey *et al.*, 1997; Salmon *et al.*, 2000). Lentiviruses integration is site specific, and integration takes place in gene-dense regions throughout the transcription units rather than promoter regions or transcription start sites (Ciuffi *et al.*, 2016). Lentiviral integration site analysis has shown to correlate to high GC content, high Alu elements, low LINE elements, light Giemsa bands (less condensed chromatin), epigenetic marks of

active transcription (H3K4me, H3K4me2, H3K9me, H3K27me, H3K36me), DNase I hypersensitive sites and acetylated histones (Ciuffi *et al.*, 2008; 2016). Due to insertional mutagenesis (viral genome insertion into the host DNA), it is possible to disrupt the host genome integrity upon integration. As reviewed by Ciuffi *et al.*, (2016), insertional mutagenesis can occur impacting the cell in a number of ways. Lentiviral integration within intergenic regions has little effect on host cell gene expression (Ciuffi *et al.*, 2016). However, integration in enhancers/ promoter regions results in changes in pro-viral gene expression (if enhancers are within the heterchromatin region, expression is reduced). Pro-viral integration within a transcription unit (in either an antisense or same orientation) also disrupts cellular gene expression. The potential impact on the cellular gene is dependent on the i) the function of the gene close to the integration event (e.g. whether the gene is pro-apoptotic or involved in cell proliferation), (ii) the way in which the gene is modified (dominant negative splice variant, gene truncation) and (iii) the impact on gene expression (i.e. over-expression or knock-down) (Knight *et al.*, 2013; Ciuffi *et al.*, 2016).

2nd Generation Lentiviral System

As the lentiviral method developed by the Trono group is established, the same method will be utilised in this work to generate immortalised HUVEC cell lines, therefore the context covered from this section onwards will focus on the 2nd generation lentiviral system. The 2nd generation lentivirus system utilises an envelope vector (pMD2.G), a packaging vector (pCMVR8.74), and an excisable transfer vector (pLOX-TERT-iresTK), (Salmon *et al.*, 2000).

The envelope vector encodes glycoprotein G of the Vesicular Stomatitis Virus (VSV-G) which is used to pseudotype (ψ) the HIV-1 envelope protein ((Salmon, Trono 2007). Compared to the HIV-1 envelope protein, the VSV-G protein on the surface of the virus will govern its specificity to a broader host cell range (Burns *et al.*, 1993). The packaging vector encodes the HIV-1 core proteins Gag, Pol, Tat and Rev that are important for packing the viral genome (Zufferey *et al.*, 1997). For safety reasons, the accessory proteins, (Vpr, Vif, Vpu, and Nef) involved in viral propagation are excluded.

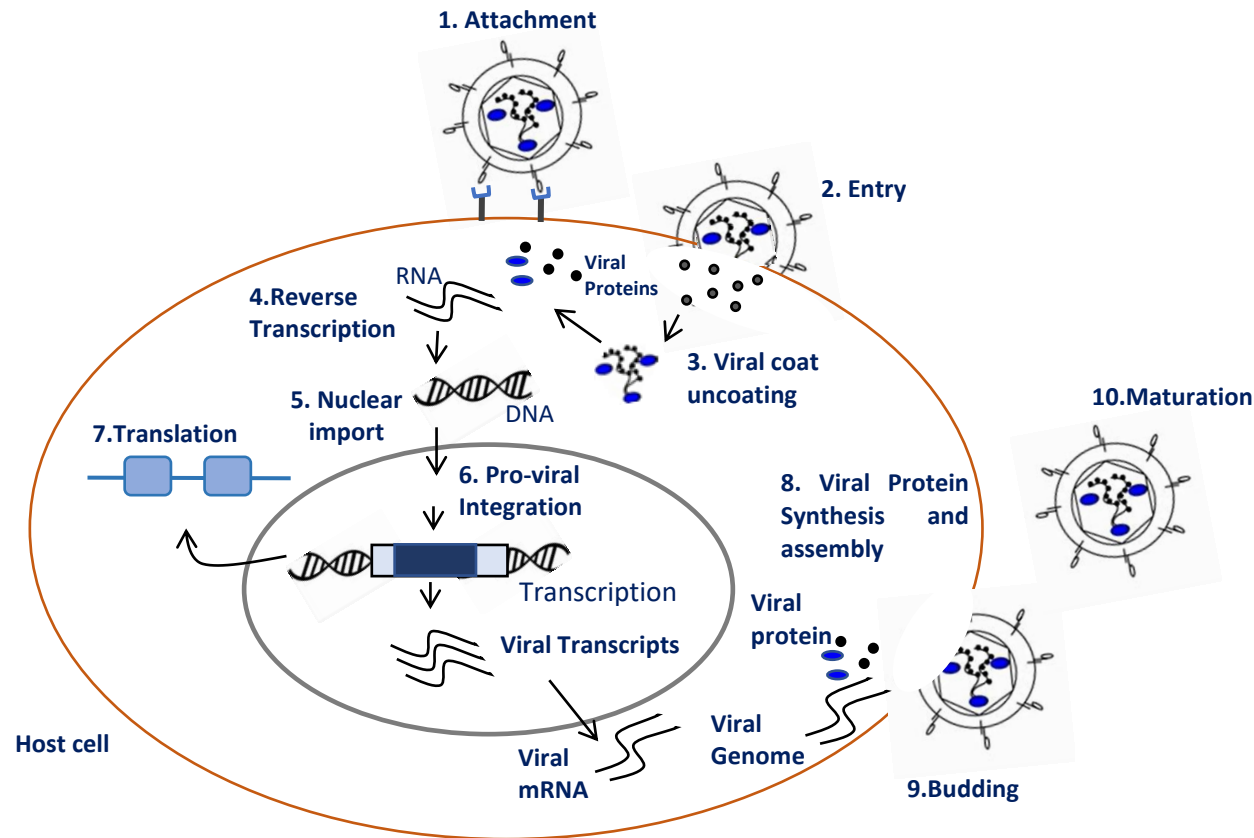


Figure 1.6 Schematic overview of a HIV-1 replication and life cycle. 1, 2 & 3. The virus attaches to the cell membrane via a viral glycoprotein binding to a receptor, permitting entry into the host cell. The viral capsid proteins, reverse transcriptase and integrase are uncoated. 4, 5 & 6. Using viral RNA as a template, RT synthesises pro-viral DNA which is exported in the nucleus followed by pro-viral integration into the host genome. 7. A copy of the transgene DNA is translated. The following are part of the HIV-1 life cycle; viral mRNA transcripts are processed according to the cellular machinery and are exported from the nucleus. 8. Viral proteins are synthesised and assembled and are exported out of the cell through a budding (9). 10. Viral particles undergo maturation upon the dimerization of Gal-Pol which gives rise to an infectious particle. (Salmon & Trono 2007; Sakuma *et al.*, 2012; Baeyens *et al.*, 2016; Sundquist *et al.*, 2012).

A lentiviral transfer vector, pLOX-TERT-iresTK, is derived from the human immunodeficiency virus (HIV-1) (Salmon *et al.*, 2000; Stadler *et al.*, 2011). The lentiviral vectors have been modified amid the safety concerns, as such they are capable of infecting only one cell. In a HIV genome, a single RNA molecule that contains the critical *cis*-acting elements carries all the coding sequence (Salmon & Trono 2007) (**Figure 1.7. A**). The lentiviral system segregates the sequences encoding the critical components through the use of multiple vectors to generate the virus. The use of multiple vectors maximises the number of complex recombination events that would be required to regenerate a fully replicative competent virus (Salmon & Trono 2007; Salmon 2013). This ensures the lentiviral vectors will only produce replicative defective viruses. The pLOX-TERT-iresTK transfer vector serves as a proxy for the virus encoding the *TERT* gene under a human cytomegalovirus (CMV) internal promoter (Salmon *et al.*, 2000). The CMV promoter is placed in the vector upstream of a bicistronic coding cassette encoding the *TERT* transgene and the Herpes simplex virus type 1 thymidine kinase (HSV TK) gene (**Figure 1.7. A**). The *TERT* and TK transgenes are linked by a DNA sequence encoding the internal ribosome entry site of encephalomyocarditis virus (IRES) (Salmon *et al.*, 2000). The IRES element acts as another ribosome recruitment site to allow the initiation of translation (independent of the 5' cap), this ensures the co-expression of the two proteins from a single mRNA.

1.6.4 Cre-Lox system

Previous studies have achieved the reversible immortalisation of primary cells through externally controllable gene expression systems for e.g. the use of a tet repressor, or inserting a dexamethasone-responsive mouse mammary tumor virus (MMTV) promoter, or a conditionally active growth promoting factor, such as the temperature-sensitive mutant of SV40 large T antigen (Efrat *et al.*, 1995; Gossen *et al.*, 1992; Lee *et al.*, 1981; Chou *et al.*, 1978). A further system relies on the specific introduction of transgenes in a configuration that permits their subsequent excision by DNA recombinases, such as that possessed by the lentivector pLOX-TERT-iresTK (**Figure 1.8 B**). This technique utilises the Cre-Lox system and involves the use of a CMV promoter regulated Cre recombinase a method developed by Stadler and colleagues (2000). The two components; Cre Recombinase and a 58bp Lox-P recognition site are

derived from the P1 bacteriophage (Salmon *et al.*, 2000) (**Figure 1.8 B**). The orientation and location of the LoxP is site specific and is inserted in the 3' LTR of the pLOX-TERT-iresTK transfer vector. This is important to prevent downstream LoxP-mediated effects and to ensure the complete excision of DNA. The U3 region of the 3'LTR of the integrated proviral *TERT* is duplicated during reverse transcription (**Figure 1.8 B**). The LoxP sites flanked on either side of the integrated proviral *TERT* allows for site specific deletion of the internal gene expression cassette by Cre recombinase, leaving behind an inert solitary LTR sequence devoid of any transcriptional activity (Salmon *et al.*, 2000). This ensures the site is not incorrectly recognised as a cryptic LoxP site, which has been shown to serve as non-specific recognition sites for the Cre recombinase (Thyagarajan *et al.*, 2000; Semprini *et al.*, 2007).

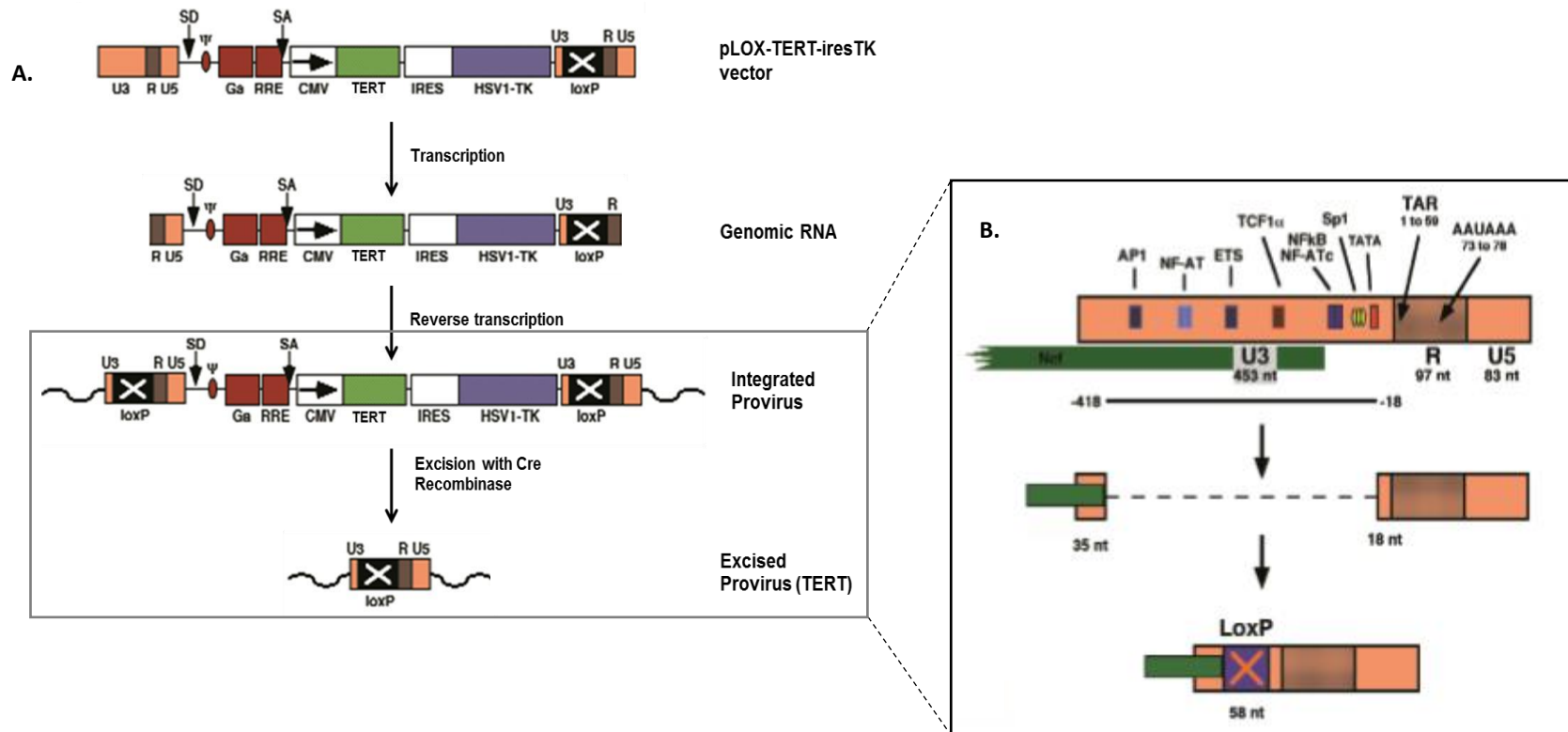


Figure 1.7 Schematic diagram of the Lox-TERT lentivirus and the Lox 3'LTR region of the integrated TERT provirus. A. The Lox-TERT vector life cycle from the point of introducing the vector into HUVEC. The critical aspect to the Cre-Lox system is the two LoxP sites flanked on either side of the expression cassette of the integrated provirus. B. The U3, R and U5 regions and sizes of the LTR sites are indicated along with the major transcriptional elements. Upon the addition of Cre the -418 to -18 segment of the LTR is removed leaving a 53 nt LoxP sequence upstream of R. The LoxP sequence (58 nt) is inserted within the SIN deletion and is transcriptionally inert. Adapted from Salmon *et al.*, 2000.

The use of a viral Cre does however raise possible issues with integration events within the host cell. As discussed previously (**section 1.6.1**), due to clonal succession, it is questionable whether the TERT+ population will remain heterogenous or will have unintentionally become clonal during the prolonged culturing period. One of the disadvantages of introducing a gene via the lentiviral gene transfer system is a single integration could lead to changes in expression another gene (Cuiffi *et al.*, 2016), which could then be responsible for any phenotype observed other than TL. If the lines are clonal, the pro-viral Cre has narrowed to a single integration then there may be a one or two insertion points of Cre incorporated within the host genome which may be detrimental to the cell. A mixed cell population is therefore preferred, however as discussed in **section 1.6.1**. heterogenous cells with different telomere lengths will still be present as the model would not prevent this.

Previous studies have observed an incomplete excision of floxed genes following the addition of Cre, resulting in a subsequent lack of phenotype in target cell types (Kimura *et al.*, 2003; Lei *et al.*, 2010). As this project involves working with a heterogenous cell population, it is possible for the small percentage of non-excised cells to have a significant growth advantage. As it is critical to achieve the complete removal of *TERT*, this experimental model system utilises a conditional built in ablation system. The HSV-1 Thymidine kinase transgene component of the pLOX-TERT-iresTK lentivector used to immortalise HUVEC is transcriptionally linked only with *TERT* via an IRES sequence (**Figure 1.7 A.**). Cells producing HSV1-TK (**Figure 1.7 A.**) are sensitive to nucleoside analogs such as Acycloguanosine (ACG) which are converted by the viral enzyme into nucleotides that are toxic upon incorporation into DNA (Salmon *et al.*, 2000). Therefore, ACG anti-viral therapy is required to eradicate any non-excised TERT+ cells (after the addition of Cre) and taking this model forward reduces the chances of any potential bystander effect of TK-negative neighbouring cells (Bendetti *et al.*, 2017).

1.7. Aims of the Project

The principle aim of the project is to investigate the biological mechanism by which shorter TL could increase the risk of CAD. This will be exploited by studying the effect of telomere length dynamics on the atherogenic potential of endothelial cells.

This will be achieved by:

- Generating experimental isogenic lines (with short and long telomeres) using primary endothelial cell lines.
- Challenging the established isogenic cell lines with proatherogenic stimuli to assess atherogenic phenotypes.

Human Umbilical Vein Endothelial cells (HUVEC) will be used to generate the experimental isogenic lines of long and short telomere lengths. Endothelial cells are a cardiovascular relevant cell-type. HUVEC undergo endothelial cell dysfunction in response to pro-atherogenic stimuli and therefore are suitable for in-vitro models of atherogenesis. The first part of this thesis aims to establish an experimental model to i) generate Lox-TERT immortalised HUVEC and ii) isolate isogenic lines of short and long TL. To assess immortalisation using *TERT*, lines will be first analysed for *TERT* expression and telomerase activity and the cells will be maintained in culture until the HUVEC have exceeded 100PDs. Cellular transformation has been associated with culturing primary cells for a prolonged period, therefore the immortalised lines will be checked for their endothelial cell phenotype by expression of established endothelial cell surface markers CD144 (VE-Cadherin), CD31 (PE-CAM-1) and cell surface antigen CD109 (VEGFR-2). Isogenic EC lines will be generated upon the addition of a self-excising viral Cre.

The second part of this thesis involves the creation of isogenic EC lines with short and long telomere lengths to investigate whether such differences in telomere length are attributed to changes in endothelial cell function in response to the proatherogenic stimuli, Tumour Necrosis Factor (TNF- α). TNF- α is a pro-inflammatory cytokine naturally secreted by endothelial cells, smooth muscle cells, neutrophils and activated lymphocytes and therefore is locally sourced at the endothelium to activate endothelial

cells. Endothelial cell activation triggers the plethora of molecular mechanisms associated with endothelial dysfunction, the initial stage of atherogenesis. This work investigates whether isogenic lines of short and long telomere length are attributed to changes in endothelial cell function in response to TNF- α , by assessing the gene expression of specific endothelial dysfunctional markers *eNOS*, *ICAM-1* and *E-SELECTIN* and further exploring the functional effect this may have on later stages of atherogenesis such as endothelial cell-monocyte adhesion binding.

CHAPTER 2

Materials & Methods

Materials & Methods

2.1 Materials

2.1.1 Bacterial culture

Ampicillin antibiotic	ThermoFisher Scientific, UK
BD™ Difco™ Agar	Thermo Fisher Scientific, UK
<i>E.coli</i> DH5α competent cells	Invitrogen Life Technologies, UK
Kanamycin antibiotic	ThermoFisher Scientific, UK
Luria Broth	Sigma Aldrich, UK
SOC media (<i>Tryptone 2% (w/v), Yeast extract 0.5% (w/v), 10mM NaCl, 2.5mM KCl, 10mM MgCl₂ and 20mM Glucose</i>)	Sigma Aldrich, UK

2.1.2 Nucleic acid extraction from human cells

DNeasy® Blood and Tissue DNA extraction kit	QIAGEN, UK
Proteinase K	Sigma Aldrich, UK
RNase A (7000 units/ml)	QIAGEN, UK
RNeasy® RNA extraction kit	QIAGEN, UK

2.1.3 PCR and RT-qPCR reagents

MyTaq™ HS DNA Polymerase kit	Bioline, MA
SensiFAST™ cDNA Synthesis Kit	Bioline, MA
SensiMix™ SYBR® No-ROX Kit	Bioline, MA
Lenti-X™ Integration Site Analysis	Clontech, USA
Nucleospin® Gel and PCR Clean-up	Macherey-Nagel, Germany

2.1.4 Gel electrophoresis

Agarose	Sigma Aldrich, UK
5X DNA Loading buffer	Bioline, MA
PAGE GelRed™	BIOTIUM Inc
GeneRuler Ultra Low Range DNA Ladder (0.1 µg/µL)	ThermoFisher Scientific, UK
Hyperladder™ 100bp	Bioline, MA
Hyperladder™ 1kb	Bioline, MA
Novex™ TBE High Density Sample Buffer 5x (0.1% bromophenol blue, 0.1% xylene cyanol)	ThermoFisher Scientific, UK
Novex™ 10% TBE non-denaturing polyacrylamide precast gel (without urea), 15-well	ThermoFisher Scientific, UK
Novex™ TBE Running Buffer	ThermoFisher Scientific, UK
TAE Buffer	Sigma Aldrich, UK

2.1.5 Plasmid preparation and cloning

Cutsmart® Buffer	New England Biolabs, MA
GenElute™ PCR Clean-Up Kit	Sigma Aldrich, UK
Glycerol	Sigma Aldrich, UK
PureYield™ Plasmid Midiprep System (Endotoxin Free)	Promega, USA
pGEM®-T Easy Vector System	Promega, USA
Restriction enzymes	New England Biolabs, MA

Plasmids

Plasmid DNA Vector	Bacterial Growth strain (<i>E.coli</i>)	Supplier	Catalogue number
pLOX-TERT-iresTK	Stbl3	Addgene, MA	12245
pLOX-GFP-iresTK	Stbl3	Addgene, MA	12243
pLOX-CW-CRE	Stbl3	Addgene, MA	12238
pMD2.G	NEB Stable	Addgene, MA	12259
pCMVR8.74	DH5- α	Addgene, MA	22036
pOG231	DH5- α	Addgene, MA	17736
pCre-pac	DH5- α	Professor Catrin Prichard (Cancer Research Centre, UoL, UK)	-

Table 2.1 Plasmid DNA vector name, bacterial growth strain, supplier/source and catalogue number

2.1.6 Cell Culture

Cell lines

HCT116 (Colorectal carcinoma cell line)	Horizon Discovery, UK
HEK293T (Human Embryonic Kidney 293T)	Horizon Discovery, UK
HUVEC (Human umbilical vein endothelial cells)	Promocell GmbH, Germany
THP-1 (Human monocytic leukaemia)	Gift from Dr Tom Webb Cardiovascular Sciences, UoL, UK

Culture media, additives and related

Acycloguanosine	Sigma Aldrich, UK
CryoSFM	Promocell GmbH, Germany
DetachKit	Promocell GmbH, Germany
DMEM (Dulbecco's modified Eagle's medium)	Sigma Aldrich, UK
DMEM/F12 (Dulbecco's Modified Eagle Medium: Nutrient Mixture F-12)	Thermo Fisher Scientific, UK

DMSO	Sigma Aldrich, UK
Endothelial cell growth media	Promocell GmbH, Germany
Human Recombinant TNF- α (50 μ g/ml)	PeptoTech, UK
Non heat activated Fetal Bovine Serum (FBS)	Gibco, Life Technologies, UK
Phosphate Buffered Saline (PBS) (10g NaCl, 0.25g KCl, 1.43g Na ₂ HPO ₄ , 0.25g KH ₂ PO ₄)	Sigma Aldrich, UK
Penicillin/Streptomycin 1% (10,000U/ml stock solution)	Hyclone (GE Healthcare Life Sciences, UK)
RPMI	Thermo Fisher Scientific, UK
Senescence cells Histochemical Staining Kit	Sigma Aldrich, UK
Trypan Blue 0.4% (w/v)	ThermoFisher Scientific, UK
Trypsin-EDTA 10x (5g/l trypsin and 2g/l EDTA)	Lonza, Switzerland

Transfection

Lipofectamine [®] 2000	ThermoFisher Scientific, UK
Opti-MEM [®] Reduced Serum Medium	Fisher Scientific, UK

2.1.7 Production of Lentivirus

PEG-it [™] Virus Precipitation Solution	System Biosciences, Cambridge UK
Transdux [™] Virus Infection Reagent 1x	Cambridge Biosciences, UK
0.45 μ m Stericup [®] PVDF disk filter	Merck, Hertfordshire UK

2.1.8 Protein detection by flow-cytometry

CD309 (VEGFR-2) human Antibody	Miltenyi Biotec, Germany
CD31 (PECAM-1) human Antibody	Miltenyi Biotec, Germany
CD144 (VE-Cadherin) human Antibody	Miltenyi Biotec, Germany
CD54 (ICAM-1)-APC, human Antibody	Miltenyi Biotec, Germany
REA Control- APC human Antibody	Miltenyi Biotec, Germany

REA Control- FITC human Antibody

Miltenyi Biotec, Germany

2.1.9 TRAP assay for telomerase activity

Bradford Reagent

Sigma Aldrich, UK

TRAPeze® Telomerase Detection kit

Merck, Hertfordshire UK

2.2.0 Equipment

Nanodrop 8000 Spectrophotometer

ThermoFisher Scientific, UK

QIAgilty liquid handling system

Qiagen, UK

GelDoc Illuminator

Invitrogen

Life Technologies, UK

GStorm Multi-Block Thermal Cycler

Gene Technologies Ltd. UK

RotorGene™ 6000 Q Thermal Cycler

Qiagen, UK

XCell SureLock® Mini-Cell system

ThermoFisher Scientific, UK

UV transilluminator

Syngene, India

2.2.1 Software

Ensembl database

Cambridgeshire, UK

GraphPad Prism 8.1.1

GraphPad software Inc. CA,
USA

ImageJ (version 1.51p)

National Institute of Health,
USA

NetPrimer

PREMIER Biosoft, USA

Primer3 (version 4.1.0)

Whitehead Institute for
Biomedical Research, USA

Rotorgene analysis software

Qiagen, UK

2.2 Methods

2.2.1 Cell Culture

Generation of the Lox-TERT experimental lines involves the use of both primary human cells and cell lines. A brief summary of each of the lines along with its uses are shown in **Table 2.2**. Key information on each of the lines including the cell name and type, the media composition and the seeding densities required for general maintenance of the lines is also shown (**Table 2.2**). Cells were cultured in the media specified unless otherwise stated. Supplemented media was stored at 4°C for up to one month. Cell culture work was performed under sterile conditions. HEK293T, HCT116 and THP-1 cells were cultured at 37°C with 20% O₂/5% CO₂. HUVEC were cultured at 37°C with 5% O₂/5% CO₂.

A total of 9 HUVEC single donors (newborn/Caucasian) were used (**Table 2.2**), HUVEC were isolated from the umbilical vein of the umbilical cord tissue (by Promocell). All donors showed acceptable viability and growth characteristics. The HUVEC were phenotypically characterised (using immunohistochemistry) positive for CD31, vWF/Factor VIII-related antigen, Dil-Ac-LDL and negative for smooth muscle α -actin. Upon receipt of the cells from Promocell, thawing and seeding of the cells was deemed passage 1.

Cell Recovery from Liquid Nitrogen storage

Working stocks of all cell lines at earlier passages were stored in liquid nitrogen until required. Upon recovery, vials were removed immediately and thawed rapidly at 37°C. Cells were added to 12ml of pre-warmed media (in a T80 culture flask). After 24 hours the media was replaced with fresh media to remove any dimethyl sulfoxide (from the cryopreservation solution) and any remnants of cell debris (as a result of inevitable cell death during recovery).

Cell washing and detachment

HUVEC, HEK293T and HCT116 cells

The appropriate cell media and solutions used for passaging the HUVEC, HEK293T and HCT116 cells are shown in **Table 2.2**. Prior to use, media, PBS, trypsin/EDTA and detachment kit (for HUVEC) was prewarmed to 37°C. All cell lines were passaged at 60-70% confluency. To passage the HEK293T and HCT116 cells the media was aspirated, cells were washed with 3ml of PBS and incubated with 2ml of trypsin for 5mins. HUVEC were first washed in 2ml of HEPES followed by 2ml of trypsin. Cells were observed under the microscope for complete cell detachment. Any remaining cells were loosened by gently tapping the side of the flask. For the HEK293T and HCT116 cells complete DMEM was used to neutralise the trypsin. For HUVEC, 2ml of Trypsin Neutralizing Solution was added to the flask. Cells were collected and then centrifuged at 300 x g for 5minutes. The cell pellet was then diluted in the appropriate of media prior to counting.

THP-1 cells

THP-1 cell suspension was collected in a falcon tube and centrifuged for 100 x g for 5 minutes. The supernatant was carefully discarded and the pellet was resuspended in 5ml of media as shown in **Table 2.2**.

Cell counting using Trypan Blue

To count the cells, 10µl of the cell suspension was mixed with an equal volume of 0.4% (w/v) Trypan Blue dye solution. The number of viable cells present on the four outer squares (1mm²) of a haemocytometer slide were counted under a light microscope.

An average viable cell count was calculated using the equation below:

$$\text{Cell count per ml} = \text{Average number of viable cells} \times 10^4 * \times 2 **$$

*the volume of one square in the haemocytometer is 10⁻⁴ ml, therefore the factor of 10⁴ converts this to 1 ml volume of the cell suspension.

**takes into account the 1:1 dilution factor of the cell suspension to Trypan Blue.

Cell Seeding

For the general passaging, the cells were seeded according to the densities outlined in **Table 2.2**. The calculated volume of cell suspension was added to 11ml of pre-equilibrated media. For THP-1 cells the required volume of cell suspension was added to 20ml of media.

Population Doublings

The Population Doubling (PDs) level were calculated for HUVEC cell lines grown in culture (during each passage using the following equation:

$$\text{PDs} = 3.32 (\log \text{ total cell yield} - \log \text{ seeding cell density to begin the next subculture})$$

The growth curve of the HUVEC cell line was then plotted as cumulative PDs versus time in culture (days).

Cell Cryopreservation

As the HUVEC cell lines will be continuously cultured for an extended period of time, cell stocks of various passages were cryopreserved in liquid nitrogen for use in future experiments. HEK293T and HCT116 cell stocks were also frozen down and revived at a later point according to as and when lentivirus generation was required. For all cell lines, a total number of $>1 \times 10^6$ total cells were resuspended in 1ml of the appropriate cryopreservation media as outlined in **Table 2.2**. To cryo-freeze cell stocks, homogenous cell suspensions were added to cryovials and were kept in a cryo-freezing container at -80°C for 24 hours. To allow the cells to freeze slowly by reducing the temperature at approximately 1°C per minute, the vials were kept in a cryo-freezing container at -80°C for 24 hours. Frozen cells were then transferred to liquid nitrogen for long term storage.

Transient Cell Transfections

The generation of high titre pseudoviral lentiviral particles initially involved the use of a cation lipid based transfection method of plasmid DNA in HEK293T cells. A day prior to the transfection procedure, the cells were seeded at 8×10^5 cells total per T75 flask.

HEK293T cells were transfected at ~70% confluency. 30min prior to the transfection, the media was replaced with pre-equilibrated DMEM with 10% FCS (containing no antibiotics).

Lipofectamine[®] 2000 (375µl) was diluted in 500µl of Opti-MEM[®] Reduced Serum Medium. The Lipofectamine[®] 2000/Opti-MEM[®] mixture was carefully mixed by gentle swirling. The mixture was incubated for 5 minutes at room temperature. During this incubation period, the transgene (60µg), envelope (30 µg) and packaging (60µg) DNA vectors were added to 2500µl of Opti-MEM[®] in a sterile tube. After the incubation, the Lipofectamine[®]2000/Opti-MEM[®] was gently swirled in the DNA/Opti-MEM[®] mix. The DNA-lipid complex was incubated for 30 minutes at room temperature and the mixture was added dropwise to each T75 flask (~1.16ml). To minimise cytotoxic effects to the HEK293T cells, the flasks were gently tilted to avoid direct contact of the DNA/lipid complex to the cells. The cells were incubated overnight at 37°C with 5% CO₂. The following morning, the media was carefully replaced with 10ml of pre-equilibrated complete DMEM. The cells were incubated at 37°C with 5% CO₂ for ~16hours.

Cell Pellets

During passaging of the lines, cell pellets were collected and subsequently kept on dry ice for 5mins and were then transferred for storage at -80°C until use for DNA/RNA/protein extraction.

Cell type	Name	Experimental Use	Growth Media	Final Supplement concentration	Seeding Densities	Detachment Method	Freezing Media
Primary human cells	HUVEC (Promocell) 9 single donors (newborn/ Caucasian)	Establish an endothelial model to generate isogenic lines of short, medium and long telomere lengths	Endothelial cell growth media (Promocell)	Fetal Calf Serum 0.02ml/ml Endothelial Cell Growth Supplement 0.004ml/ml Epidermal Growth Factor (recombinant human) 1ng/ml Heparin 90µg/ml Hydrocortisone 1µg/ml (Promocell)	2.5-3.0 x 10 ⁵ cells/ml	Detachment kit (HEPES 30mM, Trypsin (0.04%)/EDTA (0.03%) Trypsin Neutralising Solution (Promocell)	Cryo-SFM (Promocell)
Cell lines	HEK293T (Horizon Discovery)	Host cell line used to generate the TERT, CRE and GFP lentivirus	DMEM (Advanced)	Fetal Calf Serum 10% (Gibco, Life Technologies) Penicillin/Streptomycin 1% (10,000U/ml stock solution) (Hyclone)	6.0 x 10 ⁵ cells ml	Trypsin(0.5%) EDTA(0.2%) (Lonza)	DMEM with 10% DMSO (Sigma)
	HCT116	Transduced HCT116 used to titrate lentivirus	DMEM/F12	Fetal Calf Serum 10% Penicillin/Streptomycin 1%	5.6 x 10 ⁵ cells ml	Trypsin (0.5%) EDTA(0.2%)	DMEM with 10% DMSO
	THP-1	Monocyte - HUVEC cell adhesion assay	RPMI	L-Glutamine 2mM, Sodium Pyruvate 1mM, β-mercaptoethanol 0.055mM Fetal Calf Serum 10% Penicillin/Streptomycin 1%	2.5 x 10 ⁵ cells/ml	n/a	n/a

Figure 2.2. Table showing information on human primary cell lines and non-primary human cells lines. Human Umbilical Vein Endothelial cells (HUVEC), Human Embryonic Kidney-293T cells (HEK293T) (expressing a mutant version of the T-antigen), human colorectal carcinoma cell line HCT116 and human monocytic THP-1 cells. Dulbecco's Modified Eagle's Medium (DMEM); advanced DMEM is with complete supplements listed. Ethylenediaminetetraacetic acid (EDTA). Cryo-serum-free-media (Cryo-SFM). Dimethyl sulfoxide (DMSO).

2.2.2 Lentivirus Generation

As the nature of this experimental work involves a 2nd generation lentiviral vector system and ultimately genetically modification of primary cells, safety approval was required from the Health and Safety Executive. All viral work was carried out according to Class II Biohazard regulations. The TERT lentivirus used to generate the isogenic clonal lines, will be created using the host producer cell line, Human Embryonic Kidney 293T (HEK293T) cells.

Co-transfection of plasmid DNA constructs in HEK293T cells

To generate the high titre pseudoviral particles, the plasmid DNA carrying the relevant transgene (pLOX-TERT-iresTK, pLOX-GFP-iresTK or pLOX-CW-CRE) along with envelope and packaging vectors (pMD2.G and pCMVR8.74) were transiently co-transfected in HEK293T cells using a lipid based transfection method. Approximately 16 hours post transfection, the medium from the HEK293T cells was removed and carefully replaced with 10ml of pre-equilibrated complete DMEM. The cells were incubated at 37°C with 5% CO₂ overnight.

Harvesting Lentiviral Particles

Media containing the lentiviral particles was carefully collected in pre-cooled 50ml conical tubes and centrifuged for 5 min at 500 × g at 4°C to remove any detached cells and cell debris. The viral supernatant was collected and stored at 4°C. The harvested media was replaced with 10ml of pre-equilibrated complete DMEM and two further consecutive ~16hours incubations and harvests were performed. In between each harvest the viral supernatants were stored at 4°C, the lentiviral supernatant can be stored at °C for 1–4 days without significant viral titre loss, therefore a total of 3 harvests was collected.

Concentrating Lentiviral Particles with PEG-it™

The lentiviral supernatants were pooled and carefully filtered through a 0.45 µm filter. The lentivirus was then concentrated using a polyethylene glycol based reagent; PEG-it™ Virus Precipitation Solution according to the manufacturer's instructions. In brief, 1

volume of cold PEG-it™ was added to every 4 volumes of lentiviral supernatant. The tubes were mixed by gentle inversion and incubated at 4°C overnight. The lentiviral/PEG-it™ mixture was then centrifuged at 1500 × g for 30 minutes at 4°C. The lentiviral particles appeared as a beige pellet; to ensure adequate lentiviral collection the supernatant was transferred to a fresh tube and centrifuged again. The supernatant was carefully discarded and the lentiviral pellets were resuspended in cold PBS at 1/100 of the original volume (prior to concentration). The PEG-it™ Virus Precipitation Solution also acts as a cryopreservative agent, therefore lentiviral stocks were aliquoted and stored at -70°C until required.

2.2.3 Genomic DNA Extraction

Genomic DNA (gDNA) was extracted from cells using a DNeasy Blood and Tissue kit (Qiagen) according to the manufacturer's protocol.

Cell lysis and DNA isolation

Cell pellets (up to 5×10^6 cells total/pellet) were thawed and resuspended in 200µl of sterile PBS. To lyse the cells 20µl of Proteinase K was added to the cell suspension. As RNA-free genomic DNA is required, 4µl of RNase A (100 mg/ml) was added, the samples were briefly vortexed and incubated for 2min at room temperature to allow for RNA digestion. 200µl of Buffer AL (with no ethanol) was added and the tubes were vortexed immediately to yield a homogenous solution. Samples were incubated at 56°C (to provide optimal DNA binding conditions during gDNA isolation) for 10 min. After the incubation, 200µl of 100% ethanol was added and the samples were mixed thoroughly.

DNA binding and washing

To allow for DNA binding the lysate was pipetted into a silica-based spin column. The column was centrifuged at $\geq 600 \times g$ for 1 min. The flow-through was discarded and the column was placed in a new collection tube. A series of centrifugation steps were performed in the presence of a high ethanol gradient to selectively bind DNA to the membrane as contaminants pass through. To do this, 500µl of Buffer AW1 was added and the column was centrifuged for 1 min $\geq 600 \times g$. After discarding the flow-through,

the column was placed in a new collection tube and 500µl of Buffer AW2 was added. The column was centrifuged for 3min at 20,000 x g to dry the membrane. To ensure there was no residual ethanol carryover the flow-through was carefully discarded and the column was centrifuged for a further 1min at 20,000 x g.

DNA elution

For maximum DNA yield, purified DNA was eluted in 50 µl of elution buffer. The elution buffer contained 10 mM Tris Cl and 0.5 mM EDTA (pH 9.0) to ensure optimum recovery and stability of eluted DNA. The column was incubated with elution buffer for 5min at room temperature and then centrifuged at ≥ 600 x g for 1 min to elute the DNA. The concentration of purified DNA was determined using spectrophotometry (Nanodrop 8000). Genomic DNA with an A_{260}/A_{280} ratio between 1.7 and 1.9, showing a symmetric peak at 260nm confirmed high purity and was deemed acceptable for experimental use.

2.2.4 Plasmid DNA

Bacterial Culture

LB Agar Plates for Bacterial Culture

All bacterial culture work was performed under sterile conditions. Luria Broth (LB) agar plates were prepared by adding 1.5g of granulated agar (BD Difco) to 2.5g of Luria Broth (Sigma) per 100ml of distilled water. The appropriate antibiotic selection marker (**Table 2.3**) was added for each DNA plasmids. Once the plates were set, a sterile metal loop was used to streak bacteria from the *E.coli* stab culture (**Table 2.1**) onto the appropriate LB agar/antibiotic plate. All plates were incubated overnight at 37°C.

Inoculating a liquid culture of bacterial plasmid

After ~16hours, plates were checked for single colonies. A starter culture was prepared by inoculating a single colony in 5ml of LB media (containing the appropriate antibiotic). The starter cultures were incubated at 37°C in a shaking (~300rpm) incubator for 6-8hrs. At the end of the incubation time, starter cultures were observed for cloudiness. As all of the DNA plasmids of interest have a high copy number growth in bacteria therefore 0.1ml (1:1000) of the starter culture was added to a large conical flask containing 100ml

of the appropriate antibiotic selective LB media. The bacterial culture was incubated overnight.

Glycerol Stocks of Bacterial Plasmids

Bacterial glycerol stocks were prepared for long term storage of the plasmids. 500µl of the transformed *E.coli* bacterial culture was added to 500µl of 80% glycerol in a screw top cryovial. After mixing gently the cryovials were cooled on dry ice for 5-10mins and then transferred to -80°C for long term storage. To recover bacteria, the cryovials were placed on dry ice. Using an inoculation loop the bacteria was scraped from the surface and then streaked onto a LB agar plate (containing the appropriate antibiotic selection marker) and the culture was left to grow overnight at 37°C.

Plasmid DNA was isolated from *E.Coli* bacterial cells using a 'PureYield Plasmid Midiprep System– Endotoxin Free' plasmid preparation kit (Promega, Wisconsin, USA). This kit is endotoxin free to ensure the removal of protein, RNA and bacterial endotoxin contaminants from the purified plasmid DNA prior to cell transfections (to prevent an inflammatory response). Plasmid DNA was purified according to the manufacturer's protocol as described below.

Bacterial cell lysis

The transformed *E.coli* bacterial liquid cultures were pelleted by centrifugation (3082 x g for 10 minutes). The cell pellets were then resuspended in 3ml Cell Resuspension solution. To lyse the bacterial cells, 3ml of Cell Lysis Solution was added and the tube was mixed by gentle inversion and incubated for 3min at room temperature. The lysate was then neutralised with 3ml of Neutralising Solution. After gentle inversion, the tube was left in an upright position for 3 minutes (to allow for the formation of a white flocculent precipitate containing dead proteins and cell debris).

Lysate clearing and plasmid DNA binding

Lysate clearing and binding of plasmid DNA to the column was performed using a series of centrifugation steps. Upon adding the lysate to the PureYield™ clearing column, a 2

min incubation was performed to allow for the bacterial cellular debris to rise to the top. The column was centrifuged at 1,500 × g for 5 minutes. To allow for the plasmid DNA to bind to the column, the filtered lysate was added to a PureYield™ Binding Column, and the column was centrifuged at 1,500 × g for 3 minutes.

Wash

Contaminants such as endotoxins, protein, RNA and endonucleases were eliminated by adding 5ml of endotoxin wash removal (containing isopropanol). The column was centrifuged at 1,500 x g for 3 minutes and the supernatant was discarded. A second wash was performed this time using 20ml of Column Wash Solution (containing 95% ethanol). To ensure the removal of any remaining ethanol, the column was centrifuged at 1,500 x g for an additional 10mins.

DNA Plasmid Vector	Gene of interest	E.coli Host Strain	Bacterial Antibiotic Resistance gene	Vector Use
pLOX-TERT-iresTK	<i>TERT</i>	Stbl3	Ampicillin 100µg/ml	Lentiviral (transfer)
pLOX-GFP-iresTK	<i>GFP</i>	Stbl3	Ampicillin 100µg/ml	Lentiviral (transfer)
pLOX-CW-CRE	<i>CRE</i>	Stbl3	Ampicillin 100µg/ml	Lentiviral (transfer)
pMD2.G	<i>VSV G</i>	DH5α	Ampicillin 100µg/ml	Lentiviral (envelope)
pCMVR8.74	<i>gag pol tat rev</i>	DH5α	Ampicillin 100µg/ml	Lentiviral (packaging)
pCre-pac	<i>CRE</i>	DH5α	Ampicillin 100µg/ml	Transient Transfection

Table 2.3 Plasmid DNA vector. For each of the plasmid DNA information on, the gene of interest, E.coli host strain, the specific antibiotic resistant gene cloned within the plasmid, the experimental purpose of the vector and the source of obtaining the plasmids are shown. Telomerase Reverse Transcriptase (*TERT*), Green Fluorescent Protein (*GFP*), Cyclin Dependent Kinase 4 (*CDK4*), Vesicular stomatitis virus (*VSV G*)

Plasmid DNA elution

To elute the plasmid DNA, 600µl of nuclease-free water was added and the column was centrifuged at 1,500 × g for 5 minutes. The eluted plasmid DNA was transferred to a 1.5ml tube and quantified. The remaining plasmid DNA was stored at -20°C until required.

Quantification of Plasmid DNA using Spectrophotometry

Spectrophotometry (Nanodrop 8000) was used to determine the plasmid DNA concentration by measuring the absorbance at 260nm. As a measure of good DNA purity, plasmid DNA samples with a 260/280 ratio within the range of 1.8-2.0 were deemed acceptable for experimental use.

Re-transforming DH5α Competent Cells with Plasmid DNA

For re-transformation, 100ng of plasmid DNA was added to 100µl of thawed *E.coli* DH5α competent cells (Invitrogen Life Technologies) on ice. The tube was gently mixed and the competent cell/DNA mixture was incubated on ice for 20 minutes. For 'heat shock' to occur, the transformation tube was placed in a 42°C water bath for 30-40 seconds. The tube was immediately placed on ice for 2 minutes. 1ml of SOC media (containing no antibiotic) was added to the bacteria and the contents were transferred to a 15ml falcon. To allow for bacterial growth, the culture was incubated at 37°C for 60 minutes. 50µl of the transformation reaction was spread onto prewarmed LB Agar plates (containing the appropriate antibiotic) and the plate was incubated overnight at 37°C. Bacterial liquid cultures were inoculated with a single colony, bacterial cultures were grown and the plasmid was purified.

Diagnostic Restriction Digests

To verify the purified plasmid DNA, diagnostic digests were performed using specific restriction enzymes that cleave complementary restriction sites within the DNA sequences. **Table 2.4** highlights the plasmid DNA, vector backbone size and the restriction enzymes to digest the plasmid used (with details of the specific cut site within the plasmid) and the expected fragment sizes. The corresponding plasmid maps for each of the plasmid DNA vectors are shown in the **Appendix S1 (1-10)**.

Plasmid DNA	Vector backbone (bp)	Restriction enzymes (and restriction cut site on plasmid)	Expected fragment sizes (Kb)
pLOX-CW-CRE	9886	XbaI (4687bp) and BamHI (3016bp)	8.2kb and 1.7kb
pLOX- TERT-iresTK	13115	BamHI (5180bp) and XbaI (7917bp)	2.7kb and 10.4kb
pLOX-GFP-iresTK	10438	BamHI (2632bp) and XbaI (5239bp)	2.6kb and 7.8kb
pCMVr8.74	11906	XbaI (7005bp) and EcoRI (5064bp)	1.9kb and 10.0kb
pMD2.G	5824	BamHI (multiple restriction sites 2bp, 33bp, 860bp) and ScaI (5383bp)	Multiple fragments 443bp, 31bp, 827bp and 4.5kb
pCre-pac	6000	BamHI (2 restriction sites 600bp and 1600bp)	5kb and 1kb
pOG231	4800	Sall and SpeI (253bp)	4.5kb and 233bp

Table 2.4 Restriction enzymes and the expected fragment sizes for each of the plasmid vectors. Plasmid DNA is shown along with the size of the vector backbone, the restriction enzyme(s) used for the single or double diagnostic digest and the expected fragment sizes post digest.

Setting up the Restriction Digests

The DNA restriction digest reactions were set up according to **Table 2.5** shown below:

DNA restriction digest reaction set-up	
Plasmid DNA	500ng
10x CutSmart Buffer® (10mM Magnesium Acetate, 50Mm Potassium Acetate, 20Mm Tris-acetate, 100µg/ml Bovine Serum Albumine pH 7.9)	2µl
Restriction enzyme(s)	1µl
Total reaction volume	20µl

Table 2.5 DNA restriction digest reaction set-up

The restriction digest reactions were adjusted with ultrapure water to give a total reaction volume of 20µl. All reactions were performed on ice due to sensitivity of the restriction endonuclease activity. Prior to the addition of the restriction enzymes; the plasmid DNA, CutSmart Buffer® and ultrapure water were mixed. CutSmart Buffer® was chosen as the combination of chemical components listed in **Table 2.5** to allow for double digests, furthermore the addition of BSA was used to enhance the digest. The restriction enzymes were added (**Table 2.4**), and the reaction mixture was gently mixed. Reaction mixtures were then placed in a heat block at (37°C) for 1hr, the incubation time for the pCre-pac plasmid restriction digest reaction was 3hrs. Restriction digest fragments were analysed by agarose gel electrophoresis.

Agarose Gel Electrophoresis

A 0.7% agarose gel was prepared using agarose (0.7g) with 1X TAE buffer (100ml) and 10µl of GelRed nucleic acid stain (Biotium). DNA samples were prepared; 5µl of 5X loading buffer containing bromophenol blue (Blue), cresol red (Red), orange G and xylene cyanol FF (Bioline) was added to 20µl of DNA digest product and to the corresponding uncut plasmid DNA (500ng). Both the DNA digests and the uncut corresponding plasmid DNA samples were run on the agarose gel alongside 1kb and

100bp DNA ladders (Hyperladder, Bioline). The agarose gel electrophoresis was run at 100V for approximately 1.5 hours and visualised under UV light.

An example of an agarose gel showing the diagnostic digest restriction products is below:

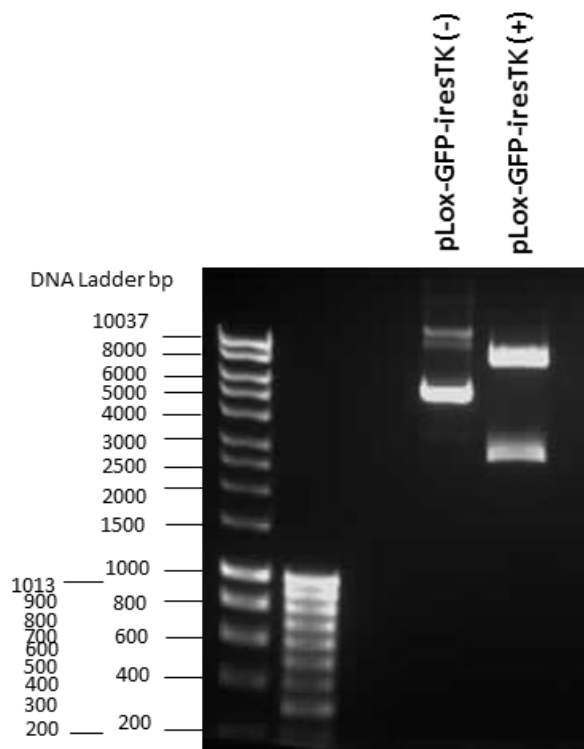


Figure 2.1 Example of DNA restriction double digest products on a gel. The uncut DNA plasmid pLox-GFP-iresTK (-) can be observed where no restriction enzyme added. The plasmid DNA cut using the restriction endonuclease BamHI and XbaI (pLox-GFP-iresTK(+)) yields two fragments at 2.6kb and 7.8kb.

Using the diagnostic digests for verification, the actual fragment sizes from the digests were compared to the expected fragment size for each of the plasmid DNA listed in **Table 2.4.**

A discrepancy in one of the bands was observed for the double digest of pLOX-CW-CRE with BamHI and XbaI. The band sizes 8.2kb and 1.7kb were expected, instead DNA fragments sizes of 8.2kb, 3.5kb and a very faint band at 400bp was found. These band

sizes have been observed by the supplier Addgene and the depositing lab is aware of the discrepancy and attributes it to mistakes during sequence assembly for the full plasmid. Nonetheless, the depositing lab have confirmed this plasmid is still functional. The plasmid pOG231 could not be verified using the fragment size yielded by the diagnostic digest (**Appendix S1 (9)**). Subsequently, new bacterial cultures were grown from isolated single colonies. This was performed within the two week recommended time period to use the bacteria within the stab culture. After plasmid purification and quantification, the double digest was repeated on the original pOG231 plasmid and the new pOG231 plasmid DNA. The same incorrect bands were yielded in both digests. Therefore this plasmid was replaced with a pCre-pac plasmid **Appendix S1 (10)**. for use in subsequent experiments.

2.2.5 RNA Extraction

Total RNA was extracted from the HUVEC using an RNeasy mini kit (Qiagen) according to manufacturer's protocol. Cells pellets were collected as described in **2.2.1**. To lyse the cells, the media was aspirated from the wells. To inactivate RNases, a denaturing guanidineisothiocyanate-containing buffer, RTL (with β -mercaptoethanol (1:100)) was added (350 μ l per well). Lysates were pipetted directly into a QIAshredder spin column (Qiagen) and the column was centrifuged at 17,000 x g for 3 minutes for cell homogenisation. To provide the appropriate conditions for RNA binding, 1 volume of 70% ethanol was mixed with the lysate. The sample was then added to a silica based RNeasy spin column and centrifuged for 15 seconds at ≥ 8000 x g. The flow-through was discarded. To ensure the removal of any residual gDNA (which may interfere with the real-time PCR application) an on-column DNase digest was performed. First to wash the spin column, 350 μ l of RW1 buffer was added and the column was centrifuged for 15 seconds at ≥ 8000 x g. The flow-through was discarded. For each reaction, 10 μ l of RNase-free DNase I (27 Kunitz units) was added to 70 μ l Buffer RDD and the tube was mixed by gentle inversion. The DNase was applied directly to the column and incubated at room temperature for 15 min. 350 μ l of Buffer RW1 was added and the column was centrifuged for 15 seconds at ≥ 8000 x g. The flow-through was discarded. To wash away contaminants and to retain only the total RNA, 500 μ l of Buffer RPE was added and the column was centrifuged for 15 seconds at ≥ 8000 x g, the flow-through was discarded.

To dry the spin column, the wash step (500µl of RPE buffer) was repeated and the column was centrifuged for 2 minutes at $\geq 8000 \times g$. The flow-through was carefully discarded and to prevent the carryover of ethanol the column was centrifuged again at full speed for 1 min. To elute the RNA, 30µl of RNase-free water was applied directly to the column and incubated for 2 minutes. The column was centrifuged for 1 min at $\geq 8000 \times g$. This extraction method purifies RNA longer than 200 nucleotides (for example mRNA) therefore RNA molecules shorter than this size are excluded (for example 5.8S rRNA, 5S rRNA, and tRNAs).

Quantification of RNA using Spectrophotometry

The RNA concentration was determined by spectrophotometry (Nanodrop 8000) by measuring the absorbance at 260nm. RNA samples with a 260/280 ratio of >2.0 was deemed suitable for experimental use.

Determining the quality of RNA by agarose gel electrophoresis

The quality, yield and integrity of the RNA in the samples was assessed by gel electrophoresis. An agarose gel (1%) was prepared with agarose (1g) and 1X TAE buffer (100ml), and 10µl of GelRed nucleic acid stain. The samples were prepared by the following; 3µl sample RNA, 2µl 5x loading dye (bioline) and 7µl distilled water. Samples were mixed and loaded into the gel alongside a 100bp ladder (Bioline). The electrophoresis ran at 80V for ~1hour. The gel was then visualised under UV light to confirm the RNA is intact (by the detection of clear 18S and 28S ribosomal RNA bands), free of gDNA contamination with minimal RNA degradation present.

cDNA synthesis

cDNA was synthesised from mRNA template using reverse transcription, to serve as a template in subsequent quantitative realtime PCR (RT-qPCR) assays. cDNA was produced using the Sensifast cDNA synthesis kit (Bioline) according to manufacturer's instructions. All reactions were prepared on ice. A mastermix was prepared 1µg RNA, 4µl of 5x TransAmp buffer (containing oligo dT primers) and 1µl of Reverse Transcriptase. The volume was adjusted to 20µl using RNase free water and mixed by

gentle pipetting. A no reverse transcriptase (NRT) control reaction was included using 1µl of RNase free water in place of the RNA. The reactions were run on a RT-PCR thermal cycler in the following order: 25°C for 10 min (for primer annealing), 42°C for 15 min (reverse transcription), 85°C for 5 min (Reverse Transcriptase inactivation) and a 4 °C hold. Upon completion of the cycle, the cDNA samples were immediately stored at -20°C, prior to use in the real-time qPCR assays.

2.2.6 Polymerase chain reaction

Primer Design

Primers sequences were designed for *TERT*, *MOB4*, *ICAM-1*, *eNOS*, *E-SELECTIN* as no primers specific to these genes were readily available in our laboratory. The Ensembl database (Cambridgeshire, UK) was used to identify the cDNA sequences of a particular transcript variant for each of the human genes. The cDNA sequences of specific exons of interest were inputted in a software (Primer3) which generated potential forward and reverse primers. To prevent amplification of non-specific DNA, stringent parameters were set when designing primers (**Table 2.6**). Primer sequences were chosen that spanned specific exon junctions to prevent amplification of any potential contamination in the RNA extract. Primers that bind to different exons were chosen, provided the introns spanning these exons were long. The NetPrimer (Premiere Biosoft) software was used to cross check the chosen primers against a set criteria (**Table 2.6**).

Melting Temperature T_m	Within +2°C of each other
Length of primer sequence	18-21 nucleotides
GC content	~ 50%
GC clamp	> 2 out of 5 is either G or C
Secondary structures associated with sequence	Avoid primer sequences that may form secondary structures (hairpin structures, self-dimers or heterodimers)
Amplicon Size	100-200bp

Table 2.6 Criteria for the design of optimum forward and reverse primers for PCR

Blast searches were performed to check the chosen primers are specific to the gene of interest. Primers were then ordered from either Eurofins Genomics (Germany) or Sigma (UK).

Standard PCR Set-up

A temperature gradient standard PCR was applied when optimising primer sets. Different annealing temperatures of the primers were initially tested, followed by the optimum cycling parameter. PCR was performed on cDNA using a MyTaq HS DNA Polymerase kit (Bioline), according to the manufacturer's protocol. A typical PCR reaction set up is shown in **Table 2.7**. DNase free water was added to give a total reaction volume of 25 µl. A NRT (no reverse transcriptase) and NTC (no template control) were included. All reactions were performed using a GStorm Multi-Block Thermal Cycler using the conditions outlined in **Table 2.8**. PCR products were visualised on a 1.5% agarose gel. The most suitable primer sets for each the genes of interest were then taken forward to the real-time platform.

Component	
5x MyTaq™ Reaction Buffer	10 µl
Template	10ng
Reverse Primer	300nM
Forward Primer	300nM
MyTaq™ HS DNA Polymerase	500 Units

Table 2.7 The components of a standard PCR set up reaction

Step	Temperature	Time	Cycles
Initial Denaturation	95°C	1 min	1
Denaturation	95°C	15 sec	30
Annealing	According to T _m of primers	15 sec	
Extension	72°C	10 sec	

Table 2.8 Standard PCR cycling conditions

Colony PCR

For colony PCR, a sterile tip was used to stab the colony and was directly added to the 25µl reaction mix shown in Table 2.6.1.a. The cycling parameters used for the colony PCR are shown in **Table 2.8**.

Integration Site Analysis

Integration site analysis was performed according to the manufacturer's protocol (Clontech, UK). Genomic DNA was first isolated from the cells using the procedure outlined in **Section 2.2.3**. The purity of experimental genomic DNA was tested by DraI (10 units/µl) digestion (overnight at 37°C) and the restriction products were analysed on a 0.6% agarose gel.

Viral DNA library	Restriction enzyme	Restriction enzyme concentration units/µl	Restriction enzyme buffer	Temperature	Incubation time of digest (hrs)
DL-1	DraI	10	10x	37°C	2
DL-2	SspI	10	10x	37°C	2
DL-2	HpaI	10	10x	37°C	2
DraI positive control	DraI	10	10x	37°C	2

Table 2.9 Blunt ended digestion of experimental genomic DNA using DraI, SspI or HpaI to generate viral integration DNA libraries. A control (human genomic DNA (lentivirus)) with high molecular weight genomic DNA that contains a single copy of the lentiviral provirus is provided in the kit. The DraI positive control is the control human genomic DNA digested with DraI.

Digestion of genomic DNA

Adapted ligated genomic DNA fragments were then constructed from the lentiviral transduced cell population to generate three different viral integration libraries. To do this gDNA (0.1µg/ml) was digested independently using the following blunt ended restriction enzymes (10 units/µl), Dral, Ssp I and HpaI according to **Table 2.9**.

Following the digest, reactions were vortexed (slow speed) for 5–10 sec and incubated at 37°C overnight (16–18 hr). The next day, to check for complete digestion 5 µl of each digestion reaction on a 0.6% agarose gel.

Purification of DNA

DNA was purified using the 'NucleoSpin Gel and PCR Clean-Up' component of the kit. In brief gDNA digests were mixed with 200 µl of Buffer NT1 and the sample was added to a column membrane. The membrane was centrifuged for 30 sec at 11,000 x g to allow for DNA binding, the flow-through was then discarded. To wash the membrane, 700µl of buffer NT3 was added to the column which was then centrifuged for 30 sec at 11,000 x g. The flow-through was discarded. To dry the membrane, the column was centrifuged for 1 min at 11,000 x g to completely remove the buffer NT3. The purified DNA was eluted using 20 µl of Buffer NE (prewarmed to 70°C), after the addition of the elution buffer the column was incubated at room temperature (18–25°C) for 1 min. The column was then centrifuged for 1 min at 11,000 x g. The DNA yield was confirmed by running 1 µl of purified digested DNA of each reaction along with unpurified digested genomic DNA on a 0.6% agarose.

Ligation of genomic DNA to adapters

Four ligation reactions were set-up (DL-1, DL-2, DL-3 and Dral Control Human Genomic DNA). Each ligation reaction contained 4.8 µl of purified DNA, 1.9 µl GenomeWalker Adaptor (25 µM), 0.8 µl 10X Ligation Buffer and 0.5 µl T4 DNA Ligase (6 units/µl). The reaction mixtures were incubated at 16°C overnight. To stop the reactions, tubes were incubated at 70°C for 5 min. To maintain stability of the gDNA during storage, 32 µl of TE (pH 7.5) was added to the samples.

PCR-Based DNA Walking in Viral Integration Libraries

Primary PCR

Primary PCR was performed (using adaptor primers (AP) and lentivirus-specific primers (LSP)) to amplify the region of gDNA surrounding the integration site (**Table 2.10**). The following primary PCR master mixture was prepared (per reaction); 117µl of distilled water, 15µl of 10X Advantage 2 PCR Buffer, 3µl dNTP (10mM), 3µl AP1 (10µM), 3µl LSP1 (10 µM) and 3µl Advantage 2 Polymerase Mix (50X). The mastermix was gently mixed and 24µl to 1µl of the corresponding DNA library was added per reaction. The primary PCR 2-step cycling parameters were as follows, 94°C 25 sec, 72°C 3 min (7 cycles); 94°C 25 sec 67°C 3 min (32 cycles) and one cycle of 67°C for 7 min after the final cycle. For quality control purposes the primary PCR products were run on a 1.5% agarose gel.

Secondary (Nested) PCR

The secondary PCR master mix was prepared as follows, 117µl of distilled water, 15µl of 10X Advantage 2 PCR Buffer, 3µl dNTP (10mM), 3µl AP2 (10µM), 3µl LSP2 (10 µM) (**Table 2.10**) and 3µl Advantage 2 Polymerase Mix (50X). 24µl of this secondary PCR master mix was gently mixed with 1 µl of each diluted corresponding primary PCR product. The secondary PCR 2-step cycling parameters were as follows 94°C 25 sec, 72°C 3 min (5 cycles); 94°C 25 sec, 67°C 3 min (20 cycles) and one cycle of 67°C for an additional 7 min. The secondary PCR products of the viral integration libraries were analysed on a 1.5% agarose for verification. For quality control purposes of the assay, the Dral-treated control library was run on the gel (which produces a 700 bp secondary PCR product).

PCR	Primer Name	Primer sequence 5' → 3'
Primary PCR	AP1	GTAATACGACTCACTATAGGGC
	LSP1	GCTTCAGCAAGCCGAGTCCTGCGTCGAG
Secondary PCR	AP2	ACTATAGGGCACGCGTGGT
	LSP2	GCTCCTCTGGTTTCCCTTTCGCTTCAA

Table 2.10. Integration Site Analysis primer sequences for the primary and secondary PCR. Adaptor primers (AP) contain sequence from the GenomeWalker Adaptor. Lentivirus specific primers (LSP) are located downstream of the 5' LTR within conserved sequences to avoid amplification of repeat sequences within the provirus.

PCR Clean-up and Direct Sequencing

Major bands from the secondary PCR products were excised from the gel and the DNA was extracted using a 'NucleoSpin Gel and PCR Clean-Up' kit. In brief the DNA fragment was carefully excised using a scalpel. 200µl of Buffer NT1 was added to each 100 mg of agarose gel. Samples were incubated for 10 min at 50 °C and gently vortexed to ensure the gel was completely dissolved. To extract the DNA, the sample was loaded on a column and centrifuged for 30 seconds at 11,000 x g. The flow-through was discarded. To wash the membrane, 700µl of Buffer NT3 was added and the column was centrifuged for 30 seconds at 11,000 x g, the flow-through was discarded. This washing step was repeated to minimise chaotropic salt carry-over. To dry the membrane, the column was spun for 1 minute at 11,000 x g. To ensure the total removal of residual ethanol, the column was incubated for 2-5 minutes at 70°C. To elute the DNA, the column was placed in a clean 1.5ml micro-centrifuge tube, 15µl of Buffer NE was then added and column was incubated at room temperature for 1 minute. The column was centrifuged for 1 minute at 11,000 x g to elute the purified DNA. Purified DNA was sequenced using AP2 and LSP2 primers (**Table 2.10**). Sequencing analysis was performed using NCBI BLAST (Altschul *et al.*, 1990) and UCSC Genome Browser (Kent *et al.*, 2002).

Real-Time Quantitative PCR

RT-qPCR set up

Real-time quantitative PCR (RT-qPCR) is a means of determining the real time detection of amplified DNA copies and the relative quantification of the starting template cDNA. Each real-time qPCR reaction was performed in triplicate. 2X SensiMix™ SYBR® No-ROX kit containing SYBR® Green I dye, dNTPs, stabilisers and enhancers was used when setting up the PCR reactions. The final reaction mix composition consisted of the following; 1x SensiMix™ SYBR® No-ROX (3mM MgCl₂), 300nM forward primer, 300nM reverse primer and the final volume was adjusted using ultrapure water. The mastermix (9.5µl per reaction) was carefully pipetted in 0.1ml strip PCR tubes (Qiagen,UK) followed by 3µl of template cDNA. As control measures, a NRT (no reverse transcriptase) and a NTC (no cDNA template control, 3µl of ultrapure water) were also run in the PCR assay. The RT-qPCR cycling profile was specific for each primer set as shown on **Table 2.1.1**. This was performed on a RotorGene™ 6000 Q Thermal Cycler (Qiagen).

Primer optimisation

The conditions for each of the primer sets to be used were optimised by a temperature gradient standard PCR. Different annealing temperatures of the primers were initially tested, followed by the optimum cycling parameter. The PCR products were visualised on a 1.5% agarose gel to confirm the expected band size was observed and only a single product was produced. The forward and reverse primer sequences of each of the primer sets and the optimum cycling conditions are shown in **Table 2.11**. The house-keepers 36B4 and PMSB4 were specifically chosen for quantification purposes due to the genes being constitutively expressed in most cell types.

SYBR-Green

During the run, the SYBR® Cycling. A Green channel was set on the Rotor-Gene Q. This allowed for optics present within the cycler to excite (at 470 ± 10 nm) when SYBR® Green is bound to the duplex double-stranded DNA. The fluorescent signal corresponds to the amount of DNA product that has been amplified during the qPCR run; an example of an amplification plot is shown (**Figure 2.2**). The SYBR® Green dye is sensitive to the non-specific binding of primers and other contaminating DNA, as a result, primer-dimers and superficial PCR product may be detected. A melt curve analysis was therefore performed to confirm the presence of a single product.

Melt curve analysis

The melt curve analysis checks the specificity of the reaction and ensures the detection of a consistent single product; the target amplicon of interest (**Figure 2.2**). The melt curve cycle was run at the end of the cycling profile; 90 seconds for the first step and 5 seconds for subsequent steps at 72 to 95°C (increments of 1°C).

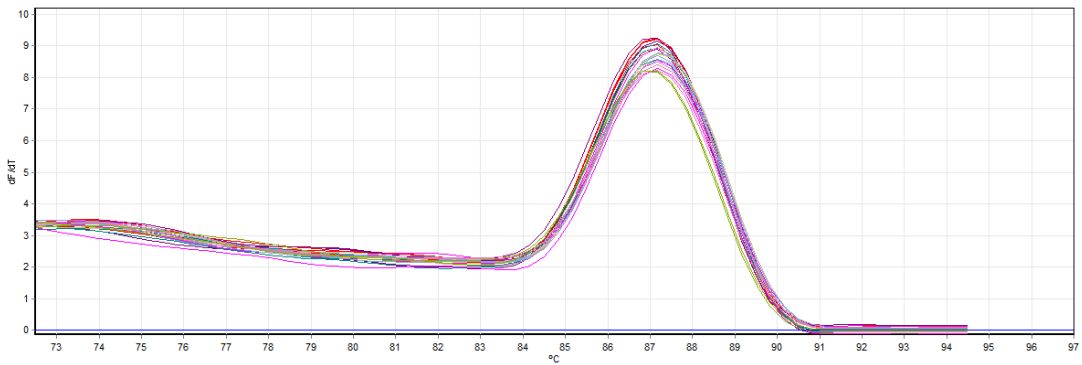


Figure 2.2 Melt Curve Analysis of *ICAM-1* standard curve obtained through the SYBR Green real-time quantitative PCR (RT-qPCR). RT-qPCR reactions were carried out using a two-fold dilution series (150ng to 1.17ng) of HUVEC cDNA. The reactions were performed using 1x SensiMix™ SYBR® No-ROX (3mM MgCl₂), 300nM forward *ICAM-1* primer and 300nM reverse *ICAM-1* primer. The RT-qPCR cycling profile was as follows, 95°C for 15 seconds, 58°C for 15 seconds and 72°C for 20 seconds. The melt curve cycle was run at the end of the cycling profile; 90 seconds for the first step and 5 seconds for subsequent steps at 72 to 95°C (increments of 1°C).

Gene	Forward Primer	Reverse Primer	RT-qPCR Cycling Conditions						Amplicon length (bp)
			Step 1 Denaturation		Step 2 Annealing		Step 3 Elongation		
			Temp °C	Time (secs)	Temp °C	Time (secs)	Temp °C	Time (secs)	
<i>ICAM-1</i>	AACCCACAGTCACCTATGG	TTCTGAGACCTCTGGCTTCG	95	15	58	15	72	20	194
<i>eNOS</i>	CTCACCGCTACAACATCCT	TGATTCCACTGCTGCCTTG	95	15	56	15	72	20	98
<i>E-SELECTIN</i>	CCAGAGCCTTCAGTGTACCT	GAGTGGTGCATTCAACCTGG	95	15	58	15	72	20	211
<i>36B4</i>	TCGACAATGGCAGCATCTAC	GCCTTGACCTTTTCAGCAAG	95	10	58	60	72	20	221
	CGTTCCGCAGAGAAAAGAGG	CGTCACATCCACCTTGACAA	95	15	59	15	72	15	212
<i>MOB4</i>	TGCCATCCAGATACTTGAC	TCCTACGGCATACTGATCCT	95	15	58	15	72	15	214
<i>vWF</i>	GACCCTTTGTGCAGAAGGAA	GGCTCACTATCTTGCCATTC	95	15	58	35	72	20	194
<i>KDR</i>	TGATCGGAAATGACACTGGA	CACGACTCCATGTTGGTCAC	95	15	58	35	72	20	131
<i>CD34</i>	AGGTATGCTCCCTGCTCCTT	GAATAGCTCTGGTGGCTTGC	95	15	58	35	72	20	181
<i>CDH5</i>	GCCAGGTATGAGATCGTGGT	GTGTCTTCAGGCACGACAAA	95	15	58	30	72	20	152

Table 2.11 Forward and reverse primer sequences and cycling conditions for real-time quantitative PCR. The forward and reverse primer sequences for each of the genes of interest are shown along with the three step cycling conditions (step 1 Denaturation, step 2 Annealing and step 3 Elongation). The number of cycles for all genes were 40 cycles with the exception of *TERT* (35 cycles) and *CDH5* (30 cycles). The total size of amplicon length (in bp) is shown for each gene.

Standard Curves

Standard curves were generated for each of the primer sets in order to establish a linear (input) cDNA template concentration range. To generate the standard curves, a two-fold dilution series of reference template cDNA (150ng to 1.17ng in a total of 8 serial dilutions) was carefully prepared. For reproducibility, the RT-qPCR reaction was set-up in triplicate for each reaction.

To generate the standard curve, the take-off values for each reaction was plotted against the log₁₀ input cDNA (ng). The amplification efficiency can be calculated from the slope of the line using the following equation:

$$\% \text{ Efficiency} = (10^{(-1/\text{slope})} - 1) \times 100$$

Efficiency between 90 and 110% was acceptable, which corresponds to a gradient ranging from -3.1 to -3.6 (with the optimal being -3.32). The coefficient of determination value, R^2 , measures how well the experimental data fits the regression line ($R^2 > 0.98$ was acceptable). A standard curve of the *ICAM-1* primer is shown in **Figure 2.3**. The linear dynamic range of the standard curve is where the line is linear and in this case likely extends past the lowest and highest values. Therefore a input cDNA concentration in the middle of the linear range (15ng) was chosen as the input cDNA concentration to be used in subsequent experiments.

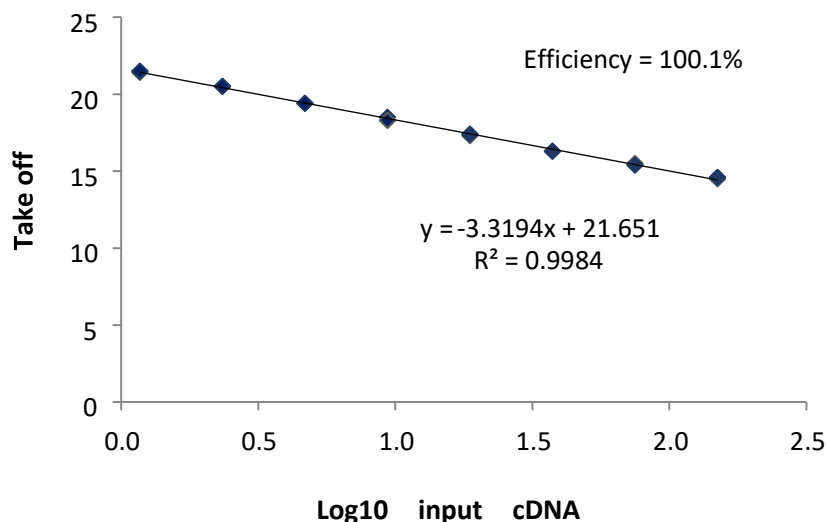


Figure 2.3 Standard curve for *ICAM-1* primer set. A linear range (14.5 – 21.5 cycles) was established, 15ng total cDNA was used for subsequent qPCR assays. All experimental data using this primer set were checked to ensure take-off values lie within this linear range. Any samples found to run outside the linear range were diluted and re-run.

Relative quantification

The real-time qPCR data was analysed by relative quantitation using the Rotor-Gene Q Series comparative quantification software. The software calculates the amount of product in the test sample relative to a set calibrator. The Rotor-Gene software calculates the concentration of the specific gene of interest in a given sample relative to a set calibrator using the equation:

$$\text{Relative concentration} = \text{MAE}^{(\text{Calibrator takeoff} - \text{Sample takeoff})}$$

To put this equation into context, the software generates a second derivative of an amplification plot which produces a peak corresponding to the maximum rate of fluorescence increase during the exponential phase of the reaction. The software calculates the take-off point of each sample defined as the cycle number that reaches a 20% threshold of the maximum level. The efficiency of the reaction is calculated as $E = 10^{(-1/\text{slope})}$. MAE is the mean amplification efficiency across all triplicates for each test sample within the PCR run to adjust for any differences between reactions.

Gene expression analysis

Relative quantification was performed for gene expression analysis (n=3 for each test sample with each sample run in triplicate) using control or baseline samples as the calibrator. Data was further normalised against the gene *36B4* which is a routine housekeeper used in our laboratory. The housekeeper assays accounts for any variations in target DNA (due to technical errors or differences in the reverse transcription efficiencies when synthesising cDNA). The relative concentrations were determined independently for *36B4*. The relative concentration for the gene of interest was divided by the reference relative concentration (for each sample) to give a ratio. The gene expression level of the gene of interest in each sample is expressed as a fold-difference relative to the comparative calibrator concentration.

Telomere length Measurements

Mean telomere length (TL) was measured in gDNA samples using a standard quantitative real time PCR (RT-qPCR)-based method which has been validated in our laboratory (Codd *et al.*, 2010, Codd *et al.*, 2013).

Genomic DNA was extracted from cells using the protocol outlined in **section 2.2.3**. Prior to the TL measurements, gDNA samples were diluted to 10ng/ μ l. TL is expressed as a T/S ratio of telomere repeat length (T) to copy number of a single copy gene, 36B4(S). Primer sequences for the telomere and house keeper (36B4) are shown in **Table 2.12**.

	Forward Primer Sequence	Reverse Primer Sequence
Telomere	Tel1b: CGGTTTGTGGGTTGGGTTGGG TTGGGTTGGGTT	Tel2b: GGCTGCCTTACCCTTACCCTTACCCT TACCCTTACCCT
Single Copy Gene (36B4)	36B4U: CAGCAAGTGGGAAGGTGTAATCC	36B4D: CCCATTCTATCATCAACGGGTACAA

Table 2.12 Telomere and Single Copy gene (36B4) primer sequences for telomere length PCR

PCR set up reactions contained, 1x SensiMix™ SYBR® NO-ROX master mix (Bioline), 300nM of Tel1b, 300nM Tel2b primers and 30ng of template gDNA. For the single copy gene 36B4 PCR, 300nM 36B4U primer and 500nM of 36B4D primer was used. The total volume for each PCR reaction was 25 μ l and DNA samples were assayed in duplicate. To standardize across assays a K562 Calibrator sample (gDNA from a K562 cell line) was used. A no template control was also set up for each TL assay. For consistency, all reactions were set up using a QIAgilty liquid handling system (Qiagen, UK) and run on a Rotor-Gene Q Thermal Cycler (Qiagen). The cycling conditions were as follows; 95°C incubation for 10mins followed by either 20 cycles (telomere) or 30 cycles (36B4) of 95°C for 15 sec and 58°C for 1min. Relative values for both T and S were calculated by relative quantification against K562 as the calibrator sample and the T/S ratio calculated.

Absolute quantification

Absolute quantification was performed for copy number quantification assays. This assay measures the lentiviral copy number stably integrated in the genome of a single target cell of a transduced HCT116 cell line by targeting the HSV Thymidine Kinase (HSV TK) transgene within the provirus.

A standard curve is generated using serial dilutions of a standard of plasmid DNA carrying the TK and the housekeeper gene albumin for normalisation. Samples for quantification are run within the same qPCR run as the standard curve. Quantification is then performed using the Rotor-Gene Q Series quantification software, which uses the diluted standard to generate the standard curve and quantifies the sample against this.

Transduction of cells with Lentivirus

Creation of albumin standard for copy number calculation

Plasmid DNA carrying the housekeeper albumin gene was required for the generation of standards for viral titre. As one was not readily available in our laboratory, a vector containing the *albumin* transgene was generated. The forward (sequence) and reverse (sequence) albumin primers were first optimised, by a temperature gradient PCR as outlined in **section 2.2.5**. DNA fragments containing *albumin* were produced by PCR amplification (124bp) of the required region on parental HCT116 genomic DNA (2.64ng/ μ l). Products were visualised on a 1.7% agarose gel for verification of the correct albumin product. The PCR amplification products were purified (from excess primers, nucleotides, DNA polymerase, oil and salts) using a GenElute™ PCR Clean-Up Kit (Sigma, UK). In brief, 0.5ml of column preparation solution was added to a GenElute plasmid mini spin column and the column was centrifuged at 12,000 x g for 1 min. After centrifugation, the eluate was discarded. Binding solution (5 volumes) was added to the PCR reaction mix (1 volume) and the mixed solution was applied to the membrane. The column was centrifuged at maximum speed for 1 min and the eluate was discarded. 0.5ml of diluted Wash Solution (containing ethanol) was added and the column was centrifuged for 1 min at maximum speed. The eluate containing contaminants was discarded. To dry the membrane from excess ethanol, the column was further

centrifuged for 2 minutes at full speed. To elute the DNA, 15µl of Elution Solution was added and the column was incubated for 1 min at room temperature. The pure PCR amplification product was eluted by centrifuging the column at maximum speed for 1min.

TA Cloning

The *albumin* insert was cloned into a pGEM[®]-T Easy Vector System according to the manufacturer's instructions (Promega, UK). Ligation reactions were set up in 0.5ml tubes as follows; 5µl 2x Rapid Ligation Buffer, pGEM[®]-T Easy Vector 50ng, *albumin* PCR product (64ng/µl), T4 DNA Ligase 3 Weiss units/µl and nuclease-free water to a final volume of 10µl. The reactions were mixed by pipetting and incubated for 1 hour at room temperature. The ligated pGMT-alb mixture was transformed into *E.coli* DH5α competent cells according to the protocol outlined in **2.2.4**.

Lentivirus Infection of HCT116 for viral titration

HCT116 cells were seeded in 12-well culture plates according to the methods outlined in **2.2.1**. Once the cells had reached 60-70% confluency, HCT116 cells were infected with 4 µl, 2 µl and 1µl of lentivirus in 500µl of fresh supplemented DMEM/F12. Two further virus dilutions included 1:100 and 1:1000.

The transduced cells were incubated for 96 hours. Cell pellets were collected and immediately kept on dry ice for 5mins. Genomic DNA was extracted from the cells according to the protocol outlined in **2.2.3**.

Lentiviral Titration Calculation

The number of assessed lentiviral DNA copies integrated in the transduced target cell was determined using qPCR by absolute quantification against known standard of plasmid DNA carrying the TERT and the housekeeper gene albumin for normalisation.

To calculate the number of integrations per cell quantification of a genomic single copy control, albumin, were performed in parallel, using known dilutions of the pGMT-alb plasmid to generate the standard curve.

Copy number was calculated using the following equation:

$$\text{Vector copy number} = (\text{Quantity mean of TK sequence} / \text{Quantity mean of Alb sequence}) \times 2.$$

This equation takes into account the Albumin sequence is present in two copies per genome.

Once the copy number was determined, the lentiviral titre was calculated according the following:

$$\text{Titre (TU/ml)} = \frac{(\text{Number of target cells} \times \text{number of copies per cell of the sample})}{\text{Volume of supernatant in (ml)}}.$$

Multiplicity of Infection (MOI) is defined as the ratio of infectious pseudoviral particles (IFU) to the population of target cells. Using the viral titre, the MOI used for the lentivirus infection in the host cell was calculated as follows:

$$\text{MOI} = \text{Titre (TU/ml)} \times \text{Volume of lentivirus (ml)} / \text{Number of target cells}$$

Lentivirus infection in the host cell

HUVEC cells were seeded in T25 culture vessels according to the methods outlined in **2.2.1**. Once the cells had reached 60-70% confluency, the lentivirus of interest was added to the cells in 5ml of fresh ECGM. For 'difficult to transfect' cell lines such as HUVEC an MOI of 100 is sufficient to transduce the cells. The transduced cells were incubated for 72 hours.

Antiviral therapy using Acycloguanosine

For generation of the isogenic lines of short and long TL, the experimental model system utilised in this work involves the use of a conditional ablation system post viral Cre excision. As the lines utilised in this work are a mixed population, the use of an anti-viral therapy is to ensure the complete removal of non-excised cells containing the TERT transgene. A cytotoxicity test to assess the concentration-response was first performed

on untransduced HUVEC. Cells were treated with 0.25-10 $\mu\text{g}/\text{ml}$ of Acycloguanosine (ACG) alongside a DMSO vehicle only control for 7 days and counted (**Figure 2.4**).

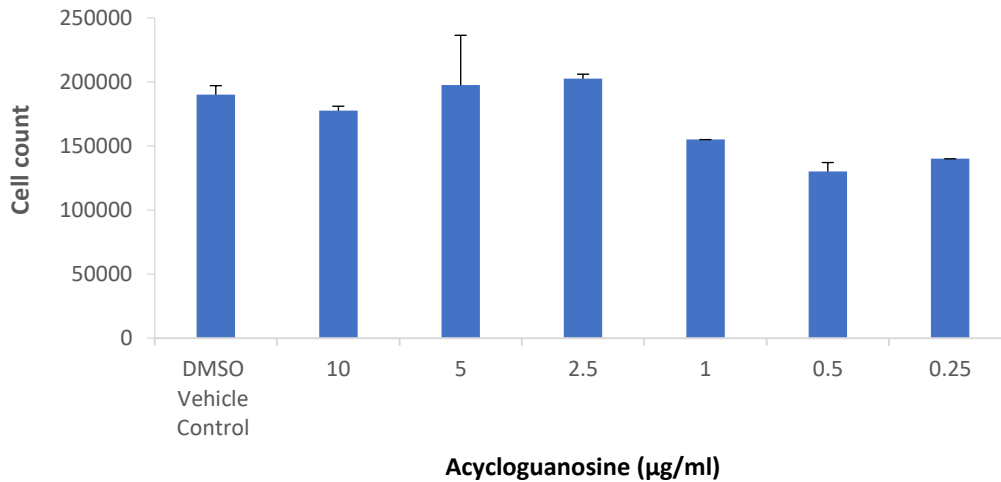


Figure 2.4 Concentration-response of Acycloguanosine on untransduced HUVEC. Cells were treated with a dose response of Acycloguanosine alongside a DMSO vehicle only control for a course of 7 days. Cells were then counted post treatment.

The cytotoxicity test results found 10 $\mu\text{g}/\text{ml}$ ACG as the optimal dose with minimal toxicity on parental HUVEC, therefore this dose was taken forward for subsequent ACG treatments.

Telomerase Repeat Amplification Protocol

Telomerase activity was measured using a PCR-based assay known as Telomerase Repeat Amplification Protocol (Kim et al 1994; 1997). This was performed using a gel-based TRAPeze[®] Telomerase Detection kit according to the manufacturer's instructions (Merck, Hertfordshire).

Extract Telomerase

1x10⁶ HUVEC were pelleted by centrifugation followed by the removal of media at 300 x g for 5 minutes. The cell pellet was washed twice with phosphate-buffered saline and after the final centrifugation all residual PBS was carefully removed. The pellets were either snap frozen in dry ice and stored at -80°C for future use or immediately resuspended in 200ul of ice-cold 1x CHAPS Lysis Buffer (10mM Tris-HCl pH 7.5, 1mM MgCl₂, 1mM EGTA, 0.1 mM Benzamidine, 5 mM β-mercaptoethanol, 0.5% CHAPS and 10% Glycerol) to a concentration of 5000 cell equivalents/μl. To allow for lysis, cells were incubated on ice for ≥30 minutes and then centrifuged at 4°C for 30 minutes at 16,200xg. The supernatant was carefully transferred to a pre-cooled 0.5ml screw-top tube and left on ice prior to measuring the protein concentration. A 25μl volume was taken from each cell lysate in order to perform protein concentration assay. For the remaining supernatant, 30μl aliquots were added to additional pre-cooled 0.5ml tubes to avoid multiple freeze-thawing, all tubes were snap-frozen on dry ice and stored at -80°C.

Protein Concentration

Protein concentration was measured using a Bradford Assay method (Bradford Reagent, Sigma Aldrich UK) against known BSA standards (2, 1.5, 1, 0.75, 0.5, 0.25, 0.125 BSA mg/ml). In a 96-well plate, cell lysate was diluted 1:50 with Bradford reagent. The plate was then placed on a shaker for 30 seconds at 230rpm and the absorbance values were immediately read on a spectrometer at a wavelength of 595nm. A TRAP PCR master mix was prepared according to **Table 2.13**.

Reagents	Volume μl
10X TRAP Reaction Buffer (200mM Tris-HCl pH 8.3, 15mM MgCl ₂ , 630mM KCl, 0.5% Tween 20, 10mM EDTA)	2.5
50X dNTP Mix (2.5mM each dATP, dTTP, dGTP and dCTP)	0.5
TS Primer	0.5
TRAP Primer Mix	0.5
Taq Polymerase (5 units/μL)	0.2 (1 unit)
PCR-grade Water (protease, DNase, and RNase-free; deionized)	18.8

Table 2.13 Mastermix PCR set up for the TRAP assay.

For valid analysis of the results, controls were included in each TRAP assay. A telomerase-positive control included a K562 cell extract (500cells/ μ l). To make this extract, cells were lysed in 200 μ l of 1x CHAPS Lysis Buffer and then diluted 1:20 (with 1x CHAPS Lysis Buffer), 2 μ l were added per TRAP assay. As telomerase is a heat-sensitive enzyme, a heat-inactivated negative control included a K562 sample extract incubated at 85°C for 10 minutes. A special feature of the TRAPEZE® Telomerase detection kit is the inclusion of an internal control to assess PCR inhibition and amplification efficiency, which in turn enables semi-quantitative analysis. The TRAP Primer Mix contains an internal control primer K1 and a TSK1 oligonucleotide template that together with the TS primer generates a 36 bp internal control (IC) band in every lane. Finally, a primer-dimer/PCR contamination control included CHAPS Lysis Buffer only. This control checks for the presence of primer-dimer/PCR artefacts, which may be due to suboptimal PCR conditions and/or amplified TRAP product carry-over contamination.

Cell test extracts were added to the PCR reaction in three different serial dilutions (2500, 500, 100 cell equivalents). 2 μ l of cell sample test extracts, heat-inactivated extracts or controls into each PCR tube to give a total reaction volume of 25 μ l. Amplification of the extension products by PCR was performed using a two-step Rotor-Gene® Q (Qiagen) thermocycler protocol according to **Table 2.14**.

PCR cycling conditions				
Elongation step	Step 1	30°C	30min	1 cycle
	Step 2	95°C	5min	1 cycle*
Amplification step	Step 3	94°C	15sec	34 cycles
		59°C	30sec	
		72°C	1min	
	Step 4	25°C	20min	1 cycle

*To heat inactivate telomerase

Table 2.14 PCR cycling conditions for the TRAP assay

Gel Electrophoresis

To visualise the amplified telomerase products, 10µl of the TRAP PCR products were diluted in 2.5µl of 5x Novex™ TBE High Density Sample Buffer (containing 0.1% bromophenol blue and 0.1% xylene cyanol). 10µl of this mixture was loaded on a Novex™ 10% TBE non-denaturing polyacrylamide gel (no urea), 15-well gels (Thermofisher). The gel is run in a XCell SureLock® Mini-Cell (Thermofisher) vertical electrophoresis tank and the reservoirs were filled with 1x Novex™ TBE Running Buffer. 1µl of a GeneRuler Ultra Low Range DNA Ladder (0.1 µg/µL) (Thermofisher Scientific) to lane 1 of the gel.

The gel was run at 160V constant for ~70 minutes (Start: 16mA, End: 8 to 10mA) until the marker dye had run ~75% of the gel/ 5mm above third line on the gel casing. After electrophoresis, the gel was carefully stained with PAGE GelRed™ (Takara, France). To do this PAGE GelRed™ solution was diluted 1:10,000 in deionised water and the PAGE GelRed/TRAP gel was incubated for 30 minutes at room temperature with gentle agitation. The gel was then visualised on a 254nm UV transilluminator (Syngene) with an ethidium bromide filter.

Semi Quantitative analysis

To quantify the telomerase reaction products, the signal of the total region corresponding to the TRAP product ladder bands from each gel lane (representative of each sample) was measured (**Figure 2.5 A**). To do this, plots were generated using the image densitometry analysis software program ImageJ 1.51. Each plot corresponds to each lane of the TRAP gel image and each peak within a plot is representative of a band of telomerase reaction product (**Figure 2.5 B**). The Area Under the Curve (AUC) was manually enclosed for each of the peaks to allow for the software to generate a value and the sum of the total telomerase products for each sample was then calculated and plotted on a graph.

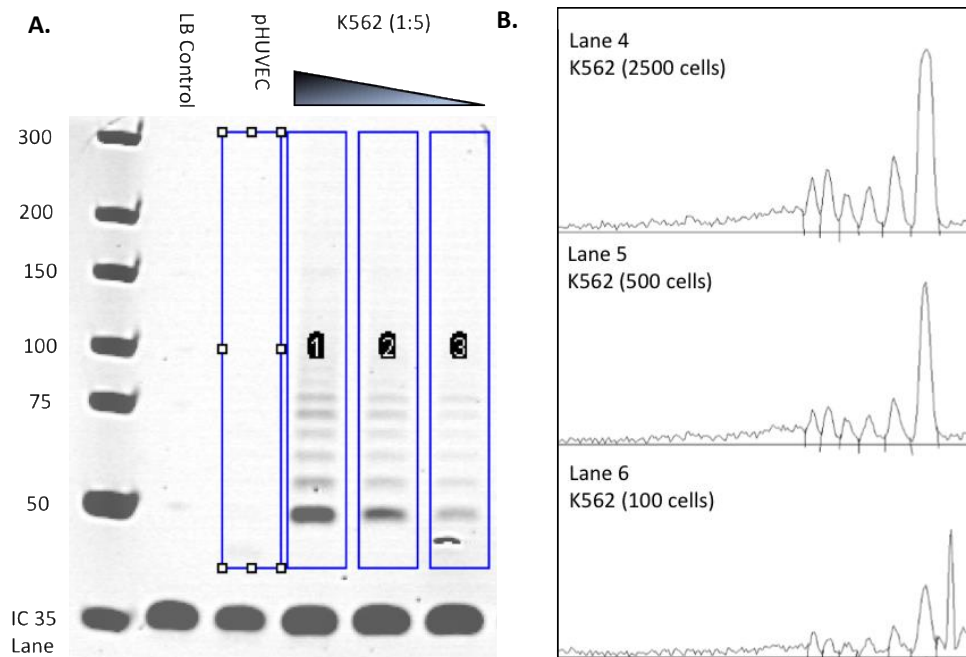


Figure 2.5 TRAP assay gel image and densitometry. A. TRAP gel image is shown where telomerase activity was detected in whole cell lysates of parental HUVEC (2500 cell equivalents) (- control) and a K562 telomerase positive cell line at 2500, 500 and 100 cell equivalents (+ control). The 35bp internal control (IC) is present for every lane to monitor PCR inhibition and serves as a control for amplification efficiency for each reaction. B. For the quantitative analysis of relative telomerase activity, densitometry is applied (using ImageJ 1.5.1). Plots for lanes 4, 5 and 6 only are shown, with each peak corresponding to each band within that lane. The Area Under the Curve (AUC) was manually enclosed for each of the peaks to which the software generates a value for each band. The total product generated is calculated as the sum of all peaks for each plot.

2.2.7 Cellular Senescence

Senescent cells within the HUVEC population were identified using a histochemical approach staining for a marker of cellular senescence β -galactosidase activity at pH 6. Increased β -galactosidase activity is detectable in senescent cells, however is not detected in quiescent, immortal or tumour cells (Dimri, I.G., *et al.*, 1995).

The senescence assay was performed according to the manufacturer's instructions (Sigma Aldrich, Germany). Prior to the assay HUVEC were seeded into 6 well cell culture plates (in triplicate) and corresponding treatments were carried out. The fixation buffer, Reagent B and Reagent C were pre-equilibrated to room temperature and mixed thoroughly before use. Ultrapure water was filtered through a 0.2 μ m filter unit prior to use. The Fixation Buffer solution (20% formaldehyde, 2% glutaraldehyde, 70.4 mM Na₂HPO₄, 14.7 mM KH₂PO₄, 1.37 M NaCl, and 26.8 mM KCl) was diluted 10-fold with ultrapure water. To avoid the formation of aggregates (that could potentially interfere with the visualisation of the stained cells), the X-Gal Solution was pre-warmed at 37°C for 1 hour. The endothelial cell growth media was aspirated from the cells and 1ml of PBS was added per well/plate to wash the cells. The entire wash solution was carefully removed. 1.5ml of 1x Fixation Buffer was added per well and the plate was incubated at room temperature for 6-7 minutes to allow for fixation of the cells. Cells were then rinsed 3 times with 1ml PBS/well. To prepare the Staining Mixture, the following components were mixed, 1ml of Staining Solution, 125 μ l Reagent B (400 mM Potassium Ferricyanide), 125 μ l Reagent C (400 mM Potassium Ferrocyanide), 0.25ml X-Gal solution (40mg/ml) and 8.5ml of ultrapure water. The Staining Mixture was then passed through a 0.2 μ m filter to ensure no aggregates remained in the solution. 1ml of the Staining Mixture was added per well, the plate was sealed with Parafilm and incubated at 37°C overnight. As the staining of the cells is pH dependent, the cells were left in an incubator without CO₂.

Cells were then visualised under an EVOS light microscope (100x magnification), to quantify the % of cells expressing β -galactosidase (senescent cells) the number of blue-stained cells and the total number of cells were counted in 5 fields of view (by two independent subjects). The staining mixture was aspirated and 1ml of 70% glycerol was added to the wells, to allow for long-term storage of the cells at 4°C.

2.2.8 THP-1 monocyte cell adhesion assay

HUVEC were seeded into 96 well plates (9,000 cells/well) according to the methods outlined in 2.2.1. On the day prior to the assay, HUVEC were treated with TNF- α (10ng/ml) for 24 hours. Fresh ECGM was added to the unstimulated HUVEC. After 24 hours, the media was removed and 100 μ l of serum free RPMI containing L-Glutamine was added to the wells and the plate was returned to the incubator. THP-1 cells (1×10^6 cells/ml) were loaded with 5 μ M Calcineurin and incubated for 30min at 37°C. Loaded THP-1 were washed twice with RPMI and 100 μ l of the THP-1 cell suspension was added to the wells containing stimulated and unstimulated HUVEC and the cells were incubated at 37°C for 90 minutes. 100 μ l of serum free RPMI (+L-Glutamine) media was added to unstimulated HUVEC only wells which served as an internal background only control for the assay. Following the incubation, the cells were washed 4x with pre-warmed serum free RPMI media. The plate was read using a NovoStar (BMG LabTech, Bucks, UK) fluorescence spectrophotometer at an excitation wavelength of 490nm and emission wavelength of 510nm. The cells were visualised and images were taken on an EVOS light microscope (ThermoFisher Scientific, UK).

2.2.9 Cell surface target detection by Flow Cytometry

Cell Staining for CD309 (VEGFR-2), CD114 (VE-Cadherin) and CD31 (PECAM-1) protein expression

FACS analysis was performed to detect the surface expression of endothelial specific proteins CD309 (VEGFR-2), CD31 (PECAM-1) and CD114 (VE-Cadherin) on the Ex1 and Ex2 isogenic lines (at 141-147 PDs). Up to 1×10^5 cells were labelled with a human conjugated antibody (1:200) or the appropriate IgG isotope control (for each run) according to **Table 2.15**. Endothelial cells were gated on the basis of their forward versus side scatter and fluorescence was measured on a Gallios FACS analyser. The Mean Fluorescence Intensity (MFI) of the logarithmic histograms (showing a normal population) was calculated using the median value derived using the Kaluza analysis software.

Cell surface protein	Human Isotype	Human IgG Isotype Control
CD309 (VEGFR-2)	CD309-APC	REA Control (S) APC
CD114 (VE-Cadherin)	CD114-APC	REA Control (S) APC
CD31 (PECAM-1)	CD31-FITC	REA Control (S) FITC
CD54 (ICAM-1)	CD54-APC	REA Control (S) APC

Table 2.15 Human isotope antibodies and the corresponding human isotope control antibody used for the detection of endothelial cell surface proteins

Cell Staining for ICAM-1 protein expression

For the HUVEC surface staining, cells were seeded into 6 well plates (0.5×10^5 cells/well) and treated if necessary with TNF- α (10ng/ml). After 24 hours, the cells were pelleted by centrifuging the cells for 200 x g for 5 minutes and resuspended in 100 μ l (per 10^7 nucleated cells) PBS containing 1mM EDTA (to avoid cell aggregates). Cells were labelled with a human CD44 (ICAM-1) conjugated antibody (1:200). Samples were also run using the appropriate IgG isotope control according to **Table 2.15**. The cells/antibody were incubated for 20 minutes in the dark at room temperature. Following the incubation, 100 μ l of PBS/EDTA was added and mixed well (to ensure a single cell suspension). The cells were transferred to 5ml polystyrene round bottom tubes (BD falcon) for analysis using a Beckman Coulter Gallios flow cytometer.

2.3.0 Statistical analysis

All data are presented as mean \pm standard deviation (SD). GraphPad Prism 8.1.1 (GraphPad software Inc.) was used to generate all graphs and for the statistical analyses. Statistical significance of the data was determined using a paired t-test. A one-way Analysis of Variance (ANOVA), following the appropriate post-test was used for comparisons between two or more groups. A P-value of <0.05 was considered statistically significant.

CHAPTER 3

GENERATION OF LOX-TERT PRIMARY HUMAN ENDOTHELIAL CELL LINES

CHAPTER 3

GENERATION OF LOX-TERT PRIMARY HUMAN ENDOTHELIAL CELL LINES

3.1 Introduction

In order to understand how telomere length (TL) may influence disease it is important to establish how telomere length may influence cellular physiology. Previous studies have focused on either inducing severe telomere dysfunction or growing cells for varying lengths of time in culture to induce telomere loss. As severe dysfunction, via removal of TRF2 function (Minamino *et al.*, 2001), will not reflect the subtle changes in telomere length associated with disease risk and growing cells for varying times in culture can introduce confounding factors (i.e. culture stress), neither are a perfect model. To overcome these difficulties I sought to establish a model system which could manipulate telomere length to examine the effects of more subtle changes in telomere length.

Endothelial cells (EC) line the blood vessel wall, endothelial dysfunction (ED) is the earliest change within the vessel wall that precedes atherogenesis. It has been shown that senescent, EC are observed on the luminal surface of atheromas in coronary arteries from patients with ischaemic heart disease (Minamino *et al.*, 2002). Telomere loss induces senescence, which is pro-inflammatory and also increases markers of endothelial dysfunction (increased *ICAM-1* expression, decreased *eNOS* activity) (Minamino *et al.*, 2002). We therefore decided to use endothelial cells in which to establish the model, with the hypothesis that shorter TL may induce ED and inflammation to drive early atherogenesis.

To investigate the role by which shorter TL could increase the risk of CAD, the effect of telomere length dynamics on the atherogenic potential of endothelial cells will be investigated. Isogenic lines of short and long telomeres will be generated, but to achieve this the immortalisation of human primary HUVEC is necessary. This procedure involves the ectopic expression of a removable form of the reverse transcriptase component of human telomerase (*TERT*) under the Cre Lox system (Salmon *et al.*, 2000, Stadler *et al.*, 2013). LoxP sites flanking either side of the integrated proviral *TERT* allows for the site specific deletion of the internal gene expression cassette by Cre recombinase.

Expression of *TERT* should allow the cell to overcome replicative senescence; a fundamental aspect of cellular immortalisation. Previous studies have immortalised normal human diploid cell strains through the reactivation/upregulation of telomerase, where cells acquired an unlimited replicative capacity through telomere length stabilisation (Bodner *et al.*, 1998; Yang *et al.*, 1999; Morales 2003). We aimed to achieve the immortalisation of HUVEC upon the addition of human *TERT* to activate telomerase. Previous studies have achieved the immortalisation of primary cells by over-expressing CDK4 in addition to telomerase (Stadler *et al.*, 2011; Zhu *et al.*, 2007). Over-expression of CDK4 sequesters the tumour suppressor protein p16^{INK4A} to allow free CDK4 to bind to cyclin D to enable cell cycle progression. Normal EC express low levels of p16^{INK4a} (Kan *et al.*, 2012), therefore over-expressing CDK4 may not be necessary in this model, which is preferable to avoid introducing another integration event which may be more detrimental to the cells.

TERT will be introduced in a HUVEC single donor line using a lentiviral transfer technique. This method is established to introduce a genetically integrated transgene into primary cells (Stadler *et al.*, 2011). Once *TERT* expression is achieved the cells will be grown in culture, either stabilisation of or increase in telomere length (TL) is expected in the cell lines with time.

Once the TL is undergoing lengthening or has become stabilised, removal of *TERT* from subcultures will produce isogenic lines with short and long telomere lengths. A schematic diagram of the proposed experimental model system is shown in **Figure 3.1**. To achieve this, *TERT* will be removed by expression of Cre at an earlier and later time point, lines will be grown in parallel, where normal TL attrition would then occur generating “short” and “long” telomere lengths without introducing confounding factors (**Figure 3.1**, Stadler *et al.*, 2011; 2013).

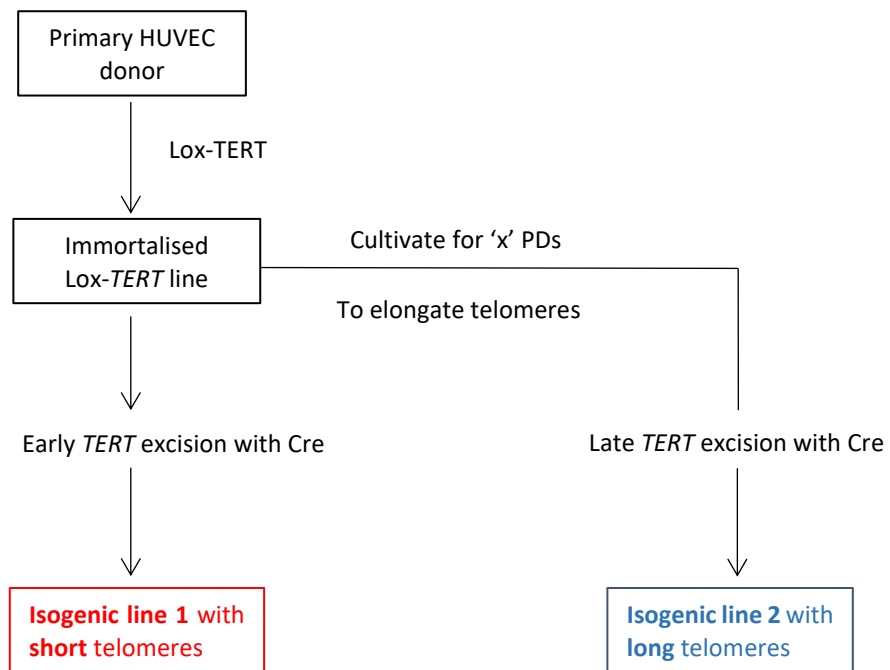
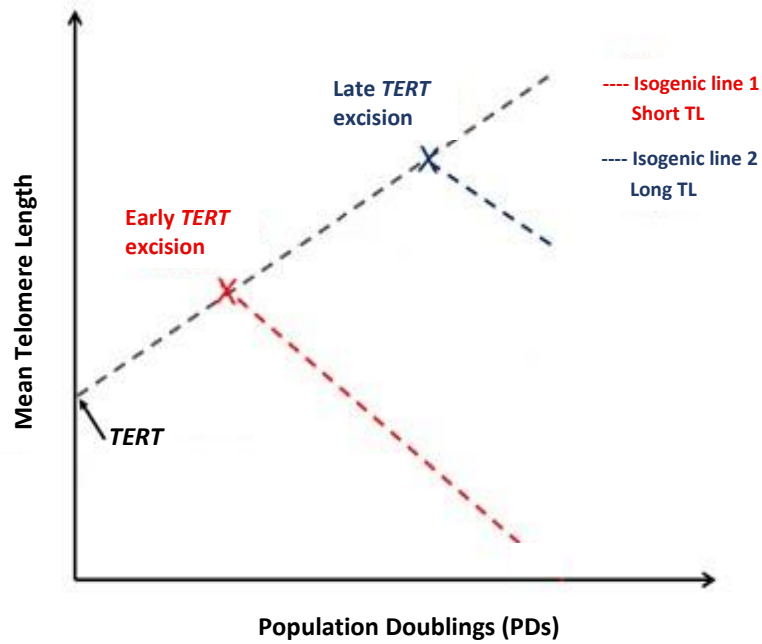


Figure 3.1. Schematic experimental design to show the generation of short and long telomeric isogenic lines from a single immortalised TERT+ HUVEC donor. At time **X** Lox-TERT will be excised by Cre recombinase at an earlier time point to generate an isogenic line with short TL (isogenic line 1). At time **X** Lox-TERT will be excised by Cre recombinase at a later time point to generate an isogenic line with long TL (isogenic line 2). The lines will be cultured for the same length of time therefore no confounding factors are introduced. The only difference between the isogenic lines will be the telomere lengths (Stadler *et al.*, 2011; 2013).

3.2 Methods

3.2.1 Lentivirus Generation

As the nature of this experimental work involves a 2nd generation lentiviral vector system and ultimately genetic modification, safety approval was gained from the Health and Safety Executive. All viral work was carried out according to Class II Biohazard regulations. To summarise, the TERT, GFP and Cre lentiviral particles were generated, titrated and infected into HUVEC according to the detailed methods described previously (**Methods 2.2.2**). A flow diagram of this is depicted in **Figure 3.2**, shown below.

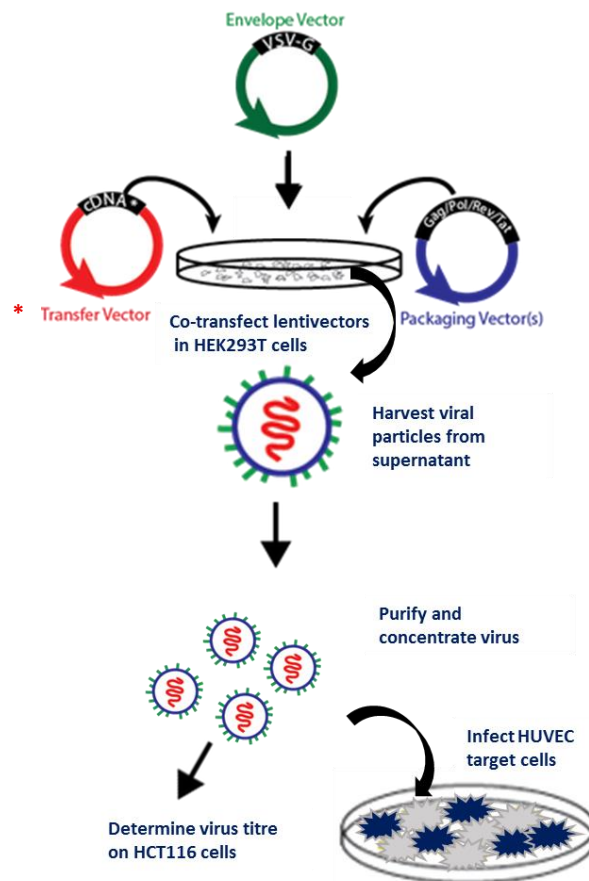


Figure 3.2 Flow diagram to show the process of lentivirus production, concentration, titration and infection into the host cell. The envelope vector pMD2.G, transfer vector *pLox-TERT-iresTK/pLox-GFP-iresTK/pLox-CW-CRE and packaging vector pCMVR8.74, were co-transfected in HEK293T cells using a lipid-based transfection method. The virus was harvested 24, 48 and 72 hours post-transduction. The harvests were then pooled, purified by filtration and concentrated by precipitation (using a polyethylene glycol-based reagent). Once the viral titre was determined, lentiviral particles were infected in HUVEC.

3.2.2 Biological Titration of TERT Lentivirus by quantitative PCR

The titer of a functional lentivector is defined as the number of infectious particles required to transduce a single cell within a defined volume (Barczak *et al.*, 2015; Salmon & Trono 2007). The lentivirus was titrated using a conventional assay based on quantitative PCR. This assay measures the lentiviral copy number stably integrated in the genome of a single target cell of a transduced HCT116 cell line by targeting the Thymidine Kinase transgene within the provirus (Forghani *et al.*, 1991). The methods utilised in this work to titrate the lentivirus were developed by the Trono Lab (**Methods 2.2.6**). Following TERT and GFP lentivirus generation, a test infection of each lentivirus was performed using HCT116 cells to confirm the lentiviruses are functional and viable and to titrate the virus. The titre was calculated using a qPCR based approach with primers targeting the HSV type 1 thymidine kinase (*HSV TK*) transgene present in the viral component of both pLOX-TERT-iresTK and pLOX-GFP-iresTK lentivectors. Absolute quantification was performed on genomic DNA extracted from the transduced HCT116 cells against standard curves generated from known dilutions of the relevant lentivector plasmid DNA. To calculate the number of integrations per cell, quantification of a genomic single copy control, albumin, was performed in parallel, using known dilutions of the pGMT alb plasmid to generate the standard curve. Copy number was then calculated using the following equation:

$$\text{Vector copy number} = (\text{Quantity mean of TK sequence} / \text{Quantity mean of Alb sequence}) \times 2.$$

This equation takes into account the Albumin sequence is present in two copies per genome.

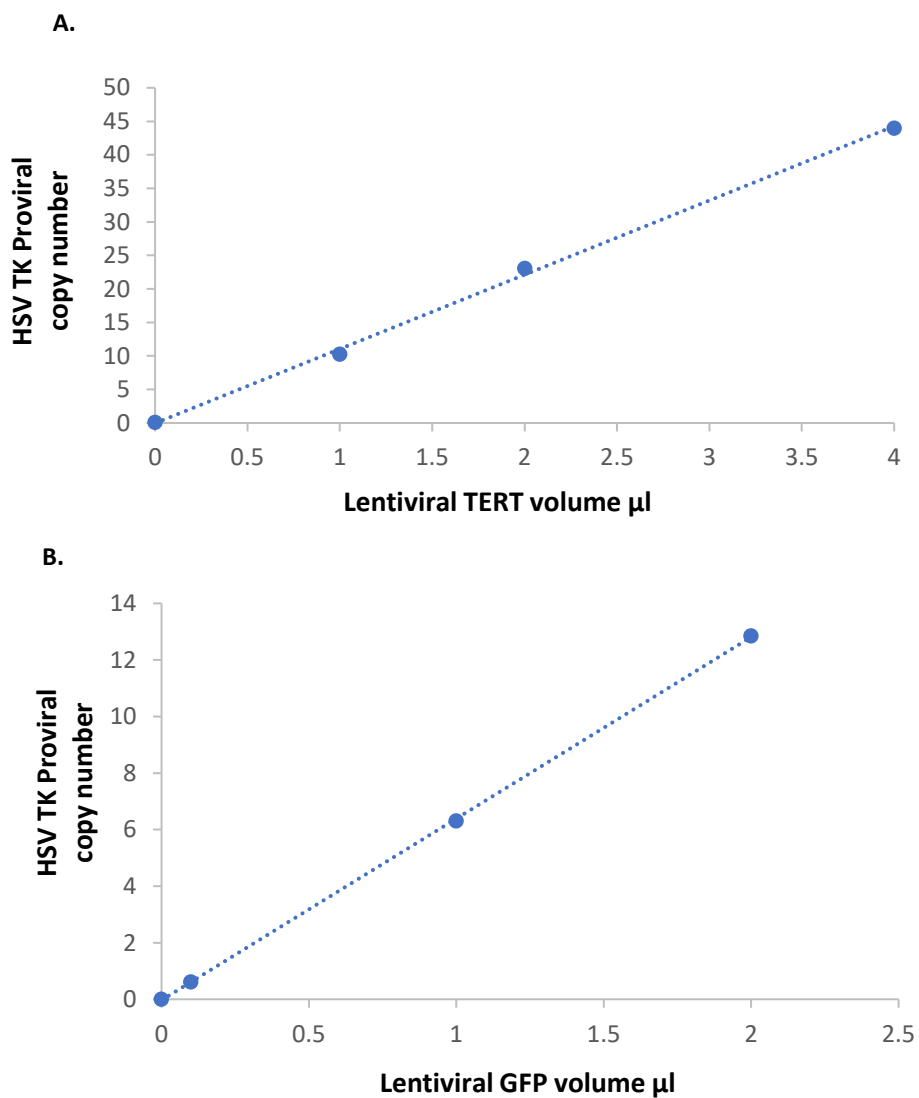
Once the copy number was determined, the lentiviral titre (Transducing Units (TU) per ml) was calculated according the following:

$$\text{Titre (TU/ml)} = \frac{(\text{Number of target cells} \times \text{number of copies per cell of the sample})}{\text{Volume of supernatant in (ml)}}.$$

Multiplicity of Infection (MOI) is defined as the ratio of infectious pseudoviral particles (IFU) to the population of target cells. Using the viral titre, the MOI used for the LV-*TERT* and LV-*GFP* titration was calculated as follows:

$$\text{MOI} = \text{Titre (TU/ml)} \times \text{Volume of lentivirus (ml)} / \text{Number of target cells}$$

The lentiviral generation protocol utilised in this work was efficacious; both the LV-*TERT* and LV-*GFP* pro-viral copy numbers increased with increasing MOI, as shown in **Figure 3.3 A & B**. The lentiviral titration results confirm the pseudoviral stocks are viable; there is a fairly stable titre between the infected doses (**Figure 3.3 C**)



C.

Sample	Lentivirus Volume μl	HSV TK Proviral Copy Number	Titre TU/ml	Multiplicity of Infection (MOI)
-ve Control	0	0.0004	0.02	-
LV- <i>TERT</i>	0.1	10.26	6.97×10^8	1.2
LV- <i>TERT</i>	1.0	23.08	7.85×10^8	14.0
LV- <i>TERT</i>	4.0	43.99	7.48×10^8	26.7
LV- <i>GFP</i>	0.1	0.62	3.69×10^8	0.7
LV- <i>GFP</i>	1.0	6.31	3.79×10^8	6.8
LV- <i>GFP</i>	2.0	12.85	3.85×10^8	13.8

Figure 3.3 Pro-viral copy number, Titre (TU/ml) and MOI for transduced *TERT* and transduced *GFP* lines. Lentiviral (LV) copy number is shown against LV infection doses in transduced HCT116 cells (56,000 cells/sample) for A. *TERT* and B. *GFP*. C. Calculated vector copy number, lentiviral titre and Multiplicity of Infection (MOI) for *TERT* or *GFP* transduced cells using varying multiplicity of infections (MOI). Negative (-ve) control is uninfected HCT116.

Lentiviral Cre Titration

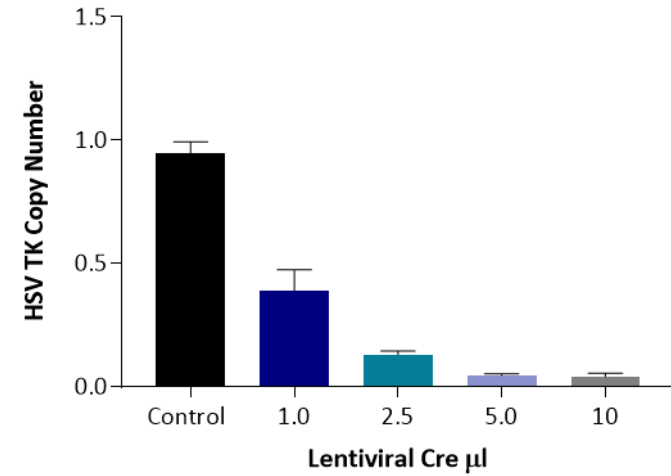
To improve the efficacy of Cre delivery into the HUVEC, the experimental model system in this work utilised a Cre lentivector to govern the excision of the TERT provirus. As the lentiviral Cre is self-excising it would not be possible to calculate titre in the same manner as removal of viral sequence will need to be measured rather than insertion. It was therefore necessary to first generate a HCT116 cell line containing a single copy of the LoxP site. To achieve this, lentiviral GFP was infected in HCT116 cells according to the methods described in **section 2.2.6 (Lentivirus infection of HCT116 for viral transduction)**. Single cell dilutions of the GFP transduced HCT116 cells were plated and grown into clonal cell lines. Positive clones for GFP were selected by fluorescence screening. The total number of positive clones for GFP are shown in **Figure 3.4 A**. HCT116/GFP Clone 4 was taken forward to the Cre titration platform as the integrated pro-viral copy of the *GFP* transgene was closest to a single copy (0.95). The Cre titration was then performed according to the method described in **3.2.2**. In brief, GFP+ clonal cells containing a single copy of the LoxP site were transduced with varying volumes of lentiviral Cre, genomic DNA was extracted from the cells post 72 hours transduction. HSV TK derived vector sequences (specific to the integrated HSV TK transgene) were amplified by quantitative real-time PCR, albumin sequences (specific for the human albumin gene) were used to normalise for the amount of genomic DNA.

The data shown in **Figure 3.4 (A-C)** confirm the LV- Cre viral stocks are functional and viable, showing increased reduction in HSV TK copy number with increasing volume of lentiviral Cre (**Figure 3.4 B-C**). GFP excision is confirmed when adding 5-10 μ l of LV-Cre; this indicates the successful excision of the *GFP* transgene is achieved when the Cre viral stock is diluted at least 1/100. Minor fluctuations in HSV TK proviral copy number are observed in the control (untransduced lines) between the two quantitative PCR assays. The copy number for Clone 4 untransduced cells from the initial screening assay is 0.95 versus 1.19 (**Figure 3.4 A & B**). However, such differences do not significantly impact the Cre titration data.

A.

HCT116/GFP Clone	Calculated Concentration Alb	Calculated Concentration TK	HSV TK proviral Copy Number
1	230000	197000	1.71
2	200000	153000	1.53
3	175000	64800	0.74
4	223000	106000	0.95
5	177000	21200	0.24
6	236000	22600	0.19
7	181000	144000	1.59
8	152000	158000	2.08
9	143000	190000	2.66
10	159000	42500	0.53

B.



C.

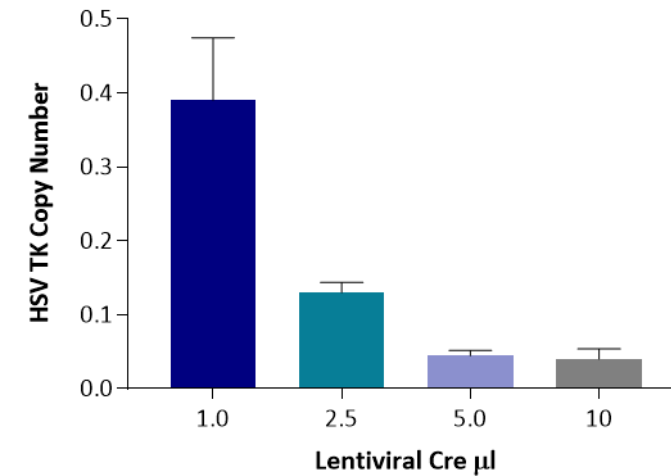


Figure 3.4 HCT116 single cell GFP clone screening and Cre titration using clone 4. A. The GFP proviral copy number for each clone is given alongside calculated *TK* and *ALBUMIN* concentrations derived by absolute quantification (real time qPCR) to calculate vector copy number. B. The HSV TK copy number for clone 4 is shown following transduction with 1-10 μ l of lentiviral Cre (LV-Cre) (n=3 for each dose) or from un-transduced cells (- control). N= 3, mean \pm SD; 0.95 \pm 0.05 (- control), 0.39 \pm 0.08 (1.0 μ l LV-Cre), 0.13 \pm 0.01 (2.5 μ l LV-Cre), 0.05 \pm 0.007 (5.0 μ l LV-Cre) and 0.04 \pm 0.01 (10.0 μ l LV-Cre). C. Due to the substantial difference in HSV TK copy number between the control and Cre transduced cells, proviral HSV TK copy number is shown for the transduced lines (1.0, 2.5, 5.0 and 10 μ l of LV-Cre) only.

3.3 Results

3.3.1 Telomere shortening in HUVEC under standard culturing conditions

Prior to the generation of the Lox-TERT cell lines, it was necessary to first understand important parameters such as the rate of telomere length (TL) decline in HUVEC under standard culturing conditions (37°C/5% CO₂/20% O₂).

The population doubling level is defined as the number of times the cell population has doubled since their primary isolation in-vitro (Hayflick 1961). **Figure 3.5 A** depicts the growth curve of a single HUVEC donor, Line 7, cultivated under standard conditions. The population doublings (PDs) against the number of days the cells were maintained in culture are shown. PDs provides a meaningful estimate on the biological age of the cell population to which telomere length is a marker (Harley & Greider 1990). The average telomere length (expressed as a Telomere/36B4 single copy gene ratio) was determined by RT-qPCR (Cawthon 2002) in the HUVEC (**Figure 3.5 B**). The cells grew steadily up to ~38days at PD 24.4; as reflected by the relatively consistent difference of population doublings (2.0-3.1 PDs) per passage. A gradual telomere length decline can be observed as the population doubling increases. As shown in **Figure 3.5 A & B**, the cellular lifespan of parental HUVEC was 55 days or 31.7 PDs (T/S ratio 1.5), at which the growth curve reaches a plateau. **Figure 3.5 B**). This falls within previous estimates of the finite lifespan of primary HUVEC which can vary between 20 and 60 PDs (Bicknell 1996). These results confirm primary HUVEC undergo a gradual telomere length shortening and the cells stop growing at around 55 days in culture.

Most lentiviral genomes have selectable markers such as an antibiotic resistance gene (e.g Puromycin) or a fluorescent GFP marker (Ben-Dor *et al.*, 2006) to enrich a stable cell population expressing the transgene. The Puromycin resistance gene confers antibiotic resistance to infected host cells. The addition of Puromycin to the growth media of the host cells would kill off any un-transduced cells that have not incorporated the lentivirus. As a result of this, cells that have incorporated the lentivirus survive and can be expanded to create stable lines. In the case of GFP selection, fluorescence activated cell sorting (FACS) can be used to separate live cells expressing GFP, which can then be

expanded into a stable cell line. The pLOX-TERT-iresTK lentivector was chosen for this model, as this plasmid had been successfully used for the reversible immortalisation of primary human cells (via the Cre-Lox system) (Salmon *et al.*, 2000). However, this lentivector does not have a specific selection cassette (e.g antibiotic resistance or GFP tag) to allow for TERT selection, most likely due to the large capacity size of the vector (backbone and insert ~1.3kb **Appendix S1. 2**). As it is not possible using this model to specifically select cells that carry the TERT transgene following transduction, this model relies on non-transduced cells reaching replicative senescence and cell death to eliminate them from the cell population to resulting in a homogenous TERT+ population. Therefore, we expect to see establishment of the Lox-TERT cells after 55 days in culture.

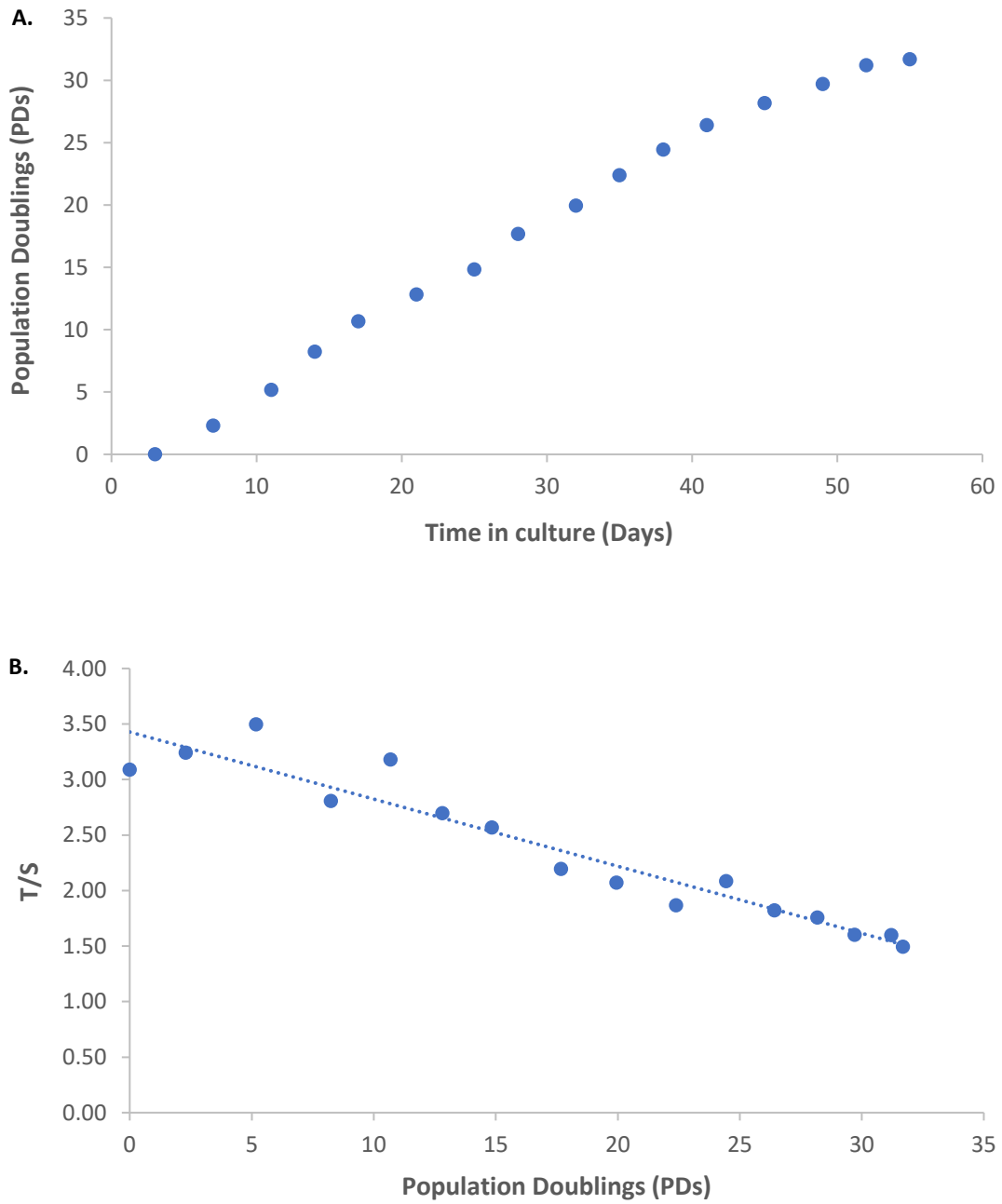


Figure 3.5 Growth curve and telomere length of HUVEC single donor cell Line 7 cultured under standard conditions. A. Population doublings (PDs) are shown against the time in culture (days). A fairly constant growth rate is observed until ~40 days when growth rate slows before stopping at day 55. B. The relative T/S ratio is shown against PDs showing a general decline in telomere length over time in culture.

3.3.2. Generation of a Lox-TERT line

Having established the lifespan of Line 7 the next step was to transduce this line with LV-*TERT*. This was performed according to **Methods 2.2.6 (Lentivirus infection in the host cell)**. As the ability of lentiviruses to infect host cell varies according to the cell type used, three different MOIs were tested (5, 50 and 100). Copy number integration was observed in a viral dose specific manner (**Figure 3.6 A**). For all experimental lines, using the average titre, LV-*TERT* was used to transduce this HUVEC line at a multiplicity of infection of 100 as this gave an integrated copy number close to 1 per target cell. LV-*TERT* copy number in the transduced population was assessed at 8 days post transduction. This showed integration at a copy number of a single copy per cell (**Figure 3.6 B**). It should be noted that this is an average number across the population, with some cells potentially carrying multiple integrations whilst others may be containing none. Expression of *TERT* was seen in the transduced line, the parental (non-transduced cells grown in parallel culture) showed no expression as expected (**Figure 3.6 C & D**). *TERT* expression was quantified relative to the *TERT* expressing K562 lymphoblastoid cell line and was seen to be expressed at high levels (120 fold relative to K562 **Figure 3.6 C**). These findings show successful integration of pro-viral *TERT* and subsequent upregulation of *TERT* in transduced HUVEC.

3.3.3 Growth of TERT+ HUVEC under standard culturing conditions

The HUVEC were grown in parallel with un-transduced control cells under standard culturing conditions (37°C/5% CO₂/20% O₂). As the growth curve depicts (**Figure 3.7 A**), the un-transduced control cells reached a growth plateau after 43 days in culture whereas the TERT+ line continued to grow steadily. To confirm the senescent status, cells were stained for β-galactosidase (β-Gal), the activity of which at pH.6 is a specific marker of cellular senescence (Dimri *et al.*, 1995). During the initial culturing period, both lines showed comparable low levels of β-Gal activity (day 8 Parental 0.8 % versus TERT+ 0.2 % β-Gal+ cells **Figure 3.7 B, C & D**). At day 48 a high proportion of the control cells reached senescence; 78% β-Gal+ cells versus 8% β-Gal+ TERT+ cells (**Figure 3.7 B, E & F**).

A small proportion of senescent cells were detected in the TERT+ lines, due to the line being a mixed cell population. It is possible for senescent cells to remain metabolically active and have a senescence-associated secretory phenotype that can affect the behavior of neighboring cells (Krtolica *et al.*, 2001; Ramirez *et al.*, 2001). In our observations, the effect of the small number of senescent parental cells is almost negligible as the growth curve depicts a stable growing population in the TERT+ line **(Figure 3.7 A)**.

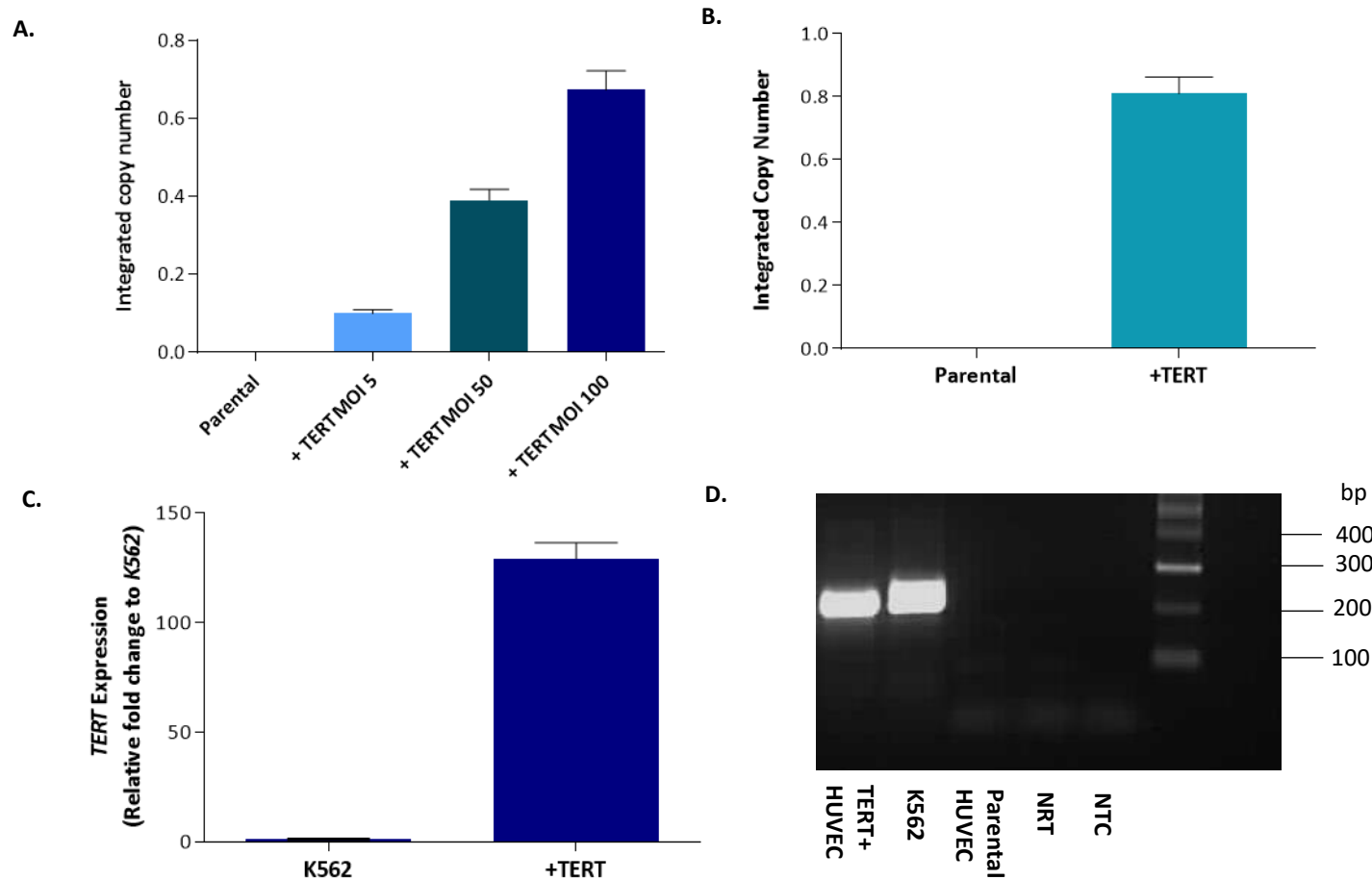


Figure 3.6. Confirmation of *TERT* pro-viral integration and *TERT* expression A. LV-*TERT* copy number (CN) integration in uninfected HUVEC (parental) and Line 7 HUVEC infected with LV-*TERT* at an MOI of 5, 50 and 100. N=3, mean \pm SD; 0.1 \pm 0.01 (MOI 5), 0.39 \pm 0.03 (MOI 10), 0.67 \pm 0.05 (MOI 100). No LV-*TERT* pro-viral copy number was detected in parental HUVEC. B. LV-*TERT* pro-viral copy number integration day 8 post infection of LV-*TERT* at MOI of 100 (0.81 \pm 0.05), as expected no LV-*TERT* copy number was detected in parental HUVEC. C. *TERT* expression (relative to a K562 cancer cell line) at day 8 post infection (1.0 \pm 0.06 K562, 129 \pm 7.3 LV-*TERT*). D. *TERT* qPCR products are shown on a 1.5% agarose gel. *TERT* is expressed in HUVEC infected with LV-*TERT* and the cancer cell line K562 (two bands are observed due to the presence of two splicing variants present in K562). No *TERT* expression is detected in normal HUVEC. No reverse transcriptase (NRT) and no template control (NTC) reactions show no amplification.

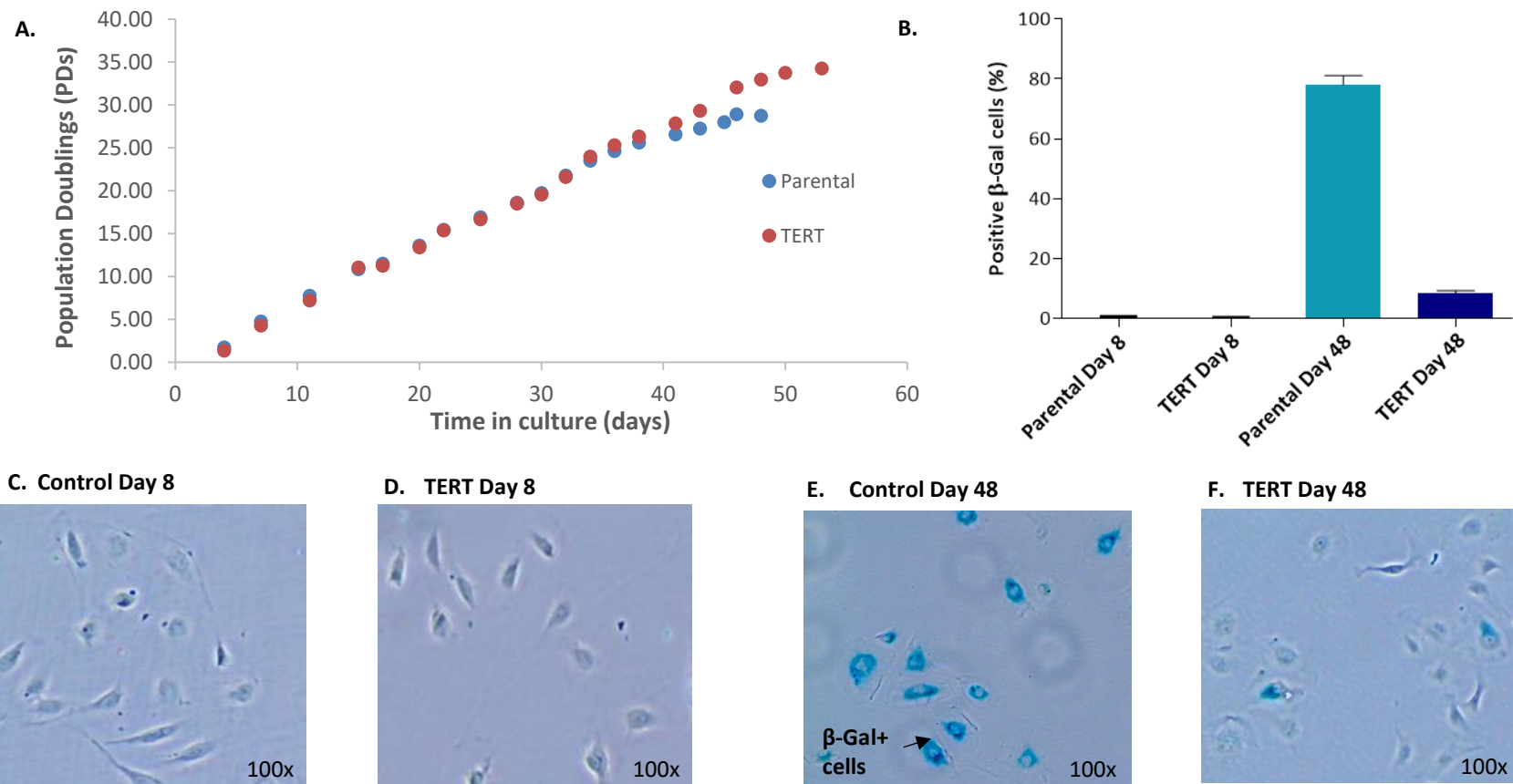


Figure 3.7. Line 7 growth curves and cellular senescence levels for parental (un-transduced) and TERT+ cells, grown under standard culturing conditions. A. Growth curve shows PD vs time in culture. The control cells reach a plateau in growth at ~45 PDs, whereas TERT+ cells continue to grow. B. β-Gal positive cells quantified (n=3) in the parental line (mean±SD; 0.3±0.45) and TERT line (0.2±0.19) at day 8 post LV-TERT infection (C & D) and in the parental line (78.1±3.00) and TERT line (8.3±0.97) at day 48, where the parental cells exhibit growth arrest. E & F. Representative images (100x magnification) of β-Gal staining used for senescence quantification.

3.3.4. Under standard culture conditions TERT is protective against stress induced senescence but does not maintain telomere length

Traditionally, “immortalisation” of cells in culture is defined as growth past 100 PDs (Yang *et al.*, 1999). To achieve this, it was necessary to continue to culture the TERT+ cells for an extended period of time. Although this line was expressing TERT and had continued to grow past the point where the parental cells reached replicative senescence, this line did not reach 100 PDs, with growth slowing and eventually stopping at 49 PDs (**Figure 3.8. A**).

The expectation was in the presence of TERT, the TL in the cells would have increased or at least stabilised due to the activity of telomerase, thereby preventing replicative senescence (**Figure 3.8 B**) (Bicknell 1996). Assessing TL throughout the time in culture, telomere length shortening was observed in the parental line and the cells eventually reached senescence (**Figure 3.8. A and C**). Unexpectedly, the TERT+ line also showed telomere length shortening despite the cell population continuing to grow (**Figure 3.8. A and C**). Premature growth arrest is associated with the upregulation of a cyclin-dependent kinase inhibitor, p16^{INK4A}, and is known to be caused by stress inflicted by prolonged culturing conditions in primary cell lines including endothelial cells (Ramirez *et al.*, 2001; 2003; Herbert *et al.*, 2002). The simplest explanation is the parental cells are undergoing stress-induced rather than replicative senescence and TERT is having a protective effect on the cells which is telomere length independent. TERT is known to be relocated to the mitochondria under conditions of oxidative stress (Haendeler *et al.*, 2009; Haendeler *et al.*, 2004; Santos *et al.*, 2004) and has been shown to be protective with increased mitochondrial function and reduced mitochondrial DNA damage in conditions of mild hyperoxia (Ahmed *et al.*, 2008; Haendeler *et al.*, 2009). Therefore, it is plausible that TERT may be protective, allowing the cells to outlive the parental cells, but immortalisation has not been achieved as this is TL independent.

Standard cell culture is performed at atmospheric O₂ levels of ~20% whereas physiological O₂ is ~3-7% (Decaris *et al.*, 2009). Primary cells grown at 5% O₂ show a 20-50% increase in PDs (Betts *et al.*, 2008; Decaris *et al.*, 2009) suggesting that atmospheric O₂ can induce cellular stress.

One study has shown that over expression of TERT in endothelial cells does not prevent telomere loss in standard culture conditions and TL is maintained when grown at 5% O₂ (Napier *et al.*, 2010). In order to establish the model system, I needed to see either stabilisation or elongation of TL upon TERT upregulation. To mimic physiological cell conditions, Line 7 cell stocks of both the parental and TERT+ line from the earliest passage were revived and maintained in culture at 5% O₂ (37°C, 5% CO₂). As seen under previously under standard culture conditions, the TERT+ cells continued to grow past the point where the parental cells exhibited growth arrest (22.1 PDs, **Figure 3.9 A**) and showed TL measurements similar to control cells until this point. However, after control cells entered growth arrest, TERT+ cells showed an increased and stable growth rate (**Figure 3.9 A**) which corresponds with an observed TL lengthening followed by stabilisation throughout subsequent culture (**Figure 3.9. B**).

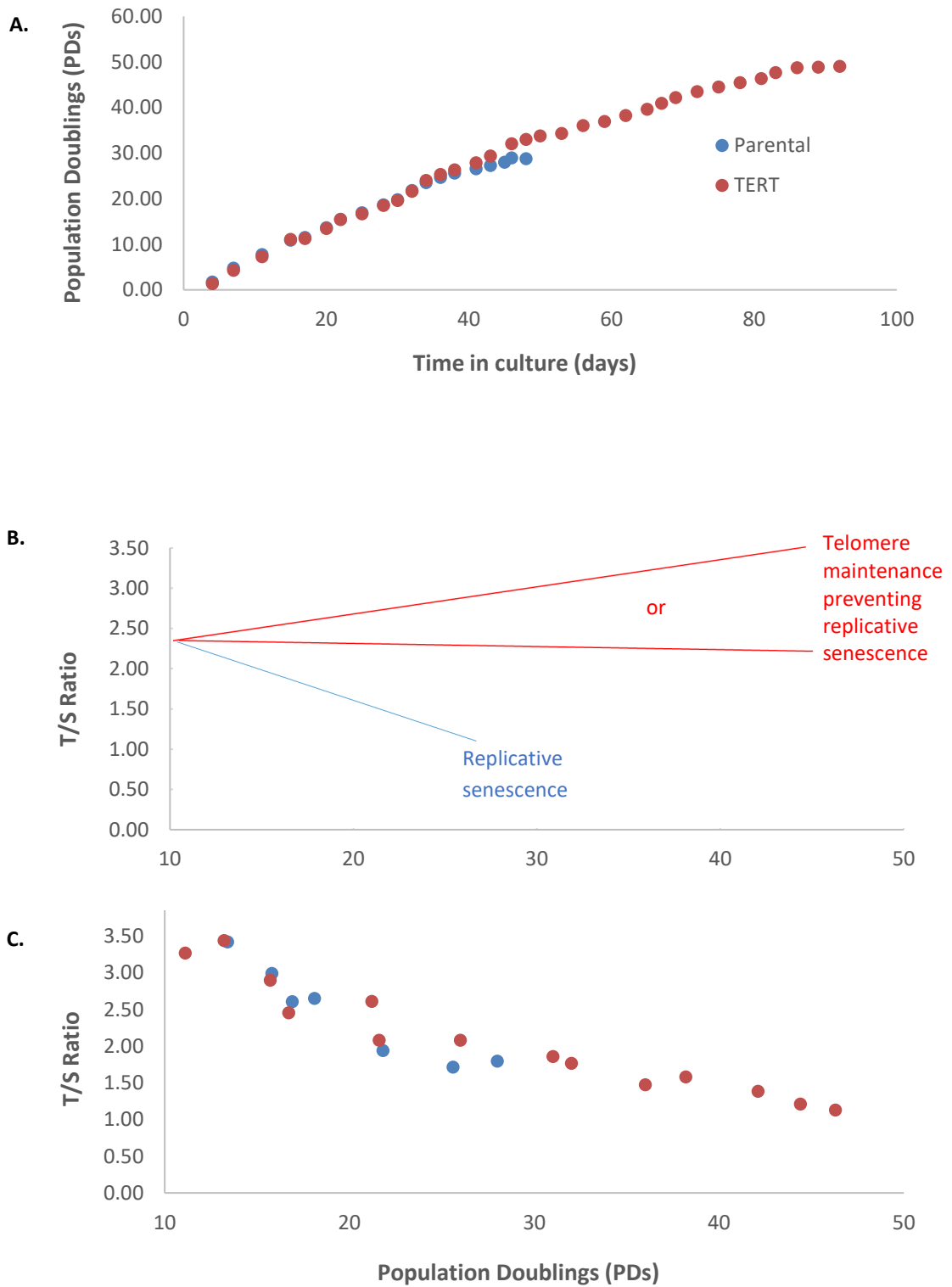


Figure 3.8. Line 7 growth and telomere measurements reveal TERT+ cells fail to immortalise. A. Growth curves for parental (uninfected) and TERT+ cells show slowing and arrest of growth in TERT + cells at 49 PDs. B. Schematic diagram of expected telomere lengths of the TERT+ HUVEC lines. C. Actual telomere length measurements in the TERT+ and control lines, showing that TERT+ cells continue to show attrition during culture and exhibit shorter TL than that observed in control cells at the point of growth arrest

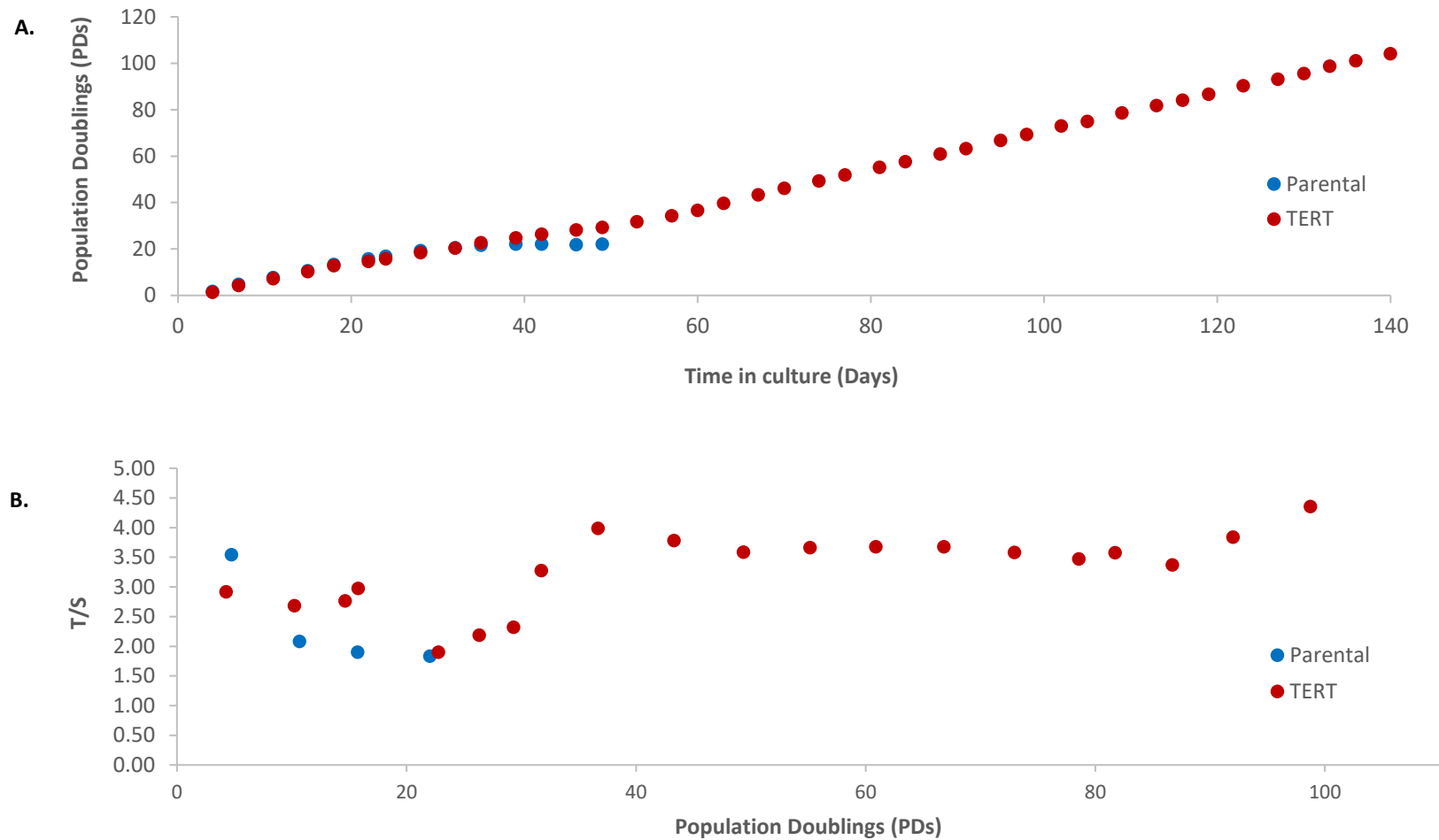


Figure 3.9. Continued growth and TL stabilisation in TERT+ cells grown under 5% oxygen A. Growth curve of TERT+ cells maintained under 5% oxygen reveals an increased, stable growth rate after 30 PDs and the growth of the cells surpassed 100PDs (therefore are deemed immortal). The parental (un-transduced) cells grew for 49 days and underwent 22 PDs. B. Telomere length stabilisation is observed in the TERT+ line maintained in culture under 5% oxygen after 30PDs, coinciding with the observed increase in growth rate. Parental cells underwent a gradual TL decline during the entirety of culture.

3.3.5 Establishment of further Lox-TERT cell lines

Once successful immortalisation of Line 7 was achieved I sought to establish a minimum of two further lines. This would be required in order to ensure downstream experimental data derived from the model were not donor specific.

In total a further 8 additional single HUVEC donors were transduced with LV-*TERT*, all donors were maintained in culture at 5% O₂ (37°C, 5% CO₂). The phenotypic profile of each of the HUVEC donors were determined at the time the cells were isolated, as described in **Methods 2.2.1 Cell Culture**. Of the 8 lines, 5 failed to immortalise, showing that despite previous success, creating further lines was not guaranteed and that limitations to this approach existed and further optimisation of this model is required for future work. First the 5 lines where immortalisation was not achieved will be discussed followed by the 3 lines which were successful.

To validate the model it was important to assess the growth kinetics, *TERT* pro-viral integration and *TERT* transgene expression in the unsuccessful donors. As shown in **Figure 3.10. A**, none of the failed immortalised lines grew long enough to surpass 100PDs. Two of the lines, Line 3 and 8 failed to outgrow the parental cells (**Figure 3.10. A**) despite the presence of *TERT* (**Figure 3.10. C**) at 114 fold and 39 fold relative to K562 respectively. In such cases, although *TERT* is being expressed, due to clonal succession, the un-transduced cells within the mixed population are outgrowing the *TERT*⁺ cells (Kay 1965; Martin *et al.*, 1993). One possible explanation is that inadvertently the line may have grown clonal within the resulting mixed *TERT*⁺ population. To address this issue, attempts were made (at the time of *TERT* transduction) to try and grow the EC to clonal *TERT*⁺ line. This approach has failed; EC are a notoriously difficult cell type to seed to a single cell dilution or even at low confluency due to contact inhibition (Noseda *et al.*, 2004).

Differences in *TERT* expression between the failed lines are observed, Lines 8 and 9 show an adequate *TERT* pro-viral copy number (**Figure 3.10. B & C**) however compared to the other HUVEC donors, lower *TERT* expression. Reduced transgene expression could

be due to epigenetic modifications such as the DNA methylation of CpG-rich regions within the provirus, particularly the CMV promoter region (He *et al.*, 2005; Kong *et al.*; 2009). Furthermore, the stable insertion of the provirus can have a significant impact on transgene expression. For example, in a cell population with an integrated copy number of >1 copy per target cell, such as the TERT+ line observed in Line 4 (**Figure 3.10. C**). insertional mutagenesis and subsequent transgene instability can occur (Lui *et al.*, 2008). As subpopulation of cells undergo subsequent divisions, cells transmit this genetic information, thereby with time it is possible for a loss of transgene expression (Christodoulou *et al.*, 2016). To investigate this, TERT expression was monitored in the Line 4 TERT+ line at numerous passages throughout the entirety of its culture. As shown in the quantitative data (**Figure 3.11**), *TERT* expression was lost during subsequent passaging of the cells up to day 106. This progressive loss of *TERT* expression coincides with the growth curve which eventually reaches a plateau (**Figure 3.10 A**).

Substantial *TERT* expression was observed in Lines 3 and 6 (**Figure 3.10 A and C**), despite this both lines failed to immortalise. To check the failure of these cells is TL dependent, this was explored in Line 6 (as this TERT+ grew longer in culture) (**Figure 3.12 A and B**). Progressive TL shortening was observed in the TERT+ line. Due to insufficient time, telomerase activity was not determined Line 6, but the TL measurements show telomere lengths are not being maintained in these cells despite the presence of *TERT* (**Figure 3.10 C**). *TERT* may have been inhibited by post-transcriptional regulators such as endogenous miR-128 which inhibits telomerase activity by directly targeting two sites within the coding sequence of *TERT* mRNA (Guzman *et al.*, 2018). This may part explain how there is a substantial upregulation in *TERT*, however telomerase is not able to function to meet the needs of TL length maintenance.

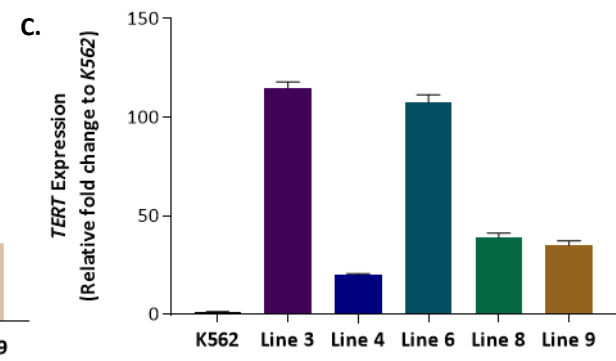
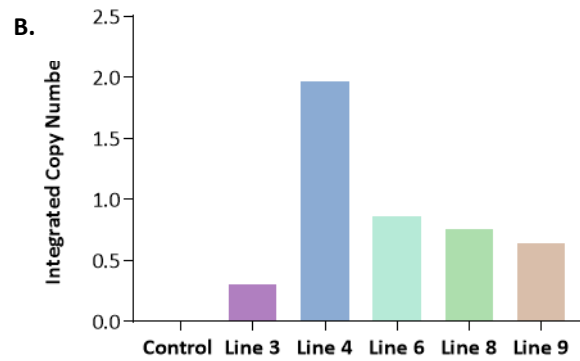
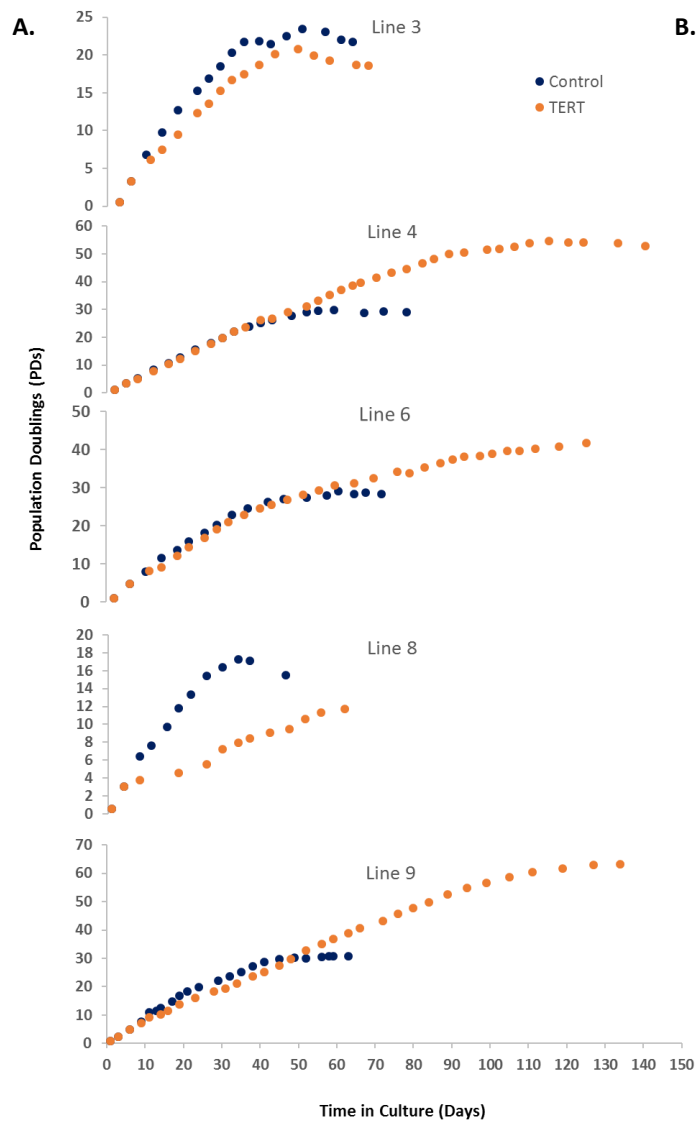


Figure 3.10. A. Growth curves, TERT pro-viral integration data and TERT expression for Line 3, 4, 6, 8 and 9 parental (uninfected) and TERT+ cells showing a failure to immortalise the HUVEC lines. A. Single donor HUVEC growth curves grown under 5% oxygen B. Integrated TERT pro-viral copy number (derived by absolute quantification) is shown for Lines 3, 4, 6, 8 and 9 infected with LV-TERT (MOI of 100) alongside an uninfected control. C. TERT transgene expression (n=3) in Lines 3, 4, 6, 8 and 9 determined using comparative quantification against the telomerase positive cancer cell line K562 (mean±SD; K562 1.0±0.02, Line 3 114.7±3.28, Line 4 20±0.70, Line 6 107.5±3.93, Line 8 39.12±2.20 and Line 9 35.03±2.29 TERT expression relative fold change to K562). All samples were normalised to a 36B4 housekeeper gene. Integrated TERT pro-viral copy number and TERT expression were determined at Day 8 (Lines 3, 6 and 9), Day 19 (Line 4) and Day 28 (Line 8) post LV-TERT infection.

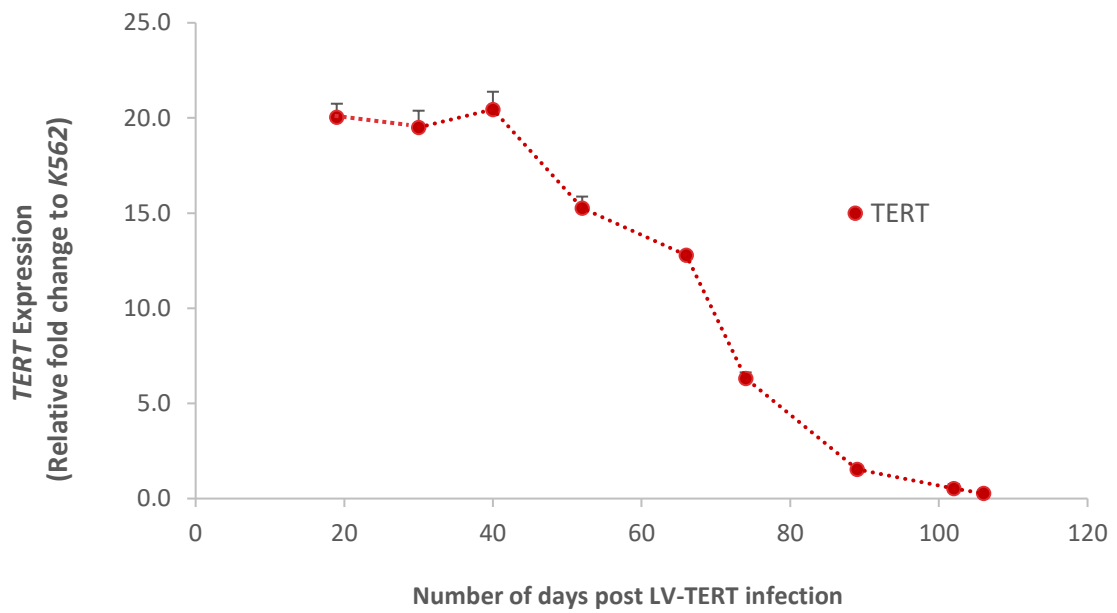


Figure 3.11. Failure to immortalise HUVEC (loss of *TERT* expression). Line 4 *TERT* expression levels relative to *K562* determined by RT-qPCR from Day 19 post LV-*TERT* infection to Day 102. A progressive loss of *TERT* expression was observed during prolonged culturing of the line. Mean±SD; Day 19 20±0.71, Day 30 19.5±0.88, Day 40 20.5±0.93, Day 52 15.3±0.61, Day 66 12.8±0.17, Day 74 6.3±0.32, Day 89 1.5±0.00, Day 102 0.5±0.24 and Day 106 0.3±0.01 *TERT* expression relative fold change to *K562*.

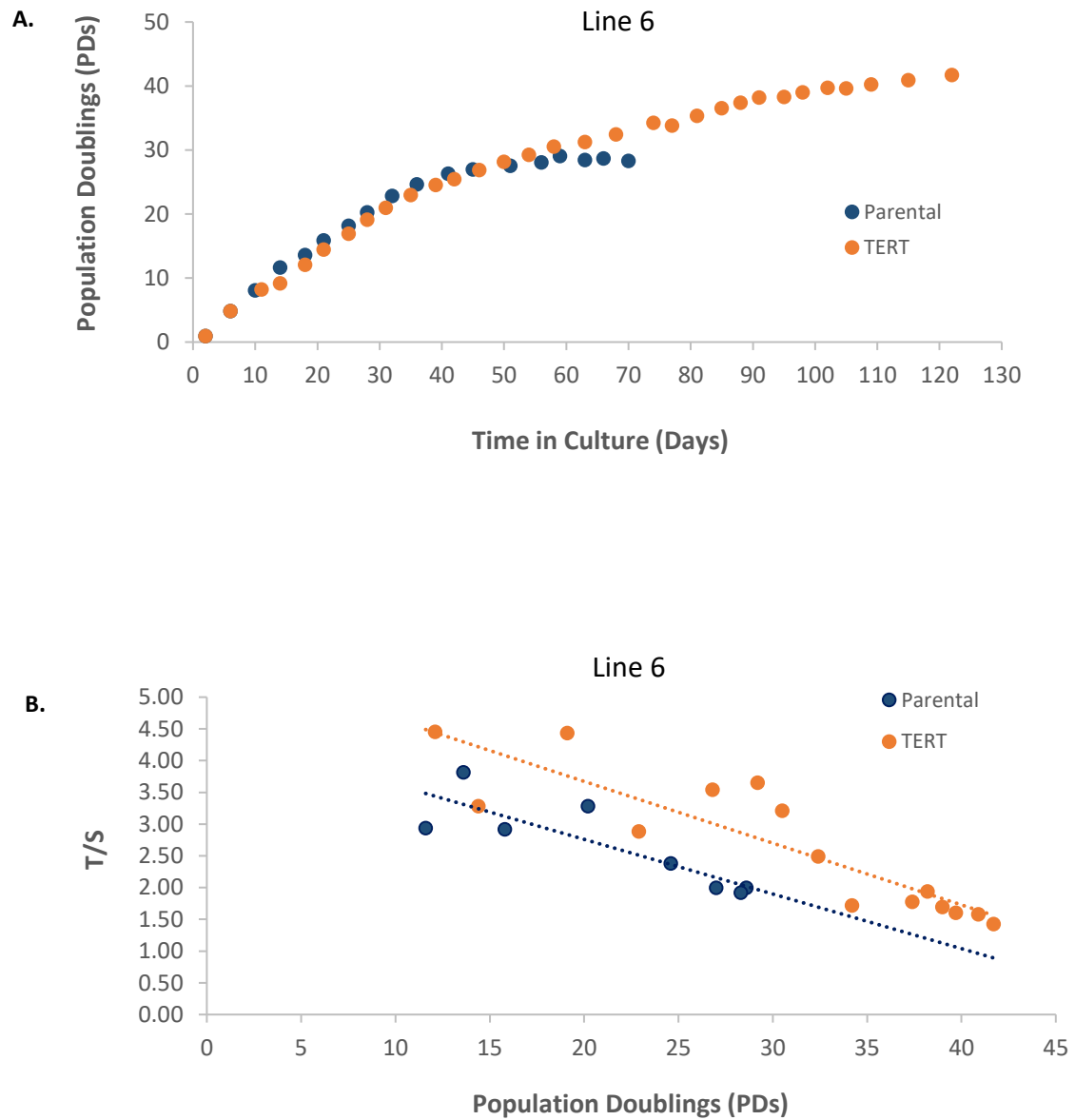


Figure 3.12. Failure to immortalise HUVEC (telomere length shortening in the TERT+ line)
 A. Line 6 Growth curve and B. Line 6 telomere length measurements across the culture from Day 18 (post LV-TERT infection) to Day 122. As the growth of the cells eventually reached a plateau at Day 74 (34 PDs) the telomere lengths continued to shorten.

3.3.6 Successful Immortalisation of HUVEC using human TERT

Improved Growth Kinetics and bypass of replicative senescence

If we look at the growth kinetics of the successful HUVEC lines over time (**Figure 3.13. A**), TERT+ cells in four lines (Line 1, 2, 7 and 10) showed a marked extension in growth and surpassed 100 PDs, so were deemed as immortalised HUVEC (iHUVEC). All of the lines showed successful pro-viral *TERT* integration (**Figure 3.13. B**) and *TERT* expression (**Figure 3.13. C**). In the 4 immortalised lines, the addition of TERT increased the replicative lifespan of these cells by >70 PDs (**Figure 3.13. A**) compared to un-transduced parental cells. There are differences in the finite replicative lifespan of each of the un-transduced control lines, with Line 2 growing the longest for 85 days (reaching a maximum population doubling of 43). As the HUVEC are derived from different donors, these differences could be due to the basal TL and rate of telomere attrition (as further discussed later in this section). As time progressed all lines showed a linear growth rate with minimal senescence levels, in contrast the uninfected control cells which eventually stopped growing at 19.7-41.0 PDs and became senescent (**Figure 3.14 A and B**).

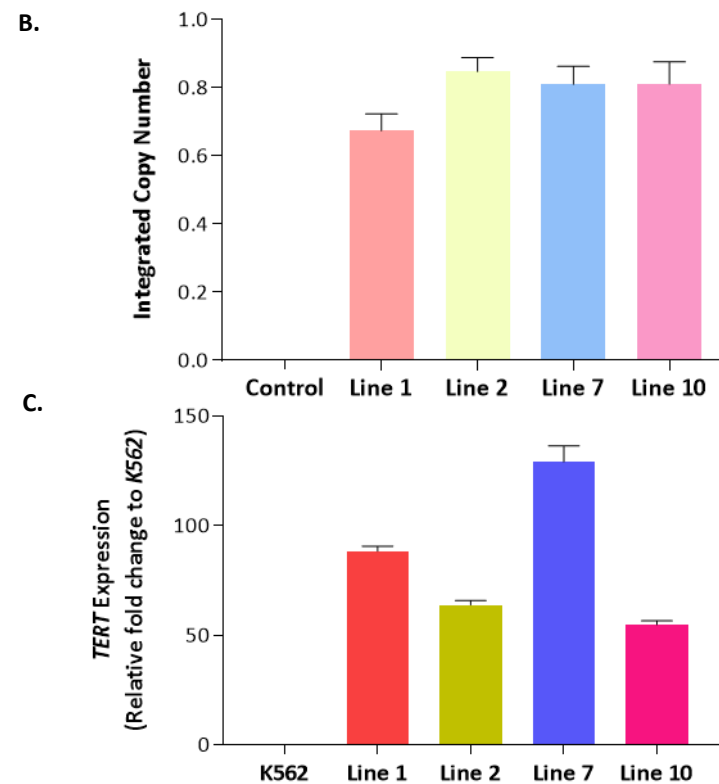
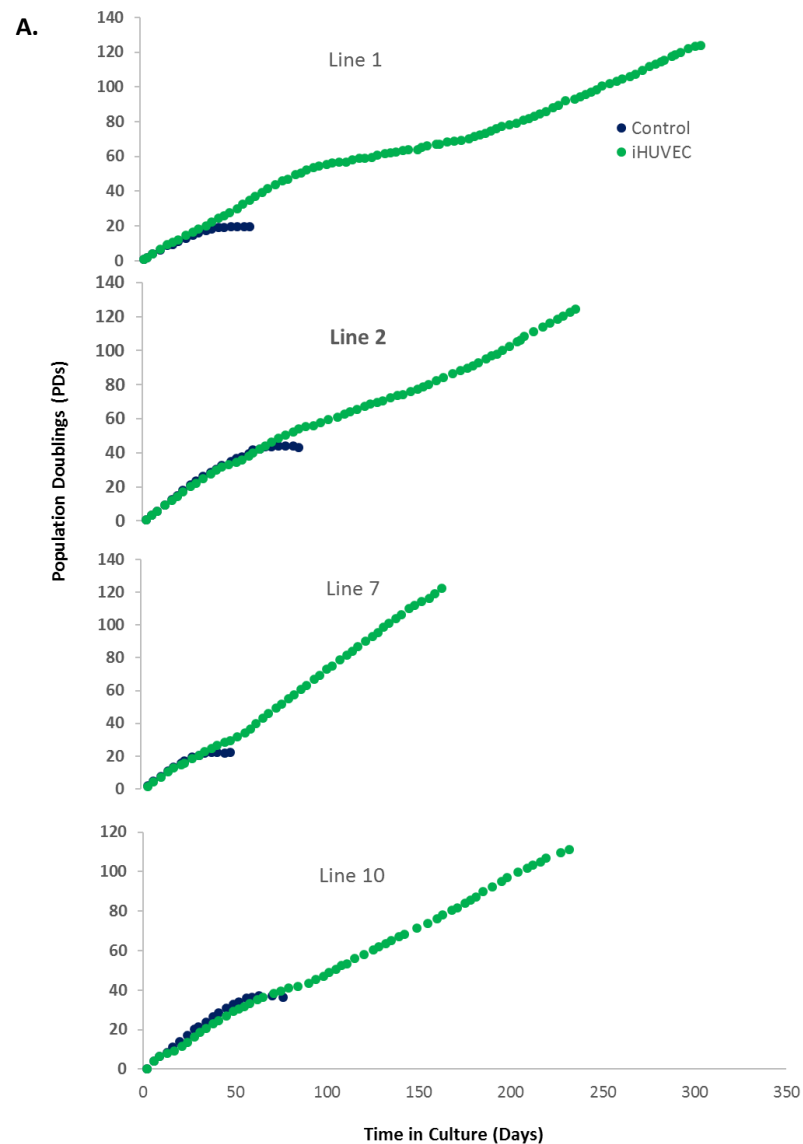


Figure 3.13. Successful immortalisation of four HUVEC lines. A. Growth kinetics of parental (un-transduced) HUVEC and immortalised HUVEC (iHUVeC) in Line 1, 2, 7 and 10 (grown under 5% oxygen). LV-*TERT* was transduced in all lines between Day 10 and 12. B. Integrated pro-viral *TERT* copy number (CN) determined by RT-qPCR (mean \pm SD; Line 1 0.67 \pm 0.05, Line 2 0.85 \pm 0.04, Line 7 0.81 \pm 0.05 and Line 10 0.81 \pm 0.07 CN). C. *TERT* mRNA expression determined by RT-qPCR (Line 1 88.4 \pm 2.27, Line 2 64.0 \pm 2.02, Line 7 129.1 \pm 7.3 and Line 10 54.9 \pm 1.79 *TERT* expression (relative fold change to K562)). Both the integrated copy number and *TERT* expression were determined in the lines 8 days post LV-*TERT* infection.

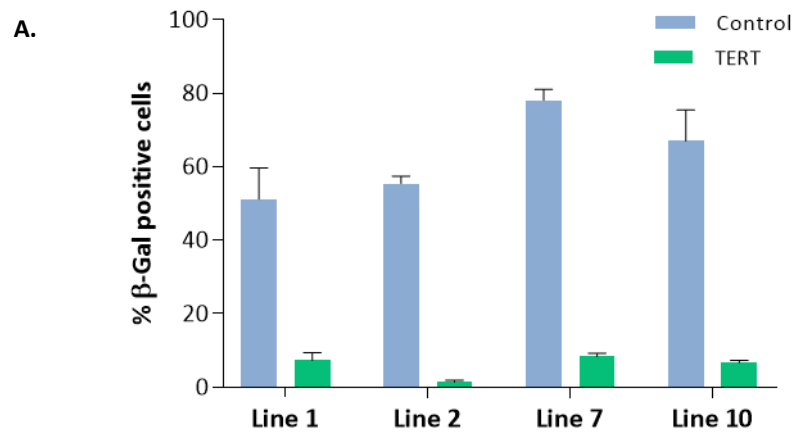
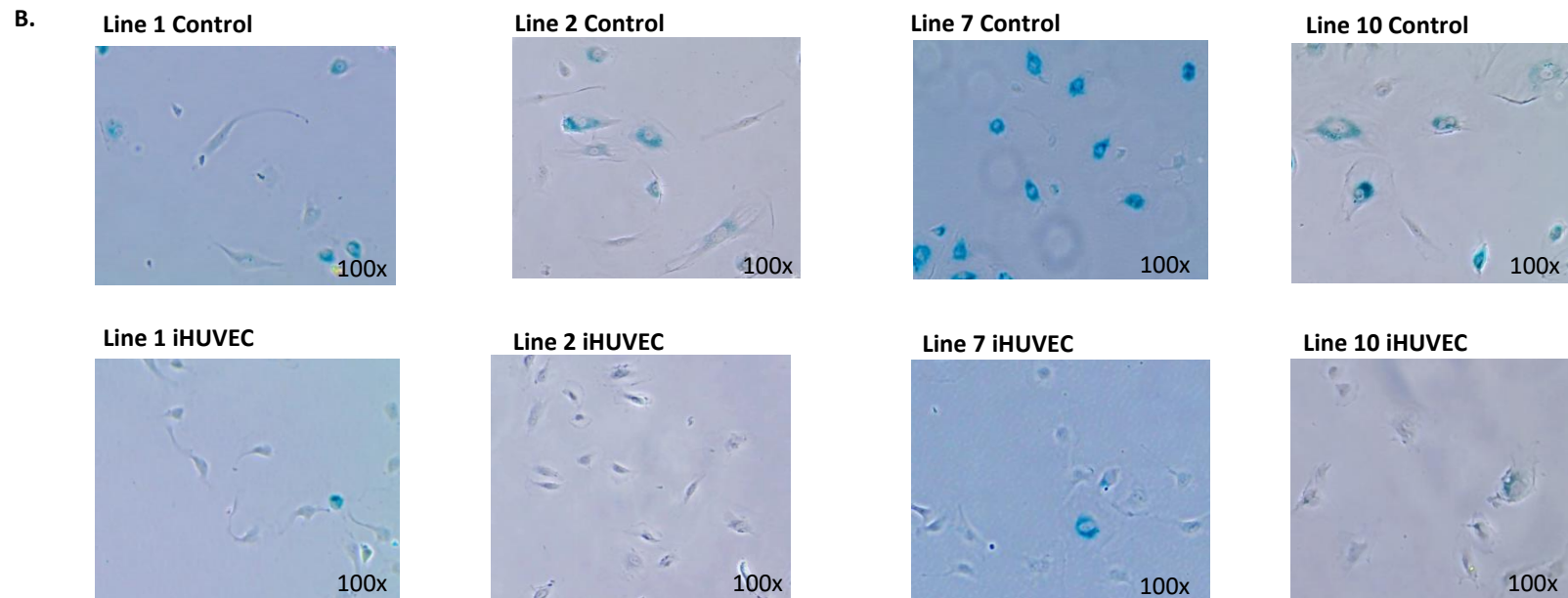


Figure 3.14 Immortalised HUVEC bypass senescence A. Quantification of β -Gal positive senescent cells in parental and iHUVEC lines (n=3) at the point where parental cells enter growth arrest (Day 60 post LV-*TERT* infection in Line 1 (51.2±8.6 Parental versus 7.3±2.2 TERT), Day 82 in Line 2 (55.5±2.0 Parental versus 1.5±0.5 TERT), Day 43 in Line 7 (78.1±3.0 Parental versus 8.3±1.0 TERT) and Day 76 in Line 10 (67.1±8.4 Parental versus 6.7±0.7 TERT). B. Representative images (taken at 100x magnification) of β -Gal staining used for quantification.



Detection of High Telomerase Activity

TERT is the rate limiting catalytic component of the telomerase enzyme (Kim *et al.*, 1995), as we know *TERT* is expressed in the iHUVeC lines, experimental work was performed to verify telomerase is active. A PCR-based telomerase activity (Feng *et al.*, 1997) detection assay known as TRAP (Telomeric Repeat Amplification Protocol) was performed according to the methods described in **2.2.6 Telomerase Repeat Amplification Protocol**. The concept involves a simple two-step process, firstly telomerase adds the nucleotides 'AG' in addition to a number of telomeric repeats (GGTTAG) onto the 3' end of a substrate oligonucleotide (TS). The products are then amplified by PCR using the telomerase substrate and reverse primers.

A ladder of telomerase products with 6 base increments starting from 50 nucleotides is detected in the telomerase positive K562 control and in Lines 7, 1 and 2 and 10 showing telomerase activity in the iHUVeC (**Figure 3.15 A**). For all the lines of interest, cell equivalents (from 2500, 500 and 100) were serially diluted, the amount of telomerase products (intensity of the bands) reflects this cell dilution in Line 7, 1 and 2. No differences were observed between the 2500, 500 and 100 cell equivalents in Line 10 due to technical differences in loading the cell lysates. As expected, no telomerase activity was detected in parental HUVEC. In all the iHUVeC lines, the level of telomerase product in the iHUVeC lines was remarkably higher compared to the telomerase positive cancer cell line K562, this finding corresponds to the substantial TERT expression (relative to K562) in these lines (**Figure 3.13 C**).

Between the iHUVeC lines, at 2500 cell equivalents varying intensities of the telomerase products can be observed. To further investigate this, the relative telomerase activity % (RTA) was quantified by calculating the total product generated per reaction using densitometry. RTA varied between donors (**Figure 3.15 A and B**) with the highest RTA in Line 10 and lowest in Line 1. The difference in telomerase activity between donors gives an idea of the TERT making it into the telomerase complex versus TERT being sequestered elsewhere (Blackburn 2005).

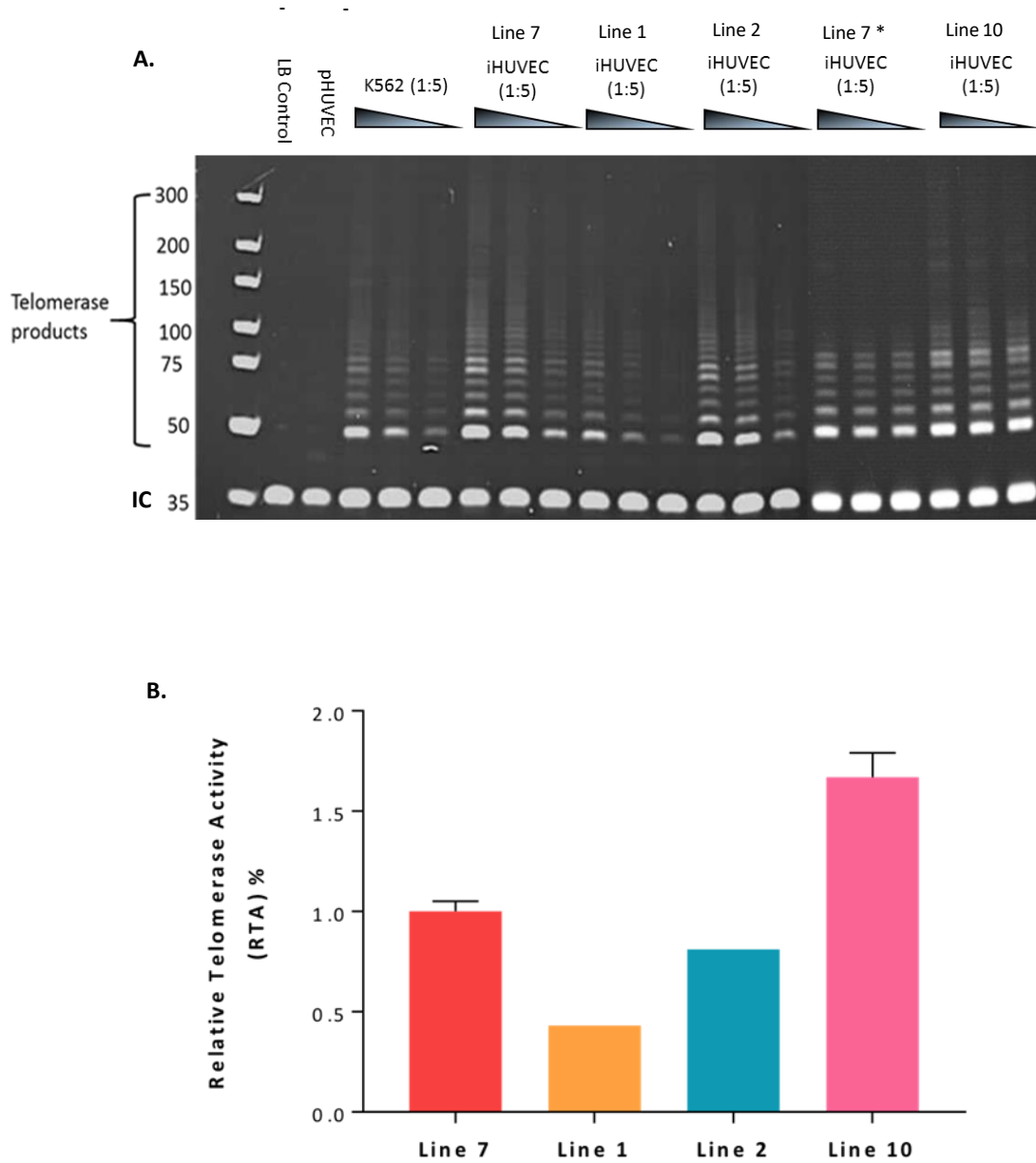


Figure 3.15 Telomerase Activity in iHUVCEC. A. Telomerase activity detected in the whole cell lysates of control parental HUVEC (-) (pHUVEC) telomerase positive cell line K562 (+), iHUVCEC cell Lines 7, 1, 2 and 10 at 2500, 500 and 100 cell equivalents. An assay negative control (Lysis Buffer only, LB) was also included. Line 7* and 10 were run on a separate gel, hence Line 7 is shown twice. The 35bp internal control (IC) is present for every lane to monitor PCR inhibition and serves as a control for amplification efficiency for each reaction. B. Quantitative analysis determined using densitometry. Relative telomerase activity in whole cell lysates of Line 7, Line 1, Line 2 and Line 10 iHUVCEC expressed as a % normalised to Line 7 at 2500 cell equivalents. Line 7 1.0 ± 0.05 (n=2), Line 1 0.43, Line 2 0.81, Line 10 1.67 ± 0.12 (n=2).

Growth rates and Telomere Length stabilisation

As telomerase activity was confirmed, next the TL was measured throughout the entirety of both the parental and iHUVeC lines in culture. TL stabilisation was confirmed in all the iHUVeC lines, compared to TL shortening in the parental cells of all lines.

In the parental cells the basal TL and subsequent TL shortening between individual donors varies considerably, it would make sense that because of this parental cells for each of the lines would reach replicative senescence at different population doublings depending on the rate of TL shortening (**Figure 3.16**). If we look at the TL measurements for parental Line 1, you would expect the cells to reach replicative senescence faster based on a faster telomere attrition (**Figure 3.16**). However, this is not quite reflected in the growth rates for this donor. Comparison of the TL shortening in the parental cells of all donors shows a greater drop in TL is observed for Line 7 parental from 5-16 PDs (T/S 3.54 to T/S 1.90), which explains replicative senescence observed 17 days earlier compared to Line 1 (**Figure 3.16**). This could be due to a number of reasons, the telomere assay used in this study measures average TL in a cell rather than an individual TL per chromosome *per se*. Whilst we assume that TERT will extend the shortest telomeres and create relatively homogenous TLs across the chromosomes within each cell, this was not investigated. Therefore senescence could have been triggered by individual chromosomes reaching a critical TL, although the average TL may be higher. Individuals may also maintain their TL differently based on genetics, leading to variance in attrition rates.

Interestingly, the level of TL stabilisation between the four donors varied and this corresponds with the level of telomerase activity detected (**Figure 3.1.5 B and 3.16**). In Lines 2, 7 and 10 TL look promising for the generation of isogenic lines, the iHUVeC were stabilised at a high level and the growth rate of the cells were maintained at ~2.2-2.6 PDs between each passage (**Figure 3.16**), thus allowing Cre excision and subsequent growth and TL attrition to generate isogenic lines with different TL.

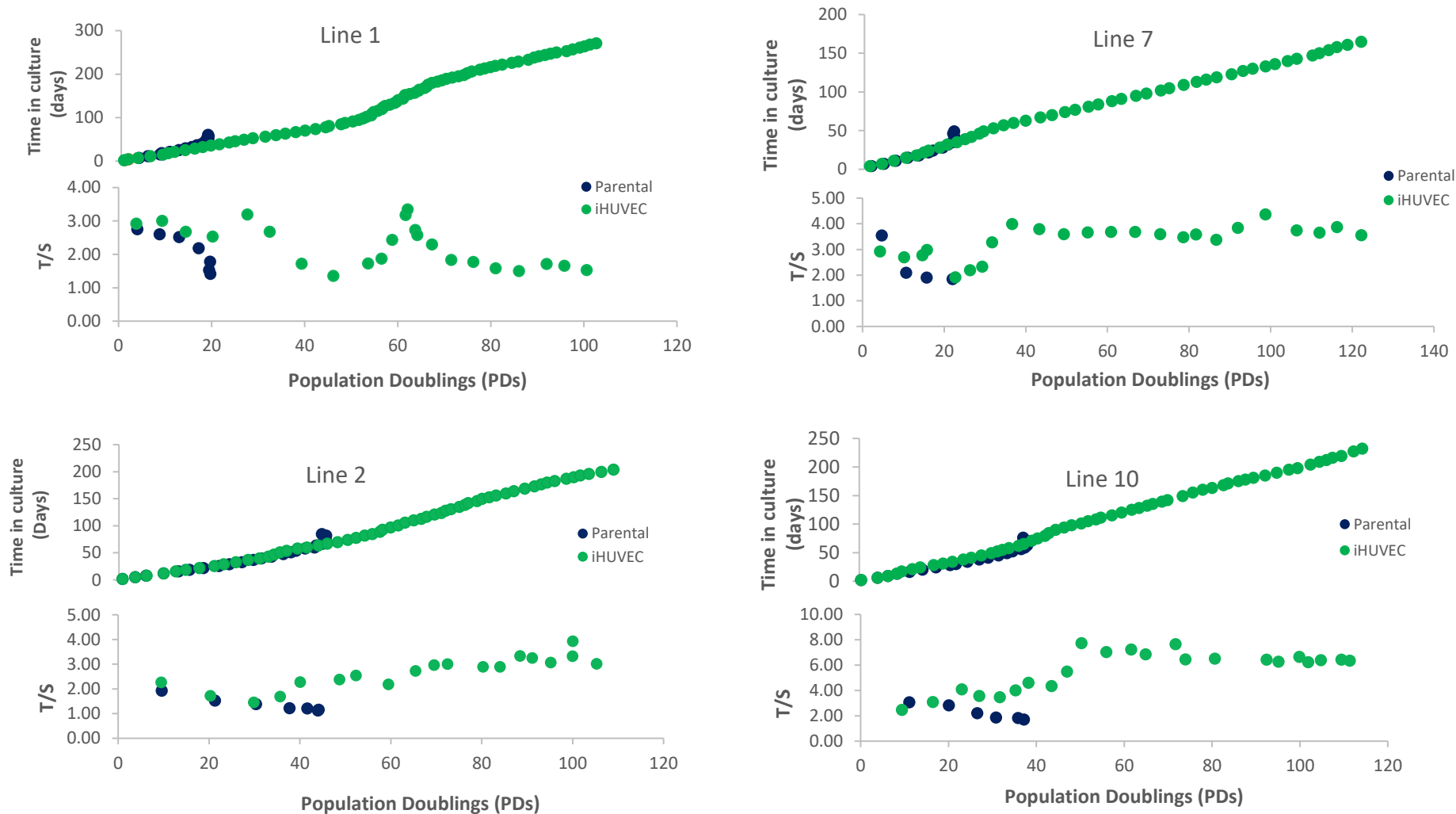


Figure 3.16 Growth rates and telomere length measurements for control (uninfected) and iHUVeC. Growth kinetics (the accumulative population doublings (PDs) against the time in culture) of parental (un-transduced) HUVeC and immortalised HUVeC (iHUVeC) in Line 1, 2, 7 and 10 (grown under 5% oxygen) are shown. Telomere lengths were measured (by RT-qPCR) throughout the entirety of the culture for each of the donors.

The telomere length dynamics of the iHUVeC reflects the growth rates, for example in Line 1 iHUVeC at 46 PDs the TL in this line increased from T/S 1.36 to its peak of 3.34 (**Figure 3.16**), increase growth rate was also detected. Although these cells have surpassed 100PDs and continued growing in culture, from the point at which the TL stabilise at a low level, the growth rate of the cells is reduced. To understand why Line 1 iHUVeC stabilised with a short telomere length, the expression of *TERT* from cells at 103 PDs was determined. **Figure 3.17** shows a 67-fold loss of *TERT* expression at mRNA level in iHUVeC (261 days post LoX-TERT transduction) compared to early TERT transduced cells (10 days post LoX-TERT transduction).

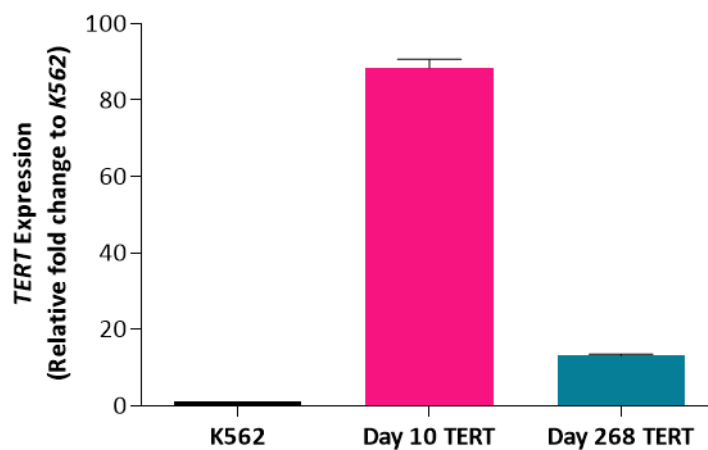


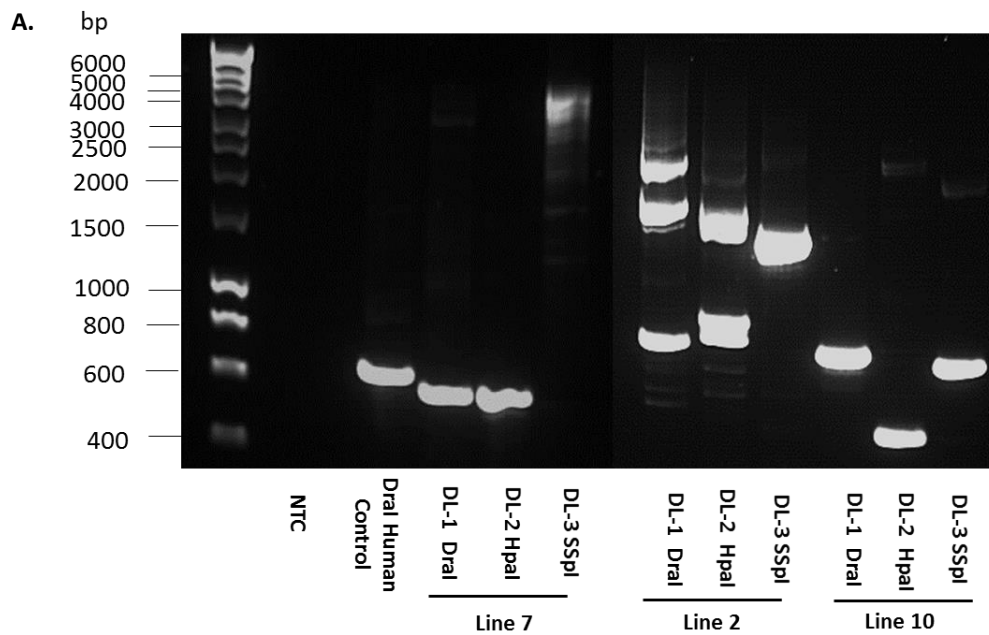
Figure 3.17 *TERT* mRNA expression in Line 1 cells transduced with LV-TERT at Day 10 (6.3 PDs) and Day 261 (103 PDs). *TERT* expression is quantified using real-time quantitative PCR (RT-qPCR) and is shown as the relative fold change to K562. *TERT* expression decreased in the Line 1 cells from Day 10 to Day 268. Mean ± SD; K562 0.98 ± 0.02, Day 10 TERT 88.4 ± 2.3, Day 268 TERT 13.1 ± 0.4 *TERT* expression (relative fold change to K562). For RT-qPCR of *TERT* expression, each sample was assayed in triplicate (n=3).

Due to the loss of *TERT* expression and the low level of TL stabilisation in the Line 1 iHUVeC this line was no longer taken forward. Had there been more time to investigate this, I would need to check whether this is a donor specific effect, an effect of the insertion site(s) or whether this was a random occurrence. Cells would need to be re-grown in culture from an earlier passage to see if the lines stabilised low again or whether it would be possible for the cells to stabilise at a higher TL. Day 32 (20 PDs) would be an ideal point to revive the cells as I observed a more linear growth and the average TL was maintained by telomerase at a high level.

Pro-viral Integration Analysis

As successful immortalisation has been achieved it is important to assess where the *TERT* transgene has been integrated into the genome. As lentivectors randomly insert into actively transcribing units of the host genome, endogenous gene expressions may be disrupted (Desfarges & Ciuffi 2010), therefore it is necessary to characterise the insert sites. Upon LV-*TERT* infection, initially there is a mixed population of both parental and *TERT*⁺ cells. After extended culture it can be assumed that any *TERT*^{-ve} cells have undergone cell death and therefore have been removed from the population. In terms of cell dynamics in culture, it is questionable whether the iHUVeC population remain heterogenous or have unintentionally become clonal during the prolonged culturing period. A clonal cell population within the iHUVeC could be a potential implication to this model system. For example, if the pro-viral *TERT* has narrowed to a single integration then there may be a one or two insertion points of *TERT* incorporated within the cell which may be detrimental to the cell. This could explain the effects seen previously in the unsuccessful HUVEC lines (**section 3.3.5 Establishment of further Lox-*TERT* lines**). One of the disadvantages of introducing a gene via the lentiviral gene transfer system is a single integration could lead to changes in the expression of another gene, which could then be responsible for any phenotype observed, rather than *TERT*. Therefore, it was next sought to characterise the *TERT* pro-viral insertion site(s) of Lines 2, 7 and 10 iHUVeC to better understand whether such changes are being observed in this model.

Lines 2, 7 and 10 iHUVeC were assessed for sites of *TERT* integration using the methods described in **methods 2.2.6 (Integration Site Analysis)**. In brief, viral integration libraries consisting of adaptor-ligated genomic DNA fragments were constructed from the *TERT* transduced HUVEC population using specific restriction enzymes (DraI, SspI and HpaI). The region of genomic DNA flanking the 5' end of the viral integration site(s) were amplified by primary PCR and a secondary 'nested' PCR. **Figure 3.18 A** shows the results of the nested PCR reaction for each of the viral integration libraries. PCR products were then excised from the gel and directly sequenced and analysed using NCBI BLAST (Altschul *et al.*, 1990) and UCSC Genome Browser (Kent *et al.*, 2002).



B.

iHUVeC Line	Chromosomal Integration site	Gene
7	Chr2q33	<i>MOB4</i>
2	Chr10q23.31	<i>PTEN</i>
2	Chr8q24.3	<i>C8orf33</i>
2	Chr20q11.22	<i>NCOA6</i>
10	Chr5q34	Intergenic

Figure 3.18 Pro-viral *TERT* Integration site analysis of Line 7, 2 and 10 iHUVeC. A. Gel image (0.6% agarose gel) of secondary PCR products from three viral integration libraries (as indicated below each lane) of *TERT* transduced iHUVeC (0.1 μ g/ μ l genomic DNA). A control digest was performed on human genomic DNA transduced with lentivirus 0.1 μ g/ μ l which showed the expected fragment size of 700bp (Dral human control). B. Sequencing Analysis of the secondary PCR products generated from the lentiviral integration libraries. Pro-viral *TERT* singly integrated in Line 7 HUVEC at location Chr2q33, within an intron of Family Member 4, Phocin (*MOB4*). Multiple pro-viral *TERT* integration events were detected in Line 2, one at Chr10q23.31 within the intron of Phosphatase and tensin homolog (*PTEN*) and LOC107987150 a sense intronic (non-coding transcript), at Chr8q24.3 within an intron of *C8orf33* and at Chr20q11.22 within an intron of *NCOA6*. A single pro-viral *TERT* integration site was detected for Line 10 at Chr5q34 and is intergenic.

Multiple integration sites within each line was expected, which would indicate a mixed population, however very few are actually observed. Two lines (7 and 10) contained a single integration, whilst three sites were found in Line 2.

Line 10 sequencing revealed a single integration within an intergenic region of Chr5q34 (**Figure 3.18 A and B**). Therefore pro-viral TERT integration should have minimal consequence on host cell gene expression as it does not obviously disrupt an endogenous gene (Ciuffi *et al.*, 2016).

Multiple pro-viral integration events were detected in Line 2 (**Figure 3.18 A and B**). One integration site is at Chr10q23.31 within an intron of *phosphatase and tensin homolog (PTEN)* and downstream of an intronic non-coding transcript (*LOC107987150*). *PTEN* is a known tumour suppressor gene and mutation of this gene has been shown to promote angiogenesis, hyperproliferation and impair vascular remodelling (Suzuki *et al.*, 2007). This is a cause for concern as disruption of these gene could adversely affect EC function. A second site was observed at Chr8q24.3 within an intron of an uncharacterised gene *chromosome 8 open reading frame 33 (C8orf33)* (**Figure 3.18 B**). A third integration was identified at Chr20q11.22, within an intron of *nuclear receptor coactivator 6 (NCOA6)*, a multifunctional gene involved in transcription, cell survival, growth and development (Mahajan & Samuels 2008). There was insufficient time to take this line further as it would first be necessary to confirm whether it was multiple insertions into the same cell or a mixed population. It would need to be assessed whether the viral integration influences expression and/or splicing of *PTEN*, *C8orf33* or *NCOA6*. The copy number data for Line 2 (**Figure 3.13 B** 0.8 copies of TERT/cell) would suggest a mixed population, in which case clonal lines can be isolated for each of the three integration sites, lines where endogenous gene expression is not altered can be carried forward.

Line 7 also showed a single integration at location Chr2q33, within intron 5 of *Family Member 4, Phocin (MOB4)* (**Figure 3.18 A and B, Appendix S2**). *MOB4*, also known as *hMOB3* directly binds to sterile 20-like kinase 1 (MST-1) in response to apoptotic stimuli, to negatively regulate apoptotic signalling. As this protein is over-expressed in Glioblastoma Multiform, it may be involved in promoting tumour growth (Tang *et al.*, 2014). The integration of *TERT* within *MOB4* may be an implication to the model as this may exert toxic effects on the cell, particularly as the protein is a negative regulator of the apoptosis signalling pathway. Therefore, it was necessary to check the endogenous expression levels of *MOB4* in both un-transduced and the iHUVeC lines. As shown in **Figure 3.19**), levels of *MOB4* remained unchanged upon integration of the *TERT* provirus confirming integration has no confounding effect on the level of endogenous *MOB4* expression. The primers for gene expression analysis were designed to bind exons either side of the integration point, so that if splicing was disrupted this would be detected. If splicing of intron 5 was inhibited either additional products and / or a reduction in the spliced transcript would be detected, neither of which were seen. Therefore, taking this line forward, it can be reassured any phenotypes observed are not due to an effect of *TERT* integration on *MOB4*.

The DL-3 integration library showed a smear of high molecule weight material at ~6kb (**Figure 3.18 A**). The presence of the smear is potentially due to a diminished suppression PCR effect (Siebert *et al.*, 1995). As shown in **Appendix S3**, the adapter sequence template size of DL3 is unexpectedly extended and forms panhandle DNA structures. This could be due to an incomplete amine modification or incomplete adaptor ligation. During PCR, the intramolecular annealing event of adaptor primer to sequence is favoured to these structures over the 'normal' adaptor primer to the adaptor sequence which in essence suppresses the PCR (Siebert *et al.*, 1995). The diminished PCR effect does not mean that products obtained with DL-1 and DL-2 are not correct, since redundancy is a part of the assay.

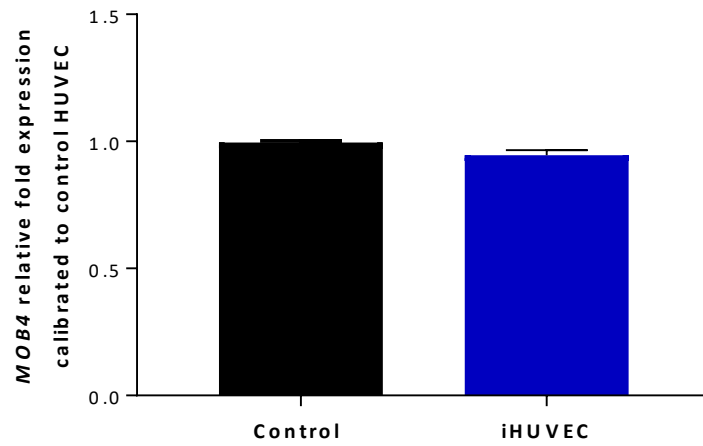


Figure 3.19 *MOB4* gene expression in control (un-transduced) and TERT+ transduced (iHUVEC) cells. *MOB4* expression was quantified in the un-transduced and TERT+ iHUVEC cells (n=3) using RT-qPCR. For the comparative quantification analysis, levels of *MOB4* in iHUVEC were calibrated to the control cells. Levels of *MOB4* are no different in both the control (untransduced) and TERT+ transduced iHUVEC (control 1.0 ± 0.01 versus iHUVEC 0.95 ± 0.02).

iHUVEC maintain the phenotypic expression of endothelial cell specific markers

Previous studies have reported prolonged constitutive expression of telomerase in TERT+ immortalised cells favoured the development of a pre-malignant transformation of endothelial cells (Kan *et al.*, 2012; Takano *et al.*, 2008). Therefore, it was necessary to verify the immortalised endothelial cell lines maintain an endothelial cell phenotype. To further characterise the lines, it was necessary to firstly verify the detection of gene expression of endothelial cell specific markers on one of the iHUVEC lines. Baseline expression of von Willebrand factor, CD34 and CDH5 (encodes VE-Cadherin) are regarded as key endothelial markers (Lin *et al.*, 1995; Cines *et al.*, 1998). Expression of the four markers was detected in both iHUVEC and parental cells at an mRNA level for all experimental lines, an example gel image for Line 7 is shown in **Figure 3.20 A**. It was next sought to quantify the protein expression of endothelial cell surface markers present at the cell surface of all the iHUVEC lines. The cell adhesion molecules CD31 (PECAM1), CD144 (VE-Cadherin) and cell surface antigen CD109 (VEGFR-2) are established markers of endothelial cells (Lampugnani *et al.*, 1992; Carmeliet *et al.*, 1999; Flores-Nascimento *et al.*, 2015), all were detected in both parental and iHUVEC at similar levels (**Figure 3.20 B**).

Taken together these findings confirm the iHUVEC maintain their endothelial phenotype at both a gene expression and protein level.

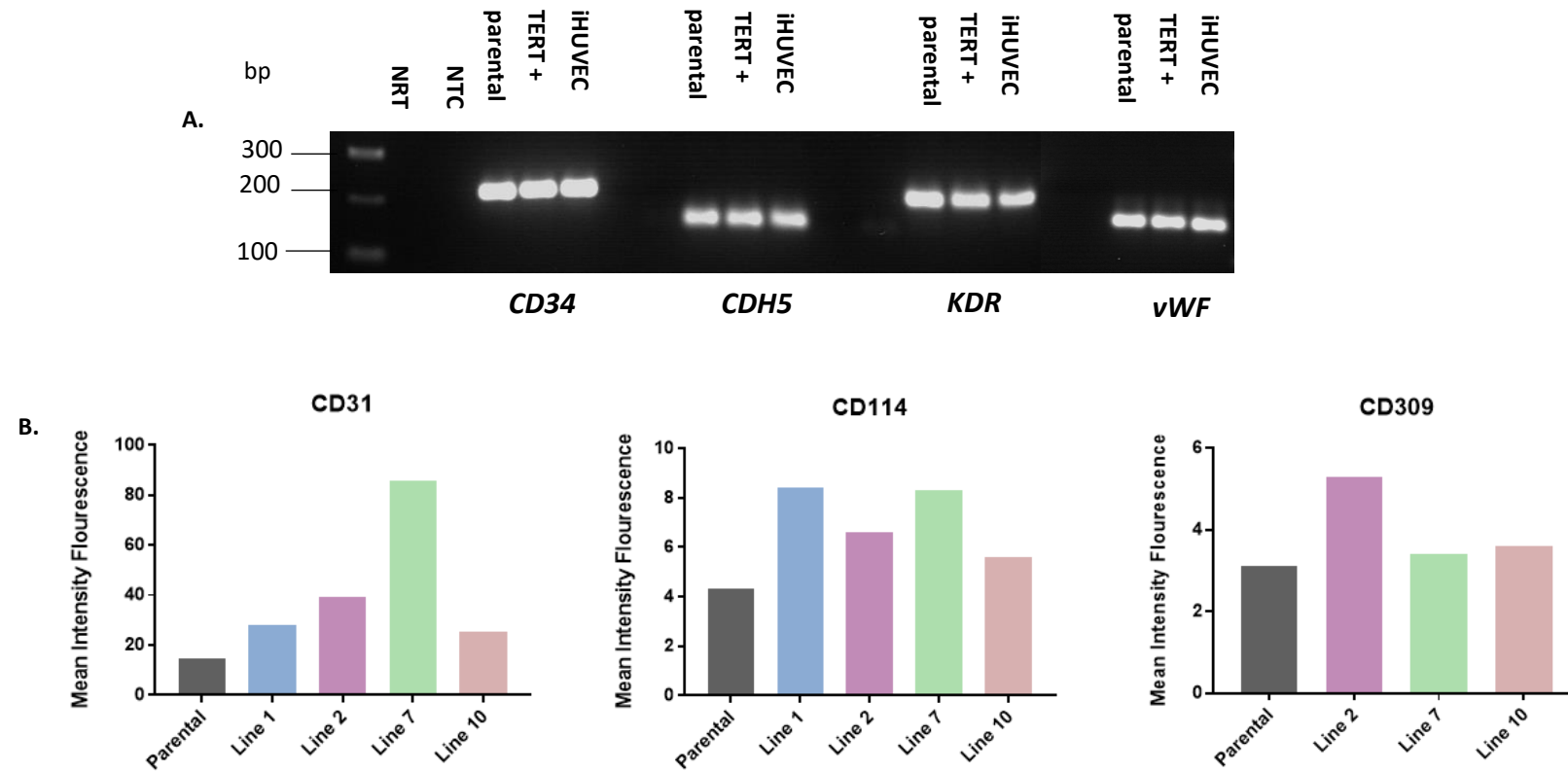


Figure 3.20 iHUVeC phenotypic profiling to normal HUVEC. A. Gene expression markers *CD34*, *CDH5*, *KDR* and *vWF* detected by PCR in early passage parental HUVEC (< 10 days in culture), TERT+ HUVEC (< 10 days in culture) and iHUVeC of Line 7. B. Flow cytometric detection of endothelial cell surface markers CD31, CD109 and CD144 in early passage parental HUVEC (<10 days in culture) and iHUVeC (between 103 - 106 PDs). Mean fluorescence intensity was calculated from histoplots and is shown normalised to either human isotope Ig G-APC or Ig G-APC control (to check the background level of non-specific antibody) (**Appendix S4**). No data is shown for CD309 expression in Line 1 due to technical errors in the procedure.

3.3.7 Ability to generate isogenic lines of varying telomere lengths from immortalised HUVEC.

Upon successful immortalisation of the HUVEC lines using TERT, the next stage was to experimentally isolate isogenic cell lines with short and long telomere lengths. In order to achieve this, the *TERT* transgene is excised using Cre recombinase. Our system relies on the introduction of the TERT vector in a configuration where upon reverse transcription, the U3 region of the 3'LTR is duplicated and LoxP sites are flanked on either side of the integrated TERT provirus (Salmon *et al.*, 2000). Both LoxP sites are recognised by Cre recombinase allowing for the complete excision of the LTR cassette and subsequent removal of the TERT transgene (Westerman *et al.*, 1996; Salmon *et al.*, 2000). The remaining LoxP site is transcriptionally inert which is important in the establishment of this model system. As this ensures the site is not incorrectly recognised as a cryptic LoxP site, which have been shown to serve as non-specific recognition sites for Cre recombinase (Thyagarajan *et al.*, 2000; Semprini *et al.*, 2007).

Transient Cre expression is not sufficient to excise Lox-TERT

To excise TERT, Cre (pCre-pac) was first transiently transfected into iHUVEC as this has been shown successful in other studies (O'Gorman *et al.*, 1997; Stadler *et al.*, 2013). As described in **section 2.2.6 (Lentiviral infection in host cell)**, Cre was transfected (for 72 hours) into a population of Line 7 iHUVEC. Although this plasmid has been successfully utilised in other studies and within our lab, no reduction in *TERT* expression was observed (**Figure 3.21**). Using transient transfection, Cre delivery was of a poor efficiency. Endothelial cells are notoriously difficult to transiently transfect, therefore to enable *TERT* removal, a viral Cre (pLOX-CW-CRE) was delivered to the cells via a lentiviral approach (Cudre-Mauroux *et al.*, 2003; Kang *et al.*, 2013; Lim *et al.*, 2010).

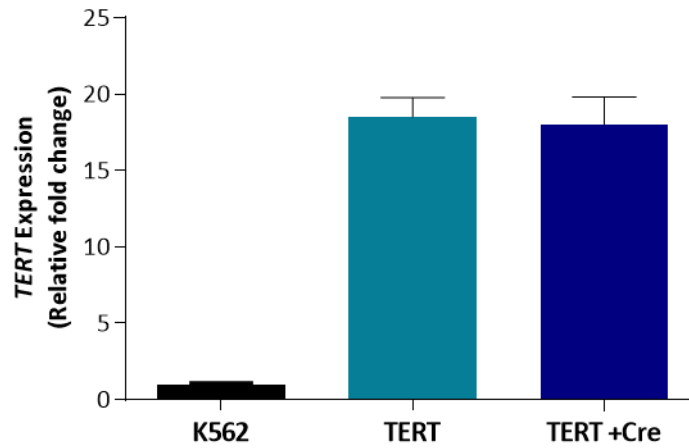


Figure 3.21. Addition of Cre recombinase by transient transfection does not remove *Lox-TERT*. *TERT* expression (relative to K562) was determined by real-time quantitative PCR in iHUVeC (n=3) and iHUVeC transiently transfected with a Cre plasmid (n=3). No reduction in *TERT* is observed after transfection with Cre (K562 1.0±0.1, TERT 18.52±1.3, TERT +Cre 18.03±1.8).

Lentiviral Cre-mediated ablation of TERT expression and telomere length shortening in test excision (Line 7)

To establish the experimental conditions to set-up the creation of isogenic lines of long and short TL, it was first necessary to perform a test infection using viral Cre in the iHUVeC. According to the methods described in **section 2.2.1** and **2.26**, a subculture of Line 7 iHUVeC were isolated post 100 PDs and transduced with lentiviral Cre. Notably, no cellular toxicity was observed upon the addition of viral Cre. For the conditional ablation of any unexcised cells, the excised line was subjected to a 7-day course of Acycloguanosine (ACG) (10 μ g/ml) treatment and the cells were maintained in culture. This isogenic line is termed Excision 1 (Ex1). *TERT* removal was verified and consequently no telomerase activity was detected in the excised line (**Figure 3.22 A & B**). To confirm the generation of this isogenic subclone was due differences in TL dynamics (compared to the iHUVeC clone), the TL lengths were measured in the excised line throughout the entirety of the culturing period from 108–174 PDs. The telomere length analysis shown on **Figure 3.22 C** shows subtle telomere length shortening was observed during this period, the telomere lengths dropped from T/S 3.8-1.36. The activity of telomerase was abolished upon *TERT* removal, therefore there was a failure for telomerase to maintain the TL in the excised subclone. In order to achieve both long and short TL isogenic lines it was important to assess the growth kinetics of the excised clone. The timing of the second excision for the generation of the long TL clone is critical so that the first excised line is still viable and will not have undergone sufficient TL attrition to reach replicative senescence / growth arrest. According to the telomere length data of the test infection, a gap of ~20days was considered optimal for creation of the experimental lines.

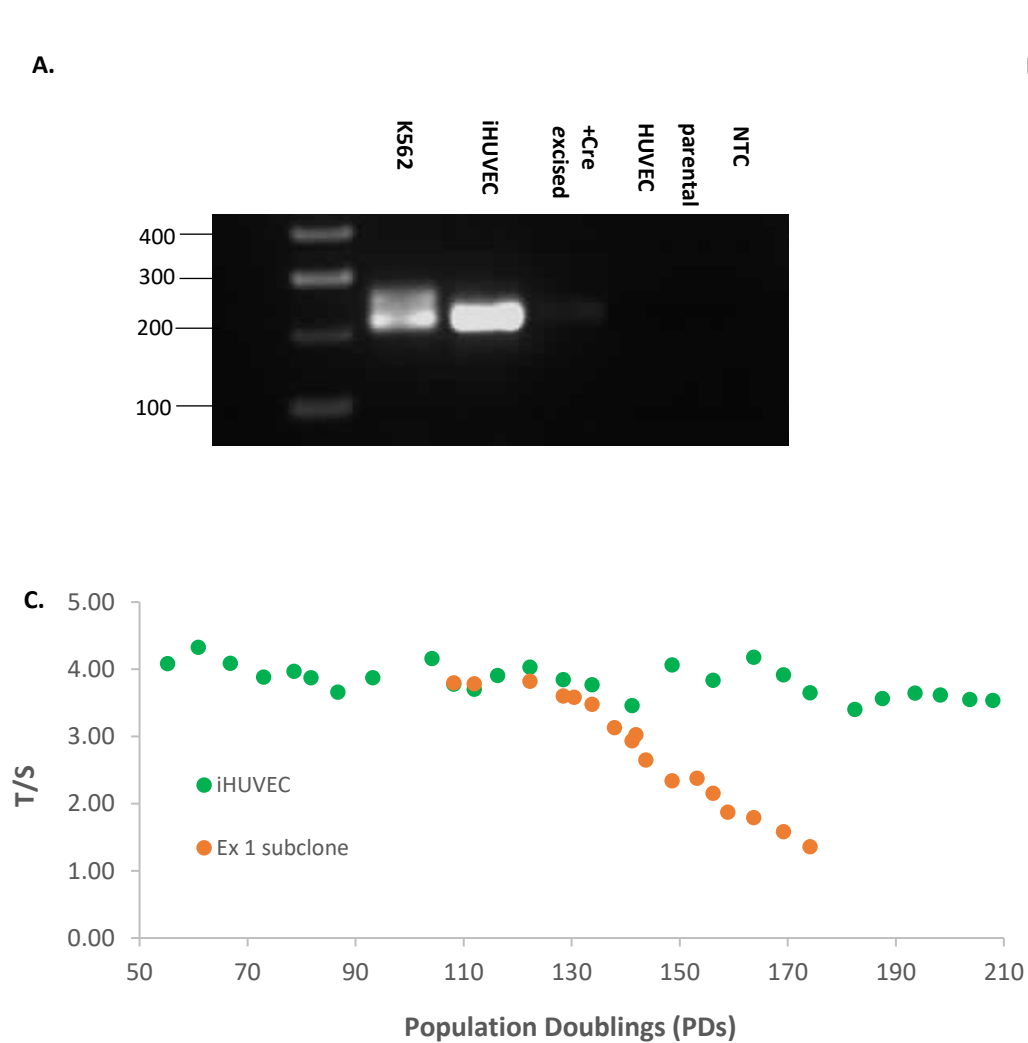


Figure 3.22 Successful removal of *TERT* from iHUVEC following the viral Cre test excision. A. Complete *TERT* removable in the Ex (Day 10 post Cre excision). B. Telomerase activity in K562 (positive control), Line 7 parental HUVEC, iHUVEC, +Cre excised subclone (Day 15 post Cre excision) whole cell lysates at 2500, 500 and 100 cell equivalents. The negative control (lysis buffer only, LB) is clear of bands. As telomerase is a heat-sensitive enzyme, heat treated (Δ) K562 (85°C) was performed as a negative control which is also clear of bands. The 35bp internal control (IC) is present for every lane to monitor PCR inhibition and serves as a control for amplification efficiency for each reaction. No detectable telomerase activity is seen in the parental and Cre excised lines. Telomerase activity is observed in K562 (+control) and iHUVEC. C. TL measurements of the iHUVEC (from 55.2 – 207 PDs) and Ex1 isogenic subclone (from 108 PDs to 174 PDs). All test samples were calibrated to K562 gDNA.

Test infection – Line 10

Three iHUVeC lines, which had been seen to show stabilised TL (Lines 2, 7 and 10) (**section 3.3.6**) were taken forward for functional experiments, with the aim to observe a consistent effect across three different donors. This would allow for any potential donor specific effects to be ruled out.

As discussed previously (**section 3.3.6**), Line 10 iHUVeC looked promising for the generation of isogenic lines as the TL of the iHUVeC were stabilised at a high level (**Figure 3.13**). Therefore, an initial infection of viral Cre (MOI of 100) was performed on Line 10 iHUVeC at day 227 (109 PDs). To verify whether the first excision had worked, cDNA from K562 (telomerase positive), Line 10 iHUVeC and the Line 10 Cre excised line were assayed by PCR for the presence or absence of *TERT* mRNA. PCR products were run on a 1.5% agarose gel. The gel image confirm the *TERT* excision was successful (**Figure 3.23**). There was insufficient time to take this line forward within scope of this thesis, although there are future plans to continue work with this line.

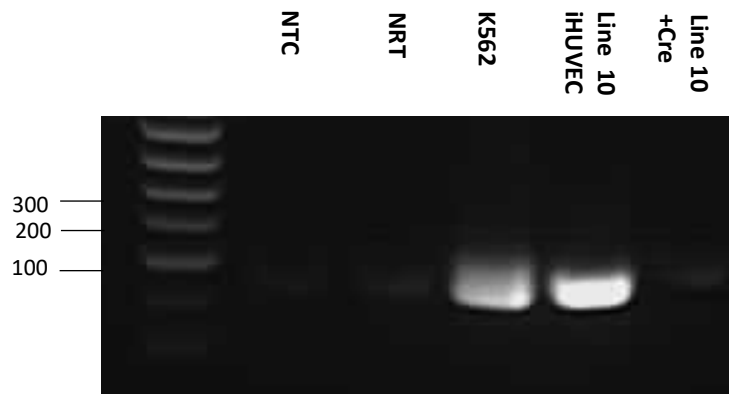


Figure 3.23 *TERT* expression in Line 10 immortalised HUVEC excised with Cre at 109 PDs. *TERT* expression (analysed by PCR) is observed in the telomerase positive cancer cell line K562 (which served as a positive control) and Line 10 iHUVeC. Complete *TERT* removal was confirmed at 10 days post Cre excision. *TERT* PCR products were run on a 0.6% agarose gel.

3.4 Conclusion

To investigate the biological mechanism by which shorter TL is causal to CAD, the aim of this project is to explore the effect of telomere length dynamics on the atherogenic potential of endothelial cells. The first aim is to generate isogenic lines of short and long telomeres. The immortalisation of human primary HUVEC using exogenous *TERT* is necessary for this process. This model system was based on an established technique where the controlled expression of a *TERT* transgene has been used successfully to immortalise myoblasts (Stadler *et al.*, 2011; 2013).

Findings show *TERT* was successfully integrated in the genome of one HUVEC donor, Line 7, and substantial *TERT* expression was observed at both RNA and protein level compared to parental HUVEC. Unexpectedly, both the parental and *TERT*+ line underwent TL shortening, the parental cells ultimately stopping growing and reached senescence whilst the *TERT*+ cell population continued growing in culture. Premature stress induced senescence is known to be caused by stress inflicted by prolonged culturing conditions in primary cell lines (Herbert *et al.*, 2002) therefore it is possible the parental cells were undergoing stress-induced rather than replicative senescence. Under oxidative stress conditions, such as mild hyperoxia, *TERT* has been reported to translocate from the nucleus to the mitochondria (Haendeler *et al.*, 2009; Haendeler *et al.*, 2004; Santos *et al.*, 2004) where it exerts protective effects such as reducing mitochondrial DNA damage (Ahmed *et al.*, 2008; Haendeler *et al.*, 2008). Therefore, it can be postulated, it is due to this protective effect that the *TERT*+ cells outlived the parental cells, however immortalisation has not been achieved as this is TL independent. Along with our findings, one study has also confirmed the over-expression of *TERT* in endothelial cells does not prevent telomere loss in standard culture conditions and the authors found TL is maintained when cells were grown at 5% O₂ (Napier *et al.*, 2010), therefore it is possible that atmospheric O₂ can induce cellular stress. Additionally, studies have shown primary cells grown at 5% O₂ show a 20-50% increase in PDs (Betts *et al.*, 2008; Martin *et al.*, 2004).

Therefore, to establish the experimental endothelial cell model, cells were maintained in culture at 5% O₂. Line 7 stocks of both parental and TERT+ cells were revived from the earliest point in culture and maintained. Following this approach, parental cells entered growth arrest, TERT+ cells exceeded 100 PDs showing no diminution in growth rate and can therefore be classified as 'immortal' (Yang *et al.*, 1999; Morales *et al.*, 2003). The immortalised cells showed TL lengthening followed by stabilisation.

To ensure any functional data derived from the model is not donor specific, a further 8 donors were subjected to the immortalisation process. Although 5 of the donors failed to immortalise, differences in pro-viral *TERT* copy number and *TERT* expression were observed in the unsuccessful lines. For one of the failing lines a downwards trajectory in *TERT* expression with increasing number of days post lentiviral TERT infection was observed. Epigenetic modifications such as DNA methylation may influence the transgene *TERT* expression (Kong *et al.*, 2009), particularly as the promoter region for *TERT* harbours a high GC content (Lu *et al.*, 2009). However, due to the prolonged culturing of the cells, it is possible because of clonal succession (Kay 1965), the untransduced cells within the mixed population are outgrowing the *TERT*+ cells thereby 'diluting' out the effects of the transgene.

3 single HUVEC donors (Line 2, 7 and 10) successfully immortalised upon the addition of lentiviral TERT, all iHUVEC showed substantial *TERT* expression. High telomerase activity was detected in all of the immortalised lines, ultimately TL stabilization was observed and the detection of CD31 (PE-CAM1), CD144 (VE-Cadherin) and the cell surface antigen CD109 (VEGFR-2) show the immortalised lines maintain an EC phenotype.

Most interestingly, the quantitative data show differences in the level of telomerase activity; with the order of activity (highest first) in Line 10, 7, 2 and lowest in Line 1. The difference in telomerase activity between donors gives an idea of TERT making it into the telomerase complex versus TERT being sequestered elsewhere (Blackburn 2005). However, there may be other factors contributing to this. As observed previously with the unsuccessful lines, the cell lines are heterogenous, it may be at an earlier point in

culture the un-transduced cells dominated the TERT+ cells and we are observing the effects. This is more reflective in the TL analysis of the immortalised cells during the entirety of culture. Compared to Line 2, 7 and 10, the growth kinetics of Line 1 is oblique, although the cells surpassed 100PDs, the TL stabilised at a low level, at which point the growth rate of the cells was reduced. This coincided with a loss of *TERT* expression at mRNA level in the iHUVeC, again reflecting how inadvertently the Line 1 cell population may have become clonal. Lines 2, 7 and 10 TL look promising for the generation of isogenic lines, the iHUVeC were stabilised at a high level and the growth rate of the cells were maintained.

As differences during the immortalisation process were observed between the donors, it was necessary to further analyse the site of pro-viral *TERT* integration in the genome of the iHUVeC as this would provide further insight on whether the line is of a mixed cell population or whether the lines are clonal. Upon infection with pro-viral *TERT*, all the iHUVeC lines exhibited a single copy of the lentiviral provirus, which adjusted for any small differences in MOI used when transducing the target cells. Although it was expected to see multiple integration sites within in each line, (which would indicate a mixed population) very few were actually observed. Multiple pro-viral *TERT* integration events were detected in Line 2 at 3 sites; one at *Chr10q23.31* within the intron of *PTEN*, at *Chr8q24.3* within an intron of *C8orf33* and at *Chr20q11.22* within an intron of *NCOA6*. As evidence of pro-viral *TERT* integration into *PTEN*, a gene involved in cell angiogenesis, hyperproliferation and impair vascular remodelling (Suzuki *et al.*, 2007) and *NCOA6*, a multifunctional gene involved in transcription, cell survival, growth and development (Mahajan & Samuels 2008) is observed, disruption of either of these genes could be deleterious to the cell. There was insufficient time to take this line further as it would first be necessary to verify whether it was multiple insertions into the same cell or the effects of a mixed population. It would also need to be confirmed whether the viral integration influences expression and/or splicing of *PTEN*, *C8orf33* or *NCOA6* compared to un-transduced Line 2 HUVEC.

Two of the Lines (7 and 10) contained a single integration, this was within *MOB4* (at Chr2q33) in Line 7 and an intergenic region (at Chr5q34) in Line 10, suggesting in the lines a single clone has become dominant within the population over time. One of the consequences of viral integration in the host cell is insertional mutagenesis which effects the host genome integrity and may cause subsequent cell death or cell proliferation depending on the function of the gene disrupted (Cuiffi *et al.*, 2016). In Line 7, endogenous expression levels of *MOB4* in both un-transduced and the iHUVeC remained unchanged upon integration of the *TERT* provirus, therefore, taking this line forward, we can be reassured any phenotypes observed are not due to an effect of *TERT* integration on *MOB4*. To avoid random integration of the *TERT* provirus into the host genome, the use of a safe harbour locus AAVS1 would be beneficial for this model. The AAVS1 located on the human chromosome 19 (locus PPP1R12C) are transcriptionally active regions with an open chromatin configuration (DeKolver *et al.*, 2010). Therefore, transgene insertion within this locus has no or minimal effect on global or local gene expression

The generation of the isogenic lines of long and short TL utilises the Cre-Lox system (Salmon *et al.*, 2000). Initial attempts at excising *TERT* using a transient Cre failed, therefore a viral Cre was delivered to the cells via an established lentiviral approach (Salmon *et al.*, 2000, Cudre-Mauroux *et al.*, 2003; Lim *et al.*, 2010). A test Cre infection was performed with Line 7, this was followed by an anti-viral Acycloguanosine therapy. Acycloguanosine treatment ensured any remaining non-excised cells within the mixed population were eliminated (Salmon *et al.*, 2000). No cellular toxicity was observed upon the addition of viral Cre, *TERT* removal was verified and telomerase activity was completely abolished in the excised line. Subtle telomere length shortening was observed and the excised line reached replicative senescence. The timing of this process is critical, as it is paramount prior to the second excision the first excised line is still viable and had not undergone sufficient TL attrition to reach replicative senescence. According to the data from this experiment, a gap of ~20days was considered optimal for the creation of the experimental lines of long and short TL as discussed in the next chapter.

CHAPTER 4

CHALLENGING ISOGENIC CELL LINES
OF SHORT AND LONG TELOMERE
LENGTHS WITH PRO-ATHEROGENIC
STRESS TO ASSESS ENDOTHELIAL
DYSFUNCTION

CHAPTER 4

CHALLENGING ISOGENIC CELL LINES OF SHORT AND LONG TELOMERE LENGTHS WITH PRO-ATHEROGENIC STRESS TO ASSESS ENDOTHELIAL DYSFUNCTION

4.1 Introduction

To understand how telomere length may influence coronary artery disease risk it is important to establish the biological mechanism by which telomere length may influence atherogenesis. The hypothesis is TL may influence the earliest stage of this process, endothelial dysfunction (ED).

Endothelial cell activation is induced by local systemic proinflammatory cytokines, including TNF- α , this triggers the plethora of molecular mechanisms associated with ED. eNOS downregulation leads to a reduction in the bioavailability of nitric oxide (NO), which is associated with changes in expression of the cell adhesion molecules vascular cell adhesion molecule 1 (VCAM-1), intercellular adhesion molecule 1 (ICAM-1) and/or E-selectin (Tiefenbacher *et al.*, 2001; Carreau *et al.*, 2011). The upregulation of these cell adhesion molecules has been shown to support the pro-inflammatory status of the EC and subsequently affects monocyte adhesion to the endothelium (Galkina *et al.*, 2007; Čejková *et al.*, 2016).

Studies to date have focused on investigating endothelial dysfunction in the presence of severe telomere dysfunction (telomere uncapping due to loss of TRF2). These vascular cells exhibit a pro-inflammatory state (increase in *ICAM-1* adhesion molecule expression, reduction in *eNOS* activity) and have shown phenotypic changes associated with senescence (van Steensel & Smogorzewska 1998; Minamino *et al.*, 2002; Karlseder *et al.*, 1999). Together with the evidence that *in-vivo* senescent EC exist in human atherosclerotic lesions (Minamino *et al.*, 2002), these studies have postulated that functional changes resulting in senescent endothelial cells *in-vivo* may play an important

role in the pathophysiology of disease. However, severe telomere dysfunction does not reflect a more gradual telomere length loss over time or the small inter-individual differences in TL associated with disease risk.

The research question is whether endothelial cells with short TL, with or without activation using a pro-inflammatory stimulus, exhibited higher levels of endothelial dysfunction compared to cells with a long TL. If so, is this effect driven through the induction of cellular senescence.

To explore the proatherogenic potential of endothelial cells with subtle changes in long and short telomere lengths, it is first necessary to isolate the effects of telomere length from other confounding factors. Chapter 3 discussed the generation of Lox-TERT primary human endothelial cell lines and the successful isolation of an isogenic lines showing progressive TL shortening. This chapter explores the creation of isogenic cell lines with short and long telomere lengths in primary HUVEC and investigates whether such differences in telomere length (in HUVEC lines maintained for the same length of time in culture) are attributed to changes in endothelial cell function in response to proatherogenic stimuli.

4.2 Methods

4.2.1 Creation of isogenic lines

The initial establishment of the model to create isogenic EC lines of varying telomere lengths is discussed in the previous chapter (**3.3.7 Ability to generate isogenic lines of varying telomere lengths from immortalised HUVEC**). Following the success of the model, a subculture of Line 7 iHUVEC were isolated at 102-106 PDs and transduced (using an MOI of 100) with lentiviral Cre according to the protocol outlined in **methods 2.2.6**. The excised line (Ex 1) was subjected to a 7-day course of Acycloguanosine (10µg/ml) treatment. A second excision (Ex 2) was performed on the iHUVEC at a later time point after ~20 days at 119-121 PDs. This second excision line was subjected to a 7-day course of Acycloguanosine (10µg/ml). The following methods were performed to validate the isogenic lines.

Validation of TERT removal

Removal of *TERT* was confirmed by assessing *TERT* mRNA expression (as described in **2.2.6 Real-time quantitative PCR**) and telomerase activity by TRAP assay (**2.2.6 Telomerase Repeat Amplification Protocol**).

MOB4 gene expression

MOB4 gene expression was quantified on both the short and long isogenic using real-time qPCR according to the methods described in (**methods 2.2.6, Real-time quantitative PCR**)

CD309 (VEGFR-2), CD144 (VE-Cadherin) and CD31 (PECAM-1) protein expression analysis by flow cytometry

FACS analysis was performed to detect the surface expression of endothelial specific proteins CD309 (VEGFR-2), CD31 (PECAM-1) and CD114 (VE-Cadherin) on the Ex1 and Ex2 isogenic lines at 141-147 PDs. A detailed method section is provided in (**methods 2.2.9**).

4.2.2 Functional experiments

Challenging the isogenic lines with proatherogenic stimuli to assess endothelial function.

For the functional experiments, subcultures of Ex1 and Ex2 lines taken between 141-147 PDs were either stimulated with human recombinant TNF- α (10ng/ml) for 24 hours or remained untreated (basal). 10ng/ml TNF- α treatment for 24 hours was shown optimum in the preliminary concentration and time-course treatment studies. Post TNF- α treatment the following EC functional assays were performed; *ICAM-1*, *E-SELECTIN* and *eNOS* gene expression was quantified by real-time qPCR, *ICAM-1* protein expression analysis was quantified by flow cytometry (according to the methods described in (**methods 2.2.9**), cell adhesion assay of THP-1 blood monocyte binding to HUVEC (**methods 2.2.8**). The senescent status of the Ex1 and Ex2 lines was verified between 144-151PDs using a β -galactosidase in situ assay for cellular senescence (Dimri *et al.*, 1995).

4.3 Results

4.3.1 Experimental HUVEC isogenic lines with long and short telomeres

As shown in the previous chapter, Line 7 iHUVEC showed TL attrition upon *TERT* removal by viral Cre addition. Experiments to investigate the physiological effects of TL on ED were initiated using this line.

In order to show a consistent and reliable result, this procedure was performed on three separate occasions to produce three experimental sets of isogenic long and short TL lines. Notably, the excisions were consistent between experiments; the first excision (Ex1) was performed between 102-106 PDs and the second excision (Ex2) at 119-121 PDs. The excised cells were cultivated for the same length of time within each experiment and approximately had the same length of time between experiments, which equated to between 141-147 PDs. **Figure 4.1** confirms complete *TERT* removal post excision (**Figure 4.1 A**) and telomerase activity in both of the excised sublines (**Figure 4.1 B**) showing the complete removal of TERT at both RNA and protein level.

For the functional experiments, subcultures of the Ex1 and Ex2 lines were purposely selected so that both isogenic lines had been subjected to the same length of time in culture. This was to eliminate any additional confounding factors associated with the prolonged culturing conditions. Prior to investigating any functional effect of the isogenic lines, it was necessary to determine the actual telomere lengths of the lines. The telomere lengths were measured for the excised lines and the average TL for the Ex1 isogenic line was shorter than that for the Ex2 isogenic line (T/S 2.39 ± 0.37 vs 4.01 ± 0.31). The TL for parental Line 7 HUVEC determined at the initial culturing period of the Line (at 4 PDs) was T/S 3.76. Therefore it can be assured, compared to the parental cells, the Ex1 excised line has a shorter TL and the Ex2 line has a longer TL. This confirms the experimental isogenic lines are different in their TL prior to the functional analysis experiments. For the remainder of this chapter the lines will be termed as short TL (previously Ex1) and long TL (previously Ex2) respectively.

MOB4 expression in isogenic lines with long and short telomeres

Previous data was shown for this donor where pro-viral *TERT* integrates at a single integration site at Chr2q33, within an intron of *MOB4* (section 3.3.6, Figure 3.18), further analysis showed levels of *MOB4* remained unchanged upon the integration of *TERT* in iHUVEC compared to parental (un-transduced cells) (section 3.3.6, Figure 3.19). Therefore the use of viral Cre, hence a second integration event, also has no effect on *MOB4* expression in either of the short and long TL line relative to iHUVEC (Figure 4.2). This means any phenotypes observed during the functional experiments are not due to an effect of Cre integration.

Phenotypic profiling of isogenic lines with long and short telomeres

In the previous chapter it was shown HUVEC immortalised using lentiviral *TERT*, maintain an endothelial cell phenotype at both RNA and protein level (Figure 3.20 A and B). Integrating viruses can carry the risk of insertional mutagenesis and subsequent malignant transformation (Mikkers *et al.*, 2003). Therefore prior to carrying out the functional experiments, it was necessary to verify whether the integration of the second virus (Cre) potentially affects the endothelial cell phenotype. The protein expression of the endothelial cell surface markers, CD309 (VEGFR-2) and CD114 (VE-Cadherin) on both short and long isogenic lines were comparable to parental HUVEC (Figure 4.3). The protein expression of CD31 (PECAM-1) was 2.7 fold higher in the short TL line (35.5) and 3.0 fold higher (39.6) in the long TL line compared to parental HUVEC (13.2). At this stage, it was important to detect whether or not the isogenic lines of different TL show CD31 expression. Had there been more time, further work is required to investigate the observed differences between the level of CD31 in the Cre excised lines versus parental.

The findings observed show the isogenic lines show a true endothelial cell phenotype and have not undergone any cellular transformations during the process of reversible immortalisation. Once the endothelial cell phenotypic profiling of the isogenic lines was confirmed, the next stage was to examine the functional effect of the HUVEC isogenic lines with short and long TL.

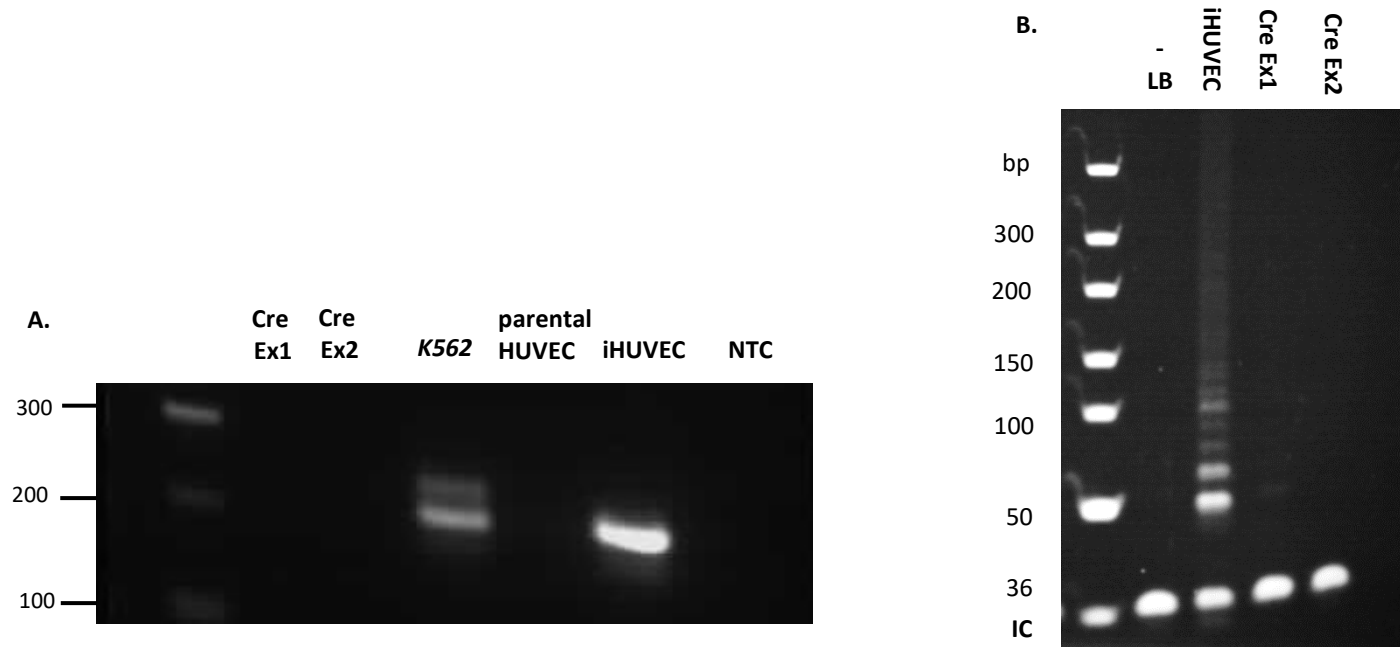


Figure 4.1. Creation of experimental isogenic lines with short and long telomere lengths. A. *TERT* expression was detected by RT-qPCR and products from cDNA amplification were run on a 1.5% agarose gel. Complete *TERT* removal is shown in the Ex1 (Day 10 post Cre excision) and Ex2 (Day 8 post Cre excision) isogenic lines. B. Telomerase activity in Line 7 parental HUVEC, iHUVEC, Ex1 isogenic line (Day 15 post Cre excision) and Ex2 isogenic line (Day 13 post Cre excision). iHUVEC is included as a positive control. No detectable telomerase activity is seen for either excised line. The negative control (lysis buffer only, LB) is clear of bands. The 35bp internal control (IC) is amplified by the TS primer and is present for every lane to monitor PCR inhibition and serves as a control for amplification efficiency for each reaction.

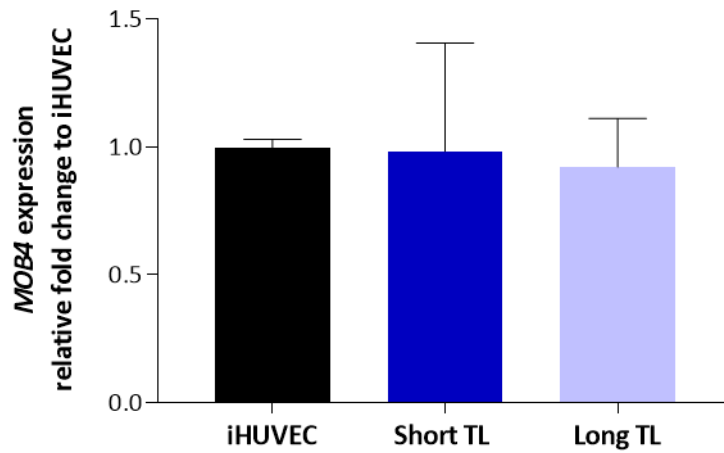


Figure 4.2 MOB4 gene expression in iHUVeC and short and long TL lines. MOB4 expression was quantified in Line 7 iHUVeC, short and long TL cells using RT-qPCR. Quantification for samples is relative to housekeeper 36B4. For the comparative quantification analysis, levels of MOB4 in the short and long TL lines were calibrated to iHUVeC. No differences in expression levels of MOB4 were observed between the iHUVeC, short and long TL lines. Mean±SD; iHUVeC 1.0±0.03, Short TL line 0.99±0.42, Long TL line 0.92±0.19).

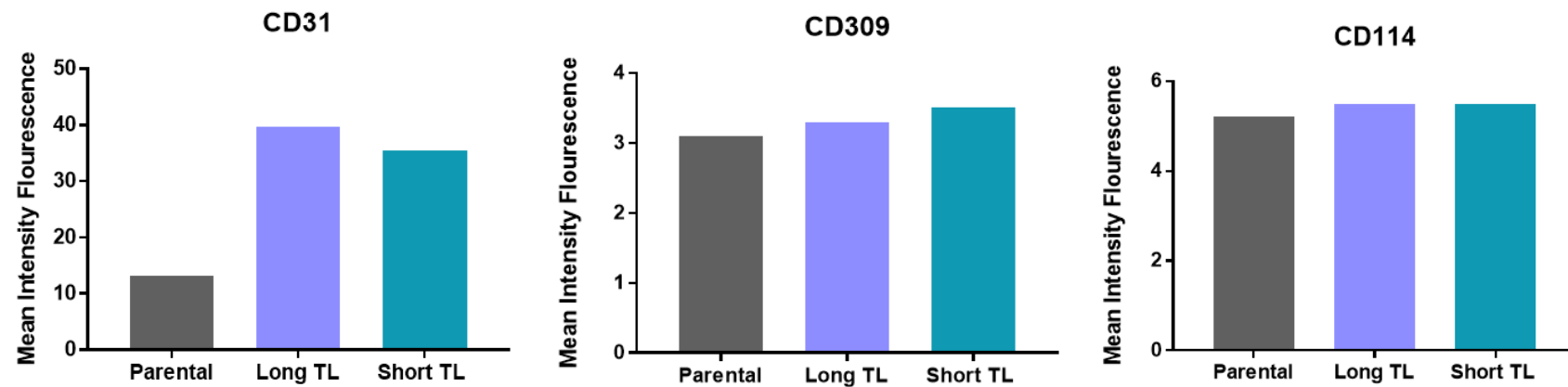


Figure 4.3. Phenotypic profiling of isogenic lines compared to parental HUVEC. Flow cytometric detection of endothelial cell surface markers CD31 (PECAM-1), CD309 (VEGFR-2) and CD144 (VE-Cadherin) in parental HUVEC, Ex1 (long) isogenic line and Ex2 (short) isogenic line (both lines are between 141-147 PDs). Human isotope Ig G-APC or Ig G-FITC controls were included for each run to check the background level of non-specific antibody. The Mean Fluorescence Intensity (MFI) of the logarithmic histoplots (showing a normal population (**Appendix S5**)) was calculated using the median (this was done independently for CD309, CD31 and CD114). Comparable levels of CD31, CD309 and CD114 protein expression is observed in the parental (untransduced) HUVEC and long and short TL lines.

4.3.2 Increased *ICAM-1* and *E-SELECTIN* gene expression at basal level in the short TL clone

To test our initial hypothesis of whether upon proatherogenic stimulation differences in endothelial function are observed in isogenic lines with short and long TL, cells were challenged with TNF- α (10ng/ml). Treatment with TNF- α was for 24 hours to evoke endothelial cell activation, this was compared to untreated cells in order to assess basal expression levels. The concentration of TNF- α (10ng/ml) and time of treatment (24 hours) was chosen as this elicited a maximum response in the gene expression of ED markers during the preliminary experiments. Several genes have been reported to be induced in endothelial dysfunction including *ICAM-1*, *E-SELECTIN* and *eNOS* (Minamino *et al.*, 2002, Kahn *et al.*, 2017). mRNA expression of these endothelial dysfunctional markers were quantified by real-time quantitative PCR, as shown in **Figure 4.4**.

No notable differences were observed in *eNOS* expression at basal and upon treatment (**Figure 4.4 C and F**). During type II activation of EC, the suppression of *eNOS* expression by TNF- α is time-dependent (hours). During this inflammatory response, a reduction in *eNOS* promoter activity has been observed after 8 hours of TNF- α exposure (Anderson *et al.*, 2004). This may explain why no changes were observed between the short and long TL lines, the 24h treatment window may be prolonged to see an effect in response to TNF- α treatment (which for *eNOS* may be acute during inflammation).

Interestingly, findings show the expression of *ICAM-1* was higher at basal in cells of the short TL isogenic line compared to cells of the long TL line (**Figure 4.4 A**). There was also increased expression of the cell adhesion molecule *E-SELECTIN* at basal in the short LT cells (**Figure 4.4 B**). As expected, upon treatment with TNF- α , there is an increase in the expression of *ICAM-1* (short TL basal 1.0 versus TNF- α 11.89 \pm 4.17, long TL basal 0.60 \pm 0.20 versus TNF- α 10.38 \pm 4.43) and *E-SELECTIN* (short TL basal 1.0 versus TNF- α 81.36 \pm 68.91, long TL basal 0.73 \pm 0.28 versus TNF- α 59.93 \pm 30.53) and decreased expression of *eNOS* (short TL basal 1.0 versus TNF- α 0.80 \pm 0.06, long TL basal 1.07 \pm 0.21 versus TNF- α 0.87 \pm 0.19), confirming both the short and long isogenic EC lines are dysfunctional upon pro-atherogenic stimulation.

Despite the differences observed in the expression of *ICAM-1* and *E-SELECTIN* between the short and long TL lines at a basal, upon TNF- α treatment this effect is diminished (**Figure 4.4 D and E**).

4.3.3 Increased *ICAM-1* gene expression in response to TNF- α stimulation

To investigate whether the effects of *ICAM-1* and *E-SELECTIN* expression in the short and long TL isogenic lines are driven by the differences observed at baseline or whether differences observed are independent of this, the fold increase (upon TNF- α stimulation) of each of the endothelial dysfunctional markers in both lines were compared. The fold increase varied between experiments; *ICAM-1* short versus long 10.6 v 18.7 (experiment 1), 8.2 v 13.5 (experiment 2), 16.8 v 22.8 (experiment 3), and *E-SELECTIN* short versus long 55.0 v 104.0 (experiment 1), 21.0 v 53.2 (experiment 2) and 170.0 v 80.4 (experiment 3). To take experimental differences into account, the fold change was standardised to that of the TNF- α treated short TL for each experiment (**Figure 4.5**). For this analysis, no differences were observed in the *E-SELECTIN* and *eNOS* between short and long TL lines (**Figure 4.5 B and C**).

As previously shown, *ICAM-1* expression is higher at basal in the short TL line compared to the long TL line (**Figure 4.4 A**). This would suggest in the long TL line, there would be greater response to TNF- α stimulation (in terms of fold change) compared to the short TL cells in order to reach the maximum response (elicited by the short TL line at basal). As expected, there is a higher upregulation in the long TL line was observed upon TNF- α treatment (**Figure 4.5 A**).

4.3.4 Isogenic lines with short telomere length show increased protein expression of *ICAM-1* at the cell surface.

As a difference in *ICAM-1* gene expression between the isogenic lines was observed at a basal level, it was next explored whether this was observed at a post-transcriptional level by quantifying *ICAM-1* protein expression. *ICAM-1* encodes a cell surface glycoprotein expressed on EC and is recognised by monocytes for the migration of monocytes across the endothelium (Meerschaert *et al.*, 1995; Vlassarav *et al.*, 1995),

therefore, a flow cytometry assay was used to detect ICAM-1 protein expression at the cell surface. Quantification of the flow cytometric analysis confirmed an increased in basal ICAM-1 protein expression in the shorter TL clone (0.31 fold increase/ 31.1% change (**Figure 4.6 A**) which mirrored the gene expression findings.

As observed with the *ICAM-1* mRNA analysis, the next question was whether the response to TNF- α stimulation is different in the short and long TL lines. To do this the fold change upon TNF- α treatment was calculated, due to experimental differences the values were standardised to the short TL clone for each experiment. The cells start with different basal levels but show no difference in the level of expression after TNF- α stimulation (**Figure 4.6 B**). Previous studies confirm ICAM-1 expression peaks by 18–24h and remains high as long as there is active TNF- α present (Pober *et al.*, 1986; Hagi-Pavli *et al.*, 2009). It may be postulated the ICAM-1 expression in both the short and long TL lines at basal lies close to the maximum threshold therefore although TNF- α stimulation evokes a response, it is not sufficient enough to show a difference between the lines.

Taken together these findings confirm the short TL clone at basal is pro-inflammatory with increased ICAM-1 expression consistent at both gene and protein level. This implies EC with a shorter TL have higher levels of pre-existing ICAM-1, which suggests these cells exist in a pro-inflammatory state. ICAM-1 is one of the key cell adhesion molecules involved in endothelial dysfunction during atherogenesis (Chi 2007). This pro-inflammatory mediator plays a role in monocyte cell recruitment to the endothelium (Lusis 2000), therefore the next question is whether this difference in ICAM-1 expression observed at basal translates to a functional finding in EC function.

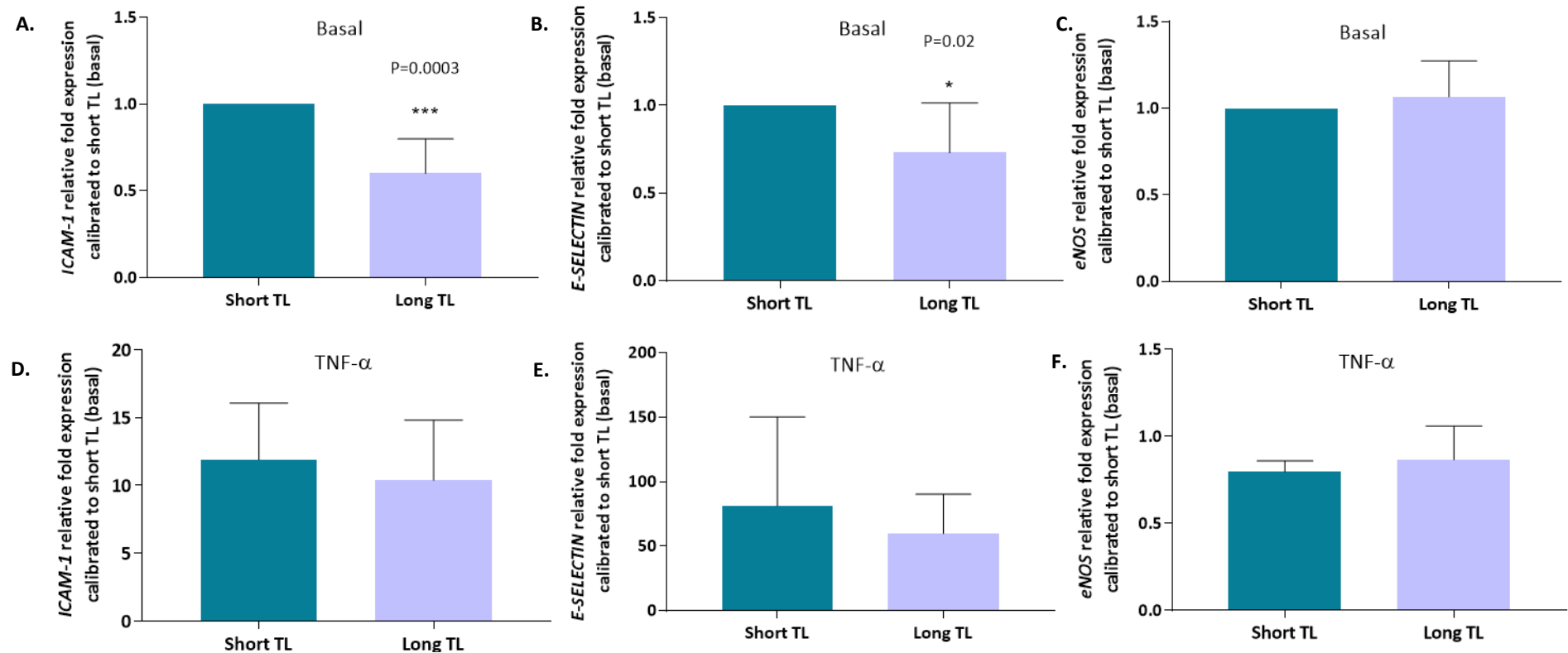


Figure 4.4 Gene expression of endothelial dysfunction markers in untreated and TNF- α stimulated cells. Isogenic lines of short and long telomere lengths (TL) were either untreated (basal) (A-C) or treated with TNF- α (10ng/ml) for 24hrs (D-F). mRNA expression of endothelial dysfunctional markers *ICAM-1*, *E-SELECTIN* and *eNOS* were quantified by RT-qPCR. For relative quantification test samples were calibrated to short TL basal. Each test sample was normalised to a *36B4* housekeeper gene. To take experimental differences into account, the fold change was standardised to that of the basal short TL for each independent experiment. Values are representative of three independent experiments (n=9 in total). Mean \pm SD, A. *ICAM-1* Basal short TL 1.0 versus long TL 0.60 \pm 0.20 P=0.0003. D. *ICAM-1* TNF- α short TL 11.89 \pm 4.17 versus long TL 10.38 \pm 4.43. B. *E-SELECTIN* Basal short TL 1.0 versus long TL 0.73 \pm 0.28 P=0.02. E. *E-SELECTIN* TNF- α short TL 81.36 \pm 68.91 versus long TL 59.93 \pm 30.53. C. *eNOS* Basal short TL 1.0 versus 1.07 \pm 0.21. F. *eNOS* TNF- α short TL 0.80 \pm 0.06 versus long TL 0.87 \pm 0.19. For statistical analysis a paired T-test was performed. Basal differences in *ICAM-1* and *E-SELECTIN* were observed between the short and long isogenic lines, with higher expression of the genes in the shorter TL clone.

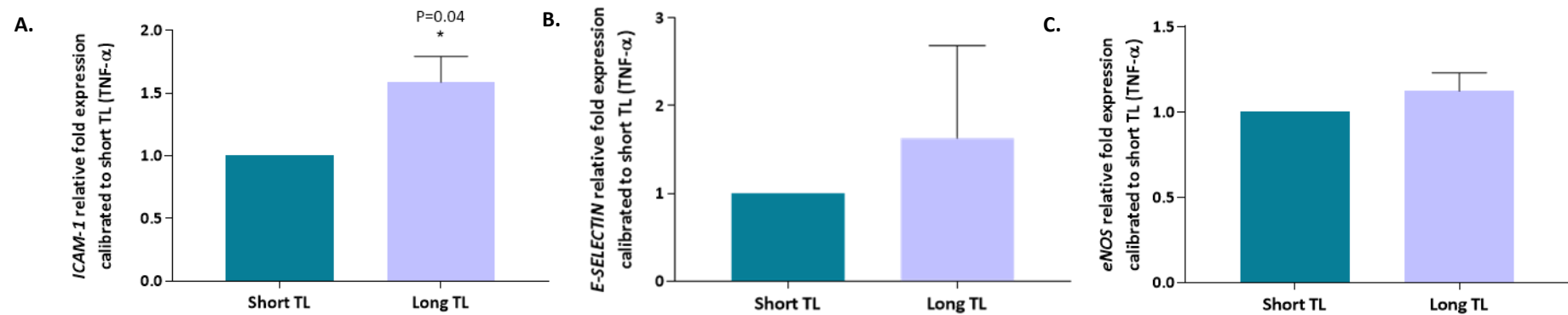


Figure 4.5. Upregulation of endothelial dysfunction marker gene expression in response to TNF- α . Isogenic lines of short and long telomere lengths treated with TNF- α (10ng/ml) for 24hrs. mRNA expression of endothelial dysfunctional markers A. *ICAM-1*, B. *E-SELECTIN* and C. *eNOS* upregulation. For relative quantification test samples were calibrated to short TL (treated with TNF- α). The data is standardised to short TL levels for each experiment. Mean \pm SD A. *ICAM-1* short TL 1.0 versus long TL 1.59 \pm 0.21. B. *E-SELECTIN* short TL versus long TL 1.63 \pm 1.06. C. *eNOS* short TL 1.0 versus long TL 1.12 \pm 0.11. For the statistical analysis a paired T-test was performed. A higher upregulation in *ICAM-1* in the long TL line was observed upon TNF- α exposure. No differences in the level of *E-SELECTIN* and *eNOS* were observed.

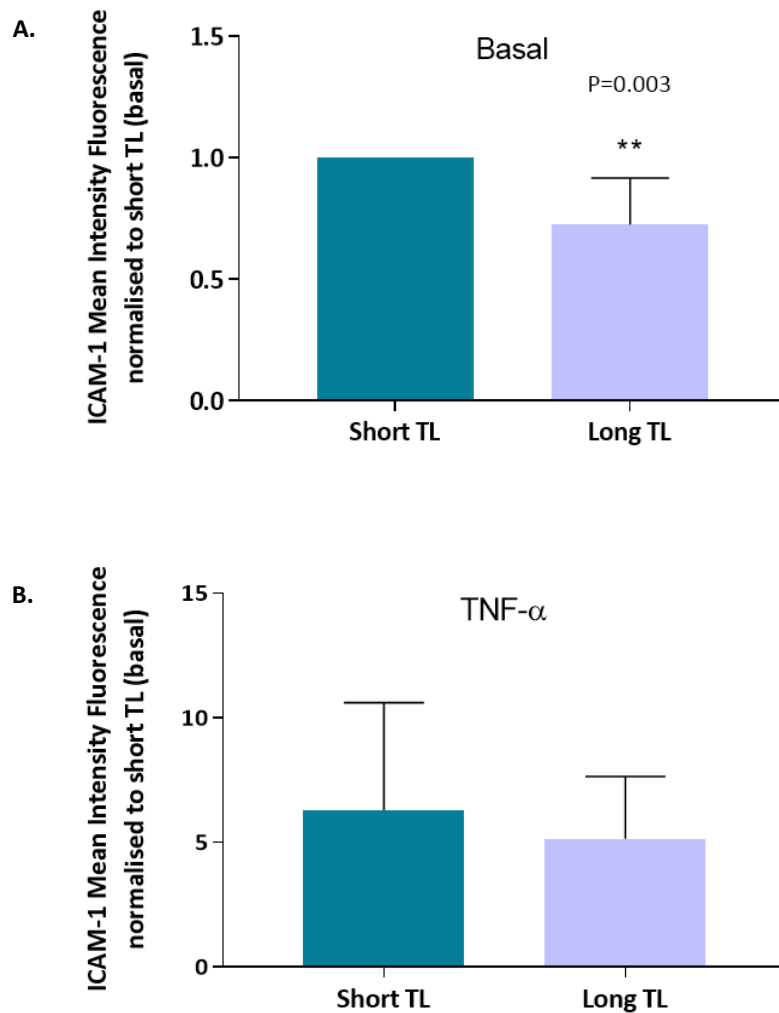


Figure 4.6 ICAM-1 protein expression in the isogenic lines with and without TNF- α stimulation. ICAM-1 expression quantified (by flow cytometric analysis) at A. basal and B. after TNF- α treatment (24 hours at 10ng/ml) in both the short and long TL. The Mean Intensity fluorescent (MIF) was calculated and normalised to an IgG isotope control to adjust for background fluorescence. Values are representative of three independent experiments (n=9 in total). All data are relative to the basal short TL. Mean \pm SD A. ICAM-1 Basal short TL 1.0 versus long TL 0.73 \pm 0.19 (P= 0.03). B. ICAM-1 TNF- α short TL 6.30 \pm 4.31 versus long TL 5.14 \pm 2.5. For statistical analysis a paired T-test was performed. At basal, cells with short TL shows an increased expression of ICAM-1 compared to cells with a long TL. As expected, treatment with TNF- α stimulated the expression of ICAM-1 in both of the lines. No differences were observed upon treatment between each of the lines.

4.3.5 HUVEC-monocyte adhesion in the short TL clone is higher at a basal and further increases upon TNF- α stimulation

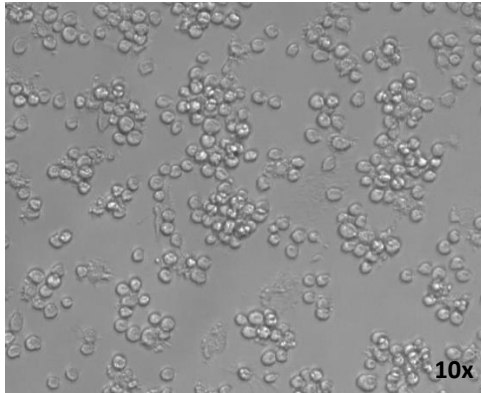
Endothelial cell activation and dysfunction influences monocyte recruitment and transmigration; accumulating evidence shows the upregulation of ICAM-1 is critical for monocyte adhesion to the endothelium during this inflammatory response (Meerschaert *et al.*, 1995; Lui *et al.*, 2017). Therefore THP-1 blood monocyte cell adhesion to the short and long TL HUVEC lines was investigated. To further explore the proinflammatory response in the isogenic lines, cells were stimulated with TNF- α (10ng/ml) for 24hours prior to the addition of the THP-1 monocytes.

As shown in **Figure 4.7**, without TNF- α stimulation minimal monocyte binding to confluent HUVEC of the short TL and long isogenic lines was observed. Binding was substantially increased in HUVEC (of both isogenic lines) treated with TNF- α (**Figure 4.7. A**). Therefore, both short and long isogenic lines are capable of binding monocytes *in-vitro* and this increases upon TNF- α stimulation as expected. Comparison of monocyte cell adhesion between the short and long TL lines revealed a significant reduction in monocyte binding in the long TL lines compared to the short TL lines, both at baseline (0.26 fold or 26.4% **Figure 4.7. B**) and after TNF- α stimulation (0.65 fold or 34.5%, **Figure 4.7. B**). Previous data shown shows ICAM-1 expression at both gene and protein level is higher in cells with short TL compared to cells with long TL (**section 4.3.3 and 4.3.4**). These findings confirm the differences observed in ICAM-1 expression do translate to a functional difference in monocyte adhesion at a basal level.

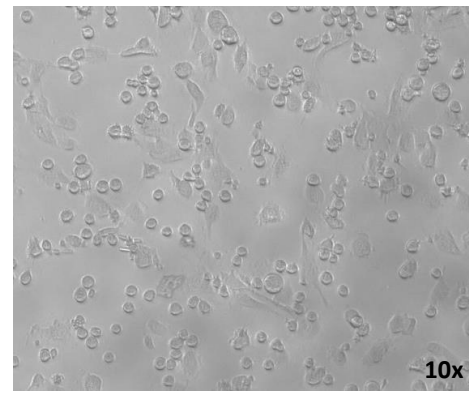
EC activation and dysfunction influences the monocyte adhesion cascade, ICAM-1 is implicated in this process. ICAM-1 binds to Mac-1 (Macrophage-1 antigen) members of the β 2 integrin family expressed on monocytes to facilitate monocyte recruitment and subsequent transmigration through the endothelium (Čejková *et al.*, 2016). Short TL cells treated with TNF- α show a greater fold increase in monocyte binding compared to cells with long TL and this is more substantial than the difference observed between the short and long TL cells at basal (**Figure 4.7 A and B**).

When investigating the effect on TNF- α stimulation of these lines, it was previously shown (**Figure 4.6**) ICAM-1 levels are the same in both short and long TL cells when treated with TNF- α . However, at a functional level, i.e. monocyte adhesion to the cells, there is a difference between the lines, where increased monocyte-EC binding occurs in the short TL line at both basal and upon treatment (**Figure 4.7 A and B**). In addition to *ICAM-1*, the cell adhesion molecules *VCAM-1*, *PECAM* and *E-SELECTIN* contributes to monocyte activation and recruitment from adventitial vessels and the arterial lumen in atherosclerosis (Davies *et al.*, 1993), which progresses to the monocyte adhesion cascade. This is important as it suggests the increased adhesion of monocytes to cells with short TL are due to additional factors of the cell adhesion cascade not measured in this work, this is further discussed later in the chapter.

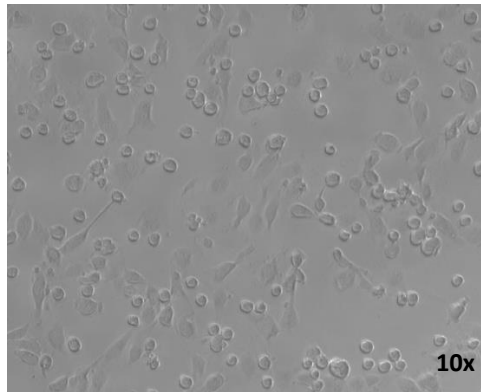
A. Short TL basal



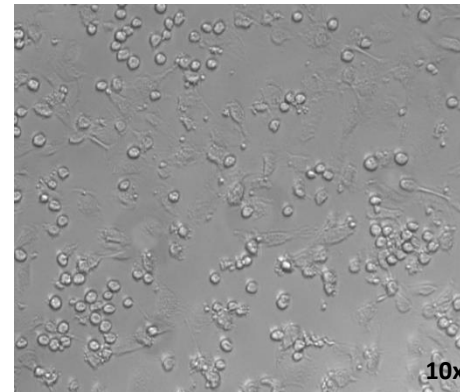
Long TL basal



Short TL +TNF-α 10ng/ml



Long TL +TNF-α 10ng/ml



B.

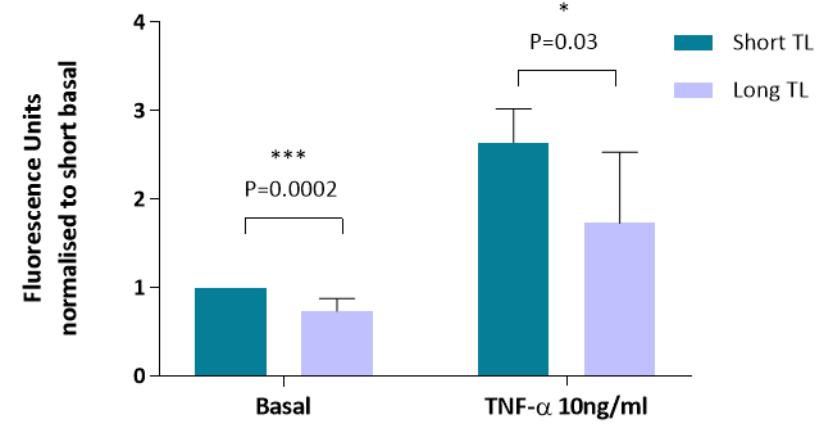


Figure 4.7 Increased HUVEC-THP-1 monocyte cell adhesion at basal in the shorter TL clone, adhesion is further increased upon TNF-α (10ng/ml) stimulation after 24hours. A. Brightfield images taken at 10x magnification showing HUVEC-THP-1 cell adhesion at basal (control) and after TNF-α treatment (10ng/ml for 24 hours) in both the short and long TL lines. Cell adhesion was quantified using a fluorometric assay. THP-1 cells were loaded with a calcineurin-AM dye and monocytes adhered to HUVEC was measured by fluorimetry using an excitation wavelength of 490nm and emission wavelength of 510nm. Fluorescence unit values are representative of three independent experiments (n=9 samples in total). All samples were normalised to short TL basal. Mean±SD Basal short TL 1.0 versus Basal long TL 0.74±0.14 (P=0.0002), TNF-α treated short TL 2.64±0.38 versus TNF-α treated long TL 1.73±0.80 (P=0.03) (Paired T-test).

4.3.6 Higher levels of endothelial dysfunction in cells with short TL is not associated with senescence.

Senescence associated secretory phenotype (SAPS) has been shown to confer characteristic changes in gene expression including the upregulation of adhesion molecules *ICAM-1*, *E-SELECTIN* associated with inflammation (Coppé *et al.*, 2008). Telomere dysfunction, which induces senescence has been associated with endothelial dysfunction (Minamino *et al.*, 2002). As there is a functional difference in cells with shorter TL, the next question is whether this was an effect being driven by differences in senescence between the short and long lines.

To assess senescence, cells with short and long TL (both subcultures had the same length of time in culture) were stained at basal and post 24 hour TNF- α treatment. The % of positive β -galactosidase cells were quantified in each of the experimental lines.

Minimal senescence was observed in the short and long TL lines at basal; no differences are observed between the two lines (**Figure 4.8 A and B**). The cell population within the isogenic lines are heterogenous consisting of both excised and non-excised (TERT+). At the time the excisions were performed, the TERT+ iHUVeC has surpassed 100PDs, due to the prolonged culturing period the senescent cells detected in this experiment at basal could be due to stress-induced senescence of the non-excised cells. We had anticipated some senescence as this was detected in our Line 7 iHUVeC as shown in Chapter 3 (**section 3.3.6 Figure 3.14**).

Treatment with TNF- α showed no further increase in senescence in either of the lines. These findings suggest senescence is not driving the pro-inflammatory phenotype of the short TL clone and endothelial dysfunction and subsequent monocyte adhesion occurs prior to the onset of replicative senescence.

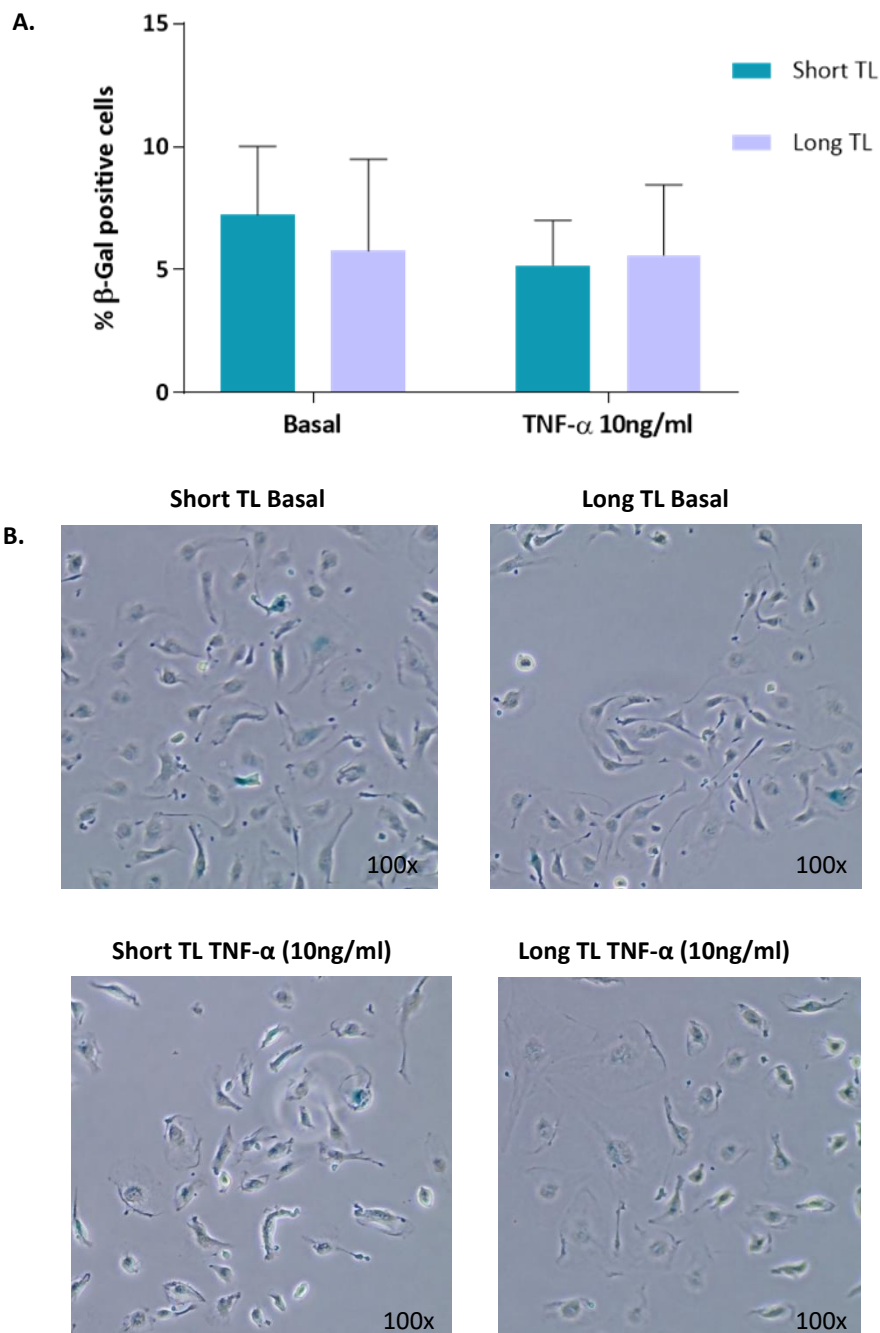


Figure 4.8 Minimal senescence detected in the short and long TL lines both at basal and upon TNF-α treatment at the time the functional experiments were performed. A. Senescence associated β-Galactosidase activity was quantified at day 218 for the short TL clone and day 212 for the long TL clone cells at basal (untreated) and after treatment with TNF-α (10ng/ml) for 24 hours. B. Brightfield images were taken of cells with short TL and Long TL at basal and post TNF-α treatment. Images shown at 100x magnification. Fluorescence unit values are representative of three independent experiments (n=9 samples in total). All samples were normalised to short TL basal. Mean±SD Basal short TL 7.23±2.78 versus Basal long TL 5.78±3.72, TNF-α short TL 5.12±1.83 versus TNF-α long TL 5.60±2.85).

4.4 Conclusion

To understand how telomere length may influence coronary artery disease risk (with particular focus on atherogenesis), it is important to establish how telomere length may influence endothelial dysfunction. We hypothesised that TL may influence the earliest stage of atherogenesis, endothelial dysfunction (ED) and shorter TL drives this process. This chapter explores the creation of isogenic cell lines with short and long telomere lengths in HUVEC and investigates whether such differences in telomere length are attributed to changes in endothelial cell function in response to proatherogenic stimuli.

Experimental HUVEC isogenic lines with long and short telomeres was successfully generated according to the model developed in Chapter 3, using an established Cre-Lox genome editing technique (Salmon *et al.*, 2000). Using a self-excising viral Cre, two excisions approx. ~20 days apart (early Ex1 and late Ex2), were performed on subcultures to produce “short” and “long” TL lines, this procedure was repeated on two further separate occasions to produce three independent experiments.

Upon the addition of viral Cre, both excised lines confirmed the complete removal of the *TERT* transgene and the total abolishment of telomerase activity. The previous chapter (**section 3.3.6**) showed pro-viral *TERT* integrated at a single integration point in Line 7, this lies within an intron (at Chr2q33) of the *MOB4* gene, levels of *MOB4* remained unchanged upon the integration of *TERT*. This model utilised a viral Cre for the generation of isogenic lines and therefore involves a second integration event which carries an additional risk of insertional mutagenesis (Cuiffi *et al.*, 2016) within this actively transcribing gene. No differences in *MOB4* expression was observed upon further Cre viral integration. Therefore, it can be assured any differences observed with this line are not due to an effect of *Cre* integration. The Line 7 immortalised HUVEC maintain protein expression of the EC surface markers CD309, CD31 and CD144 (**section 3.3.6**). We show the isogenic lines maintain this endothelial cell phenotype during the process of reversible immortalisation. This is consistent with other another study (Noguchi *et al.*, 2002), that has utilised the Cre-Lox system to remove TERT from HUVEC

which emphasizes the viability of using HUVEC in this model without compromising cell phenotype.

During phenotyping, both the short and long isogenic lines showed a marked increase (of >2 fold) in the expression of CD31 (PECAM-1). This is a multi-functional molecule involved in vascular inflammation and transendothelial cell migration (Woodfin *et al.*, 2009), therefore the increased expression in lines with a shorter TL compared to parental is an interesting finding and warrants further investigation. There was insufficient time within the scope of this project to investigate differences between the level of CD31 (PECAM-1) in the Cre excised lines versus parental.

TL analysis revealed the average TL for the Ex1 clone was shorter than for the Ex2 sub clone (T/S Ex1 2.39 ± 0.37 vs Ex2 4.01 ± 0.31), confirming subtle differences the TL of the short and long isogenic lines. This is a different approach to the Minamino study (2002) which induced catastrophic differences in TL (through expression of a dominant negative TRF-2 knockdown) to assess ED.

The functional analysis of the short and long isogenic lines in response to pro-inflammatory TNF- α stimulation, unexpectedly showed higher basal differences of the endothelial dysfunctional markers, *ICAM-1* and *E-SELECTIN* in the shorter TL line. No further differences in these genes were observed upon stimulation with TNF- α which confirms the effects are driven by the differences observed at baseline. Due to this effect of higher *ICAM-1* expression at basal levels in the short TL clone, our findings show upon TNF- α there is a higher level of upregulation in the long TL clone in order to reach the same expression level as the short TL clone upon stimulation in response to EC activation (Poher & Sessa 2007, Paffen& DeMaat 2006). As a result of this process, a higher upregulation in *ICAM-1* expression the long TL line was observed upon TNF- α exposure. During acute inflammation, type II activation of endothelial cells mediated by TNF- α is a slow response (hours compared to minutes for Type I activation) that depends on pro-inflammatory gene expression changes (Poher 2007). No differences were observed in *eNOS* expression at basal and upon treatment, reduction in the *eNOS* promoter activity

is time-dependent and has been observed after 8 hours of TNF- α exposure (Anderson *et al.*, 2004). The TNF- α treatments were 24 hours, it is therefore possible to have missed the pro-inflammatory response for *eNOS* which may be acute during inflammation.

Following the gene expression analysis, further experiments on the isogenic lines revealed *ICAM-1* was higher (31%) at a protein level, in the short TL clone. As with the *ICAM-1* gene expression findings, long and short lines showed no difference in *ICAM-1* gene or protein expression following TNF- α treatment. Consistent findings in the up-regulation of *ICAM-1*, (at both an RNA and protein level) in basal levels of the shorter TL, prompted the exploration of investigation the functional effect between the isogenic lines.

ICAM-1 is an important mediator in monocyte cell recruitment to the endothelium during the initial stages of atherogenesis (Lusis 2000). Endothelial cell activation and dysfunction is known to drive this process (Lui *et al.*, 2017). As expected, the functional analysis of the short and long isogenic lines showed in response to TNF- α , increased THP-1 blood monocyte cell adhesion, compared to basal in both the short and long TL HUVEC. Prior to TNF- α treatment (at basal), a significant reduction in monocyte binding was observed in the long TL lines compared to the short TL lines. This shows the differences observed in *ICAM-1* expression (at both gene/protein expression level) at basal contributes in part to a functional difference in monocyte adhesion. Further experimental work to validate the role of *ICAM-1* in this process is discussed in the following chapter (**section 5.3**).

As expected, both the protein and gene expression levels of *ICAM-1* increased upon TNF- α stimulation, however no differences were observed in *ICAM-1* between cells with short and long TL. Interestingly, an increase in the number of monocyte binding to cells with short TL were observed at basal and upon TNF- α treatment. Although differences were observed in *ICAM-1* gene/protein expression between the two lines, we are seeing an enhanced functional effect in monocyte binding most likely due to additional factors. Differences in the level of *E-SELECTIN* were observed, which was marginally higher in the short TL clone. Due to time constraints this was not followed through to protein level but *E-SELECTIN* may play a role in driving this process. There are other factors, not

measured in this study, which may contribute to monocytic cell adhesion process. A key cell adhesion molecule, VCAM-1 (expressed on EC) binds to the ligand integrin $\alpha 4\beta 1$ (VLA-4) expressed on monocytes, this is important for the adhesion of circulating monocytes to the vascular endothelium (Čejková *et al.*, 2016). In addition, TNF- α stimulation of HUVEC, induces the expression of chemokines including CXCL2, CXCL6, colony stimulating factor 1 and fractalkine (Viemann *et al.*, 2006) and other cell adhesion molecules such as VCAM-1, E-SELECTIN and P-SELECTIN (Lorenzon *et al.*, 1998; Hang *et al.*, 1993) which orchestrate the adhesion cascade to greatly enhance cell adhesion. Therefore future work, would involve quantifying protein levels of additional cell adhesion molecules VCAM-1, E-SELECTIN and P-SELECTIN to assess whether these are additional players implicated in driving ED in the shorter TL line.

One other study has shown catastrophic telomere loss (via the removal of TRF-2) induced EC as shown by increased *ICAM-1* and decreased *eNOS* is driven by senescence (Minamino *et al.*, 2002). Using our experimental model, it was assessed whether differences in *ICAM-1* observed at basal were driven by senescence and found this is not the case, showing that differences in *ICAM-1* at both gene/protein level are most likely attributed to TL. Minimal senescence was observed in the short and long TL lines at basal; no differences are observed between the two lines. The detection of senescence in both the long and short lines at basal is observed as the Line 7 isogenic cells are of a mixed population in nature, therefore any senescent HUVEC are due any existing unexcised cells within the population. This is not a cause for concern as validation of *TERT* removal was confirmed prior to the functional experiments. These findings suggest senescence is not driving the pro-inflammatory phenotype of the short TL clone and endothelial dysfunction and subsequent monocyte adhesion occurs prior to the onset of replicative senescence.

Although preliminary this work suggests TL may influence CAD risk through increased recruitment of monocytes to the endothelium. Further work is needed to investigate whether this functional effect is seen in other donors (to assess whether this is a genotype specific effect) and / or lines of the same donor with different integration sites (to show this is not affected by integration site of the *TERT* provirus).

CHAPTER 5

DISCUSSION

CHAPTER 5

DISCUSSION

5.1 Summary of key findings

The aim of this project was to establish a model system to enable us to manipulate TL without the presence of confounding factors and to test the effects of more subtle changes in TL, reflective of the inter-individual differences seen within the population. The model could then be used to test possible biological mechanisms by which shorter TL leads to increased CAD risk.

The model could potentially be applied to various different cardiovascular cell types (e.g. VSMC, EC) to allow us to assess the potential role of TL during atherogenesis. VSMCs undergo telomere dependent senescence, the markers of senescence SA β -gal and cyclin-dependent kinase inhibitors p16 and p21 are detected in advanced atherosclerotic plaques (Minamino *et al.*, 2003; Matthews *et al.*, 2006). However, VSMC are a difficult cell type for this model as the cells undergo a reversible phenotypic switching from a quiescent contractile phenotype to a proliferative synthetic state during the atherosclerotic process (Bennett *et al.*, 2016; Chang *et al.*, 2014). Furthermore, it would be challenging to target VSMC dysfunction as this cell type is involved in different stages of the atherosclerotic disease process (e.g. during atherogenesis and also plaque instability during advanced atherosclerosis), which would add a level of complexity to the *in-vitro* model system.

To explore the role of TL dynamics during the earliest stage of atherosclerosis, endothelial dysfunction, endothelial cells were used. Although primary Human Coronary Artery Endothelial cells may seem like the obvious cell type, Human Umbilical Vein Endothelial cells were specifically chosen. EC derived from umbilical cord are a relevant EC type (Onat *et al.*, 2011), most importantly, it can be assured the population doublings of the cells are kept to a minimum prior to utilising the cells in this model.

The initial stage of this procedure was to produce immortalised lines via a lentiviral transfer method (Salmon *et al.*, 2000) that contained a removable copy of the *TERT* transgene. The use of classical retroviral vectors is another technique used to transfer exogenous *TERT* to primary cells (Counter *et al.* 1998). This is a low efficiency process, and alongside *TERT*, growth promoter or cell cycle inducers are used in combination including the SV40 T-antigen (O'Hare *et al.*, 2001; Wen *et al.*, 2006; Chang *et al.*, 2005; Shao *et al.*, 2004), human papilloma virus E6 and E7 oncogenes (Kiyono *et al.*, 1998) or Bim-1 (Jacobs *et al.*, 1998). This approach was not favoured, as many of the studies reported malignant cellular transformation. The findings from this study are consistent with other studies where immortalisation of primary cells was achieved using human *TERT* alone (Yang *et al.*, 1999; Ouellette *et al.*, 2000; Vaziri *et al.*, 1998).

Cellular immortalisation is achieved when cells have exceeded growth past 100 PDs in culture (Yang *et al.*, 1999). Therefore, it was necessary to culture the *TERT*+ cells for an extended period of time. During the first attempt to immortalise HUVEC using *TERT*, the *TERT* transduced cells showed successful integration of the provirus at a copy number of 1.0 per cell followed by substantial *TERT* upregulation. Although the *TERT*+ line had outlived the parental cells, this line did not reach 100 PDs. Telomere length shortening was observed in the parental and unexpectedly in the *TERT*+ line. Despite this the *TERT*+ cell population continued to grow. Stress inflicted upon prolonged culturing conditions is a contributing factor to the premature growth arrest of cells, and is telomere-independent (Kiyono *et al.*, 1998; Dickson *et al.*, 2000). The most logical explanation behind these findings, is the parental cells are undergoing stress-induced rather than replicative senescence and *TERT* is having a protective effect on the cells. Premature growth arrest is associated with the upregulation of a cyclin-dependent kinase inhibitor, p16^{INK4A}, and is known to be caused by stress inflicted by prolonged culturing conditions (Ramirez *et al.*, 2001; 2003; Herbert *et al.*, 2002). On the other hand, over-expression of the cell cycle regulator, CDK4 sequesters p16^{INK4A} to allow free CDK4 to bind to cyclin D to enable cell cycle progression. Although there was insufficient time to verify this, premature senescence can be confirmed in the parental (untransduced) cells grown in 20% oxygen by quantifying expression levels of p16^{INK4A}/CDK4; where levels of p16^{INK4A} are expected to be higher.

Standard culturing conditions are considered hyperoxic to the cell and may inflict cellular stress (Jagannathan *et al.*, 2016). The protective role of TERT has been previously reported, under conditions of oxidative stress such as mild hyperoxia, TERT is known to be relocated to the mitochondria (Haendeler *et al.*, 2009; Haendeler *et al.*, 2004; Santos *et al.*, 2004) where it protects the mitochondrial genome from reactive oxygen species (Ahmed *et al.*, 2008; Haendeler *et al.*, 2009). This could be verified in the TERT+ cells grown in 20% oxygen, by looking at levels of mitochondrial protective markers, such as catalase, superoxide dismutase in comparison to ROS levels.

The nuclear localisation is dependent on residues 965-981 of the human TERT polypeptide which constitutes a nucleolar-targeting signal essential for this process (Lin *et al.*, 2008). Due to this dual-canonical function of TERT, it seemed plausible that TERT may be protective, allowing the cells to outlive the parental cells, but immortalisation has not been achieved as this process is TL independent. A well established marker of DNA damage is the phosphorylation of Histone H2A variant, H2AX (γ -H2AX), where telomere associated γ -H2AX foci exist under conditions of stress induced senescence in the presence of short telomeres (Hewitt *et al.*, 2012). To confirm the protective role of telomerase (in TERT+ cells grown in 20% oxygen), the levels of γ -H2AX foci should be determined. As telomerase protects the mitochondrial genome from reactive oxygen species (Ahmed *et al.*, 2008), levels of DNA damage γ -H2AX are expected to be low even in the presence of the short telomeres in the TERT+ cells grown under 5% oxygen.

Physiologically relevant lower oxygen levels have been used in studies and cells show a 20-50% increase in PDs (Betts *et al.*, 2008). Furthermore, one study has shown that over expression of TERT in endothelial cells does not prevent telomere loss in standard culture conditions however TL is maintained when grown under 5% O₂ (Napier *et al.*, 2010). Therefore, this method was adopted in this study and cells were revived from the earliest passage and regrown under 5% oxygen (20% CO₂ at 37°C). The cell culture dynamics diverged with this approach, as expected, un-transduced control cells entered growth arrest after 49 days in culture whereas the TERT+ cells continued to show an increased and stable growth rate. Most importantly, the growth kinetics of the

TERT+ cells corresponded with an observed TL lengthening followed by stabilisation throughout subsequent culture.

In total 9 HUVEC donors were originally infected with lentiviral *TERT*, 4 of which successfully immortalised and 5 failed. The unsuccessful lines are further discussed in the next section, in the context of 'Limitations of the *in-vitro* experimental model system'. Successful *TERT* expression at both gene and protein level was detectable in all 4 immortalised lines, telomere lengths were stabilised, and the cells retained EC phenotypic and morphological characteristics. The immortalised lines showed unique differences in telomerase activity and the level of TL stabilisation. Comparison of the lines show Line 10 immortalised with a high level of stabilisation and showed the highest relative telomerase activity whereas Line 1 immortalised with a low level of stabilisation and showed the lowest relative telomerase activity. However, further analysis with Line 1 iHUVEC revealed TERT expression was significantly lost during the culture period of 251 days. Prior to the stabilisation at a low TL, after ~40 PDs there is a period where the TL dynamics in Line 1 iHUVEC are sporadic, which may explain the altered T/S kinetics of this line. Fragile telomeres develop aberrant structures due to replication defects in telomeric repeats that can be detected on metaphase chromosomes, this process has been shown to contribute to telomere shortening (Boccardi *et al.*, 2018). Therefore, to further investigate Line 1 iHUVEC, the cells can be karyotyped to check the telomere in individual chromosome arms using Q-FISH (Perner *et al.*, 2003). Visualisation of the metaphase spread of chromosomes, will give an idea of whether there are chromosome fusions/chromosomal aberrations which will explain the altered T/S kinetics of this Line. This may be a donor specific effect, an effect of the insertion site(s) of the TERT provirus (which will be discussed later in this section) or a random occurrence. This experimental model utilises a heterogenous population of cells, therefore it is possible at an earlier point in culture for clonal selection to have randomly occurred where the un-transduced cells dominated the cell population giving rise to a clonal line (Kay 1965; Martin *et al.*, 1993). Future work with this line would involve re-growing the cells from a point where a linear growth rate was observed where the average TL was maintained by telomerase at a high level. This would be to assess the TL dynamics and see if the lines stabilised low again or whether it would be possible for the cells to stabilise at a higher TL.

Multiple *TERT* pro-viral integration events were detected in Line 2, one within an intron of the tumour suppressor protein *PTEN* and downstream of an intronic non-coding transcript (*LOC107987150*). Mutations in *PTEN* have been shown to promote angiogenesis, hyperproliferation and impair vascular remodelling (Suzuki *et al.*, 2007), therefore disruption of this gene upon *TERT* integration could adversely affect our model. A second site was observed at Chr8q24.3 within an intron of an uncharacterised gene *C8orf33*. A third integration was identified at Chr20q11.22, within an intron of *nuclear receptor coactivator 6* (*NCOA6*), a multifunctional gene involved in transcription, cell survival, growth and development (Mahajan & Samuels 2008). There was insufficient time to take this line further as additional validation work is required to check whether multiple integrations within the same cell or a population of three clones.

Further verification to assess whether the viral integration influences expression and/or splicing of *PTEN*, *C8orf33* or *NCOA6* is necessary. It is important to note, the assay used measure copy number is on a diploid genome (using a mixed population of HUVEC) therefore this is not an unequivocal measure and does not reflect a true copy number/cell but rather an average measurement. The copy number data for Line 2 (~0.8 copies of *TERT* provirus/cell) would suggest a mixed population. Therefore, attempts could be made to obtain clonal lines for each of the three integration sites and proceed with the lines where endogenous gene expression is not altered.

Pro-viral *TERT* integrated at a single integration point in Line 7, this lies within an intron (at Chr2q33) of *MOB4*. *MOB4*, negatively regulates apoptotic signalling, over-expression of the protein form is observed in Glioblastoma Multiform, therefore the protein may be involved in promoting tumour growth (Tang *et al.*, 2014). We show *TERT* integration within this gene does not alter the level of endogenous *MOB4* expression, therefore it can be assured any phenotypes observed are not due to an effect of *TERT* integration on *MOB4*.

Once the experimental model system was established, isogenic lines of short and long telomere lengths were successfully created from one of the immortalised donors using an established Cre-Lox genome editing technique (Salmon *et al.*, 2000). In our model, a self-excising viral Cre effectively removed the *TERT* transgene which led to total

abolishment of telomerase activity. Successful *TERT* excision was observed for both Line 7 and Line 10, these donors showed TL stabilisation at a high level (comparable to the TL of the lines in early culture stages). However, due to time constraints only Line 7 was taken into a full experimental model.

Two excisions, approx. ~20 days apart, were performed on subcultures to produce “short” and “long” TL isogenic lines. The ‘20 days’ timing of the second excision for the generation of the long TL clone is critical. The model confirms this window is optimum; the first excised line is still viable and has not have undergone sufficient TL attrition to reach replicative senescence / growth arrest whilst still achieving an acceptable difference in TL between the two lines.

This procedure was repeated on two further separate occasions to produce three independent experiments. To assess whether there are functional differences between the short and long TL lines, the gene expression of the cell adhesion molecules, *ICAM-1*, *E-SELECTIN* and *eNOS*, *ICAM-1* protein expression and endothelial cell-monocyte binding were measured both at baseline and in response to pro-inflammatory TNF- α stimulation. Unexpectedly marginally higher basal differences were observed in the endothelial dysfunctional markers, *ICAM-1* and *E-SELECTIN* in the shorter TL line. Due to the higher expression of *ICAM-1* at basal in cells with short TL (compared to cells with long TL), *ICAM-1* increase in cells with long TL line upon stimulation with TNF- α . This suggests the basal level of *ICAM-1* in the short TL line may lie close to the maximum level, therefore this finding may be due to a greater response to TNF- α treatment observed in the long TL line due to the lower basal level.

Further experiments on the isogenic lines revealed *ICAM-1* protein level at the endothelial cell surface, was higher (31%) in the short TL clone. Endothelial dysfunction was further confirmed through the monocyte EC adhesion assay, the shorter TL line showed an increase in monocytic adhesion both at basal levels and upon stimulation with TNF- α . Although preliminary this work suggests TL at a ‘basal’ cellular level may

influence CAD risk through increased recruitment of monocytes to the endothelium. Further work is needed to investigate whether this effect is seen in other donors to rule out any genotype specific effects.

TL as a marker for biological age in premature ageing diseases including Dyskeratosis Congenita and Aplastic Anemia (AA) has been discussed (**section 1.2.3 and 1.2.4**). Such diseases have obvious mutations in telomere binding proteins including *TERT/TERC* which induces catastrophic telomere length loss and replicative senescence (Beier *et al.*, 2012; Vulliamy *et al.*, 2008). In AA cell types such as haemopoietic cells of the bone marrow that naturally have a high turnover rate. On the other hand, CAD, is an age associated disease, the telomere length shortening dynamics are that of subtle changes and the effect of this may occur over a longer period of time (as symptoms of CAD do not manifest straightaway). There is only one previous study that has investigated telomere length at the earliest stage of atherogenesis, ED (Minamino *et al.*, 2002). However catastrophic telomere loss, via the removal of TRF-2 induced ED as shown by increased *ICAM-1* and decreased *eNOS*. The authors concluded this inflammatory process was driven by senescence however no other functional studies were performed (Minamino *et al.*, 2002). Aberrant chromosomal fusions and large metaphase spreads are a prominent feature of cells with catastrophic *TRF2* knockdown (Rai *et al.*, 2016) which does not reflect subtle changes in TL observed at an inter-individual level within the human population (Madrid *et al.*, 2016). This study therefore assessed whether differences in *ICAM-1*, due to subtle changes in TL, were driven by senescence and found this is not the case, showing that differences in *ICAM-1* at both gene/protein level was most likely attributed to TL.

In addition to higher levels of ED, at a functional level, monocyte binding in the shorter TL line was increased. It is confirmed the functional effect of monocyte EC adhesion is not driven by senescence and therefore may be occurring as an effect of shorter TL. Yanaka *et al.*, (2011) observed an increase in a number of adhesion molecules (*ICAM-1*, *E-SELECTIN*, *CCL2*, *ITGB3*, *ITGAV* and *ITGB1*) promoting monocytic adhesion and this process was significantly promoted by ageing. These observations are in line with our findings based on the hypothesis that TL is a marker of ageing. To our knowledge no

other studies have reports basal endothelial dysfunction associated with subtle telomere length differences which is more reflective of the inter-individual differences observed in the human population.

5.2 Limitations of the *in-vitro* experimental model system

Despite the initial success, 5 further single HUVEC donors failed to immortalise, this shows a challenge in our experimental model system; creating further lines was not guaranteed and limitations exist to this approach.

Two of these lines failed to outlive the parental cells despite high *TERT* expression (114 fold and 39-fold relative to a telomerase positive K562 lymphoblastoid cell line) observed ~10days post lentiviral *TERT* infection. As addressed in the previous section, one possible explanation is that inadvertently line may have grown from a mixed population to clonal and we are observing the effect of this. To address this issue, attempts were made (at the time of *TERT* transduction when *TERT* was substantially expressed) to try and grow the EC to clonal *TERT*+ line. This approach has failed; EC are a very difficult cell type to maintain in culture at low confluency/single cell due to contact inhibition (Nosedá *et al.*, 2004).

There are other explanations accountable for the failure of cells to immortalise. One of the donors that failed to immortalise (Line 4) showed a pro-viral copy number of 2.0 and a significant loss of *TERT* expression over time. Viral integration and cellular genotoxicity is related to the number of vector copies integrated per cell and high pro-viral copy number has been associated with gene silencing of the integrated cassette (Lui *et al.*, 2008). This may explain the low level of *TERT* transgene upon initial infection (compared to the other infected lines) and the subsequent loss of *TERT* during culture.

This model does not ambiguously control for the random integration of provirus *TERT*, this has been shown to be an implication in both the successful and unsuccessful donors. Lentiviruses integration is site specific, and integration takes place in gene-dense regions

throughout the transcription units, with 60-70% within transcriptionally active loci (Ciuffi *et al.*, 2016), therefore the chances of insertional mutagenesis is high. In Line 7 iHUEC, TERT integrated within an intron (of Chr2q33) of *MOB4* an actively transcribing gene, although expression levels of this gene were unaffected compared to parental. However, using this model system, it cannot be controlled where TERT is integrated in other lines. If this is within *cis* regulatory elements such as enhancers, insulators or repressors this will be detrimental to the cell. Enhancers are short motifs that contain binding sites for transcription factors; which activate the target genes without regard to orientation (Bulger & Groudine 2011). Repressors suppress gene expression and/or confine it within specific chromatin boundaries (chromatin insulators) (Maeda & Karch 2011; Yang & Corces 2011). Inevitably, proviral integration within such elements e.g. a repressor, will suppress the expression of nearby genes as well as regulating transcription rates of the transgene itself, which may indeed be the case for Line 4 (where *TERT* expression was lost over time). The safe harbour locus, *Rosa26* in mouse (Zambrowicz *et al.*, 1997) or AAVS1 in human located on chromosome 19 (locus PPP1R12C) (DeKever *et al.*, 2010) are transcriptionally active regions with an open chromatin configuration. The use of AAVS1 would be an alternative approach in this model as transgene insertion within this locus has no or minimal effect on global or local gene expression and can therefore resolve the problem of transgene silencing.

Two of the donors, Line 3 and 6 failed to immortalise despite a substantial upregulation in *TERT* observed early in the culture period. Line 6 showed progressive TL shortening in the TERT+ line; although *TERT* expression was not checked continuously during the culturing time where TL shortening is observed, there is a possibility *TERT* may have been inhibited by posttranscriptional regulators. MicroRNA (miRNAs) are small noncoding RNAs that bind to the 3' UTR of target mRNAs. Subsequent translational suppression or degradation of the RNA–DNA duplex mediated by the RNA-induced silencing complex (RISC) causes a reduction in protein expression (Eulalio *et al.*, 2012). Endogenous miR-128 inhibits telomerase activity by directly binding to the coding sequence of *TERT* mRNA (Guzman *et al.*, 2018). To specify the function of miR-128 in the TERT transduced lines, miR-128 can be transfected Line 6 at a point where it is certain TERT expression is high (this was observed day 8 post LV-TERT transduction). The

expression of miR-128 can be under control of the α -myosin heavy chain (α -MHC) promoter, which has shown to overexpress miR-128 (Huang *et al.*, 2018). As TERT is the rate limiting catalytic component of telomerase (Kim *et al.*, 1995), this will part explain how telomerase is unable to function to meet the needs of TL length maintenance. To verify miR-128 activity, *miR-128* can be knocked down using a specific miR-128 inhibitor. To validate *miR-128* knockdown, *TERT* in the LV-TERT transduced HUVEC should remain high, consequently TL should be stabilised/increased. miR-128 is an interesting miRNA in the cardiovascular field, most recently it is shown to be a critical regulator of cardiomyocytes (CM) proliferation and cardiac function. Deletion of *miR-128* promotes cell cycle re-entry of adult CMs, thereby reducing the levels of fibrosis, and attenuating cardiac dysfunction in response to MI (Huang *et al.*, 2018).

In the TERT+ lines clonal lines are emerging from the mixed population, this is evident in Line 7 and 10 where pro-viral *TERT* lies within a single integration point, suggesting that a single clone has become dominant within the population over time. As discussed earlier in this chapter (**section 5.1**), at the very initial stages of this work, Line 7 failed to immortalise under standard (20% oxygen culturing conditions). This was amidst the speculation that the line failed to immortalise as TERT has been shown to be protective under mild hyperoxia, allowing the cells to outlive the parental cells and this process is TL independent. The Line 7 TERT+ line was subsequently revived at the earliest point in culture and regrown under 5% oxygen. The time from which the cells were transduced with TERT (under standard oxygen) to the point at which the cells were frozen is ~17days which for Line 7, equates to ~14PDs. During this time we cannot absolutely rule out that the TERT+ line was a mixed cell population, it is possible a different (untransduced) clone became dominant. The integration site analysis of this line was performed only after the cells had undergone immortalisation (largely because this was not anticipated) at which a clonal line may have already been established. We have discussed how other HUVEC lines failed to immortalise even at 5% oxygen, counter-intuitively these cells may not be any different to the Line 7 TERT+ cells cultured at atmospheric oxygen and in our model oxygen levels in the cell may have no effect on the function of TERT. Reasons to address this are discussed further in this chapter.

We have used an additional viral transduction to add Cre, inevitably this introduces further integration sites. As clonal succession following TERT transduction has been observed, the same process may occur following Cre transduction. Inadvertently lines may be clonal where the integration does have an effect and these dominant clones differ between the first and second excision lines. Integration site will be difficult to assess for Cre as it is self-excising. A better approach therefore would be to optimise the method of transient Cre delivery, to avoid further integration. If this is not possible then an alternative could be to use a SIN (self-inactivating) lentivector derivative. The LTR region of 2nd generation transgene lentivectors contains the *cis*-element TATA box and binding site for transcriptional factors Sp1 (Specificity protein 1) and NF-κB (Naldini *et al.*, 1996). In a SIN (self-inactivating) vector the 5'-LTR U3 region has been replaced with a CMV promoter and a deletion in the U3 region of the 3'-LTR (Miyoshi *et al.*, 1998), this reduces the effects of random integration of the pro-virus to activate adjacent cellular genes.

However, despite these potential issues our data from short and long TL lines were obtained from three independent experiments and the functional data looks encouraging, which showed consistent effects between experiments. Therefore, it is unlikely that clonal succession following Cre excision is responsible for the observed functional effects. To show the observed effects are due to TL, the model will need replication in other lines / donors to show this is not affected by integration site or donor/genotype specific effects are required.

5.3 Future Work

This project successfully established a model system to generate isogenic HUVEC with short and long TL using one donor, the model showed a difference in endothelial function, particularly in monocyte binding during early atherogenesis. Following this, there is scope for future work.

Line 10 iHUVEC TERT integrated at a single event within an intergenic region. This line showed the highest relative telomerase activity and high level of TL stabilisation, therefore this line looks promising for the generation of isogenic lines of short and long TL. To show the observed effects are due to TL, the model will need replication in other lines/donors to show this is not affected by integration site or donor/genotype specific effects are required.

Cell adhesion mediated by ICAM-1 is an important mediator in monocyte cell recruitment to the endothelium which is critical for the trans-endothelial migration of leukocytes during the atherogenic process (Lusis 2000; Zuckerman *et al.*, 1998). This process is driven by endothelial cell dysfunction (Albrecht *et al.*, 2004; Lui *et al.*, 2017). Functional analysis of the short and long isogenic lines showed a significant reduction in monocyte binding in cells with long TL compared to cells with short TL at both basal and in response to TNF- α stimulation. This shows the differences observed in ICAM-1 expression (at both gene/protein expression level) at basal contributes in part to a functional difference in monocyte adhesion. To further validate the role of ICAM-1 in the monocyte adhesion process, the specificity of this adhesion molecule can be explored. ICAM-1 binds to the β 2 family of integrins including CD11c/CD18 (p150,95) (expressed on monocytes), this interaction is via the Ig domains 3/4 (Frick *et al.*, 2005). Residue E²⁵⁴DEGTQRL of domain 3 is a critical primary binding site for the α X I-domain of the α X β 2 integrin CD11c/CD18 (p150,95) (Choi *et al.*, 2010). HUVEC was short and long TL can be pre-treated with a neutralising ICAM-1 antibody against the E²⁵⁴DEGTQRL residue of domain 3. Compared to non-antibody incubated controls one would expect, in the presence of the antibody binding of ICAM-1 to Mac-1 will be abolished therefore, the TNF- α induced HUVEC will fail to induce monocyte adhesion.

As expected, both the long and short TL cells show increased ICAM-1 protein expression in response to TNF- α , however differences were not observed between the short and long TL lines. A functional difference in monocyte binding was seen between the isogenic lines; with increased monocyte binding to cells with short LT both at basal and in response to TNF- α . This exemplifies how the observed functional effects are not solely due to ICAM-1 (as upon in response to TNF- α no differences in ICAM-1 were observed, and additional molecules are driving this process). In addition to *ICAM-1*, the expression of the cell adhesion molecules *VCAM-1*, *PECAM* and *E-SELECTIN* contributes to monocyte activation and recruitment from adventitial vessels and the arterial lumen in atherosclerosis (Davies *et al.*, 1993), which progresses to the monocyte adhesion cascade. Capture, the initiation stage of the adhesion cascade, is mediated mainly by L-selectin and P-selectin (Čejková *et al.*, 2016). Therefore, in association with the EC-monocyte adhesion data future work with the isogenic lines of short and long TL would involve looking at the protein expression of these cell adhesion molecules on the surface of the cells by flow cytometry.

In this study, to assess the functional effect of HUVEC with short and long TL, cells were treated with the pro-inflammatory cytokine, TNF- α , to evoke EC activation (Pober *et al.*, 1986; Albrecht *et al.*, 2004). Additional pro-inflammatory stimuli such as interleukin-1 β (IL-1 β) can be tested on the model system. TNF- α and IL-1 β are both released from activated leukocytes to mediate type II EC activation (Pober *et al.*, 1986). Pro-inflammatory responses induced by TNF- α and IL-1 β cytokines initiate the transcription of specific genes within the nucleus (by NF- κ B and AP1) and are translated into adhesion molecules (ICAM-1, VCAM-1, E-SELECTIN) and chemokines (CC-chemokine ligand 2 (CCL2)) that bind leukocytes (Pober *et al.*, 2007, Makó *et al.*, 2010). Future work will involve treating HUVEC lines with short and long TL with IL-1 β to initially assess the expression of the ED markers at a gene/protein level (Pober *et al.*, 1986).

This model of generating isogenic lines with different TL has been successfully established using one donor (Line 7) where a functional difference is observed in EC-monocyte adhesion which is dependent on TL. Therefore, there is scope to implement

further *in-vitro* assays to explore the functional effect of the short and long TL lines. EC proliferation and migration occurs during early atherogenesis (Ross 1999). The proliferation of EC and the adhesion of monocytes increase at branch orifices in atherosclerosis prone regions (Azuma *et al.*, 2003). EC proliferation in cells with short and long TL can be measured by incorporation of BrdU (5-bromo-2'-deoxyuridine) into DNA, this method allows living cells to be counted. To measure EC migration, a wound 'scratch' assay can be performed. Isogenic cells of short and long TL are plated (independently) in the centre of the chamber well, once the EC reach 70-80% confluency, a physical 'scratch' is produced perpendicular to the well axis. The distance the cells have migrated within that region can be counted after a certain number of hours (e.g. 4h or 8h) and the percentage of the closed area compared with the initial wound area is then quantified.

Angiogenesis (formation of new blood vessels from pre-existing vasculature) is a pathobiological process that occurs during atherogenesis and involves endothelial cell proliferation, migration, tube and lumen formation (Herrmann *et al.*, 2006). Differences in TL may effect the angiogenic potential of EC, therefore for future work an angiogenesis assay can be performed using the lines. Cells can be plated and treated with the pro-angiogenic stimuli VEGF. The formation of vascular structures can be monitored over a period of time (e.g. 4 hours). For quantification, photographs can be taken with an optical inverted microscope and an automated analysis of quantification (incorporating total master segment lengths and NB master junction parameters) can be performed using an ImageJ software (Luna *et al.*, 2015).

Atherogenesis is a slow progressive process characterised by multifocal structural alterations of EC within the vascular wall. Dysregulation of EC apoptosis is implicated in this process, where increased EC turnover and apoptosis is observed in atherosclerosis-prone regions of the vasculature. A recent review by Paone & colleagues (2019) covers a more prominent role of EC apoptosis in the progression of atherosclerosis through EC derived membrane-bound extracellular vesicles (Paone *et al.*, 2019). Future work can address the level of EC apoptosis in the isogenic lines using a Terminal deoxynucleotidyl transferase-mediated dUTP nick-end labelling (TUNEL) assay. This assay examines

apoptosis via DNA fragmentation where DNA strand breaks are detected by enzymatically labeling the free 3'-OH termini with modified nucleotides (Gavrieli *et al.*, 1992). TUNEL-positive EC can be quantified in both the short and long lines as a measure of apoptosis.

The Telomere Position Effect (TPE) is the spreading of telomeric heterochromatin within telomeres to silence nearby genes as a function of length and has been shown to be implicated in age-related diseases (e.g. facioscapulohumeral muscular dystrophy) (Baur *et al.*, 2001; Mondoux & Zakian 2006). TPE has an effect on gene expression locally (Salmon *et al.*, 2013). This effect is progressive with decreasing TL and occurs long before terminal telomere shortening would induce replicative senescence. Evidence also suggests that TL may be affecting the gene expression changes further afield than those genes proximal to the telomere (Robin *et al.*, 2014; Kim *et al.*, 2016;). As isogenic lines of short and long TL with Line 7 have been established, more global gene expression changes could be measured. A custom gene expression array can be performed to look at genes expressed at the sub-telomeric region or adjacent regions in isogenic short and long TL lines. A Hi-C chromosome capture can be applied to enrich for specific genomic regions, followed by high-throughput sequencing microarray. Differentially expressed genes can then be confirmed using digital droplet PCR within the telomeric region. This approach may unveil novel information about which genes and cellular pathways may be regulated that are solely attributed to changes in TL.

This project successfully established a model system to generate isogenic HUVEC with short and long TL and findings showed a difference in endothelial function, particularly during the monocyte adhesion process during early atherogenesis. This can further be explored by other avenues. A previous study shows that statin treatment specifically benefits individuals with shorter TL (Brouillette *et al.*, 2007) but not via the modulation of lipids. Furthermore, statin treatment on endothelial cells reduce protein levels of E-SELECTIN and ICAM-1 and the inflammatory marker C-reactive peptide, therefore there is evidence that statins may influence EC function; by reducing the adhesion of inflammatory cells (Altun *et al.*, 2014). Using the established model and findings from

this work, future work can investigate how statin may influence the cellular response to TNF- α in a TL dependent manner.

In this work, the differences observed in pro-viral integration events, level of telomerase activity and TL stabilisation (with similar CN and *TERT* expression levels) in the immortalised donors is important, as gene therapy using lentivectors is emerging (Cesani *et al.*, 2015). However, if EC from individuals respond to this level of immortalisation differently, this is an important avenue for further research. Currently our model does not unambiguously control for this. Future work to address this will focus on looking at the effect of insertion site versus donor specific effects. We can generate lines from the same donor with different insertion sites, Line 2 would be an ideal candidate due to the presence of multiple integrative events in this donor. If we observe consistent effects this is unlikely due to the multiple insertions of pro-viral *TERT*. To investigate donor specific effects, the same integration would need to be imposed. This would require modification to the method to allow for site directed insertion, it is possible to manipulate lentiviral target site selection using a molecular tethering strategy. The stable transfer of foreign DNA into host genomes can be achieved using a non-viral *Sleeping Beauty (SB)* transposable element, which can integrate into targeted sites of the mammalian host cell chromosomes using a well-defined transposition mechanism without disrupting non-specific actively transcribing genes (Ivics *et al.*, 1997; Yant *et al.*, 2005; 2007). Another method to investigate donor specific effects, would be to develop a model in which the endogenous gene can be manipulated.

TL specific effects can also be investigated, this would require a combination of different insertions in multiple donors and then to see the effect this has on the functional experiments. In broader terms it may be interesting to further investigate what leads the TL to stabilise high in some lines and low in others as this could have implications in cancer therapy. *TERT* silencing has been looked into as a therapeutic intervention (Rahme *et al.*, 2018; Reyes-Urbe *et al.*, 2018). Our findings show removal of *TERT* in a line that has stabilised with short TL leads to imminent cell death, whereas the long TL lines continue to grow, therefore targeting *TERT* would be less effective in a cancer cell where TL has stabilised at longer lengths.

In terms of a therapeutic perspective, telomerase treatment may be suitable for some individuals but not others. A recent review by Martínez & Blasco (2018) unveiled an insight into the development of therapeutic strategies based on telomerase activation in the context of cardiovascular diseases (CVD). Telomere maintenance by telomerase is important in cardiac regeneration, therapeutic strategies are aimed at lengthening telomeres and restoring the proliferative potential of adult mammalian cardiomyocytes (CM). Telomerase activation in the adult mouse heart by AAV9-*Tert* gene therapy has been shown to confer cardioprotection and significantly reduce mortality associated with heart failure after acute MI (Bär *et al.*, 2014). In this proof of concept study, an increase in CM TL and a lower abundance of cells with short telomeres (compared to control hearts), suggest that TL recovery in the myocardium decreases the associated risk of heart failure. Upon telomerase reactivation, high levels of the proliferation marker phosphohistone H3 was observed in CM, however when normalised to the number of CM required for regeneration of the infarct scar, the level of CM proliferation was insufficient for cardiac regeneration. Compared to this project, the AAV9-*Tert* gene therapy model addressed a later disease stage of the atherosclerosis process. Furthermore different cardiac cell types possess variable turnover rates; EC have a high turnover (>15% per year) whereas CM a low turnover that gradually decreases throughout life (<1% per year) (Martínez & Blasco 2018) which reflects differences in TL dynamics.

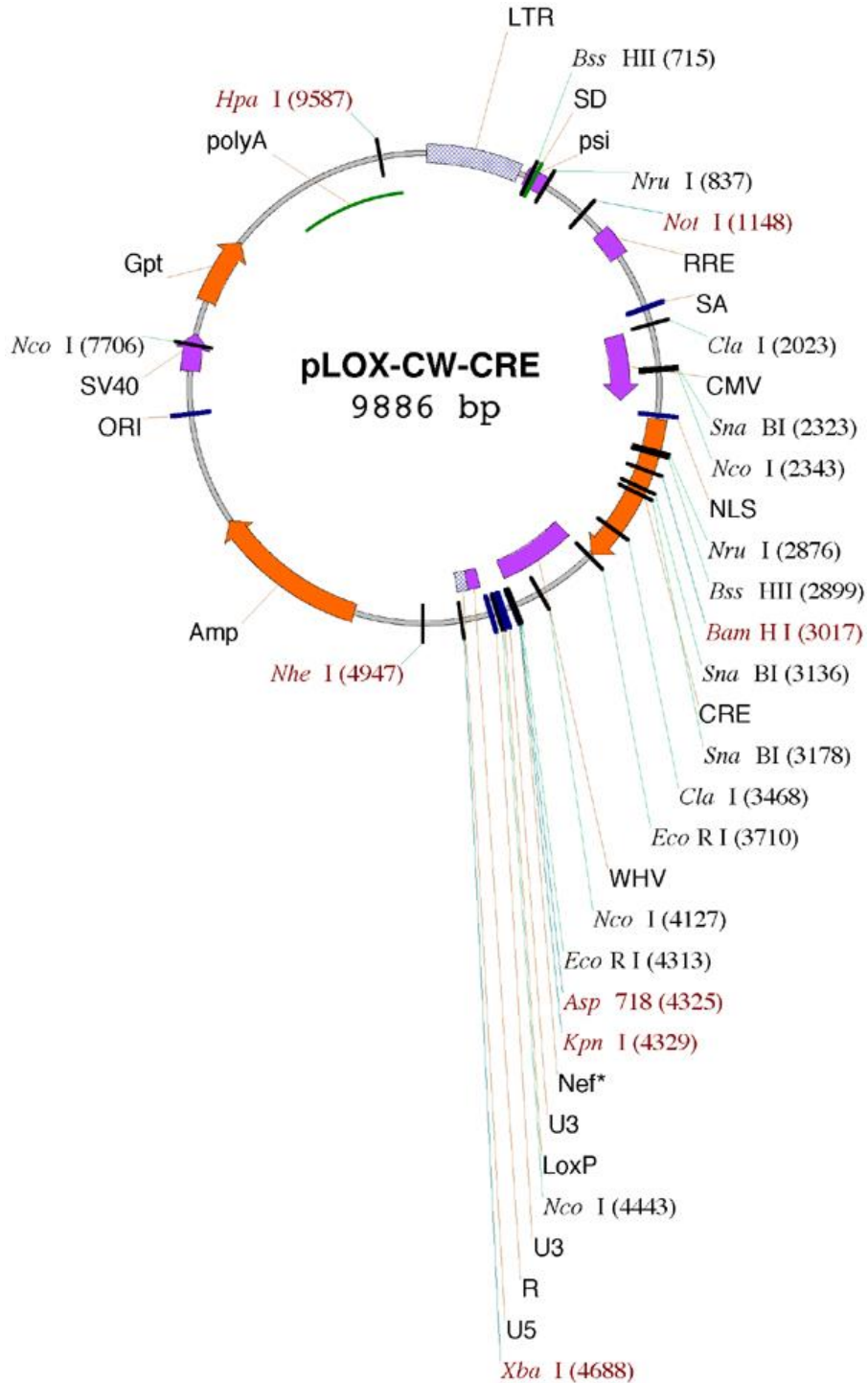
The safety of utilising TERT therapeutically has its limitations and strategies for telomerase activation have raised safety concerns. As mentioned previously, constitutive reactivation of endogenous telomerase is a key aspect to tumorigenesis (Artandi *et al.*, 2002; González-Suárez *et al.*, 2001; Canela *et al.*, 2004). Although, it has been shown AAV9-mediated *TERT* over expression in the context of an oncogenic *K-RAS* induced lung cancer mouse model does not accelerate tumorigenesis (Muñoz-Lorente *et al.*, 2018). This strengthens the feasibility of utilising *in-vitro* models to reactivate telomerase and subsequent genome editing (such as Cre-Lox system) to manipulate TL. Nonetheless, there is still a real need for further investigation to address safe strategies for transient and controllable telomerase reactivation from a therapeutic perspective using transferable gene expression *in-vitro* model systems.

APPENDIX

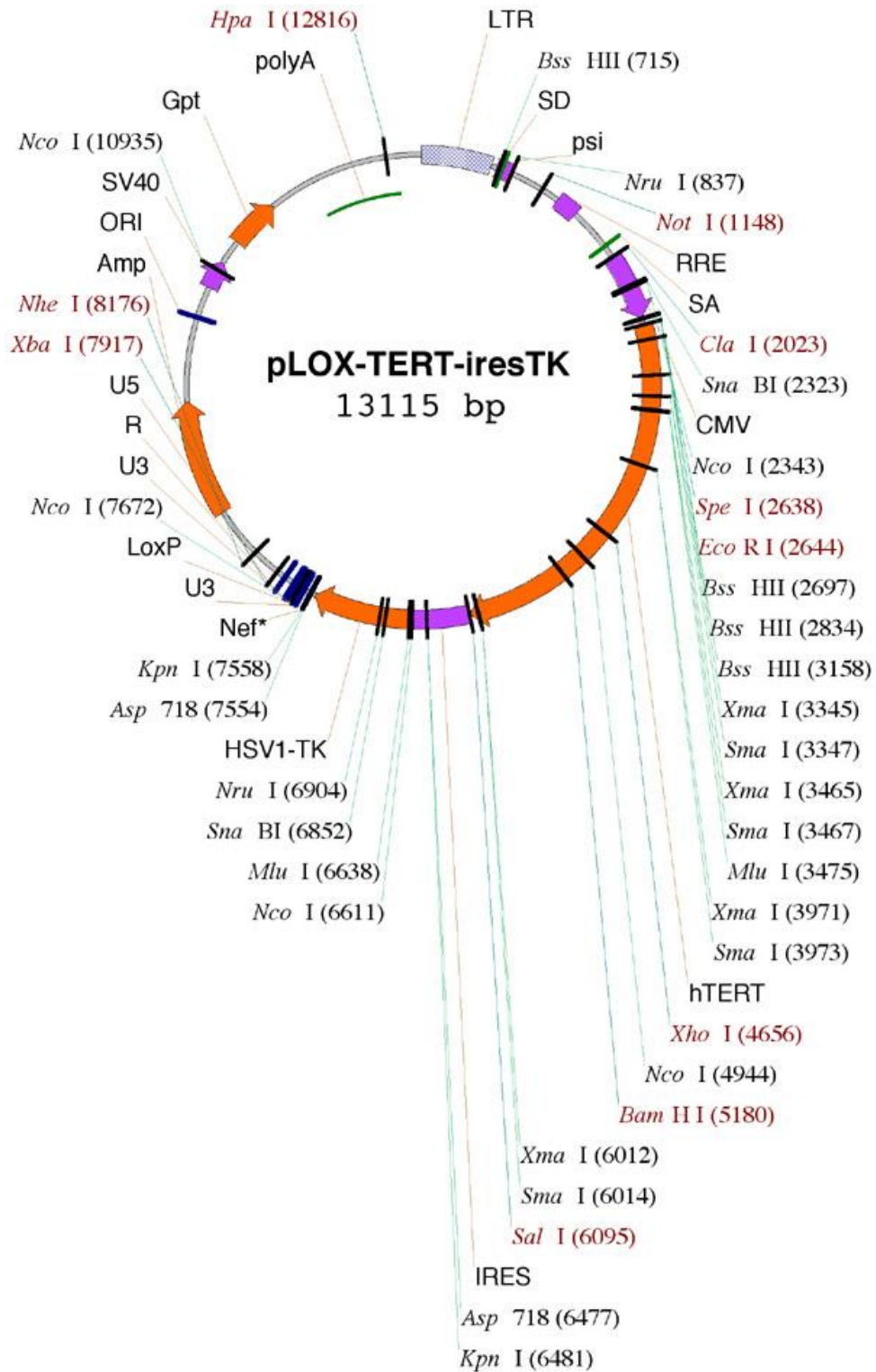
Appendix

S1.1-10 The plasmid maps for all the plasmid vectors used experimentally in this project are shown.

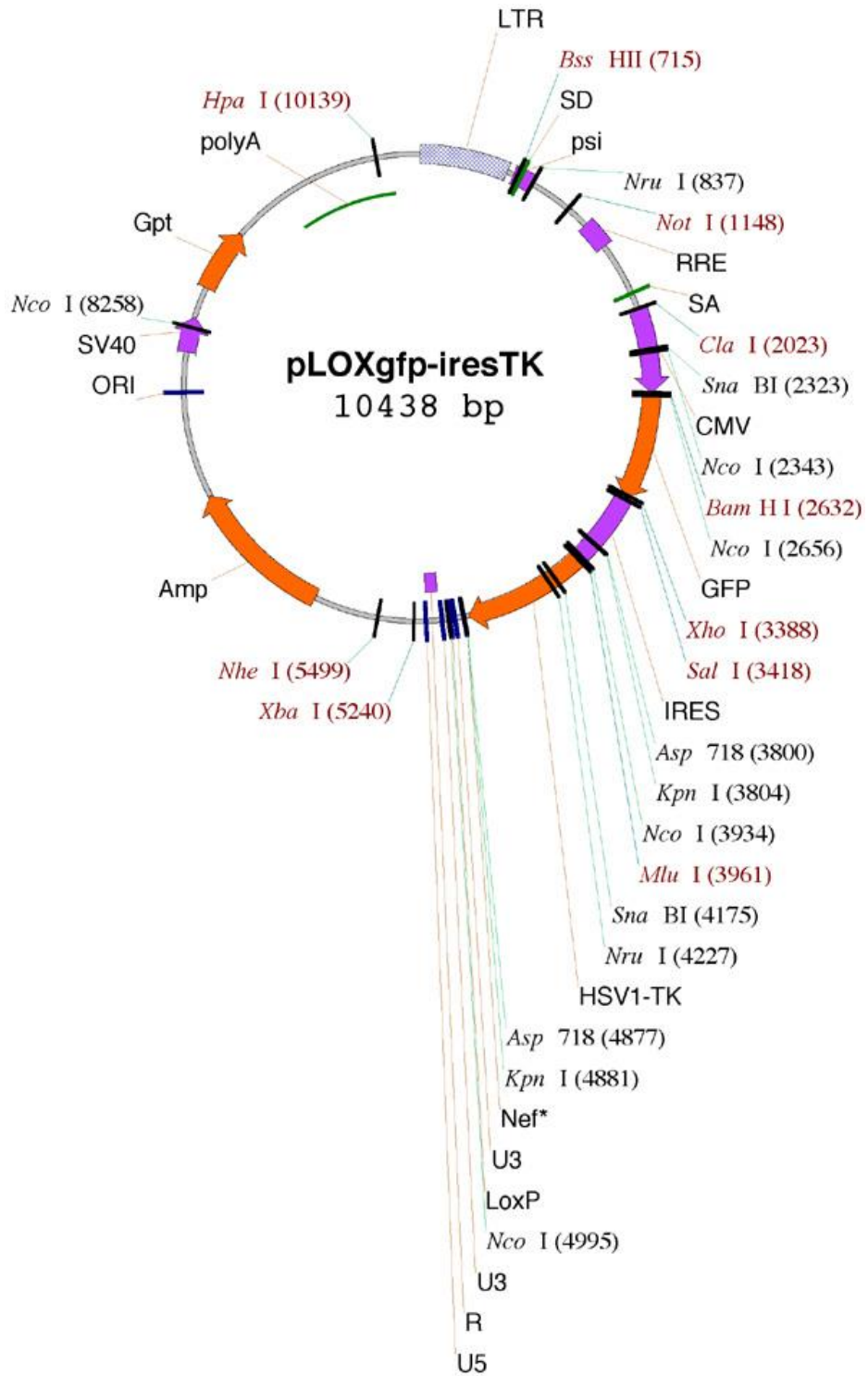
1. pLOX-CW-CRE



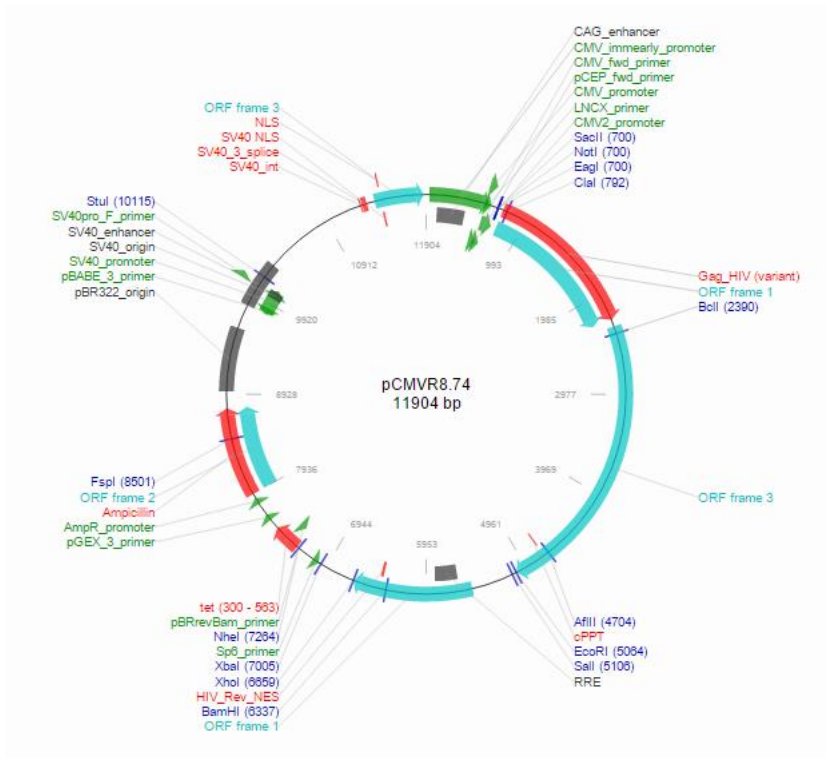
2. pLOX-TERT-iresTK



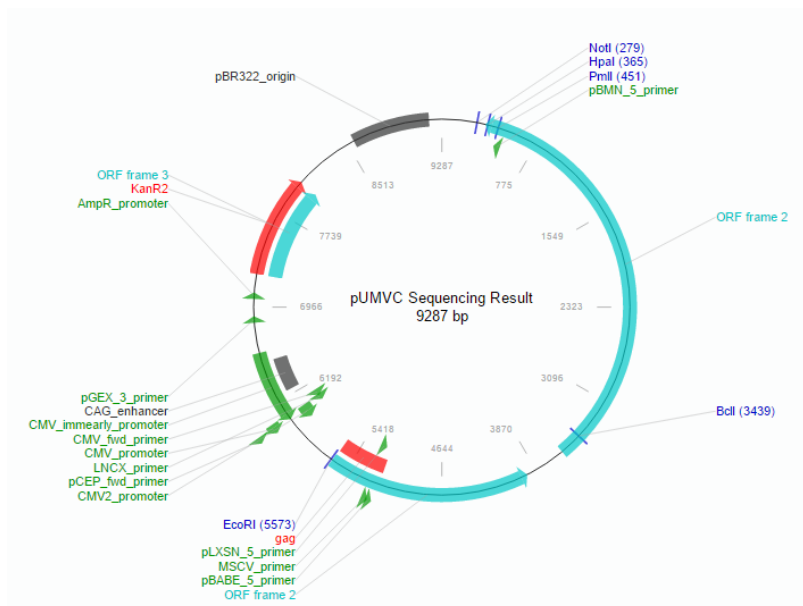
3. pLOX-GFP-iresTK



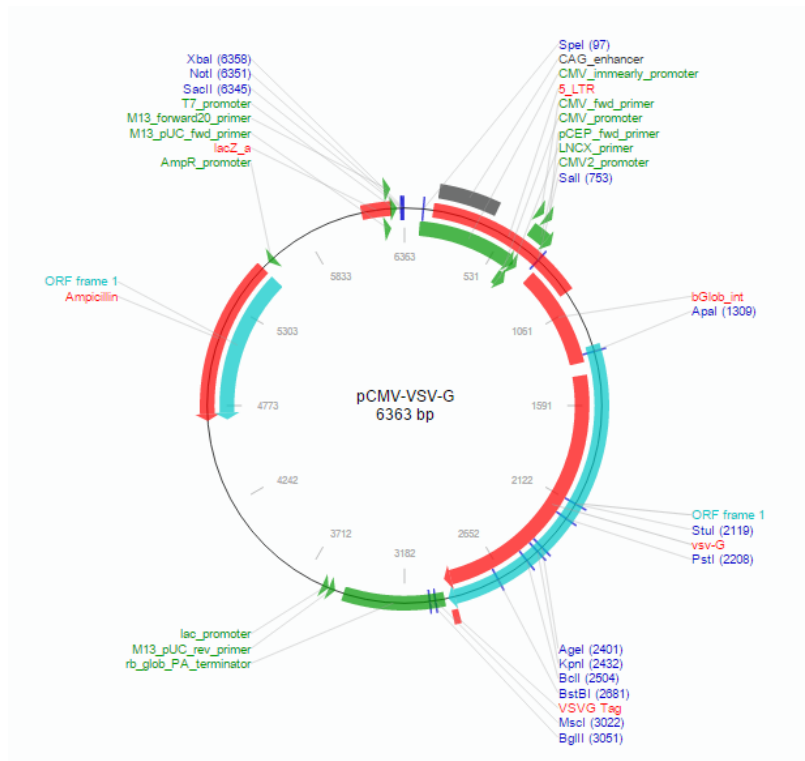
4. pCMVR8.74



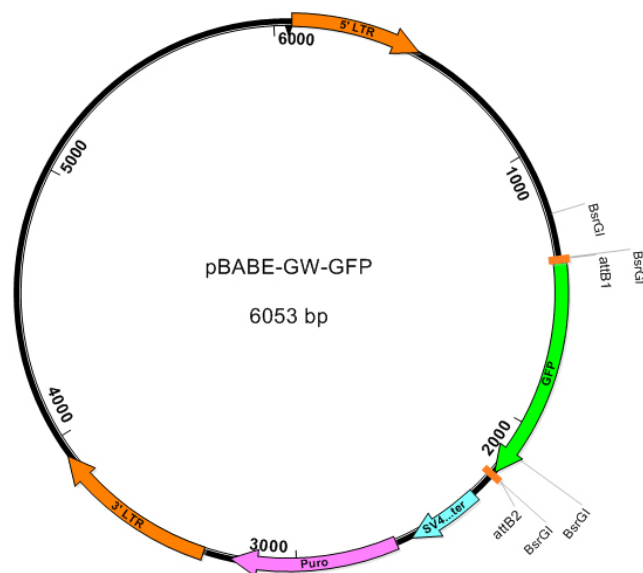
5. pUMVC



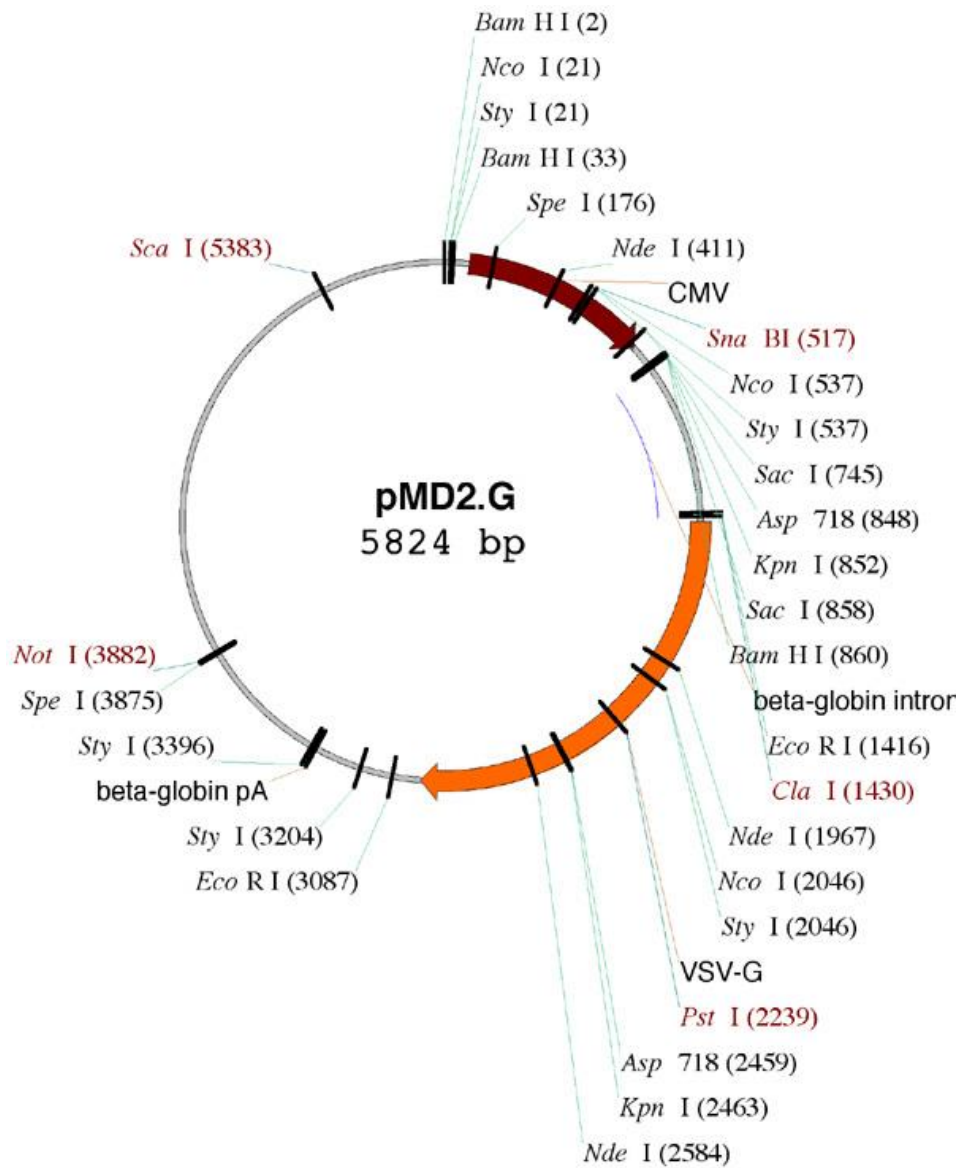
6. pCMV-VSV-G



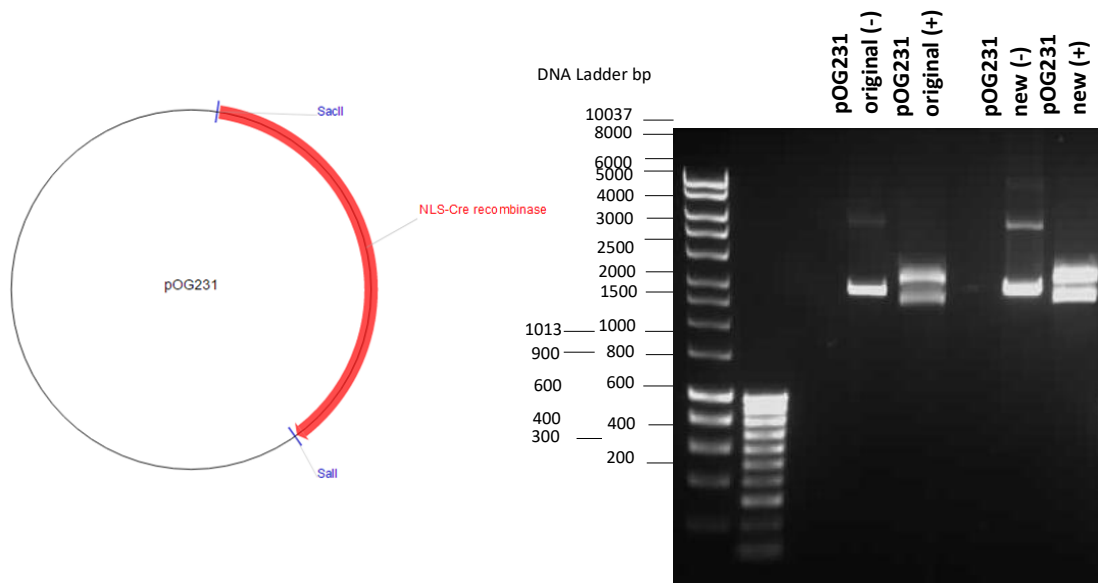
7. pBABE-GW-GFP



8. pMD2.G

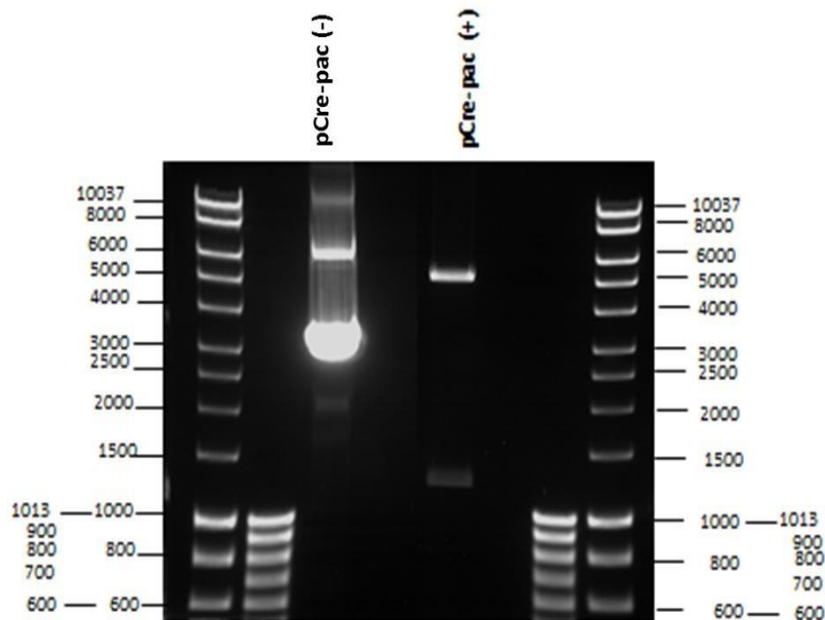
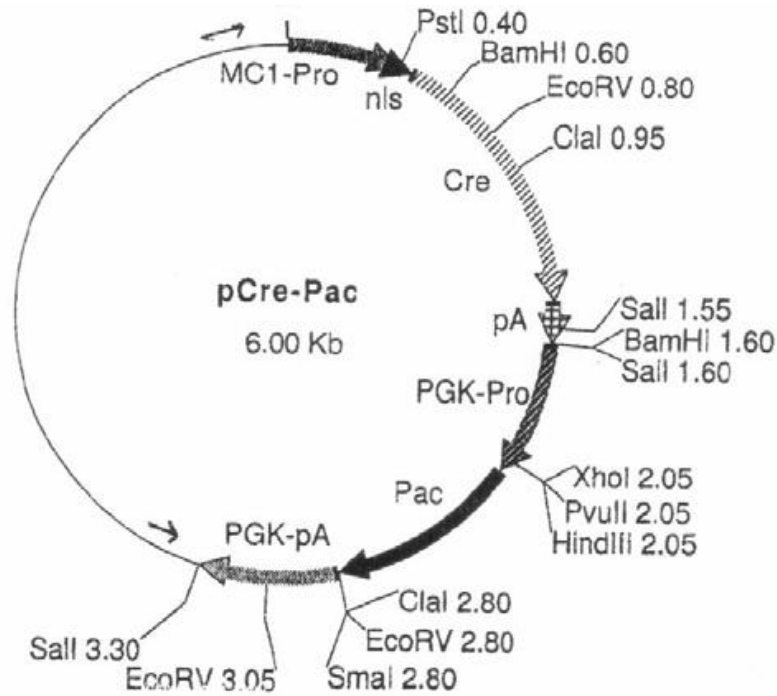


9. pOG231



S1 (9) Plasmid map and gel image of restriction digest of pOG231 using Sall and Spe I. The plasmid pOG231 could not be verified using the fragment size yielded by the diagnostic digest, expected band size 4.5kb and 233bp. New bacterial cultures were grown from isolated single colonies. After plasmid purification and quantification, the double digest was repeated on the original pOG231 plasmid and the new pOG231 plasmid DNA. The same incorrect bands were yielded in both digests. Due to discrepancy in the diagnostic digest results after bacterial culture and plasmid purification, this plasmid was replaced by pCre-pac for subsequent experiments.

10. pCre-Pac



S1 (10). pCre-pac plasmid map and restriction digest The uncut DNA plasmid (pCre-pac (-)) with no restriction enzyme added is observed as supercoiled DNA and runs slower down the gel (a smear is therefore observed). The plasmid DNA cut using the restriction endonuclease BamHI (pCre-pac (+)) yields two digest fragments at 5.0kb and 1.2kb*. * The size of fragment 2 has been confirmed by another scientist in our lab whom had also carried out this pCre-pac restriction digest using BamHI

Pro-viral TERT cDNA

```
tACATTCTCA CTAACTAGG CATCAGAGTA ATCAATAGTT CTTCTATCA 50
AAAGAAATAA TCTGAACAAA AACCTAAACA GGCGTATCTC AATCATTACA 100
CAGTAGATAT CAGCACAATG TGACAGATGT TAATCCGTAA TAGCCAGTGG 150
ATCATGAAGT GAGTCTAGC CCATGTAATT GCCCAATTAT GAAAAATGAT 200
GCTTATCATA AGAAATCCTA AAATAGCACT GCAGTAACAA CTTACAACA 250
AGCAACTCAA AATGAAATAG CAAAATGAAC AGTGAACTAA
```

Genomic chr2 (reverse strand):

```
aaaaaagagc aaaaacaaaa actgctactg cctatagtct taccttgaca 197540864
aaaaactaat aaggagaaaa acaacatgaa tattttaaag ctcaaaagta 197540814
ACATTTCTAC TTAaACTAGG CATCAGAGTA ATCAATAGTT CTTCTATCA 197540764
AAAGAAATAA TCTGAACAAA AACCTAAACA GGCGTATCTC AATCATTACA 197540714
CAGTAGATAT CAGCACAATG TGACAGATGT TAATCCGTAA TAGCCAGTGG 197540664
ATCATGAAGT GAGTCTAGC CCATGTAATT GCCCAATTAT GAAAAATGAT 197540614
GCTTATCATA AGAAATCCTA AAATAGCACT GCAGTAACAA CTTACAACA 197540564
AGCAACTCAA AATGAAATAG CAAAATGAAC AGTGAACTAA aaaccctaaa 197540514
aacttgctca acattgtctt gagagagatt taggtataa taatttt|att 197540464
agttactcta tttcataaat cctcacctct tttggagttt
```

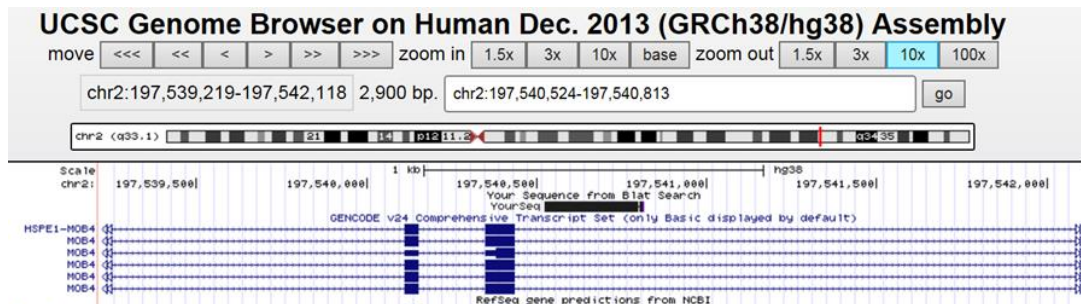


Figure S2 Integration site analysis of pro-viral *TERT* in Line 7 *iHUVEC*. A) UCSC Genome Browser analysis BLAT reveals alignment of pro-viral *TERT* sequence to lead transcript MOB4. B) Pro-viral *TERT* cDNA sequence alone and pro-viral *TERT* sequence integrated at Chr2q33 within the MOB4 genomic sequence (Altschul *et al.*, 1990; Kent *et al.*, 2002).

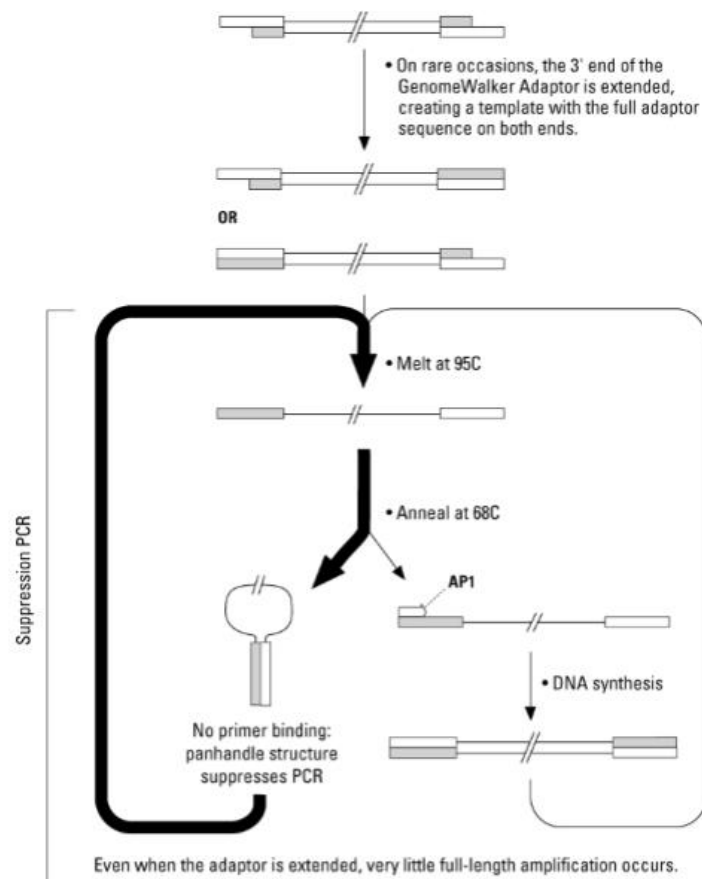


Figure S3 PCR suppression effects during DNA walking (Integration Site Analysis). In rare cases, the 3' end of the adaptor sequence gets extended, due to incomplete oligonucleotide synthesis/adaptor ligation. As a result, for targets longer than ~6kb, full-length adaptor sequences are present on both ends that serve as a template for end-to-end amplification. In suppression PCR as the adapter primer is shorter than the adapter sequence, no primer binding leads to the formation of panhandle DNA structures which are unable to be extended. During PCR, the intramolecular annealing event of this stable panhandle DNA structure is favored (block arrow) over the adaptor primer to the adaptor sequence. Without suppression PCR, such rare events would lead to unacceptable backgrounds as a result of conventional PCR amplification. Taken from Siebert *et al.*, 1995.

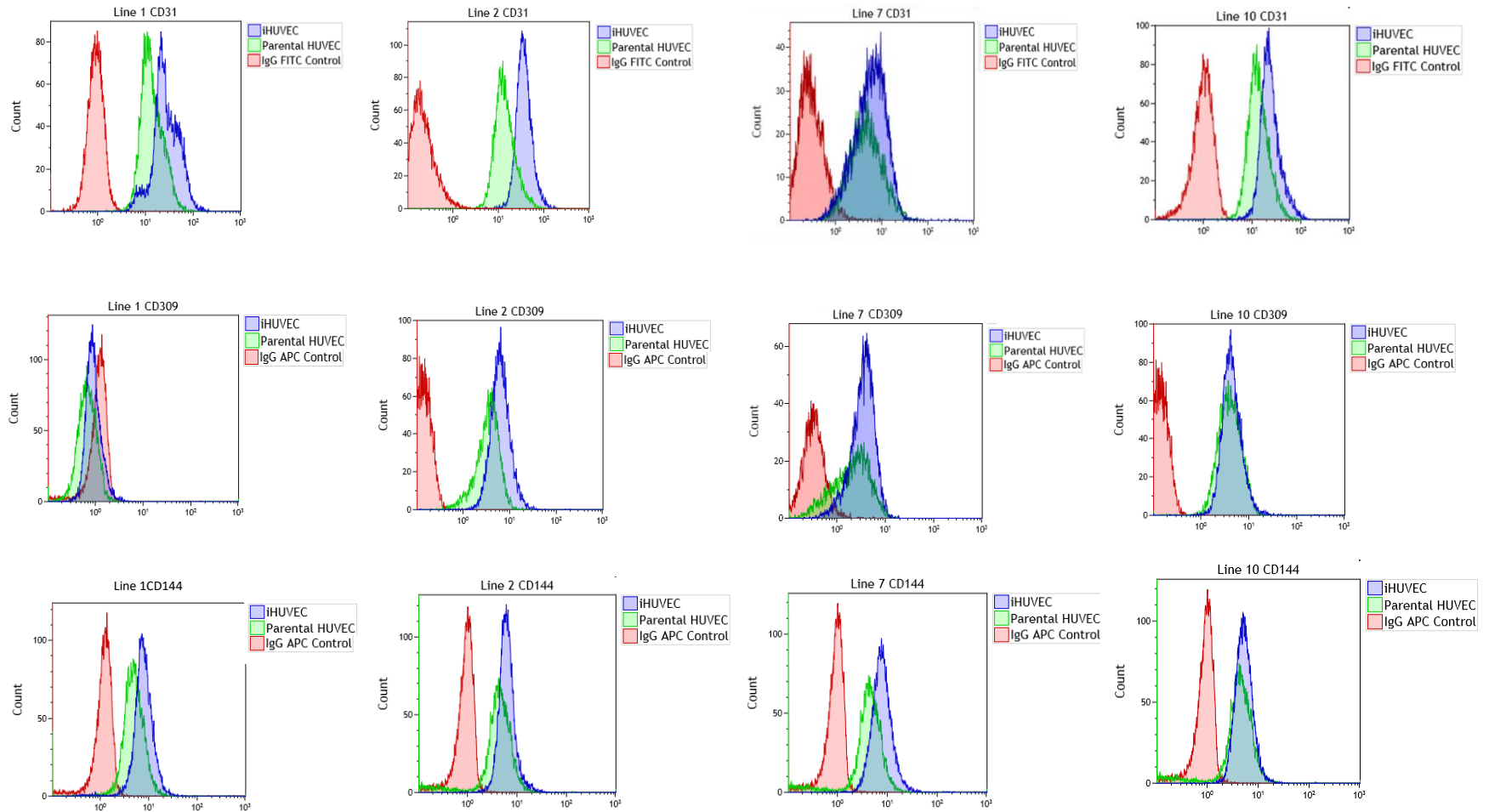


Figure S4 flow cytometric detection (histoplots) of endothelial cell surface markers CD31, CD309 and CD144 (in Line 1, 2, 7 and 10) early passage parental HUVEC (<10 days in culture) and iHUVEC. Human isotope Ig G-APC or Ig G-APC controls was included for each run to check the background level of non-specific antibody.

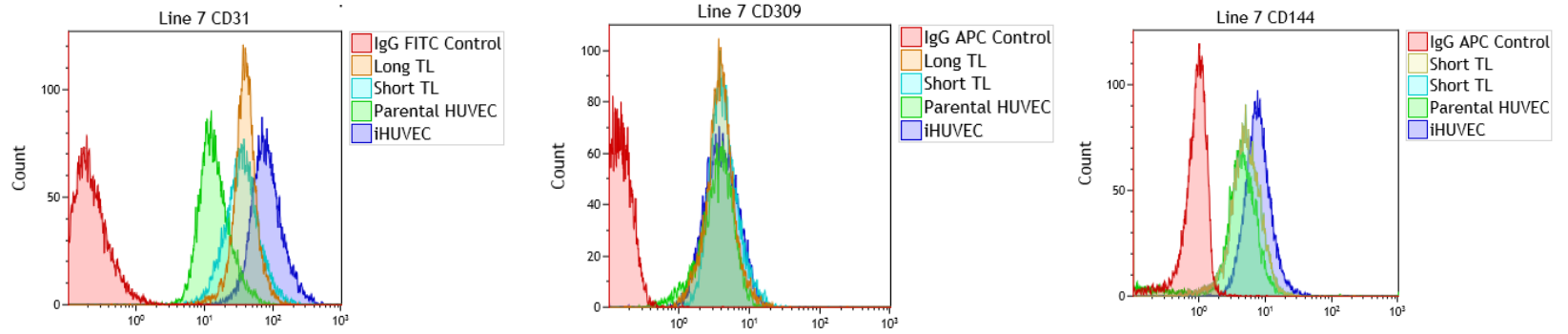


Figure S5 flow cytometric detection (histoplots) of endothelial cell surface markers CD31, CD309 and CD144 in parental HUVEC, immortalised HUVEC (iHUVEC) (<10 days in culture) and short and long TL lines Human isotope Ig G-APC or Ig G-APC controls was included for each run to check the background level of non-specific antibody.

REFERENCES

- Abreu, E., Aritonovska, E., Reichenbach, P., Cristofari, G., Culp, B., Terns, R.M., Lingner, J., Terns, M.P., 2010. TIN2-tethered TPP1 recruits human telomerase to telomeres in vivo. *Molecular and Cellular Biology*. **30**, 2971-2982.
- Ades, E.W., Candal, F.J., Swerlick, R.A., George, V.G., Summers, S., Bosse, D.C., Lawley, T.J., 1992. HMEC-1: establishment of an immortalized human microvascular endothelial cell line. *The Journal of Investigative Dermatology*. **99**, 683-690.
- Ahmed, S., Passos, J.F., Birket, M.J., Beckmann, T., Brings, S., Peters, H., Birch-Machin, M.A., von Zglinicki, T., Saretzki, G., 2008. Telomerase does not counteract telomere shortening but protects mitochondrial function under oxidative stress. *Journal of Cell Science*. **121**, 1046-1053.
- Albrecht, E.A., Chinnaiyan, A.M., Varambally, S., Kumar-Sinha, C., Barrette, T.R., Sarma, J.V., Ward, P.A., 2004. C5a-induced gene expression in human umbilical vein endothelial cells. *The American Journal of Pathology*. **164**, 849-859.
- Allsopp, R.C., Vaziri, H., Patterson, C., Goldstein, S., Younglai, E.V., Futcher, A.B., Greider, C.W., Harley, C.B., 1992. Telomere length predicts replicative capacity of human fibroblasts. *Proceedings of the National Academy of Sciences of the United States of America*. **89**, 10114-10118.
- Altschul, S.F., Gish, W., Miller, W., Myers, E.W., Lipman, D.J., 1990. Basic local alignment search tool. *Journal of Molecular Biology*. **215**, 403-410.
- Altun, I., Oz, F., Arkaya, S.C., Altun, I., Bilge, A.K., Umman, B., Turkoglu, U.M., 2014. Effect of statins on endothelial function in patients with acute coronary syndrome: a prospective study using adhesion molecules and flow-mediated dilatation. *Journal of Clinical Medicine Research*. **6**, 354-361.
- An, G., Wang, H., Tang, R., Yago, T., McDaniel, J.M., McGee, S., Huo, Y., Xia, L., 2008. P-selectin glycoprotein ligand-1 is highly expressed on Ly-6Chi monocytes and a major determinant for Ly-6Chi monocyte recruitment to sites of atherosclerosis in mice. *Circulation*. **117**, 3227-3237.
- Ancuta, P., Rao, R., Moses, A., Mehle, A., Shaw, S.K., Luscinskas, F.W., Gabuzda, D., 2003. Fractalkine preferentially mediates arrest and migration of CD16+ monocytes. *The Journal of Experimental Medicine*. **197**, 1701-1707.
- Anderson, H.D., Rahmutula, D., Gardner, D.G., 2004. Tumor necrosis factor-alpha inhibits endothelial nitric-oxide synthase gene promoter activity in bovine aortic endothelial cells. *The Journal of Biological Chemistry*. **279**, 963-969.
- Andrew, T., Aviv, A., Falchi, M., Surdulescu, G.L., Gardner, J.P., Lu, X., Kimura, M., Kato, B.S., Valdes, A.M., Spector, T.D., 2006. Mapping genetic loci that determine leukocyte telomere length in a large sample of unselected female sibling pairs. *The American Journal of Human Genetics*. **78**, 480-486.
- Arat, N.O. & Griffith, J.D., 2012. Human Rap1 interacts directly with telomeric DNA and regulates TRF2 localization at the telomere. *The Journal of Biological Chemistry*. **287**, 41583-41594.
- Armanios, M. & Blackburn, E.H., 2012. The telomere syndromes. *Nature Reviews Genetics*. **13**, 693-704.

- Armanios, M., Chen, J.L., Chang, Y.P., Brodsky, R.A., Hawkins, A., Griffin, C.A., Eshleman, J.R., Cohen, A.R., Chakravarti, A., Hamosh, A., Greider, C.W., 2005. Haploinsufficiency of telomerase reverse transcriptase leads to anticipation in autosomal dominant dyskeratosis congenita. *Proceedings of the National Academy of Sciences of the United States of America*. **102**, 15960-15964.
- Armanios, M.Y., Chen, J.J., Cogan, J.D., Alder, J.K., Ingersoll, R.G., Markin, C., Lawson, W.E., Xie, M., Vulto, I., Phillips III, J.A., 2007. Telomerase mutations in families with idiopathic pulmonary fibrosis. *New England Journal of Medicine*. **356**, 1317-1326.
- Armanios, M., 2009. Syndromes of telomere shortening. *Annual Review of Genomics and Human Genetics*. **10**, 45-61.
- Arnoult, N., Schluth-Bolard, C., Letessier, A., Drascovic, I., Bouarich-Bourimi, R., Campisi, J., Kim, S.H., Boussouar, A., Ottaviani, A., Magdinier, F., Gilson, E., Londono-Vallejo, A., 2010. Replication timing of human telomeres is chromosome arm-specific, influenced by subtelomeric structures and connected to nuclear localization. *PLoS Genetics*. **6**, e1000920.
- Artandi, S.E., Chang, S., Lee, S., Alson, S., Gottlieb, G.J., Chin, L., DePinho, R.A., 2000. Telomere dysfunction promotes non-reciprocal translocations and epithelial cancers in mice. *Nature*. **406**, 641-645.
- Artandi, S.E., Alson, S., Tietze, M.K., Sharpless, N.E., Ye, S., Greenberg, R.A., Castrillon, D.H., Horner, J.W., Weiler, S.R., Carrasco, R.D., DePinho, R.A., 2002. Constitutive telomerase expression promotes mammary carcinomas in aging mice. *Proceedings of the National Academy of Sciences of the United States of America*. **99**, 8191-8196.
- Aviv, A., Chen, W., Gardner, J.P., Kimura, M., Brimacombe, M., Cao, X., Srinivasan, S.R., Berenson, G.S., 2009. Leukocyte telomere dynamics: longitudinal findings among young adults in the Bogalusa Heart Study. *American Journal of Epidemiology*. **169**, 323-329.
- Azuma, K., Watada, H., Niihashi, M., Otsuka, A., Sato, F., Kawasumi, M., Shimada, S., Tanaka, Y., Kawamori, R., Mitsumata, M., 2003. A new En face method is useful to quantitate endothelial damage in vivo. *Biochemical and Biophysical Research Communications*. **309**, 384-390.
- Azzalin, C.M., Reichenbach, P., Khoriauli, L., Giulotto, E., Lingner, J., 2007. Telomeric repeat containing RNA and RNA surveillance factors at mammalian chromosome ends. *Science (New York, N.Y.)*. **318**, 798-801.
- Baeyens, A., Naessens, E., Van Nuffel, A., Weening, K.E., Reilly, A.M., Claeys, E., Trypsteen, W., Vandekerckhove, L., Eyckerman, S., Gevaert, K., Verhasselt, B., 2016. HIV-1 Vpr N-terminal tagging affects alternative splicing of the viral genome. *Scientific Reports*. **6**, 34573.
- Bakaysa, S.L., Mucci, L.A., Slagboom, P.E., Boomsma, D.I., McClearn, G.E., Johansson, B., Pedersen, N.L., 2007. Telomere length predicts survival independent of genetic influences. *Aging Cell*. **6**, 769-774.
- Ball, S.E., Gibson, F.M., Rizzo, S., Tooze, J.A., Marsh, J.C., Gordon-Smith, E.C., 1998. Progressive telomere shortening in aplastic anemia. *Blood*. **91**, 3582-3592.

- Bär, C., Bernardes de Jesus, B., Serrano, R., Tejera, A., Ayuso, E., Jimenez, V., Formentini, I., Bobadilla, M., Mizrahi, J., de Martino, A., Gomez, G., Pisano, D., Mulero, F., Wollert, K.C., Bosch, F., Blasco, M.A., 2014. Telomerase expression confers cardioprotection in the adult mouse heart after acute myocardial infarction. *Nature Communications*. **5**, 5863.
- Bär, C., Povedano, J.M., Serrano, R., Benitez-Buelga, C., Popkes, M., Formentini, I., Bobadilla, M., Bosch, F., Blasco, M.A., 2016. Telomerase gene therapy rescues telomere length, bone marrow aplasia, and survival in mice with aplastic anemia. *Blood*. **127**, 1770-1779.
- Barbieri, M., Paolisso, G., Kimura, M., Gardner, J.P., Boccardi, V., Papa, M., Hjelmberg, J.V., Christensen, K., Brimacombe, M., Nawrot, T.S., 2009. Higher circulating levels of IGF-1 are associated with longer leukocyte telomere length in healthy subjects. *Mechanisms of Ageing and Development*. **130**, 771-776.
- Baur, J.A., Zou, Y., Shay, J.W., Wright, W.E., 2001. Telomere position effect in human cells. *Science (New York, N.Y.)*. **292**, 2075-2077.
- Bazzoni, G. & Dejana, E., 2004. Endothelial cell-to-cell junctions: molecular organization and role in vascular homeostasis. *Physiological Reviews*. **84**, 869-901.
- Bechter, O.E., Shay, J.W., Wright, W.E., 2004. The frequency of homologous recombination in human ALT cells. *Cell Cycle*. **3**, 545-547.
- Beier, F., Foronda, M., Martinez, P., Blasco, M.A., 2012. Conditional TRF1 knockout in the hematopoietic compartment leads to bone marrow failure and recapitulates clinical features of dyskeratosis congenita. *Blood*. **120**, 2990-3000.
- Bekaert, S., De Meyer, T., Rietzschel, E.R., De Buyzere, M.L., De Bacquer, D., Langlois, M., Segers, P., Cooman, L., Van Damme, P., Cassiman, P., 2007. Telomere length and cardiovascular risk factors in a middle-aged population free of overt cardiovascular disease. *Ageing Cell*. **6**, 639-647.
- Belsky, D.W., Caspi, A., Houts, R., Cohen, H.J., Corcoran, D.L., Danese, A., Harrington, H., Israel, S., Levine, M.E., Schaefer, J.D., Sugden, K., Williams, B., Yashin, A.I., Poulton, R., Moffitt, T.E., 2015. Quantification of biological aging in young adults. *Proceedings of the National Academy of Sciences of the United States of America*. **112**, E4104-10.
- Ben-Dor, I., Itsykson, P., Goldenberg, D., Galun, E., Reubinoff, B.E., 2006. Lentiviral vectors harboring a dual-gene system allow high and homogeneous transgene expression in selected polyclonal human embryonic stem cells. *Molecular Therapy: The Journal of the American Society of Gene Therapy*. **14**, 255-267.
- Benjamin, E.J., Muntner, P., Alonso, A., Bittencourt, M.S., Callaway, C.W., Carson, A.P., Chamberlain, A.M., Chang, A.R., Cheng, S., Das, S.R., Delling, F.N., Djousse, L., Elkind, M.S.V., Ferguson, J.F., Fornage, M., Jordan, L.C., Khan, S.S., Kissela, B.M., Knutson, K.L., Kwan, T.W., Lackland, D.T., Lewis, T.T., Lichtman, J.H., Longenecker, C.T., Loop, M.S., Lutsey, P.L., Martin, S.S., Matsushita, K., Moran, A.E., Mussolino, M.E., O'Flaherty, M., Pandey, A., Perak, A.M., Rosamond, W.D., Roth, G.A., Sampson, U.K.A., Satou, G.M., Schroeder, E.B., Shah, S.H., Spartano, N.L., Stokes, A., Tirschwell, D.L., Tsao, C.W., Turakhia, M.P., VanWagner, L.B., Wilkins, J.T., Wong, S.S., Virani, S.S., American Heart Association Council on Epidemiology and Prevention Statistics Committee and Stroke Statistics Subcommittee, 2019. Heart Disease and Stroke Statistics-2019 Update: A Report From the American Heart Association. *Circulation*. **139**, e56-e528.

- Benn, P.A., 1976. Specific chromosome aberrations in senescent fibroblast cell lines derived from human embryos. *American Journal of Human Genetics*. **28**, 465-473.
- Bennett, M.R., Evan, G.I., Schwartz, S.M., 1995. Apoptosis of human vascular smooth muscle cells derived from normal vessels and coronary atherosclerotic plaques. *The Journal of Clinical Investigation*. **95**, 2266-2274.
- Bennett, M.R., Gibson, D.F., Schwartz, S.M., Tait, J.F., 1995. Binding and phagocytosis of apoptotic vascular smooth muscle cells is mediated in part by exposure of phosphatidylserine. *Circulation Research*. **77**, 1136-1142.
- Bennett, M.R., Macdonald, K., Chan, S.W., Boyle, J.J., Weissberg, P.L., 1998. Cooperative interactions between RB and p53 regulate cell proliferation, cell senescence, and apoptosis in human vascular smooth muscle cells from atherosclerotic plaques. *Circulation Research*. **82**, 704-712.
- Bennett, M.R., 2002. Apoptosis in the cardiovascular system. *Heart (British Cardiac Society)*. **87**, 480-487.
- Bennett, M.R., Sinha, S., Owens, G.K., 2016. Vascular Smooth Muscle Cells in Atherosclerosis. *Circulation Research*. **118**, 692-702.
- Bernal, A. & Tusell, L., 2018. Telomeres: Implications for Cancer Development. *International Journal of Molecular Sciences*. **19**, 10.3390/ijms19010294.
- Bettin, N., Oss Pegorar, C., Cusanelli, E., 2019. The Emerging Roles of TERRA in Telomere Maintenance and Genome Stability. *Cells*. **8**, 10.3390/cells8030246.
- Betts, D.H., Perrault, S.D., King, W.A., 2008. Low oxygen delays fibroblast senescence despite shorter telomeres. *Biogerontology*. **9**, 19-31.
- Bicknell, R. (ed.) (1996) *Endothelial Cell Culture*. Cambridge: Cambridge University Press (Handbooks in Practical Animal Cell Biology). Doi 10.1017/CBO9780511608452
- Blackburn, E.H. & Gall, J.G., 1978. A tandemly repeated sequence at the termini of the extrachromosomal ribosomal RNA genes in Tetrahymena. *Journal of Molecular Biology*. **120**, 33-53.
- Blackburn, E.H., 2005. Telomeres and telomerase: their mechanisms of action and the effects of altering their functions. *FEBS Letters*. **579**, 859-862.
- Blasco, M.A., 2005. Telomeres and human disease: ageing, cancer and beyond. *Nature Reviews Genetics*. **6**, 611-622.
- Boccardi, V., Pelini, L., Ercolani, S., Ruggiero, C., Mecocci, P., 2015. From cellular senescence to Alzheimer's disease: The role of telomere shortening. *Ageing Research Reviews*. **22**, 1-8.
- Boccardi, V., Cari, L., Nocentini, G., Riccardi, C., Cecchetti, R., Ruggiero, C., Arosio, B., Paolisso, G., Herbig, U., Mecocci, P., 2018. Telomeres Increasingly Develop Aberrant Structures in Aging Humans. *The Journals of Gerontology. Series A, Biological Sciences and Medical Sciences*. **X**, 1-6.

- Bodnar, A., Lichtsteiner, S., Kim, N., Trager, J., 1997. Reconstitution of human telomerase with the template RNA component hTR and the catalytic protein subunit hTERT. *Nat Genet.* **17**, 498-502.
- Bodnar, A.G., Ouellette, M., Frolkis, M., Holt, S.E., Chiu, C.P., Morin, G.B., Harley, C.B., Shay, J.W., Lichtsteiner, S., Wright, W.E., 1998. Extension of life-span by introduction of telomerase into normal human cells. *Science (New York, N.Y.)*. **279**, 349-352.
- Boehm, J.S., Hession, M.T., Bulmer, S.E., Hahn, W.C., 2005. Transformation of human and murine fibroblasts without viral oncoproteins. *Molecular and Cellular Biology*. **25**, 6464-6474.
- Böger, R.H., Vallance, P., Cooke, J.P., 2003. Asymmetric dimethylarginine (ADMA): a key regulator of nitric oxide synthase. *Atherosclerosis Supplements*. **4**, 1-3.
- Borges, A. & Liew, C., 1997. Telomerase activity during cardiac development. *Journal of Molecular and Cellular Cardiology*. **29**, 2717-2724.
- Boyle, J.J., Bowyer, D.E., Weissberg, P.L., Bennett, M.R., 2001. Human blood-derived macrophages induce apoptosis in human plaque-derived vascular smooth muscle cells by Fas-ligand/Fas interactions. *Arteriosclerosis, Thrombosis, and Vascular Biology*. **21**, 1402-1407.
- Broccoli, D., Young, J.W., de Lange, T., 1995. Telomerase activity in normal and malignant hematopoietic cells. *Proceedings of the National Academy of Sciences of the United States of America*. **92**, 9082-9086.
- Broccoli, D., Smogorzewska, A., Chong, L., de Lange, T., 1997. Human telomeres contain two distinct Myb-related proteins, TRF1 and TRF2. *Nature Genetics*. **17**, 231-235.
- Broer, L., Codd, V., Nyholt, D.R., Deelen, J., Mangino, M., Willemsen, G., Albrecht, E., Amin, N., Beekman, M., de Geus, E.J., Henders, A., Nelson, C.P., Steves, C.J., Wright, M.J., de Craen, A.J., Isaacs, A., Matthews, M., Moayyeri, A., Montgomery, G.W., Oostra, B.A., Vink, J.M., Spector, T.D., Slagboom, P.E., Martin, N.G., Samani, N.J., van Duijn, C.M., Boomsma, D.I., 2013. Meta-analysis of telomere length in 19,713 subjects reveals high heritability, stronger maternal inheritance and a paternal age effect. *European Journal of Human Genetics : EJHG*. **21**, 1163-1168.
- Brouillette, S., Singh, R.K., Thompson, J.R., Goodall, A.H., Samani, N.J., 2003. White cell telomere length and risk of premature myocardial infarction. *Arteriosclerosis, Thrombosis, and Vascular Biology*. **23**, 842-846.
- Brouillette, S.W., Moore, J.S., McMahon, A.D., Thompson, J.R., Ford, I., Shepherd, J., Packard, C.J., Samani, N.J., West of Scotland Coronary Prevention Study Group, 2007. Telomere length, risk of coronary heart disease, and statin treatment in the West of Scotland Primary Prevention Study: a nested case-control study. *The Lancet*. **369**, 107-114.
- Brouillette, S.W., Whittaker, A., Stevens, S.E., van der Harst, P., Goodall, A.H., Samani, N.J., 2008. Telomere length is shorter in healthy offspring of subjects with coronary artery disease: support for the telomere hypothesis. *Heart (British Cardiac Society)*. **94**, 422-425.

- Bryan, T.M., Englezou, A., Dalla-Pozza, L., Dunham, M.A., Reddel, R.R., 1997. Evidence for an alternative mechanism for maintaining telomere length in human tumors and tumor-derived cell lines. *Nature Medicine*. **3**, 1271-1274.
- Bulger, M. & Groudine, M., 2011. Functional and mechanistic diversity of distal transcription enhancers. *Cell*. **144**, 327-339.
- Burke, A. & FitzGerald, G.A., 2003. Oxidative stress and smoking-induced vascular injury. *Progress in Cardiovascular Diseases*. **46**, 79-90.
- Burns, J.C., Friedmann, T., Driever, W., Burrascano, M., Yee, J.K., 1993. Vesicular stomatitis virus G glycoprotein pseudotyped retroviral vectors: concentration to very high titer and efficient gene transfer into mammalian and nonmammalian cells. *Proceedings of the National Academy of Sciences of the United States of America*. **90**, 8033-8037.
- Cai, H. & Harrison, D.G., 2000. Endothelial dysfunction in cardiovascular diseases: the role of oxidant stress. *Circulation Research*. **87**, 840-844.
- Canela, A., Martin-Caballero, J., Flores, J.M., Blasco, M.A., 2004. Constitutive expression of tert in thymocytes leads to increased incidence and dissemination of T-cell lymphoma in Lck-Tert mice. *Molecular and Cellular Biology*. **24**, 4275-4293.
- Canela, A., Vera, E., Klatt, P., Blasco, M.A., 2007. High-throughput telomere length quantification by FISH and its application to human population studies. *Proceedings of the National Academy of Sciences of the United States of America*. **104**, 5300-5305.
- Carmeliet, P., Lampugnani, M.G., Moons, L., Breviaro, F., Compernelle, V., Bono, F., Balconi, G., Spagnuolo, R., Oosthuysen, B., Dewerchin, M., Zanetti, A., Angellilo, A., Mattot, V., Nuyens, D., Lutgens, E., Clotman, F., de Ruiter, M.C., Gittenberger-de Groot, A., Poelmann, R., Lupu, F., Herbert, J.M., Collen, D., Dejana, E., 1999. Targeted deficiency or cytosolic truncation of the VE-cadherin gene in mice impairs VEGF-mediated endothelial survival and angiogenesis. *Cell*. **98**, 147-157.
- Carreau, A., Kieda, C., Grillon, C., 2011. Nitric oxide modulates the expression of endothelial cell adhesion molecules involved in angiogenesis and leukocyte recruitment. *Experimental Cell Research*. **317**, 29-41.
- Cawthon, R.M., 2002. Telomere measurement by quantitative PCR. *Nucleic Acids Research*. **30**, e47.
- Čejková, S., Králová-Lesná, I. and Poledne, R., 2016. Monocyte adhesion to the endothelium is an initial stage of atherosclerosis development. *Cor et vasa*. **58**, 4, e419, 1959-2011
- Celermajer, D.S., Sorensen, K.E., Georgakopoulos, D., Bull, C., Thomas, O., Robinson, J., Deanfield, J.E., 1993. Cigarette smoking is associated with dose-related and potentially reversible impairment of endothelium-dependent dilation in healthy young adults. *Circulation*. **88**, 2149-2155.
- Cesani, M., Plati, T., Lorioli, L., Benedicenti, F., Redaelli, D., Dionisio, F., Biasco, L., Montini, E., Naldini, L., Biffi, A., 2015. Shedding of clinical-grade lentiviral vectors is not detected in a gene therapy setting. *Gene Therapy*. **22**, 496-502.

- Chacko, B.K., Scott, D.W., Chandler, R.T., Patel, R.P., 2011. Endothelial surface N-glycans mediate monocyte adhesion and are targets for anti-inflammatory effects of peroxisome proliferator-activated receptor gamma ligands. *The Journal of Biological Chemistry*. **286**, 38738-38747.
- Chang, E. & Harley, C.B., 1995. Telomere length and replicative aging in human vascular tissues. *Proceedings of the National Academy of Sciences of the United States of America*. **92**, 11190-11194.
- Chang, S., Song, S., Lee, J., Yoon, J., Park, J., Choi, S., Park, J.K., Choi, K., Choi, C., 2014. Phenotypic modulation of primary vascular smooth muscle cells by short-term culture on micropatterned substrate. *PLoS One*. **9**, e88089.
- Chen, Y., Yang, Y., van Overbeek, M., Donigian, J.R., Baciu, P., de Lange, T., Lei, M., 2008. A shared docking motif in TRF1 and TRF2 used for differential recruitment of telomeric proteins. *Science (New York, N.Y.)*. **319**, 1092-1096.
- Chi, Z. & Melendez, A.J., 2007. Role of cell adhesion molecules and immune-cell migration in the initiation, onset and development of atherosclerosis. *Cell Adhesion & Migration*. **1**, 171-175.
- Choi, J., Choi, J., Nham, S.U., 2010. Characterization of the residues of alphaX I-domain and ICAM-1 mediating their interactions. *Molecules and Cells*. **30**, 227-234.
- Chou, J.Y., 1978. Human placental cells transformed by tsA mutants of simian virus 40: a model system for the study of placental functions. *Proceedings of the National Academy of Sciences of the United States of America*. **75**, 1409-1413.
- Chow, T.T., Zhao, Y., Mak, S.S., Shay, J.W., Wright, W.E., 2012. Early and late steps in telomere overhang processing in normal human cells: the position of the final RNA primer drives telomere shortening. *Genes & Development*. **26**, 1167-1178.
- Christodoulou, I., Patsali, P., Stephanou, C., Antoniou, M., Kleanthous, M., Lederer, C.W., 2016. Measurement of lentiviral vector titre and copy number by cross-species duplex quantitative PCR. *Gene Therapy*. **23**, 113-118.
- Cines, D.B., Pollak, E.S., Buck, C.A., Loscalzo, J., Zimmerman, G.A., McEver, R.P., Pober, J.S., Wick, T.M., Konkle, B.A., Schwartz, B.S., Barnathan, E.S., McCrae, K.R., Hug, B.A., Schmidt, A.M., Stern, D.M., 1998. Endothelial cells in physiology and in the pathophysiology of vascular disorders. *Blood*. **91**, 3527-3561.
- Ciuffi, A., 2008. Mechanisms governing lentivirus integration site selection. *Current Gene Therapy*. **8**, 419-429.
- Ciuffi, A., 2016. The benefits of integration. *Clinical Microbiology and Infection : The Official Publication of the European Society of Clinical Microbiology and Infectious Diseases*. **22**, 324-332.
- Codd, V., Mangino, M., van der Harst, P., Braund, P.S., Kaiser, M., Beveridge, A.J., Rafelt, S., Moore, J., Nelson, C., Soranzo, N., 2010. Common variants near TERC are associated with mean telomere length. *Nature Genetics*. **42**, 197-199.

Codd, V., Nelson, C.P., Albrecht, E., Mangino, M., Deelen, J., Buxton, J.L., Hottenga, J.J., Fischer, K., Esko, T., Surakka, I., Broer, L., Nyholt, D.R., Mateo Leach, I., Salo, P., Hagg, S., Matthews, M.K., Palmén, J., Norata, G.D., O'Reilly, P.F., Saleheen, D., Amin, N., Balmforth, A.J., Beekman, M., de Boer, R.A., Bohringer, S., Braund, P.S., Burton, P.R., de Craen, A.J., Denniff, M., Dong, Y., Douroudis, K., Dubinina, E., Eriksson, J.G., Garlaschelli, K., Guo, D., Hartikainen, A.L., Henders, A.K., Houwing-Duistermaat, J.J., Kananen, L., Karssen, L.C., Kettunen, J., Klopp, N., Lagou, V., van Leeuwen, E.M., Madden, P.A., Magi, R., Magnusson, P.K., Mannisto, S., McCarthy, M.I., Medland, S.E., Mihailov, E., Montgomery, G.W., Oostra, B.A., Palotie, A., Peters, A., Pollard, H., Pouta, A., Prokopenko, I., Ripatti, S., Salomaa, V., Suchiman, H.E., Valdes, A.M., Verweij, N., Vinuela, A., Wang, X., Wichmann, H.E., Widen, E., Willemsen, G., Wright, M.J., Xia, K., Xiao, X., van Veldhuisen, D.J., Catapano, A.L., Tobin, M.D., Hall, A.S., Blakemore, A.I., van Gilst, W.H., Zhu, H., CARDIoGRAM consortium, Erdmann, J., Reilly, M.P., Kathiresan, S., Schunkert, H., Talmud, P.J., Pedersen, N.L., Perola, M., Ouwehand, W., Kaprio, J., Martin, N.G., van Duijn, C.M., Hovatta, I., Gieger, C., Metspalu, A., Boomsma, D.I., Jarvelin, M.R., Slagboom, P.E., Thompson, J.R., Spector, T.D., van der Harst, P., Samani, N.J., 2013. Identification of seven loci affecting mean telomere length and their association with disease. *Nature Genetics*. **45**, 422-7, 427e1-2.

Cong, Y.S., Wright, W.E., Shay, J.W., 2002. Human telomerase and its regulation. *Microbiology and Molecular Biology Reviews : MMBR*. **66**, 407-25, table of contents.

Coppe, J.P., Patil, C.K., Rodier, F., Sun, Y., Munoz, D.P., Goldstein, J., Nelson, P.S., Desprez, P.Y., Campisi, J., 2008. Senescence-associated secretory phenotypes reveal cell-nonautonomous functions of oncogenic RAS and the p53 tumor suppressor. *PLoS Biology*. **6**, 2853-2868.

Counter, C.M., Avilion, A.A., LeFeuvre, C.E., Stewart, N.G., Greider, C.W., Harley, C.B., Bacchetti, S., 1992. Telomere shortening associated with chromosome instability is arrested in immortal cells which express telomerase activity. *The EMBO Journal*. **11**, 1921-1929.

Counter, C.M., Meyerson, M., Eaton, E.N., Ellisen, L.W., Caddle, S.D., Haber, D.A., Weinberg, R.A., 1998. Telomerase activity is restored in human cells by ectopic expression of hTERT (hEST2), the catalytic subunit of telomerase. *Oncogene*. **16**, 1217-1222.

Cudre-Mauroux, C., Occhiodoro, T., Konig, S., Salmon, P., Bernheim, L., Trono, D., 2003. Lentivector-mediated transfer of Bmi-1 and telomerase in muscle satellite cells yields a duchenne myoblast cell line with long-term genotypic and phenotypic stability. *Human Gene Therapy*. **14**, 1525-1533.

Cusanelli, E., Romero, C.A., Chartrand, P., 2013. Telomeric noncoding RNA TERRA is induced by telomere shortening to nucleate telomerase molecules at short telomeres. *Molecular Cell*. **51**, 780-791.

Daniali, L., Benetos, A., Susser, E., Kark, J.D., Labat, C., Kimura, M., Desai, K., Granick, M., Aviv, A., 2013. Telomeres shorten at equivalent rates in somatic tissues of adults. *Nature Communications*. **4**, 1597.

Davies, M.J., Gordon, J., Gearing, A., Pigott, R., Woolf, N., Katz, D., Kyriakopoulos, A., 1993. The expression of the adhesion molecules ICAM-1, VCAM-1, PECAM, and E-selectin in human atherosclerosis. *The Journal of Pathology*. **171**, 223-229.

Davignon, J. & Ganz, P., 2004. Role of endothelial dysfunction in atherosclerosis. *Circulation*. **109**, III27-32.

- De Lange, T., 2005. Telomere-related genome instability in cancer. *Cold Spring Harbor Symposia on Quantitative Biology*. **70**, 197-204.
- De Maria, G.L., Patel, N., Kassimis, G., Banning, A.P., 2013. Spontaneous and Procedural Plaque Embolisation in Native Coronary Arteries: Pathophysiology, Diagnosis, and Prevention. *Scientifica*. **2013** .
- De Meyer, T., Rietzschel, E.R., De Buyzere, M.L., De Bacquer, D., Van Criekinge, W., De Backer, G.G., Gillebert, T.C., Van Oostveldt, P., Bekaert, S., Asklepios investigators, 2007. Paternal age at birth is an important determinant of offspring telomere length. *Human Molecular Genetics*. **16**, 3097-3102.
- De Meyer, T., Rietzschel, E.R., De Buyzere, M.L., Van Criekinge, W., Bekaert, S., 2008. Studying telomeres in a longitudinal population based study. *Frontiers in Bioscience : A Journal and Virtual Library*. **13**, 2960-2970.
- De Meyer, T., Rietzschel, E.R., De Buyzere, M.L., Van Criekinge, W., Bekaert, S., 2011. Telomere length and cardiovascular aging: the means to the ends? *Ageing Research Reviews*. **10**, 297-303.
- De Meyer, T., Nawrot, T., Bekaert, S., De Buyzere, M.L., Rietzschel, E.R., Andres, V., 2018. Telomere Length as Cardiovascular Aging Biomarker: JACC Review Topic of the Week. *Journal of the American College of Cardiology*. **72**, 805-813.
- Decaris, M.,L., Lee, C.,I., Yoder, M.,C., Tarantal, A.,F., Leach, J., 2009. Influence of the oxygen microenvironment on the proangiogenic potential of human endothelial colony forming cells. *Angiogenesis*. **12**, 303-311.
- DeKolver, R.C., Choi, V.M., Moehle, E.A., Paschon, D.E., Hockemeyer, D., Meijsing, S.H., Sancak, Y., Cui, X., Steine, E.J., Miller, J.C., Tam, P., Bartsevich, V.V., Meng, X., Rupniewski, I., Gopalan, S.M., Sun, H.C., Pitz, K.J., Rock, J.M., Zhang, L., Davis, G.D., Rebar, E.J., Cheeseman, I.M., Yamamoto, K.R., Sabatini, D.M., Jaenisch, R., Gregory, P.D., Urnov, F.D., 2010. Functional genomics, proteomics, and regulatory DNA analysis in isogenic settings using zinc finger nuclease-driven transgenesis into a safe harbor locus in the human genome. *Genome Research*. **20**, 1133-1142.
- DePinho, R.A., 2000. The age of cancer. *Nature*. **408**, 248-254.
- Desfarges, S. & Ciuffi, A., 2010. Retroviral integration site selection. *Viruses*. **2**, 111-130.
- Dickson, M.A., Hahn, W.C., Ino, Y., Ronfard, V., Wu, J.Y., Weinberg, R.A., Louis, D.N., Li, F.P., Rheinwald, J.G., 2000. Human keratinocytes that express hTERT and also bypass a p16(INK4a)-enforced mechanism that limits life span become immortal yet retain normal growth and differentiation characteristics. *Molecular and Cellular Biology*. **20**, 1436-1447.
- Dimmeler, S., Hermann, C., Zeiher, A.M., 1998. Apoptosis of endothelial cells. Contribution to the pathophysiology of atherosclerosis? *European Cytokine Network*. **9**, 697-698.
- Dimri, G.P., Lee, X., Basile, G., Acosta, M., Scott, G., Roskelley, C., Medrano, E.E., Linskens, M., Rubelj, I., Pereira-Smith, O., 1995. A biomarker that identifies senescent human cells in culture and in aging skin in vivo. *Proceedings of the National Academy of Sciences of the United States of America*. **92**, 9363-9367.

- Dokal, I. & Vulliamy, T., 2010. Inherited bone marrow failure syndromes. *Haematologica*. **95**, 1236-1240.
- Donato, A.J., Gano, L.B., Eskurza, I., Silver, A.E., Gates, P.E., Jablonski, K., Seals, D.R., 2009. Vascular endothelial dysfunction with aging: endothelin-1 and endothelial nitric oxide synthase. *American Journal of Physiology. Heart and Circulatory Physiology*. **297**, H425-32.
- Du, H.Y., Pumbo, E., Ivanovich, J., An, P., Maziarz, R.T., Reiss, U.M., Chirnomas, D., Shimamura, A., Vlachos, A., Lipton, J.M., Goyal, R.K., Goldman, F., Wilson, D.B., Mason, P.J., Bessler, M., 2009. TERC and TERT gene mutations in patients with bone marrow failure and the significance of telomere length measurements. *Blood*. **113**, 309-316.
- Efrat, S., Fusco-DeMane, D., Lemberg, H., al Emran, O., Wang, X., 1995. Conditional transformation of a pancreatic beta-cell line derived from transgenic mice expressing a tetracycline-regulated oncogene. *Proceedings of the National Academy of Sciences of the United States of America*. **92**, 3576-3580.
- Epel, E.S., Blackburn, E.H., Lin, J., Dhabhar, F.S., Adler, N.E., Morrow, J.D., Cawthon, R.M., 2004. Accelerated telomere shortening in response to life stress. *Proceedings of the National Academy of Sciences of the United States of America*. **101**, 17312-17315.
- Epel, E.S., Lin, J., Wilhelm, F.H., Wolkowitz, O.M., Cawthon, R., Adler, N.E., Dolbier, C., Mendes, W.B., Blackburn, E.H., 2006. Cell aging in relation to stress arousal and cardiovascular disease risk factors. *Psychoneuroendocrinology*. **31**, 277-287.
- Epel, E.S., Merkin, S.S., Cawthon, R., Blackburn, E.H., Adler, N.E., Pletcher, M.J., Seeman, T.E., 2008. The rate of leukocyte telomere shortening predicts mortality from cardiovascular disease in elderly men. *Aging*. **1**, 81-88.
- Eulalio, A., Mano, M., Dal Ferro, M., Zentilin, L., Sinagra, G., Zacchigna, S., Giacca, M., 2012. Functional screening identifies miRNAs inducing cardiac regeneration. *Nature*. **492**, 376-381.
- Fakhoury, J., Marie-Egyptienne, D.T., Londono-Vallejo, J.A., Autexier, C., 2010. Telomeric function of mammalian telomerases at short telomeres. *Journal of Cell Science*. **123**, 1693-1704.
- Feng, J., Funk, W.D., Wang, S.S., Weinrich, S.L., Avilion, A.A., Chiu, C.P., Adams, R.R., Chang, E., Allsopp, R.C., Yu, J., 1995. The RNA component of human telomerase. *Science (New York, N.Y.)*. **269**, 1236-1241.
- Fischer, U., Huber, J., Boelens, W.C., Mattaj, I.W., Luhrmann, R., 1995. The HIV-1 Rev activation domain is a nuclear export signal that accesses an export pathway used by specific cellular RNAs. *Cell*. **82**, 475-483.
- Flanary, B.E., Sammons, N.W., Nguyen, C., Walker, D., Streit, W.J., 2007. Evidence that aging and amyloid promote microglial cell senescence. *Rejuvenation Research*. **10**, 61-74.
- Flores-Nascimento, M.C., Alessio, A.M., de Andrade Orsi, F.L., Annichino-Bizzacchi, J.M., 2015. CD144, CD146 and VEGFR-2 properly identify circulating endothelial cell. *Revista Brasileira De Hematologia e Hemoterapia*. **37**, 98-102.

- Fogarty, P.F., Yamaguchi, H., Wiestner, A., Baerlocher, G.M., Sloand, E., Zeng, W.S., Read, E.J., Lansdorp, P.M., Young, N.S., 2003. Late presentation of dyskeratosis congenita as apparently acquired aplastic anaemia due to mutations in telomerase RNA. *The Lancet*. **362**, 1628-1630.
- Fontijn, R., Hop, C., Brinkman, H.J., Slater, R., Westerveld, A., van Mourik, J.A., Pannekoek, H., 1995. Maintenance of vascular endothelial cell-specific properties after immortalization with an amphotrophic replication-deficient retrovirus containing human papilloma virus 16 E6/E7 DNA. *Experimental Cell Research*. **216**, 199-207.
- Frick, C., Odermatt, A., Zen, K., Mandell, K.J., Edens, H., Portmann, R., Mazzucchelli, L., Jaye, D.L., Parkos, C.A., 2005. Interaction of ICAM-1 with beta 2-integrin CD11c/CD18: characterization of a peptide ligand that mimics a putative binding site on domain D4 of ICAM-1. *European Journal of Immunology*. **35**, 3610-3621.
- Fuster, V., Moreno, P.R., Fayad, Z.A., Corti, R., Badimon, J.J., 2005. Atherothrombosis and high-risk plaque: part I: evolving concepts. *Journal of the American College of Cardiology*. **46**, 937-954.
- Galkina, E. & Ley, K., 2007. Vascular adhesion molecules in atherosclerosis. *Arteriosclerosis, Thrombosis, and Vascular Biology*. **27**, 2292-2301.
- Gavrieli, Y., Sherman, Y., Ben-Sasson, S.A., 1992. Identification of programmed cell death in situ via specific labeling of nuclear DNA fragmentation. *The Journal of Cell Biology*. **119**, 493-501.
- Geng, Y.J. & Libby, P., 1995. Evidence for apoptosis in advanced human atheroma. Colocalization with interleukin-1 beta-converting enzyme. *The American Journal of Pathology*. **147**, 251-266.
- Gerhardt, T. & Ley, K., 2015. Monocyte trafficking across the vessel wall. *Cardiovascular Research*. **107**, 321-330.
- Gilley, D., Tanaka, H., Herbert, B., 2005. Telomere dysfunction in aging and cancer. *The International Journal of Biochemistry & Cell Biology*. **37**, 1000-1013.
- Gimbrone, M.A., Jr & Garcia-Cardena, G., 2016. Endothelial Cell Dysfunction and the Pathobiology of Atherosclerosis. *Circulation Research*. **118**, 620-636.
- Goldman, F., Bouarich, R., Kulkarni, S., Freeman, S., Du, H.Y., Harrington, L., Mason, P.J., Londono-Vallejo, A., Bessler, M., 2005. The effect of TERC haploinsufficiency on the inheritance of telomere length. *Proceedings of the National Academy of Sciences of the United States of America*. **102**, 17119-17124.
- Gong, Y. & de Lange, T., 2010. A Shld1-controlled POT1a provides support for repression of ATR signaling at telomeres through RPA exclusion. *Molecular Cell*. **40**, 377-387.
- Gordon, S. & Taylor, P.R., 2005. Monocyte and macrophage heterogeneity. *Nature Reviews Immunology*. **5**, 953-964.
- Gorenne, I., Kavurma, M., Scott, S., Bennett, M., 2006. Vascular smooth muscle cell senescence in atherosclerosis. *Cardiovascular Research*. **72**, 9-17.

- Gossen, M. & Bujard, H., 1992. Tight control of gene expression in mammalian cells by tetracycline-responsive promoters. *Proceedings of the National Academy of Sciences of the United States of America*. **89**, 5547-5551.
- Graham, M.K., Principessa, L., Antony, L., Meeker, A.K., Isaacs, J.T., 2017. Low p16(INK4a) Expression in Early Passage Human Prostate Basal Epithelial Cells Enables Immortalization by Telomerase Expression Alone. *The Prostate*. **77**, 374-384.
- Gramatges, M.M. & Bertuch, A.A., 2013. Short telomeres: from dyskeratosis congenita to sporadic aplastic anemia and malignancy. *Translational Research : The Journal of Laboratory and Clinical Medicine*. **162**, 353-363.
- Greider, C.W. & Blackburn, E.H., 1985. Identification of a specific telomere terminal transferase activity in Tetrahymena extracts. *Cell*. **43**, 405-413.
- Griffith, J.D., Comeau, L., Rosenfield, S., Stansel, R.M., Bianchi, A., Moss, H., De Lange, T., 1999. Mammalian telomeres end in a large duplex loop. *Cell*. **97**, 503-514.
- Gu, P., Min, J.N., Wang, Y., Huang, C., Peng, T., Chai, W., Chang, S., 2012. CTC1 deletion results in defective telomere replication, leading to catastrophic telomere loss and stem cell exhaustion. *The EMBO Journal*. **31**, 2309-2321.
- Guo, X., Deng, Y., Lin, Y., Cosme-Blanco, W., Chan, S., He, H., Yuan, G., Brown, E.J., Chang, S., 2007. Dysfunctional telomeres activate an ATM-ATR-dependent DNA damage response to suppress tumorigenesis. *The EMBO Journal*. **26**, 4709-4719.
- Guzman, H., Sanders, K., Idica, A., Bochnakian, A., Jury, D., Daugaard, I., Zisoulis, D.G., Pedersen, I.M., 2018. miR-128 inhibits telomerase activity by targeting TERT mRNA. *Oncotarget*. **9**, 13244-13253.
- Hackett, J.A. & Greider, C.W., 2002. Balancing instability: dual roles for telomerase and telomere dysfunction in tumorigenesis. *Oncogene*. **21**, 619-626.
- Haendeler, J., Hoffmann, J., Diehl, J.F., Vasa, M., Spyridopoulos, I., Zeiher, A.M., Dimmeler, S., 2004. Antioxidants inhibit nuclear export of telomerase reverse transcriptase and delay replicative senescence of endothelial cells. *Circulation Research*. **94**, 768-775.
- Haendeler, J., Drose, S., Buchner, N., Jakob, S., Altschmied, J., Goy, C., Spyridopoulos, I., Zeiher, A.M., Brandt, U., Dimmeler, S., 2009. Mitochondrial telomerase reverse transcriptase binds to and protects mitochondrial DNA and function from damage. *Arteriosclerosis, Thrombosis, and Vascular Biology*. **29**, 929-935.
- Hahn, W.C., Counter, C.M., Lundberg, A.S., Beijersbergen, R.L., Brooks, M.W., Weinberg, R.A., 1999. Creation of human tumour cells with defined genetic elements. *Nature*. **400**, 464-468.
- Hahn, W.C., Dessain, S.K., Brooks, M.W., King, J.E., Elenbaas, B., Sabatini, D.M., DeCaprio, J.A., Weinberg, R.A., 2002. Enumeration of the simian virus 40 early region elements necessary for human cell transformation. *Molecular and Cellular Biology*. **22**, 2111-2123.
- Hanahan, D. & Weinberg, R.A., 2000. The hallmarks of cancer. *Cell*. **100**, 57-70.

- Hansson, G.K., 2005. Inflammation, atherosclerosis, and coronary artery disease. *The New England Journal of Medicine*. **352**, 1685-1695.
- Hansson, G.K. & Libby, P., 2006. The immune response in atherosclerosis: a double-edged sword. *Nature Reviews.Immunology*. **6**, 508-519.
- Harley, C.B., Futcher, A.B., Greider, C.W., 1990. Telomeres shorten during ageing of human fibroblasts. *Nature*. **345**, 458-460.
- Harrison, D.G., 1997. Endothelial function and oxidant stress. *Clinical Cardiology*. **20**, II-11-7.
- Harrison, S.C., 2005. Mechanism of membrane fusion by viral envelope proteins. *Advances in Virus Research*. **64**, 231-261.
- Hashimoto, M., Ishinaga, Y., Honda, M., Ohoka, M., Morioka, S., Moriyama, K., 1991. Age-related increase in the uptake of acetylated low density lipoprotein into cultured endothelial cells from rat aorta. *Experimental Gerontology*. **26**, 397-406.
- Hayflick, L. & Moorhead, P.S., 1961. The serial cultivation of human diploid cell strains. *Experimental Cell Research*. **25**, 585-621.
- Hayflick, L., 1965. The limited in vitro lifetime of human diploid cell strains. *Experimental Cell Research*. **37**, 614-636.
- He, J., Yang, Q., Chang, L.J., 2005. Dynamic DNA methylation and histone modifications contribute to lentiviral transgene silencing in murine embryonic carcinoma cells. *Journal of Virology*. **79**, 13497-13508.
- Henderson, E.R. & Blackburn, E.H., 1989. An overhanging 3' terminus is a conserved feature of telomeres. *Molecular and Cellular Biology*. **9**, 345-348.
- Henry, C.B. & Duling, B.R., 2000. TNF-alpha increases entry of macromolecules into luminal endothelial cell glycocalyx. *American Journal of Physiology.Heart and Circulatory Physiology*. **279**, H2815-23.
- Herbert, B.S., Wright, W.E., Shay, J.W., 2002. p16(INK4a) inactivation is not required to immortalize human mammary epithelial cells. *Oncogene*. **21**, 7897-7900.
- Herrmann, J., Lerman, L.O., Mukhopadhyay, D., Napoli, C., Lerman, A., 2006. Angiogenesis in atherogenesis. *Arteriosclerosis, Thrombosis, and Vascular Biology*. **26**, 1948-1957.
- Hewitt, G., Jurk, D., Marques, F.D., Correia-Melo, C., Hardy, T., Gackowska, A., Anderson, R., Taschuk, M., Mann, J., Passos, J.F., 2012. Telomeres are favoured targets of a persistent DNA damage response in ageing and stress-induced senescence. *Nature Communications*. **3**, 708.
- Hoeijmakers, J.H., 2009. DNA damage, aging, and cancer. *The New England Journal of Medicine*. **361**, 1475-1485.

- Huang, W., Feng, Y., Liang, J., Yu, H., Wang, C., Wang, B., Wang, M., Jiang, L., Meng, W., Cai, W., Medvedovic, M., Chen, J., Paul, C., Davidson, W.S., Sadayappan, S., Stambrook, P.J., Yu, X.Y., Wang, Y., 2018. Loss of microRNA-128 promotes cardiomyocyte proliferation and heart regeneration. *Nature Communications*. **9**, 700-018-03019-z.
- Ivics, Z., Hackett, P.B., Plasterk, R.H., Izsvak, Z., 1997. Molecular reconstruction of Sleeping Beauty, a Tc1-like transposon from fish, and its transposition in human cells. *Cell*. **91**, 501-510.
- Jagannathan, L., Cuddapah, S., Costa, M., 2016. Oxidative stress under ambient and physiological oxygen tension in tissue culture. *Current Pharmacology Reports*. **2**, 64-72.
- Jansen, H., Samani, N.J., Schunkert, H., 2014. Mendelian randomization studies in coronary artery disease. *European Heart Journal*. **35**, 1917-1924.
- Jeanclous, E., Schork, N.J., Kyvik, K.O., Kimura, M., Skurnick, J.H., Aviv, A., 2000. Telomere length inversely correlates with pulse pressure and is highly familial. *Hypertension*. **36**, 195-200.
- Johnstone, M.T., Creager, S.J., Scales, K.M., Cusco, J.A., Lee, B.K., Creager, M.A., 1993. Impaired endothelium-dependent vasodilation in patients with insulin-dependent diabetes mellitus. *Circulation*. **88**, 2510-2516.
- Kan, C.Y., Wen, V.W., Pasquier, E., Jankowski, K., Chang, M., Richards, L.A., Kavallaris, M., MacKenzie, K.L., 2012. Endothelial cell dysfunction and cytoskeletal changes associated with repression of p16(INK4a) during immortalization. *Oncogene*. **31**, 4815-4827.
- Kang, S., Lu, K., Leelawattanachai, J., Hu, X., Park, S., Park, T., Min, I.M., Jin, M.M., 2013. Virus-mimetic polyplex particles for systemic and inflammation-specific targeted delivery of large genetic contents. *Gene Therapy*. **20**, 1042-1052.
- Karlseder, J., Broccoli, D., Dai, Y., Hardy, S., de Lange, T., 1999. p53- and ATM-dependent apoptosis induced by telomeres lacking TRF2. *Science (New York, N.Y.)*. **283**, 1321-1325.
- Karlseder, J., Hoke, K., Mirzoeva, O.K., Bakkenist, C., Kastan, M.B., Petrini, J.H., de Lange, T., 2004. The telomeric protein TRF2 binds the ATM kinase and can inhibit the ATM-dependent DNA damage response. *PLoS Biology*. **2**, 1150-1156.
- Kay, H.E., 1965. How Many Cell-Generations? *Lancet (London, England)*. **2**, 418-419.
- Khaidakov, M., Wang, X., Mehta, J.L., 2011. Potential involvement of LOX-1 in functional consequences of endothelial senescence. *PLoS One*. **6**, 20.
- Kim, N.W., Piatyszek, M.A., Prowse, K.R., Harley, C.B., West, M.D., Ho, P.L., Coviello, G.M., Wright, W.E., Weinrich, S.L., Shay, J.W., 1994. Specific association of human telomerase activity with immortal cells and cancer. *Science (New York, N.Y.)*. **266**, 2011-2015.
- Kim, S., Kaminker, P., Campisi, J., 1999. TIN2, a new regulator of telomere length in human cells. *Nature Genetics*. **23**, 405-412.

- Kim, W., Ludlow, A.T., Min, J., Robin, J.D., Stadler, G., Mender, I., Lai, T.P., Zhang, N., Wright, W.E., Shay, J.W., 2016. Regulation of the Human Telomerase Gene TERT by Telomere Position Effect-Over Long Distances (TPE-OLD): Implications for Aging and Cancer. *PLoS Biology*. **14**, e2000016.
- Kiyono, T., Foster, S.A., Koop, J.I., McDougall, J.K., Galloway, D.A., Klingelutz, A.J., 1998. Both Rb/p16INK4a inactivation and telomerase activity are required to immortalize human epithelial cells. *Nature*. **396**, 84-88.
- Knight, S., Collins, M., Takeuchi, Y., 2013. Insertional mutagenesis by retroviral vectors: current concepts and methods of analysis. *Current Gene Therapy*. **13**, 211-227.
- Kondo, T., Oue, N., Yoshida, K., Mitani, Y., Naka, K., Nakayama, H., Yasui, W., 2004. Expression of POT1 is associated with tumor stage and telomere length in gastric carcinoma. *Cancer Research*. **64**, 523-529.
- Kong, Q., Wu, M., Huan, Y., Zhang, L., Liu, H., Bou, G., Luo, Y., Mu, Y., Liu, Z., 2009. Transgene expression is associated with copy number and cytomegalovirus promoter methylation in transgenic pigs. *PLoS One*. **4**, e6679.
- Krtolica, A., Parrinello, S., Lockett, S., Desprez, P.Y., Campisi, J., 2001. Senescent fibroblasts promote epithelial cell growth and tumorigenesis: a link between cancer and aging. *Proceedings of the National Academy of Sciences of the United States of America*. **98**, 12072-12077.
- Kurz, D.J., Decary, S., Hong, Y., Trivier, E., Akhmedov, A., Erusalimsky, J.D., 2004. Chronic oxidative stress compromises telomere integrity and accelerates the onset of senescence in human endothelial cells. *Journal of Cell Science*. **117**, 2417-2426.
- Lampugnani, M.G., Resnati, M., Raiteri, M., Pigott, R., Pisacane, A., Houen, G., Ruco, L.P., Dejana, E., 1992. A novel endothelial-specific membrane protein is a marker of cell-cell contacts. *The Journal of Cell Biology*. **118**, 1511-1522.
- Lee, F., Mulligan, R., Berg, P., Ringold, G., 1981. Glucocorticoids regulate expression of dihydrofolate reductase cDNA in mouse mammary tumour virus chimaeric plasmids. *Nature*. **294**, 228-232.
- Lei, M., Podell, E.R., Cech, T.R., 2004. Structure of human POT1 bound to telomeric single-stranded DNA provides a model for chromosome end-protection. *Nature Structural & Molecular Biology*. **11**, 1223-1229.
- Levy, D., Neuhausen, S.L., Hunt, S.C., Kimura, M., Hwang, S.J., Chen, W., Bis, J.C., Fitzpatrick, A.L., Smith, E., Johnson, A.D., Gardner, J.P., Srinivasan, S.R., Schork, N., Rotter, J.I., Herbig, U., Psaty, B.M., Sastry, M., Murray, S.S., Vasan, R.S., Province, M.A., Glazer, N.L., Lu, X., Cao, X., Kronmal, R., Mangino, M., Soranzo, N., Spector, T.D., Berenson, G.S., Aviv, A., 2010. Genome-wide association identifies OBFC1 as a locus involved in human leukocyte telomere biology. *Proceedings of the National Academy of Sciences of the United States of America*. **107**, 9293-9298.
- Liao, J.K., 2013. Linking endothelial dysfunction with endothelial cell activation. *The Journal of Clinical Investigation*. **123**, 540-541.

- Libby, P., Ridker, P.M., Maseri, A., 2002. Inflammation and atherosclerosis. *Circulation*. **105**, 1135-1143.
- Libby, P., Ridker, P.M., Hansson, G.K., 2011. Progress and challenges in translating the biology of atherosclerosis. *Nature*. **473**, 317-325.
- Libby, P., 2013. Mechanisms of acute coronary syndromes and their implications for therapy. *The New England Journal of Medicine*. **368**, 2004-2013.
- Lim, F., Martin-Bermejo, M.J., Garcia-Escudero, V., Gallego-Hernandez, M.T., Garcia-Gomez, A., Rabano, A., Diaz-Nido, J., Avila, J., Moreno-Flores, M.T., 2010. Reversibly immortalized human olfactory ensheathing glia from an elderly donor maintain neuroregenerative capacity. *Glia*. **58**, 546-558.
- Lin, G., Finger, E., Gutierrez-Ramos, J.C., 1995. Expression of CD34 in endothelial cells, hematopoietic progenitors and nervous cells in fetal and adult mouse tissues. *European Journal of Immunology*. **25**, 1508-1516.
- Lin, J., Jin, R., Zhang, B., Chen, H., Bai, Y.X., Yang, P.X., Han, S.W., Xie, Y.H., Huang, P.T., Huang, C., Huang, J.J., 2008. Nucleolar localization of TERT is unrelated to telomerase function in human cells. *Journal of Cell Science*. **121**, 2169-2176.
- Londono-Vallejo, J.A., DerSarkissian, H., Cazes, L., Thomas, G., 2001. Differences in telomere length between homologous chromosomes in humans. *Nucleic Acids Research*. **29**, 3164-3171.
- López-Otín, C., Blasco, M.A., Partridge, L., Serrano, M., Kroemer, G., 2013. The hallmarks of aging. *Cell*. **153**, 1194-1217.
- Lorenzon, P., Vecile, E., Nardon, E., Ferrero, E., Harlan, J.M., Tedesco, F., Dobrina, A., 1998. Endothelial cell E- and P-selectin and vascular cell adhesion molecule-1 function as signaling receptors. *The Journal of Cell Biology*. **142**, 1381-1391.
- Lowe, G., Rumley, A., Norrie, J., Ford, I., Shepherd, J., Cobbe, S., Macfarlane, P., Packard, C., 2000. Blood rheology, cardiovascular risk factors, and cardiovascular disease: the West of Scotland Coronary Prevention Study. *Thrombosis and Haemostasis*. **84**, 553-558.
- Ludmer, P.L., Selwyn, A.P., Shook, T.L., Wayne, R.R., Mudge, G.H., Alexander, R.W., Ganz, P., 1986. Paradoxical vasoconstriction induced by acetylcholine in atherosclerotic coronary arteries. *New England Journal of Medicine*. **315**, 1046-1051.
- Luna, C., Carmona, A., Alique, M., Carracedo, J., Ramirez, R., 2015. TNFalpha-Damaged-HUVECs Microparticles Modify Endothelial Progenitor Cell Functional Activity. *Frontiers in Physiology*. **6**, 395.
- Madrid, A., Rode, L., Nordestgaard, B.G., Bojesen, S.E., 2016. Short Telomere Length and Ischemic Heart Disease: Observational and Genetic Studies in 290 022 Individuals. *Clinical Chemistry*. **62**, 1140-1149.
- Maeda, R.K. & Karch, F., 2011. Gene expression in time and space: additive vs hierarchical organization of cis-regulatory regions. *Current Opinion in Genetics & Development*. **21**, 187-193.

- Mahajan, M.A. & Samuels, H.H., 2008. Nuclear receptor coactivator/coregulator NCoA6(NRC) is a pleiotropic coregulator involved in transcription, cell survival, growth and development. *Nuclear Receptor Signaling*. **6**, e002.
- Maier, S.F., Wiertelak, E.P., Martin, D., Watkins, L.R., 1993. Interleukin-1 mediates the behavioral hyperalgesia produced by lithium chloride and endotoxin. *Brain Research*. **623**, 321-324.
- Makó, V., Czúcz, J., Weiszhar, Z., Herczenik, E., Matkó, J., Prohászka, Z., Cervenak, L., 2010. Proinflammatory activation pattern of human umbilical vein endothelial cells induced by IL-1 β , TNF- α , and LPS. *Cytometry Part A*. **77**, 962-970.
- Malim, M.H., Hauber, J., Le, S.Y., Maizel, J.V., Cullen, B.R., 1989. The HIV-1 rev trans-activator acts through a structured target sequence to activate nuclear export of unspliced viral mRNA. *Nature*. **338**, 254-257.
- Marsh, J.C., Ball, S.E., Cavenagh, J., Darbyshire, P., Dokal, I., Gordon-Smith, E.C., Keidan, J., Laurie, A., Martin, A., Mercieca, J., Killick, S.B., Stewart, R., Yin, J.A., British Committee for Standards in Haematology, 2009. Guidelines for the diagnosis and management of aplastic anaemia. *British Journal of Haematology*. **147**, 43-70.
- Martin-Ruiz, C.M., Gussekloo, J., Heemst, D., Zglinicki, T., Westendorp, R.G., 2005. Telomere length in white blood cells is not associated with morbidity or mortality in the oldest old: a population-based study. *Aging Cell*. **4**, 287-290.
- Martin, G.M., Sprague, C.A., Norwood, T.H., Pendergrass, W.R., 1974. Clonal selection, attenuation and differentiation in an in vitro model of hyperplasia. *The American Journal of Pathology*. **74**, 137-154.
- Martin, G.M., 1993. Clonal attenuation: causes and consequences. *Journal of Gerontology*. **48**, B171-2.
- Martínez, P. & Blasco, M.A., 2011. Telomeric and extra-telomeric roles for telomerase and the telomere-binding proteins. *Nature Reviews Cancer*. **11**, 161-176.
- Martínez, P. & Blasco, M.A., 2015. Replicating through telomeres: a means to an end. *Trends in Biochemical Sciences*. **40**, 504-515.
- Martinez, P. & Blasco, M.A., 2018. Heart-Breaking Telomeres. *Circulation Research*. **123**, 787-802.
- Martorana, A., Bulati, M., Buffa, S., Pellicanò, M., Caruso, C., Candore, G., Colonna-Romano, G., 2012. Immunosenescence, inflammation and Alzheimer's disease. *Longevity Healthspan*. **1**, b69.
- Matthews, C., Gorenne, I., Scott, S., Figg, N., Kirkpatrick, P., Ritchie, A., Goddard, M., Bennett, M., 2006. Vascular smooth muscle cells undergo telomere-based senescence in human atherosclerosis: effects of telomerase and oxidative stress. *Circulation Research*. **99**, 156-164.
- Maus, U., Henning, S., Wenschuh, H., Mayer, K., Seeger, W., Lohmeyer, J., 2002. Role of endothelial MCP-1 in monocyte adhesion to inflamed human endothelium under physiological flow. *American Journal of Physiology. Heart and Circulatory Physiology*. **283**, H2584-91.

- Meerschaert, J. & Furie, M.B., 1995. The adhesion molecules used by monocytes for migration across endothelium include CD11a/CD18, CD11b/CD18, and VLA-4 on monocytes and ICAM-1, VCAM-1, and other ligands on endothelium. *Journal of Immunology (Baltimore, Md.: 1950)*. **154**, 4099-4112.
- Michiels, C., 2003. Endothelial cell functions. *Journal of Cellular Physiology*. **196**, 430-443.
- Mikkers, H. & Berns, A., 2003. Retroviral insertional mutagenesis: tagging cancer pathways. *Advances in Cancer Research*. **88**, 53-99.
- Minamino, T., Miyauchi, H., Yoshida, T., Ishida, Y., Yoshida, H., Komuro, I., 2002. Endothelial cell senescence in human atherosclerosis: role of telomere in endothelial dysfunction. *Circulation*. **105**, 1541-1544.
- Minamino, T., Yoshida, T., Tateno, K., Miyauchi, H., Zou, Y., Toko, H., Komuro, I., 2003. Ras induces vascular smooth muscle cell senescence and inflammation in human atherosclerosis. *Circulation*. **108**, 2264-2269.
- Mitchell, J.R., Wood, E., Collins, K., 1999. A telomerase component is defective in the human disease dyskeratosis congenita. *Nature*. **402**, 551-555.
- Miyoshi, H., Blomer, U., Takahashi, M., Gage, F.H., Verma, I.M., 1998. Development of a self-inactivating lentivirus vector. *Journal of Virology*. **72**, 8150-8157.
- Mondoux, M.A. & Zakian, V.A., 2006. Telomere Position Effect: Silencing Near the End. *Cold Spring Harbor Monograph Archive*. **45**, 261-316.
- Morales, C.P., Gandia, K.G., Ramirez, R.D., Wright, W.E., Shay, J.W., Spechler, S.J., 2003. Characterisation of telomerase immortalised normal human oesophageal squamous cells. *Gut*. **52**, 327-333.
- Moskalev, A.A., Shaposhnikov, M.V., Plyusnina, E.N., Zhavoronkov, A., Budovsky, A., Yanai, H., Fraifeld, V.E., 2013. The role of DNA damage and repair in aging through the prism of Koch-like criteria. *Ageing Research Reviews*. **12**, 661-684.
- Moyzis, R.K., Buckingham, J.M., Cram, L.S., Dani, M., Deaven, L.L., Jones, M.D., Meyne, J., Ratliff, R.L., Wu, J.R., 1988. A highly conserved repetitive DNA sequence, (TTAGGG)_n, present at the telomeres of human chromosomes. *Proceedings of the National Academy of Sciences of the United States of America*. **85**, 6622-6626.
- Mudau, M., Genis, A., Lochner, A., Strijdom, H., 2012. Endothelial dysfunction: the early predictor of atherosclerosis: review article. *Cardiovascular Journal of Africa*. **23**, 222-231.
- Muñoz-Lorente, M.A., Martinez, P., Tejera, A., Whittemore, K., Moises-Silva, A.C., Bosch, F., Blasco, M.A., 2018. AAV9-mediated telomerase activation does not accelerate tumorigenesis in the context of oncogenic K-Ras-induced lung cancer. *PLoS Genetics*. **14**, e1007562.
- Münzel, T., Sinning, C., Post, F., Warnholtz, A., Schulz, E., 2008. Pathophysiology, diagnosis and prognostic implications of endothelial dysfunction. *Annals of Medicine*. **40**, 180-196.

- Nakao, S., 1997. Immune mechanism of aplastic anemia. *International Journal of Hematology*. **66**, 127-134.
- Nakayama, J., Tahara, H., Tahara, E., Saito, M., Ito, K., Nakamura, H., Nakanishi, T., Tahara, E., Ide, T., Ishikawa, F., 1998. Telomerase activation by hTERT in human normal fibroblasts and hepatocellular carcinomas. *Nature Genetics*. **18**, 65-68.
- Napier, C.E., Veas, L.A., Kan, C.Y., Taylor, L.M., Yuan, J., Wen, V.W., James, A., O'Brien, T.A., Lock, R.B., MacKenzie, K.L., 2010. Mild hyperoxia limits hTERT levels, telomerase activity, and telomere length maintenance in hTERT-transduced bone marrow endothelial cells. *Biochimica Et Biophysica Acta*. **1803**, 1142-1153.
- Nelson, N.D. & Bertuch, A.A., 2012. Dyskeratosis congenita as a disorder of telomere maintenance. *Mutation Research*. **730**, 43-51.
- Newby, A.C., Libby, P., van der Wal, A.C., 1999. Plaque instability--the real challenge for atherosclerosis research in the next decade? *Cardiovascular Research*. **41**, 321-322.
- Newby, A.C., 2005. Dual role of matrix metalloproteinases (matrixins) in intimal thickening and atherosclerotic plaque rupture. *Physiological Reviews*. **85**, 1-31.
- Noguchi, H., Kobayashi, N., Westerman, K.A., Sakaguchi, M., Okitsu, T., Totsugawa, T., Watanabe, T., Matsumura, T., Fujiwara, T., Ueda, T., Miyazaki, M., Tanaka, N., Leboulch, P., 2002. Controlled expansion of human endothelial cell populations by Cre-loxP-based reversible immortalization. *Human Gene Therapy*. **13**, 321-334.
- Nordfjall, K., Svenson, U., Norrback, K., Adolfsson, R., Lenner, P., Roos, G., 2009. The individual blood cell telomere attrition rate is telomere length dependent. *PLoS Genet*. **5**, e1000375.
- Nosedá, M., Chang, L., McLean, G., Grim, J.E., Clurman, B.E., Smith, L.L., Karsan, A., 2004. Notch activation induces endothelial cell cycle arrest and participates in contact inhibition: role of p21Cip1 repression. *Molecular and Cellular Biology*. **24**, 8813-8822.
- O'Gorman, S., Dagenais, N.A., Qian, M., Marchuk, Y., 1997. Protamine-Cre recombinase transgenes efficiently recombine target sequences in the male germ line of mice, but not in embryonic stem cells. *Proceedings of the National Academy of Sciences of the United States of America*. **94**, 14602-14607.
- O'Hare, M.J., Bond, J., Clarke, C., Takeuchi, Y., Atherton, A.J., Berry, C., Moody, J., Silver, A.R., Davies, D.C., Alsop, A.E., Neville, A.M., Jat, P.S., 2001. Conditional immortalization of freshly isolated human mammary fibroblasts and endothelial cells. *Proceedings of the National Academy of Sciences of the United States of America*. **98**, 646-651.
- Ogami, M., Ikura, Y., Ohsawa, M., Matsuo, T., Kayo, S., Yoshimi, N., Hai, E., Shirai, N., Ehara, S., Komatsu, R., Naruko, T., Ueda, M., 2004. Telomere shortening in human coronary artery diseases. *Arteriosclerosis, Thrombosis, and Vascular Biology*. **24**, 546-550.
- Oh, B., Kim, Y., Park, C., Park, Y.N., 2005. Up-regulation of telomere-binding proteins, TRF1, TRF2, and TIN2 is related to telomere shortening during human multistep hepatocarcinogenesis. *The American Journal of Pathology*. **166**, 73-80.

- Okamoto, K., Bartocci, C., Ouzounov, I., Diedrich, J.K., Yates, J.R.,3rd, Denchi, E.L., 2013. A two-step mechanism for TRF2-mediated chromosome-end protection. *Nature*. **494**, 502-505.
- Olovnikov, A.M., 1973. A theory of marginotomy: the incomplete copying of template margin in enzymic synthesis of polynucleotides and biological significance of the phenomenon. *Journal of Theoretical Biology*. **41**, 181-190.
- Onat, D., Brillon, D., Colombo, P.C., Schmidt, A.M., 2011. Human vascular endothelial cells: a model system for studying vascular inflammation in diabetes and atherosclerosis. *Current Diabetes Reports*. **11**, 193-202.
- Ouellette, M.M., Liao, M., Herbert, B.S., Johnson, M., Holt, S.E., Liss, H.S., Shay, J.W., Wright, W.E., 2000. Subsenescent telomere lengths in fibroblasts immortalized by limiting amounts of telomerase. *The Journal of Biological Chemistry*. **275**, 10072-10076.
- Paffen, E. & DeMaat, M.P., 2006. C-reactive protein in atherosclerosis: A causal factor? *Cardiovascular Research*. **71**, 30-39.
- Panossian, L., Porter, V., Valenzuela, H., Zhu, X., Reback, E., Masterman, D., Cummings, J., Effros, R., 2003. Telomere shortening in T cells correlates with Alzheimer's disease status. *Neurobiology of Aging*. **24**, 77-84.
- Paone, S., Baxter, A.A., Hulett, M.D., Poon, I.K.H., 2019. Endothelial cell apoptosis and the role of endothelial cell-derived extracellular vesicles in the progression of atherosclerosis. *Cellular and Molecular Life Sciences : CMLS*. **76**, 1093-1106.
- Pellegrini, L., 2012. The Pol alpha-primase complex. *Sub-Cellular Biochemistry*. **62**, 157-169.
- Perner, S., Bruderlein, S., Hasel, C., Waibel, I., Holdenried, A., Ciloglu, N., Chopurian, H., Nielsen, K.V., Plesch, A., Hogel, J., Moller, P., 2003. Quantifying telomere lengths of human individual chromosome arms by centromere-calibrated fluorescence in situ hybridization and digital imaging. *The American Journal of Pathology*. **163**, 1751-1756.
- Philpott, N.J., Scopes, J., Marsh, J.C., Gordon-Smith, E.C., Gibson, F.M., 1995. Increased apoptosis in aplastic anemia bone marrow progenitor cells: possible pathophysiologic significance. *Experimental Hematology*. **23**, 1642-1648.
- Pober, J.S., Gimbrone, M.A.,Jr, Lapierre, L.A., Mendrick, D.L., Fiers, W., Rothlein, R., Springer, T.A., 1986. Overlapping patterns of activation of human endothelial cells by interleukin 1, tumor necrosis factor, and immune interferon. *Journal of Immunology (Baltimore, Md.: 1950)*. **137**, 1893-1896.
- Pober, J.S. & Sessa, W.C., 2007. Evolving functions of endothelial cells in inflammation. *Nature Reviews Immunology*. **7**, 803-815.
- Podlevsky, J.D., Bley, C.J., Omana, R.V., Qi, X., Chen, J.J., 2008. The telomerase database. *Nucleic Acids Research*. **36**, D339-43.
- Podlevsky, J.D. & Chen, J.J., 2012. It all comes together at the ends: telomerase structure, function, and biogenesis. *Mutation Research*. **730**, 3-11.

- Porro, A., Feuerhahn, S., Delafontaine, J., Riethman, H., Rougemont, J., Lingner, J., 2014. Functional characterization of the TERRA transcriptome at damaged telomeres. *Nature Communications*. **5**, 5379.
- Poston, R., Britten, K., Nitkunan, T., Wilson, V., Thomas, C., Ward, J., Burnand, K., 1996. Macrophage-associated growth factor and growth factor receptor expression in human atherosclerosis. *J Vasc Res*. **33**, 79.
- Povedano, J.M., Martinez, P., Flores, J.M., Mulero, F., Blasco, M.A., 2015. Mice with Pulmonary Fibrosis Driven by Telomere Dysfunction. *Cell Reports*. **12**, 286-299.
- Quillard, T., Araujo, H.A., Franck, G., Shvartz, E., Sukhova, G., Libby, P., 2015. TLR2 and neutrophils potentiate endothelial stress, apoptosis and detachment: implications for superficial erosion. *European Heart Journal*. **36**, 1394-1404.
- Rahme, G.J., Gaskell, E., Bernstein, B.E., 2018. GABPbeta1L Wakes Up TERT. *Cancer Cell*. **34**, 358-360.
- Rai, R., Zheng, H., He, H., Luo, Y., Multani, A., Carpenter, P.B., Chang, S., 2010. The function of classical and alternative non-homologous end-joining pathways in the fusion of dysfunctional telomeres. *The EMBO Journal*. **29**, 2598-2610.
- Rai, R., Chen, Y., Lei, M., Chang, S., 2016. TRF2-RAP1 is required to protect telomeres from engaging in homologous recombination-mediated deletions and fusions. *Nature Communications*. **7**, 10881.
- Ramirez, R.D., Morales, C.P., Herbert, B.S., Rohde, J.M., Passons, C., Shay, J.W., Wright, W.E., 2001. Putative telomere-independent mechanisms of replicative aging reflect inadequate growth conditions. *Genes & Development*. **15**, 398-403.
- Ramirez, R.D., Herbert, B., Vaughan, M.B., Zou, Y., Gandia, K., Morales, C.P., Wright, W.E., Shay, J.W., 2003. Bypass of telomere-dependent replicative senescence (M1) upon overexpression of Cdk4 in normal human epithelial cells. *Oncogene*. **22**, 433-444.
- Reveal, P.M., Henkels, K.M., Turchi, J.J., 1997. Synthesis of the mammalian telomere lagging strand in vitro. *The Journal of Biological Chemistry*. **272**, 11678-11681.
- Reyes-Uribe, P., Adrianzen-Ruesta, M.P., Deng, Z., Echevarria-Vargas, I., Mender, I., Saheb, S., Liu, Q., Altieri, D.C., Murphy, M.E., Shay, J.W., Lieberman, P.M., Villanueva, J., 2018. Exploiting TERT dependency as a therapeutic strategy for NRAS-mutant melanoma. *Oncogene*. **37**, 4058-4072.
- Ribes-Zamora, A., Indiviglio, S.M., Mihalek, I., Williams, C.L., Bertuch, A.A., 2013. TRF2 interaction with Ku heterotetramerization interface gives insight into c-NHEJ prevention at human telomeres. *Cell Reports*. **5**, 194-206.
- Roberts, W.C., 1972. Coronary arteries in fatal acute myocardial infarction. *Circulation*. **45**, 215-230.

- Robin, J.D., Ludlow, A.T., Batten, K., Magdinier, F., Stadler, G., Wagner, K.R., Shay, J.W., Wright, W.E., 2014. Telomere position effect: regulation of gene expression with progressive telomere shortening over long distances. *Genes & Development*. **28**, 2464-2476.
- Ross, R. & Glomset, J.A., 1976. The pathogenesis of atherosclerosis (first of two parts). *The New England Journal of Medicine*. **295**, 369-377.
- Ross, R., 1999. Atherosclerosis—an inflammatory disease. *New England Journal of Medicine*. **340**, 115-126.
- Rudijanto, A., 2007. The role of vascular smooth muscle cells on the pathogenesis of atherosclerosis. *Acta Med Indones*. **39**, 86-93.
- Said, M.A., Eppinga, R.N., Hagemeyer, Y., Verweij, N., van der Harst, P., 2017. Telomere Length and Risk of Cardiovascular Disease and Cancer. *Journal of the American College of Cardiology*. **70**, 506-507.
- Sakuma, T., Barry, M.A., Ikeda, Y., 2012. Lentiviral vectors: basic to translational. *The Biochemical Journal*. **443**, 603-618.
- Salmon, P., Oberholzer, J., Occhiodoro, T., Morel, P., Lou, J., Trono, D., 2000. Reversible immortalization of human primary cells by lentivector-mediated transfer of specific genes. *Molecular Therapy*. **2**, 404-414.
- Salmon, P. & Trono, D., 2007. Production and titration of lentiviral vectors. *Current Protocols in Human Genetics*. 12.10. 1-12.10. 24.
- Salmon, P., 2013. Generation of human cell lines using lentiviral-mediated genetic engineering. *Epithelial Cell Culture Protocols*. Springer. 417-448.
- Samani, N.J., Boulton, R., Butler, R., Thompson, J.R., Goodall, A.H., 2001. Telomere shortening in atherosclerosis. *The Lancet*. **358**, 472-473.
- Samani, N.J. & van der Harst, P., 2008. Biological ageing and cardiovascular disease. *Heart (British Cardiac Society)*. **94**, 537-539.
- Sandoo, A., van Zanten, J.J., Metsios, G.S., Carroll, D., Kitas, G.D., 2010. The endothelium and its role in regulating vascular tone. *The Open Cardiovascular Medicine Journal*. **4**, 302-312.
- Sarkar, J. & Liu, Y., 2016. Fanconi anemia proteins in telomere maintenance. *DNA Repair*. **43**, 107-112.
- Sato, I., Morita, I., Kaji, K., Ikeda, M., Nagao, M., Murota, S., 1993. Reduction of nitric oxide producing activity associated with in vitro aging in cultured human umbilical vein endothelial cell. *Biochemical and Biophysical Research Communications*. **195**, 1070-1076.
- Schachinger, V., Britten, M.B., Zeiher, A.M., 2000. Prognostic impact of coronary vasodilator dysfunction on adverse long-term outcome of coronary heart disease. *Circulation*. **101**, 1899-1906.

- Schonbeck, U., Mach, F., Sukhova, G.K., Murphy, C., Bonnefoy, J.Y., Fabunmi, R.P., Libby, P., 1997. Regulation of matrix metalloproteinase expression in human vascular smooth muscle cells by T lymphocytes: a role for CD40 signaling in plaque rupture? *Circulation Research*. **81**, 448-454.
- Scopes, J., Bagnara, M., Gordon-Smith, E.C., Ball, S.E., Gibson, F.M., 1994. Haemopoietic progenitor cells are reduced in aplastic anaemia. *British Journal of Haematology*. **86**, 427-430.
- Semprini, S., Troup, T.J., Kotelevtseva, N., King, K., Davis, J.R., Mullins, L.J., Chapman, K.E., Dunbar, D.R., Mullins, J.J., 2007. Cryptic loxP sites in mammalian genomes: genome-wide distribution and relevance for the efficiency of BAC/PAC recombineering techniques. *Nucleic Acids Research*. **35**, 1402-1410.
- Sfeir, A., Kosiyatrakul, S.T., Hockemeyer, D., MacRae, S.L., Karlseder, J., Schildkraut, C.L., de Lange, T., 2009. Mammalian telomeres resemble fragile sites and require TRF1 for efficient replication. *Cell*. **138**, 90-103.
- Sfeir, A., Kabir, S., van Overbeek, M., Celli, G.B., de Lange, T., 2010. Loss of Rap1 induces telomere recombination in the absence of NHEJ or a DNA damage signal. *Science (New York, N.Y.)*. **327**, 1657-1661.
- Shay, J.W., Wright, W.E., Werbin, H., 1991. Defining the molecular mechanisms of human cell immortalization. *Biochimica Et Biophysica Acta (BBA)-Reviews on Cancer*. **1072**, 1-7.
- Shay, J. & Bacchetti, S., 1997. A survey of telomerase activity in human cancer. *European Journal of Cancer*. **33**, 787-791.
- Shay, J.W. & Wright, W.E., 2019. Telomeres and telomerase: three decades of progress. *Nature Reviews Genetics*. **20**, 299-309.
- Siebert, P.D., Chenchik, A., Kellogg, D.E., Lukyanov, K.A., Lukyanov, S.A., 1995. An improved PCR method for walking in uncloned genomic DNA. *Nucleic Acids Research*. **23**, 1087-1088.
- Slagboom, P.E., Droog, S., Boomsma, D.I., 1994. Genetic determination of telomere size in humans: a twin study of three age groups. *American Journal of Human Genetics*. **55**, 876-882.
- Soldatos, G., Cooper, M.E., Jandeleit-Dahm, K.A., 2005. Advanced-glycation end products in insulin-resistant states. *Current Hypertension Reports*. **7**, 96-102.
- Sprung, C.N., Afshar, G., Chavez, E.A., Lansdorp, P., Sabatier, L., Murnane, J.P., 1999. Telomere instability in a human cancer cell line. *Mutation Research/Fundamental and Molecular Mechanisms of Mutagenesis*. **429**, 209-223.
- Stadler, G., Chen, J.C., Wagner, K., Robin, J.D., Shay, J.W., Emerson, C.P., Jr, Wright, W.E., 2011. Establishment of clonal myogenic cell lines from severely affected dystrophic muscles - CDK4 maintains the myogenic population. *Skeletal Muscle*. **1**, 12-5040-1-12.
- Stadler, G., Rahimov, F., King, O.D., Chen, J.C., Robin, J.D., Wagner, K.R., Shay, J.W., Emerson Jr, C.P., Wright, W.E., 2013. Telomere position effect regulates DUX4 in human facioscapulohumeral muscular dystrophy. *Nature Structural & Molecular Biology*. **20**, 671-678.

- Steinberg, D., 2009. The LDL modification hypothesis of atherogenesis: an update. *Journal of Lipid Research*. **50 Suppl**, S376-81.
- Stewart, S.A., Ben-Porath, I., Carey, V.J., O'Connor, B.F., Hahn, W.C., Weinberg, R.A., 2003. Erosion of the telomeric single-strand overhang at replicative senescence. *Nature Genetics*. **33**, 492-496.
- Suzuki, A., Hamada, K., Sasaki, T., Mak, T.W., Nakano, T., 2007. Role of PTEN/PI3K pathway in endothelial cells. *Biochemical Society Transactions*. **35**, 172-176.
- Tahara, H., Nakanishi, T., Kitamoto, M., Nakashio, R., Shay, J.W., Tahara, E., Kajiyama, G., Ide, T., 1995. Telomerase activity in human liver tissues: comparison between chronic liver disease and hepatocellular carcinomas. *Cancer Research*. **55**, 2734-2736.
- Takano, H., Murasawa, S., Asahara, T., 2008. Functional and gene expression analysis of hTERT overexpressed endothelial cells. *Biologics : Targets & Therapy*. **2**, 547-554.
- Tan, S.M., Hyland, R.H., Al-Shamkhani, A., Douglass, W.A., Shaw, J.M., Law, S.K., 2000. Effect of integrin beta 2 subunit truncations on LFA-1 (CD11a/CD18) and Mac-1 (CD11b/CD18) assembly, surface expression, and function. *Journal of Immunology (Baltimore, Md.: 1950)*. **165**, 2574-2581.
- Tang, F., Zhang, L., Xue, G., Hynx, D., Wang, Y., Cron, P.D., Hundsrucker, C., Hergovich, A., Frank, S., Hemmings, B.A., Schmitz-Rohmer, D., 2014. hMOB3 modulates MST1 apoptotic signaling and supports tumor growth in glioblastoma multiforme. *Cancer Research*. **74**, 3779-3789.
- Thomas, P., O'Callaghan, N.J., Fenech, M., 2008. Telomere length in white blood cells, buccal cells and brain tissue and its variation with ageing and Alzheimer's disease. *Mechanisms of Ageing and Development*. **129**, 183-190.
- Thyagarajan, B., Guimaraes, M.J., Groth, A.C., Calos, M.P., 2000. Mammalian genomes contain active recombinase recognition sites. *Gene*. **244**, 47-54.
- Tiefenbacher, C.P., 2001. Tetrahydrobiopterin: a critical cofactor for eNOS and a strategy in the treatment of endothelial dysfunction? *American Journal of Physiology.Heart and Circulatory Physiology*. **280**, H2484-8.
- Torzewski, J., Torzewski, M., Bowyer, D.E., Frohlich, M., Koenig, W., Waltenberger, J., Fitzsimmons, C., Hombach, V., 1998. C-reactive protein frequently colocalizes with the terminal complement complex in the intima of early atherosclerotic lesions of human coronary arteries. *Arteriosclerosis, Thrombosis, and Vascular Biology*. **18**, 1386-1392.
- Toussaint, O., Dumont, P., Remacle, J., Dierick, J.F., Pascal, T., Fripiat, C., Magalhaes, J.P., Zdanov, S., Chainiaux, F., 2002. Stress-induced premature senescence or stress-induced senescence-like phenotype: one in vivo reality, two possible definitions? *TheScientificWorldJournal*. **2**, 230-247.
- Valdes, A.M., Andrew, T., Gardner, J.P., Kimura, M., Oelsner, E., Cherkas, L.F., Aviv, A., Spector, T.D., 2005. Obesity, cigarette smoking, and telomere length in women. *The Lancet*. **366**, 662-664.

van Steensel, B. & de Lange, T., 1997. Control of telomere length by the human telomeric protein TRF1. *Nature*. **385**, 740-743.

van Steensel, B., Smogorzewska, A., de Lange, T., 1998. TRF2 protects human telomeres from end-to-end fusions. *Cell*. **92**, 401-413.

Vaziri, H. & Benchimol, S., 1998. Reconstitution of telomerase activity in normal human cells leads to elongation of telomeres and extended replicative life span. *Current Biology : CB*. **8**, 279-282.

Viemann, D., Goebeler, M., Schmid, S., Nordhues, U., Klimmek, K., Sorg, C., Roth, J., 2006. TNF induces distinct gene expression programs in microvascular and macrovascular human endothelial cells. *Journal of Leukocyte Biology*. **80**, 174-185.

Vlassara, H., Fuh, H., Donnelly, T., Cybulsky, M., 1995. Advanced glycation endproducts promote adhesion molecule (VCAM-1, ICAM-1) expression and atheroma formation in normal rabbits. *Molecular Medicine (Cambridge, Mass.)*. **1**, 447-456.

Voight, B.F., Peloso, G.M., Orho-Melander, M., Frikke-Schmidt, R., Barbalic, M., Jensen, M.K., Hindy, G., Holm, H., Ding, E.L., Johnson, T., Schunkert, H., Samani, N.J., Clarke, R., Hopewell, J.C., Thompson, J.F., Li, M., Thorleifsson, G., Newton-Cheh, C., Musunuru, K., Pirruccello, J.P., Saleheen, D., Chen, L., Stewart, A., Schillert, A., Thorsteinsdottir, U., Thorgeirsson, G., Anand, S., Engert, J.C., Morgan, T., Spertus, J., Stoll, M., Berger, K., Martinelli, N., Girelli, D., McKeown, P.P., Patterson, C.C., Epstein, S.E., Devaney, J., Burnett, M.S., Mooser, V., Ripatti, S., Surakka, I., Nieminen, M.S., Sinisalo, J., Lokki, M.L., Perola, M., Havulinna, A., de Faire, U., Gigante, B., Ingelsson, E., Zeller, T., Wild, P., de Bakker, P.I., Klungel, O.H., Maitland-van der Zee, A.H., Peters, B.J., de Boer, A., Grobbee, D.E., Kamphuisen, P.W., Deneer, V.H., Elbers, C.C., Onland-Moret, N.C., Hofker, M.H., Wijmenga, C., Verschuren, W.M., Boer, J.M., van der Schouw, Y.T., Rasheed, A., Frossard, P., Demissie, S., Willer, C., Do, R., Ordovas, J.M., Abecasis, G.R., Boehnke, M., Mohlke, K.L., Daly, M.J., Guiducci, C., Burt, N.P., Surti, A., Gonzalez, E., Purcell, S., Gabriel, S., Marrugat, J., Peden, J., Erdmann, J., Diemert, P., Willenborg, C., Konig, I.R., Fischer, M., Hengstenberg, C., Ziegler, A., Buyschaert, I., Lambrechts, D., Van de Werf, F., Fox, K.A., El Mokhtari, N.E., Rubin, D., Schrezenmeir, J., Schreiber, S., Schafer, A., Danesh, J., Blankenberg, S., Roberts, R., McPherson, R., Watkins, H., Hall, A.S., Overvad, K., Rimm, E., Boerwinkle, E., Tybjaerg-Hansen, A., Cupples, L.A., Reilly, M.P., Melander, O., Mannucci, P.M., Ardisino, D., Siscovick, D., Elosua, R., Stefansson, K., O'Donnell, C.J., Salomaa, V., Rader, D.J., Peltonen, L., Schwartz, S.M., Altshuler, D., Kathiresan, S., 2012. Plasma HDL cholesterol and risk of myocardial infarction: a mendelian randomisation study. *Lancet (London, England)*. **380**, 572-580.

Von Zglinicki, T., 2002. Oxidative stress shortens telomeres. *Trends in Biochemical Sciences*. **27**, 339-344.

Vulliamy, T.J., Knight, S.W., Mason, P.J., Dokal, I., 2001. Very short telomeres in the peripheral blood of patients with X-linked and autosomal dyskeratosis congenita. *Blood Cells, Molecules, and Diseases*. **27**, 353-357.

Vulliamy, T., Marrone, A., Dokal, I., Mason, P.J., 2002. Association between aplastic anaemia and mutations in telomerase RNA. *The Lancet*. **359**, 2168-2170.

- Vulliamy, T., Marrone, A., Szydlo, R., Walne, A., Mason, P.J., Dokal, I., 2004. Disease anticipation is associated with progressive telomere shortening in families with dyskeratosis congenita due to mutations in TERC. *Nature Genetics*. **36**, 447-449.
- Vulliamy, T.J., Walne, A., Baskaradas, A., Mason, P.J., Marrone, A., Dokal, I., 2005. Mutations in the reverse transcriptase component of telomerase (TERT) in patients with bone marrow failure. *Blood Cells, Molecules, and Diseases*. **34**, 257-263.
- Vulliamy, T., Beswick, R., Kirwan, M., Marrone, A., Digweed, M., Walne, A., Dokal, I., 2008. Mutations in the telomerase component NHP2 cause the premature ageing syndrome dyskeratosis congenita. *Proceedings of the National Academy of Sciences of the United States of America*. **105**, 8073-8078.
- Walne, A.J., Vulliamy, T., Marrone, A., Beswick, R., Kirwan, M., Masunari, Y., Al-Qurashi, F.H., Aljurf, M., Dokal, I., 2007. Genetic heterogeneity in autosomal recessive dyskeratosis congenita with one subtype due to mutations in the telomerase-associated protein NOP10. *Human Molecular Genetics*. **16**, 1619-1629.
- Walsh, K.M., Wiencke, J.K., Lachance, D.H., Wiemels, J.L., Molinaro, A.M., Eckel-Passow, J.E., Jenkins, R.B., Wrensch, M.R., 2015. Telomere maintenance and the etiology of adult glioma. *Neuro-Oncology*. **17**, 1445-1452.
- Wang, J.C. & Bennett, M., 2012. Aging and atherosclerosis: mechanisms, functional consequences, and potential therapeutics for cellular senescence. *Circulation Research*. **111**, 245-259.
- Wang, C., Zhao, L., Lu, S., 2015. Role of TERRA in the Regulation of Telomere Length. *International Journal of Biological Sciences*. **11**, 316.
- Watson, J.D., 1972. Origin of concatemeric T7DNA. *Nature*. **239**, 197-201.
- Weber, C. & Noels, H., 2011. Atherosclerosis: current pathogenesis and therapeutic options. *Nature Medicine*. **17**, 1410-1422.
- Wei, P., Garber, M.E., Fang, S.M., Fischer, W.H., Jones, K.A., 1998. A novel CDK9-associated C-type cyclin interacts directly with HIV-1 Tat and mediates its high-affinity, loop-specific binding to TAR RNA. *Cell*. **92**, 451-462.
- Wen, V.W., Wu, K., Baksh, S., Hinshelwood, R.A., Lock, R.B., Clark, S.J., Moore, M.A., Mackenzie, K.L., 2006. Telomere-driven karyotypic complexity concurs with p16INK4a inactivation in TP53-competent immortal endothelial cells. *Cancer Research*. **66**, 10691-10700.
- Wentzensen, I.M., Mirabello, L., Pfeiffer, R.M., Savage, S.A., 2011. The association of telomere length and cancer: a meta-analysis. *Cancer Epidemiology, Biomarkers & Prevention: A Publication of the American Association for Cancer Research, Cosponsored by the American Society of Preventive Oncology*. **20**, 1238-1250.
- Westerman, K.A. & Le Boulch, P., 1996. Reversible immortalization of mammalian cells mediated by retroviral transfer and site-specific recombination. *Proceedings of the National Academy of Sciences of the United States of America*. **93**, 8971-8976.

- Wilcox, J.N., Subramanian, R.R., Sundell, C.L., Tracey, W.R., Pollock, J.S., Harrison, D.G., Marsden, P.A., 1997. Expression of multiple isoforms of nitric oxide synthase in normal and atherosclerotic vessels. *Arteriosclerosis, Thrombosis, and Vascular Biology*. **17**, 2479-2488.
- Willeit, P., Willeit, J., Brandstatter, A., Ehrlenbach, S., Mayr, A., Gasperi, A., Weger, S., Oberhollenzer, F., Reindl, M., Kronenberg, F., Kiechl, S., 2010. Cellular aging reflected by leukocyte telomere length predicts advanced atherosclerosis and cardiovascular disease risk. *Arteriosclerosis, Thrombosis, and Vascular Biology*. **30**, 1649-1656.
- Willis, A.I., Pierre-Paul, D., Sumpio, B.E., Gahtan, V., 2004. Vascular smooth muscle cell migration: current research and clinical implications. *Vascular and Endovascular Surgery*. **38**, 11-23.
- Wilson, W.R., Herbert, K.E., Mistry, Y., Stevens, S.E., Patel, H.R., Hastings, R.A., Thompson, M.M., Williams, B., 2008. Blood leucocyte telomere DNA content predicts vascular telomere DNA content in humans with and without vascular disease. *European Heart Journal*. **29**, 2689-2694.
- Wolman, S., Hirschhorn, K., Todaro, G., 1964. Early chromosomal changes in SV40-infected human fibroblast cultures. *Cytogenetic and Genome Research*. **3**, 45-61.
- Won, J., Yim, J., Kim, T.K., 2002. Sp1 and Sp3 recruit histone deacetylase to repress transcription of human telomerase reverse transcriptase (hTERT) promoter in normal human somatic cells. *The Journal of Biological Chemistry*. **277**, 38230-38238.
- Woodfin, A., Voisin, M.B., Imhof, B.A., Dejana, E., Engelhardt, B., Nourshargh, S., 2009. Endothelial cell activation leads to neutrophil transmigration as supported by the sequential roles of ICAM-2, JAM-A, and PECAM-1. *Blood*. **113**, 6246-6257.
- Wright, W.E., 1996. Telomerase Activity in Human Germine and Embryonic Tissues and Cells. *Developmental Genetics*. **18**, 173-179.
- Xin, H., Liu, D., Wan, M., Safari, A., Kim, H., Sun, W., O'Connor, M.S., Songyang, Z., 2007. TPP1 is a homologue of ciliate TEBP-beta and interacts with POT1 to recruit telomerase. *Nature*. **445**, 559-562.
- Xu, F., Sun, Y., Chen, Y., Sun, Y., Li, R., Liu, C., Zhang, C., Wang, R., Zhang, Y., 2009. Endothelial cell apoptosis is responsible for the formation of coronary thrombotic atherosclerotic plaques. *The Tohoku Journal of Experimental Medicine*. **218**, 25-33.
- Yamaguchi, H., Baerlocher, G.M., Lansdorp, P.M., Chanock, S.J., Nunez, O., Sloand, E., Young, N.S., 2003. Mutations of the human telomerase RNA gene (TERC) in aplastic anemia and myelodysplastic syndrome. *Blood*. **102**, 916-918.
- Yamaguchi, H., Calado, R.T., Ly, H., Kajigaya, S., Baerlocher, G.M., Chanock, S.J., Lansdorp, P.M., Young, N.S., 2005. Mutations in TERT, the gene for telomerase reverse transcriptase, in aplastic anemia. *New England Journal of Medicine*. **352**, 1413-1424.
- Yanaka, M., Honma, T., Sato, K., Shinohara, N., Ito, J., Tanaka, Y., Tsuduki, T., Ikeda, I., 2011. Increased monocytic adhesion by senescence in human umbilical vein endothelial cells. *Bioscience, Biotechnology, and Biochemistry*. **75**, 1098-1103.

- Yang, J., Chang, E., Cherry, A.M., Bangs, C.D., Oei, Y., Bodnar, A., Bronstein, A., Chiu, C.P., Herron, G.S., 1999. Human endothelial cell life extension by telomerase expression. *The Journal of Biological Chemistry*. **274**, 26141-26148.
- Yang, J. & Corces, V.G., 2011. Chromatin insulators: a role in nuclear organization and gene expression. *Advances in Cancer Research*. **110**, 43-76.
- Yant, S.R., Wu, X., Huang, Y., Garrison, B., Burgess, S.M., Kay, M.A., 2005. High-resolution genome-wide mapping of transposon integration in mammals. *Molecular and Cellular Biology*. **25**, 2085-2094.
- Yant, S.R., Huang, Y., Akache, B., Kay, M.A., 2007. Site-directed transposon integration in human cells. *Nucleic Acids Research*. **35**, e50.
- Ye, J.Z., Donigian, J.R., van Overbeek, M., Loayza, D., Luo, Y., Krutchinsky, A.N., Chait, B.T., de Lange, T., 2004. TIN2 binds TRF1 and TRF2 simultaneously and stabilizes the TRF2 complex on telomeres. *The Journal of Biological Chemistry*. **279**, 47264-47271.
- Yu, G.L., Bradley, J.D., Attardi, L.D., Blackburn, E.H., 1990. In vivo alteration of telomere sequences and senescence caused by mutated Tetrahymena telomerase RNAs. *Nature*. **344**, 126-132.
- Zambrowicz, B.P., Imamoto, A., Fiering, S., Herzenberg, L.A., Kerr, W.G., Soriano, P., 1997. Disruption of overlapping transcripts in the ROSA beta geo 26 gene trap strain leads to widespread expression of beta-galactosidase in mouse embryos and hematopoietic cells. *Proceedings of the National Academy of Sciences of the United States of America*. **94**, 3789-3794.
- Zhang, J., Kong, Q., Zhang, Z., Ge, P., Ba, D., He, W., 2003. Telomere dysfunction of lymphocytes in patients with Alzheimer disease. *Cognitive and Behavioral Neurology : Official Journal of the Society for Behavioral and Cognitive Neurology*. **16**, 170-176.
- Zhao, J., Miao, K., Wang, H., Ding, H., Wang, D.W., 2013. Association between telomere length and type 2 diabetes mellitus: a meta-analysis.
- Zhu, C.H., Mouly, V., Cooper, R.N., Mamchaoui, K., Bigot, A., Shay, J.W., Di Santo, J.P., Butler-Browne, G.S., Wright, W.E., 2007. Cellular senescence in human myoblasts is overcome by human telomerase reverse transcriptase and cyclin-dependent kinase 4: consequences in aging muscle and therapeutic strategies for muscular dystrophies. *Aging Cell*. **6**, 515-523.
- Zuckerman, L.A., Pullen, L., Miller, J., 1998. Functional consequences of costimulation by ICAM-1 on IL-2 gene expression and T cell activation. *Journal of Immunology (Baltimore, Md.: 1950)*. **160**, 3259-3268.
- Zufferey, R., Nagy, D., Mandel, R.J., Naldini, L., Trono, D., 1997. Multiply attenuated lentiviral vector achieves efficient gene delivery in vivo. *Nature Biotechnology*. **15**, 871-875.